

1 NOVEMBER 1987

JPL CONTRACT 951290

DESIGN STUDY OF THE JPL S-BAND
TURNAROUND RANGING TRANSPONDER

FINAL ENGINEERING REPORT

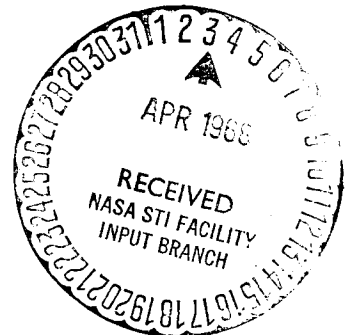
GPO PRICE \$
CSFTI PRICE(S) \$
Hard copy (HC) 300
Microfiche (MF) .65

ff 653 July 65

Submitted to:

JET PROPULSION LABORATORY
California Institute of Technology
Pasadena, California

This work was performed for the Jet Propulsion Laboratory,
California Institute of Technology, sponsored by the
National Aeronautics and Space Administration under
Contract NAS7-100.



N68-19390

FACILITY FORM 602

(ACCESSION NUMBER)

219

(PAGES)

CR-93669

(NASA CR OR TMX OR AD NUMBER)

(THRU)

(CODE)

(CATEGORY)

07

SRS TECHNICAL REPORT

JPL CONTRACT 951290

DESIGN STUDY OF THE JPL S-BAND

TURNAROUND RANGING TRANSPONDER

FINAL ENGINEERING REPORT

1 November 1967

Submitted to:

JET PROPULSION LABORATORY
California Institute of Technology
Pasadena, California

This work was performed for the Jet Propulsion Laboratory,
California Institute of Technology, sponsored by the
National Aeronautics and Space Administration under
Contract NAS7-100.

Prepared by:

PHILCO CORPORATION
A Subsidiary of Ford Motor Company
SRS Division
Palo Alto, California

TABLE OF CONTENTS

<u>Section</u>		<u>Page</u>
1	INTRODUCTION	1-1
2	SUMMARY	2-1
2.1	Original JPL Transponder Design Deficiencies	2-1
2.2	Phase I	2-3
2.3	Phase II	2-5
2.3.1	Ranging System Evaluation	2-5
2.3.2	S-Band Phase Evaluation	2-6
2.3.3	Analysis and Study	2-6
2.3.4	Recommended Changes	2-7
3	EVALUATION TESTS (Phase II)	3-1
3.1	Transponder Overall S-Band /"VCO"/ Ranging Phase vs Temperature	3-1
3.1.1	Entire Transponder	3-9
3.1.2	Six Packs (3)	3-15
3.1.3	Individual Modules (13)	3-32
3.2	Diagnostic Tests	3-55
3.2.1	Module	3-55
3.2.2	Special	3-78
4	ANALYSIS AND STUDY (Phase II)	4-1
4.1	Ranging Delay and Ranging Delay Variation	4-1
4.1.1	Ranging Delay due to Interstage Coupling Networks	4-4
4.1.2	Delay Variation Produced in the Demodulation Process	4-13

TABLE OF CONTENTS (Cont'd)

<u>Section</u>		<u>Page</u>
	4.2 Transponder Phase Relationships	4-18
	4.2.1 General Relationships	4-18
	4.2.2 Ranging Delay Produced by VCO Crystal Temperature Characteristic	4-21
	4.2.3 "Cog" Phase Jumps	4-24
	4.3 Frequency Ratio Study	4-27
5	VIDEO AMPLIFIER	
	5.1 Functional Description	5-1
	5.2 Specification Requirements	5-1
	5.3 Problems in Mariner C Design	5-1
	5.4 SRS Module Design	5-3
	5.5 Test Data	5-6
	5.6 Comparison with Mariner C Module	5-6
6	CONCLUSIONS AND RECOMMENDATIONS	
	6.1 Discussion and Review	6-1
	6.2 Recommendations for Future Work	6-4
APPENDIX (PHASE II)		
I	Phase Shift and Group Delay vs Detuning for Single and Transitional Coupled Double Tuned Filters	A.1-1
II	Demodulations of a Trapezoidal Phase Modulated Carrier	A.2-1
III	Delay Produced in the Demodulation Process	
	3.1 Distorted Ranging Signal	A.3-1
	3.2 Detector Reference Signal	A.3-5
IV	Spectrum Analysis of a Trapezoidal Modulated Carrier	A.4-1
V	Transponder Phase Analysis	A.5-1
VI	Frequency Ratio Study	A.6-1
VII	Ranging Test Information	A.7-1

SECTION 1

DESIGN STUDY
OF THE
S-BAND TURNAROUND RANGING TRANSPONDER
FINAL ENGINEERING REPORT

1.0 INTRODUCTION

JPL Contract 951290 provides for a design study program of the JPL S-Band Turnaround Ranging Transponder directed toward improving the Transponder performance. The program was divided into two parts: Phase I and Phase II.

The required overall effort is divided into three broad areas which include:

- a. A review of all the transponder circuitry directed toward improving the unit's performance, stability, efficiency, and reliability.
- b. A detail analysis of specific transponder problem areas which have evolved through previous use of the unit in the Mariner C Mars Mission.
- c. Transponder in-lock ranging and S-band carrier phase stability as a function of temperature, using JPL-supplied transponder.

The "Interim Engineering Report," WDL-TR3066, provides the results of the

Phase I effort which accomplished "a" and "b" above. Included is a complete presentation of the design investigation, analysis and testing accomplished in the Phase I effort.

This "Final Engineering Report" provides a summary of the Phase I effort plus the results accomplished in "c" above.

SECTION 2

SUMMARY

2.1 ORIGINAL JPL TRANSPONDER DESIGN DEFICIENCIES

The original JPL S-band transponder was developed during 1962 for an S-band Mariner-Mars Mission in 1964. Some of the circuitry was left identical to its L-band predecessor designed in 1959. Although the transponder has performed exceedingly well, there have been a number of problems which have occurred during calibration, test and mission operation. In addition, many improvements have been made in component technology and reliability which should be incorporated to update the design.

Of specific concern are the following items which have received specific attention during the program:

1. Self lock - the mechanism by which the Transponder receiver is caused to phase lock onto a Transponder-generated signal when the turnaround ranging module is turned on was studied and analyzed.
2. Turnaround ranging response - the turnaround response to modulation was analyzed for purposes of both improving the phase stability over the operating temperature range and providing reproducibility from unit to unit.
3. Modulation bandwidth - the required modulation bandwidth was difficult to achieve and required very careful and time-consuming alignment of the exciter stages.

4. Phase modulator - the sensitivity and stability of the phase modulator was studied and methods for improvement recommended.
5. Automatic gain control (AGC) - the AGC circuits and the AGC-controlled circuits were analyzed to improve performance and stability over the operating temperature range.
6. Receiver best-lock-frequency drift - the receiver best-lock-frequency which drifts extensively with time and temperature was studied and improved.
7. Auxiliary oscillator frequency - the auxiliary oscillator frequency was sensitive to the value of the transfer command voltage.
8. Power supply and monitor point lead filtering - the power supply and monitor point lead filtering and decoupling was analyzed for possible reduction in low-frequency feedback and radio frequency (RF) leakage.
9. Varactor multipliers - the design of the varactor multipliers was analyzed to improve the reliability and minimize spurious outputs from the exciter.
10. Part Selection - by adequate design and tolerance analysis, a reduction in the number of parts which required selection of parameters during the assembly and testing phase was made.
11. Receiver noise figure - the receiver circuitry was analyzed to reduce the receiver noise figure within the constraints of the conventional circuitry now used.
12. Component type reduction - where possible by adequate design, a reduction in the number of types of components required was made.

In addition to the detailed analysis of these specific transponder areas a review was performed of all the transponder's circuitry. This effort was directed toward improving the units performance, stability, efficiency, and reliability.

2.2 PHASE I

Phase I of this program was divided into two major areas of detail module design and transponder system analysis.

Table 2-1 provides a summary of the module study, design, and test efforts completed.

The transponder system analysis, design, and test was divided into five major areas as follows:

- a. Transponder Self-Lock
- b. Ranging Delay and Bandwidth
- c. Automatic Gain Control System
- d. DC Power Considerations
- e. Reliability Improvement.

Specific details of the Phase I effort are included in WDL-TR3066, "Design Study of the JPL S-Band Turnaround Ranging Transponder, Interim Engineering Report" dated 19 September, 1966.

TABLE 2-1

S-BAND TRANSPONDER DESIGN STUDY PHASE I MODULE EFFORT ACCOMPLISHED

Module	Analyzed	Tested	Redesigned And Tested
Mixer Preamplifier	X	X	(1)
47 Mc IF Amplifier	X	X	X
9.56 Mc IF Amplifier	X	X	X
Phase Detector			
AGC Detector	X	X	
Frequency Divider	X		
VCO	X	X	(2)
X36 Multiplier	X		
Auxiliary Oscillator	X	X	(2)
X30 Multiplier	X	X	X
Isolation Amplifier	X	X	
Video Amplifier			

(1) Mixer Portion Only

(2) Oscillator Portion Only

2.3 PHASE II

A major part of the Phase II effort was spent in a test program with the purpose of evaluating and isolating the causes of S-band carrier phase shift and ranging delay variation in the Mariner C transponder, as a function of temperature.

In addition to these tests, specific diagnostic tests were performed on several of the modules.

The principal goal of the analysis and study effort was to relate the ranging delay and S-band phase temperature data to transponder circuit functions. In addition to this, a study was made to determine the optimum transmit-to-receive frequency ratio, from the transponder viewpoint, for the proposed change in the DSIF band occupancy.

Finally, an SRS version of the Video Amplifier was developed as part of the Phase II effort.

2.3.1 Ranging System Evaluation

Measurements show that the major cause of ranging delay variations in the JPL Mariner "C" transponder under temperature varying conditions is due to the following two conditions:

- a. Distortion of the ranging signal.
- b. Variation in the alignment of the ranging detector reference phase relative to the carrier.

The combined effect of these two conditions is to produce an incremental range delay that varies nonlinearly as a function of the misalignment.

The major cause of distortion is due to reactive loading at the second mixer, due to the input impedance of the crystal filter. The 9.56 MHz I.F. Amplifier is the major cause of reference phase variations in the ranging detector.

2.3.2 S-Band Phase Evaluation

Measurements show that the S-band Phase shifted fairly linearly with temperature in the case of the entire transponder. The total variation throughout the temperature range is 22.2 cycles.

Four modules were mainly responsible for the phase shift. These are, in order:

- a. VCO and X3 Multiplier (13 cycles)
- b. Aux-Osc., Mod., and X4 Multiplier (5.1 cycles)
- c. X30 Multiplier (4.4 cycles)
- d. X36 Multiplier (3.5 cycles)

The large variation in S-band phase caused by the VCO was not expected. One reason for the large variation is due to the fact that the phase multiplication following the VCO is 120 times.

The results of the S-band phase measurements are summarized in Table 2.3.1-

2.3.3 Analysis and Study

The analysis and study efforts combined with the various measurements made in the program indicate that:

- a. Group delay in RF stages due to bandpass interstage coupling networks, and phase shift of the fundamental component of the 498 KH_2 square wave in video stages, is responsible for almost all of the measured ranging delay time in the transponder. These are normal, unavoidable delay phenomenon and result mainly from bandwidth limiting requirements.
- b. Ranging delay variations measured in the JPL transponder are produced principally in the demodulation process, and are caused by variations in the reference phase relative to the carrier. This phenomenon can be corrected to acceptable limits.

A module-to-module analysis was performed in order to obtain calculated values for nominal ranging delay and ranging delay variation due to interstage coupling networks so that expected and measured data at normal operating temperatures and temperature varying conditions could be compared directly when possible. The overall transponder expected ranging delay and ranging delay variation due to interstage coupling networks is then taken to be equal to the sum of the individual module values. The results are presented in Table 2.3.1-2.

2.3.4 Recommended Changes

The recommended design changes are listed as follows:

- a. Isolate the crystal filter from the second mixer by adding a unity gain isolation amplifier in the 47.8 MH_2 I.F. module.
- b. Tighten the phase specification of the 9.56 MH_2 I.F. module to ± 10 degrees over the operating temperature range.

- c. Specify the Frequency Divider module phase variation between its three outputs: ± 3 degrees over the operating temperature.
- d. Specify that 4.78 MHz output of the Frequency Divider shall be at least -60 db below the 9.56 MHz output.
- e. Control the overall misalignment between reference and carrier in the ranging detector to ± 20 degrees over the operating temperature.
- f. Provide adequate isolation to impedance variations at the input of Frequency Divider module and the output of the VCO module.
- g. Provide a transient-free bias source to the varicap in the VCO module.
- h. Eliminate the switching transient caused by turning on the ranging channel.
- i. Replace the JPL Video Amplifier module with the new SRS version.

SECTION 3

EVALUATION TESTS

3.0 GENERAL

A major part of the Phase II effort was spent in a test program with the purpose of evaluating and isolating the causes of S-band carrier phase shift and ranging delay variation in the Mariner C transponder, as a function of temperature. The transponder used was JPL-supplied; a list of pertinent serial numbers is given in Table 3.0-1.

In addition to these tests, specific diagnostic tests were performed on several of the modules of the above mentioned JPL-supplied transponder.

A block diagram of the Mariner 'C' transponder is presented in Figure 3.0-1, and is intended for general reference purposes for the various sections of the report.

3.1 TRANSPONDER OVERALL S-BAND/"VCO"/RANGING PHASE VERSUS TEMPERATURE

The transponder was connected in a normally operating condition for each of these tests, and the various component parts of the transponder were separately subjected to temperature variations, with all of the remaining component parts held at constant temperature. The test set up block diagram is shown in Figure 3.1-1. As shown in this figure, a transponder (REFERENCE TRANSPONDER) similar to the subject transponder (TEST TRANSPONDER) was held at constant temperature and used to provide stable phase coherent reference signals for the measurement of the S-band and "VCO" phases. The reference and measured signals are taken at corresponding points in the two transponders.

The major points of interest are listed for convenience as follows:

- S-band phase shift is the carrier phase shift of the 2295MHz RF output of the Exciter, relative to the S-band reference signal. The data at +25°C is used as a reference point. In effect, this measurement is equivalent to an S-band input to output overall transponder phase measurement.

Table 3.0-1

JPL - Supplied Transponder Serial Numbers

<u>No.</u>	<u>Identifying Name</u>	<u>S/N</u>
1.	Preselector	15
2.	Mixer-Preamplifier Module	10
3.	47.8 Mc I.F. Module	(obscured)
4.	9.56 Mc I.F. Module	4
5.	X36 Multiplier Module	4
6.	AGC Detector Module	4
7.	Phase Detector Module	4
8.	VCO Module	4
9.	Frequency Divider Module	5
10.	Isolation Amplifier Module	5
11.	Video Amplifier Module	4
12.	Auxiliary Oscillator Module	8
13.	X30 Multiplier Module	21
14.	Receiver, Six Pack No. 1	4
15.	Receiver, Six Pack No. 2	4
16.	Exciter, Six Pack	4

The following units were also supplied, but were not used in the tests.

17.	Auxiliary Oscillator Module	7
18.	X30 Multiplier Module	14
19.	Power Supply	3
20.	Power Supply	5

18

TR-DA1522A

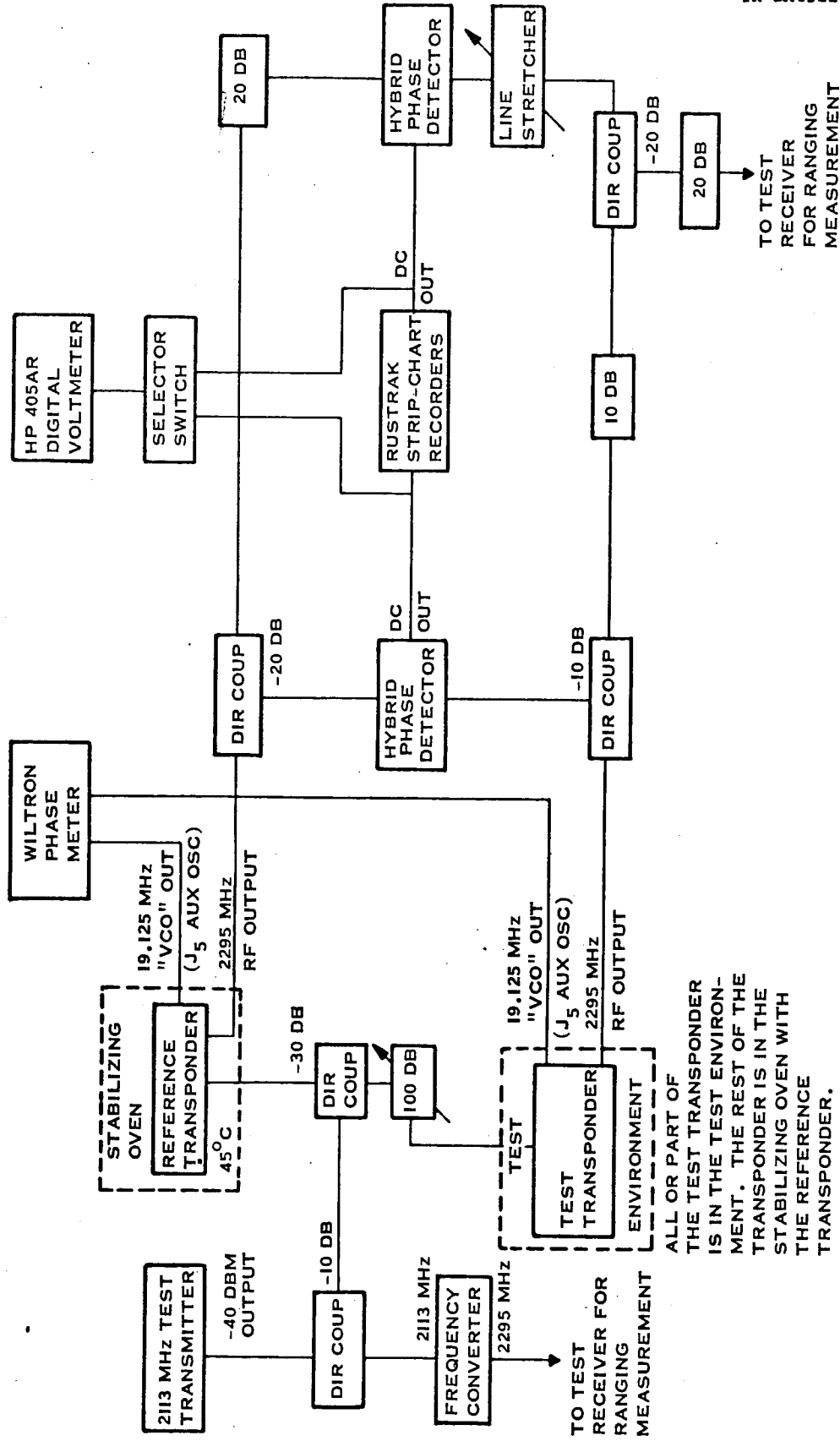


Figure 3.1-1 Block Diagram of the Test Setup for S-Band/'VCO'/Ranging Phase Shift vs. Temperature

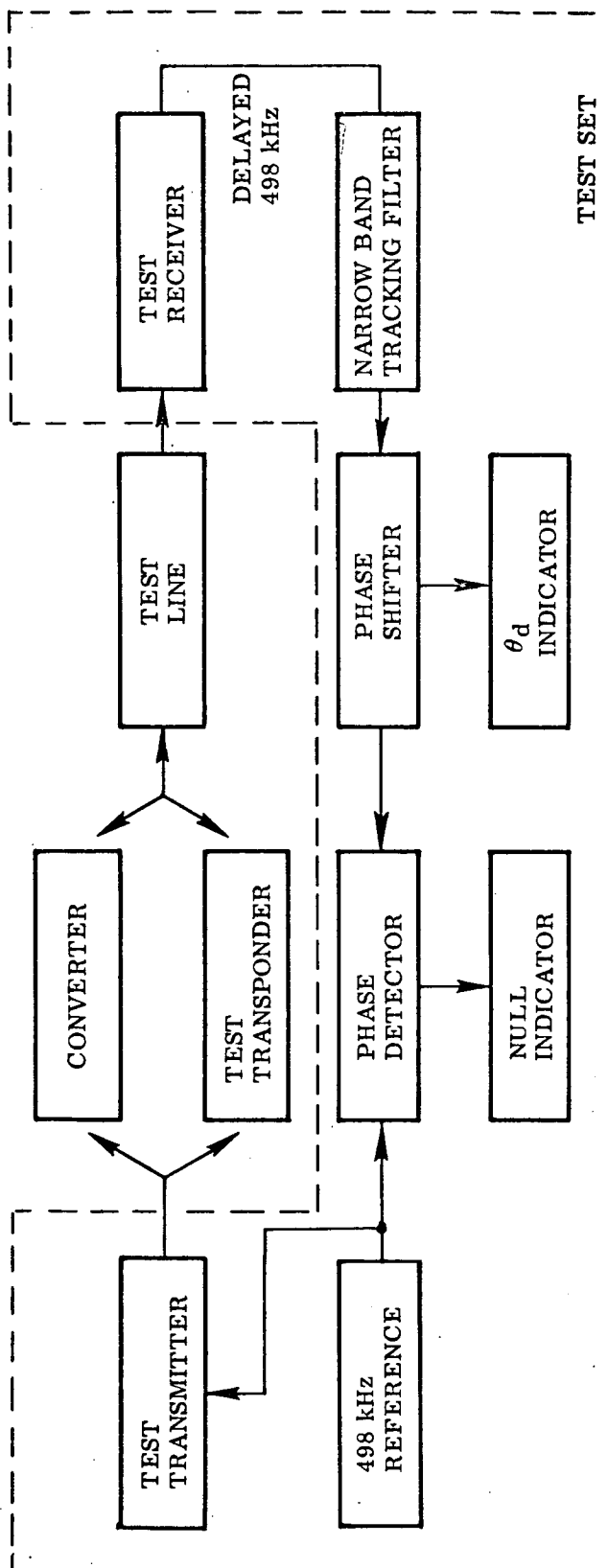
- Two quadrature-related measurements are used in order to avoid ambiguity and provide greater accuracy in the S-band phase readings (S-band phase shifts typically exceed 90 degrees for each temperature increment).
- "VCO" phase shift is the phase shift of the 19-1/8 MHz VCO output signal (i.e., the exciter input drive signal) relative to the "VCO" reference signal. In effect, this measurement is equivalent to an S-band input to VCO output overall receiver phase measurement.
- The ranging delay measurement technique is based upon comparing the phase of the fundamental component of the delayed 498 KHz ranging signal with a reference signal in the test set. See Figure 3.1-2 for further details. Note that the reference transponder is not involved in the ranging measurements.

Further information on test methods and procedures is presented in Appendix VII. A list of pertinent serial numbers for the test set are presented in the appendix; Table A.7-1.

In the tests to be described next, the temperature increments were, in the order taken:

- | | |
|--------------------------|--------------------------|
| a. -10°C | e. $+40^{\circ}\text{C}$ |
| b. 0°C | f. $+50^{\circ}\text{C}$ |
| c. $+10^{\circ}\text{C}$ | g. $+60^{\circ}\text{C}$ |
| d. $+25^{\circ}\text{C}$ | h. $+75^{\circ}\text{C}$ |

S-band and "VCO" phase data were taken at input signal levels of -70 to -140 dbm in 10 db steps, and ranging phase data were taken at -70, -90, and -110 dbm.



NOTES:

$$(1) \quad \theta_d \approx \frac{\tau_{xpndr}}{5.58} \approx \underbrace{\theta_{xpndr} + \text{test set}}_{\text{MEAS. \#1}} - \underbrace{\theta_{conv} + \text{test set}}_{\text{MEAS. \#2}}$$

where:

τ is time delay in nanoseconds

θ is phase angle delay in degrees

$\theta_{conv} \ll \theta_{xpndr}$

Note: The diagram is simplified, in order to show the measurement philosophy.

- (2) $+\Delta$ length of test line $\propto +\Delta\theta_d$ is used to check the proper angular segment between the two measured angles in order to avoid ambiguity with the complementary segment.

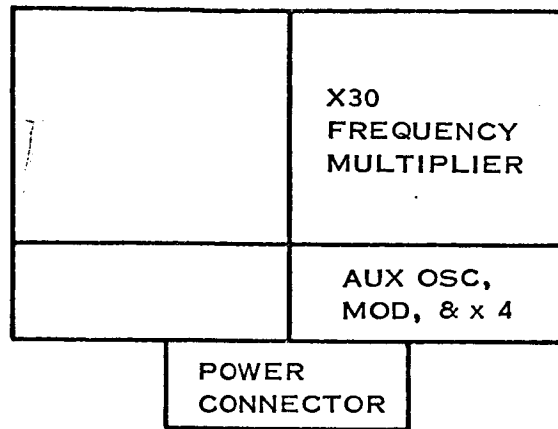
Figure 3.1-2 Ranging Delay Measurement Block Diagram

The order of the temperature tests were as follows:

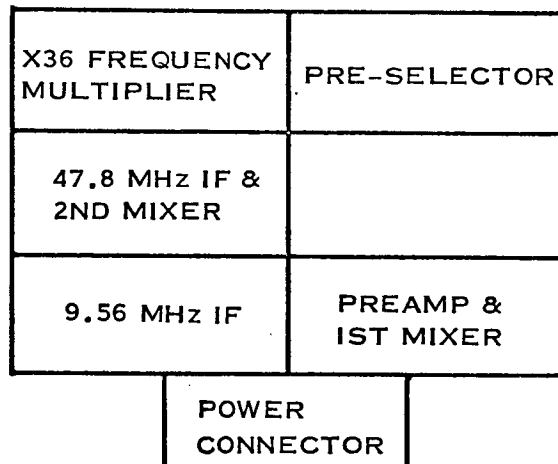
- a. Entire Transponder
- b. Individual Six Packs (3)
- c. Individual Modules (13)

The results of these tests are presented next. The module arrangement within the six-packs is shown in Figure 3.1-3 for reference purposes.

EXCITER
SIX PACK



RECEIVER,
SIX PACK NO.1



RECEIVER,
SIX PACK NO.2

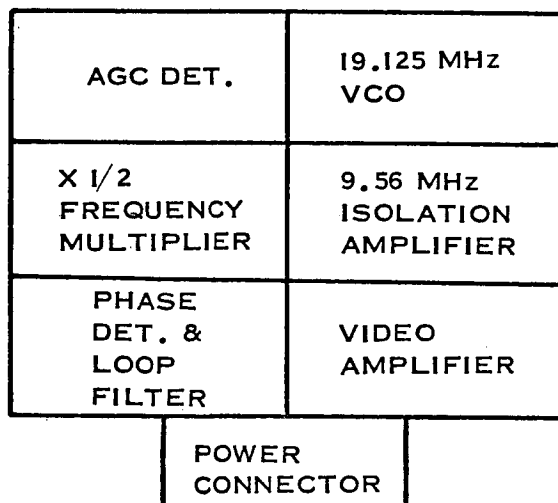


Figure 3.1-3 Module Arrangement Within the Six Packs

3.1.1 Entire Transponder Evaluation Test

Figure 3.1.1-1 indicates that, in the case of the entire transponder, the S-Band phase shifted fairly linearly with temperature. The total variation throughout the temperature range is 22.2 cycles. This large phase shift is the result of many small phase shifts resulting from circuit detuning which are multiplied by various factors in the frequency multipliers. Figure 3.1.1-2 is the phase shift measured at the VCO signal input to the Auxiliary Oscillator module. Since the Exciter Six Pack multiplies this frequency (and therefore phase variations with temperature) by 120, the total VCO shift noticed in this figure can be used to determine what portion of the total S-Band phase shift was caused by the Receiver Six Packs. In this case, the total VCO variation of 40.3° multiplied by $120/360^\circ$ equals 13.4 cycles variation at S-Band. The remaining 8.8 cycles variation was caused by the Exciter Six Pack.

The values for the VCO phase shift were read directly from the Wiltron phase meter. Since the transponder will lock to the incoming signal at many different VCO phases (see Section 4.2.3), only the relative shift with temperature should be considered. This explains the difference in the absolute value of VCO phase shift that will be noticed in these graphs in the following sections.

As seen in Figure 3.1.1-3, ranging delay did not vary linearly with temperature. Most of the ranging delay variation was determined to be caused by the subsequent misalignment between the reference and the signal at the ranging detector as temperature varied (see Section 4.1.2).

Figure 3.1.1-4 and 3.1.1-5 show the comparison of S-Band phase shift and ranging delay variation measured directly while the entire transponder was under test and the sum of the data measured while the individual six packs were under test. The contributions of each module toward these variations are quite dissimilar in direction and magnitude. This means,

TR-DA1522A

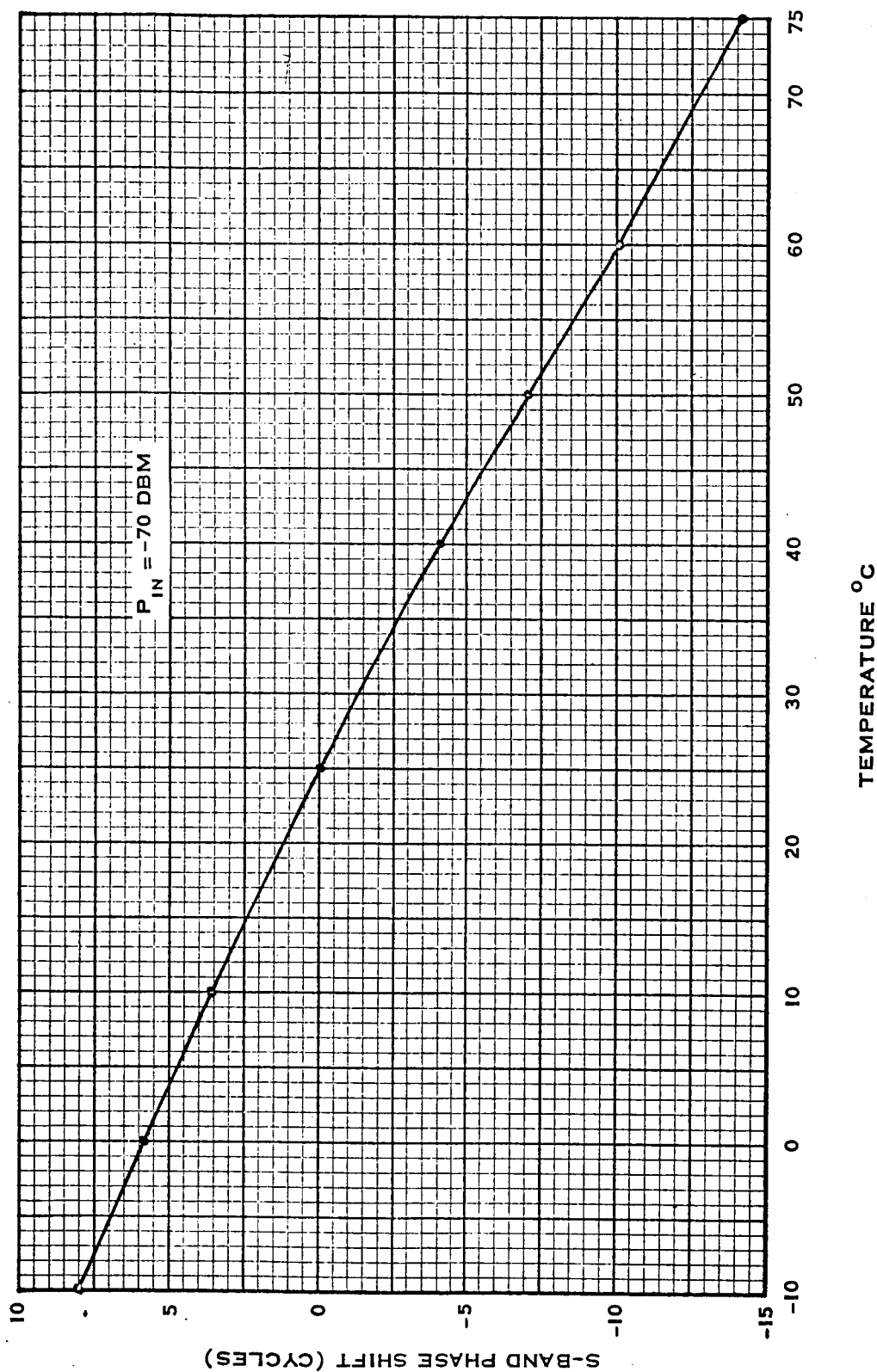


Figure 3.1.1-1 S-Band Phase Shift Vs. Temperature of the Entire Transponder.

3-10

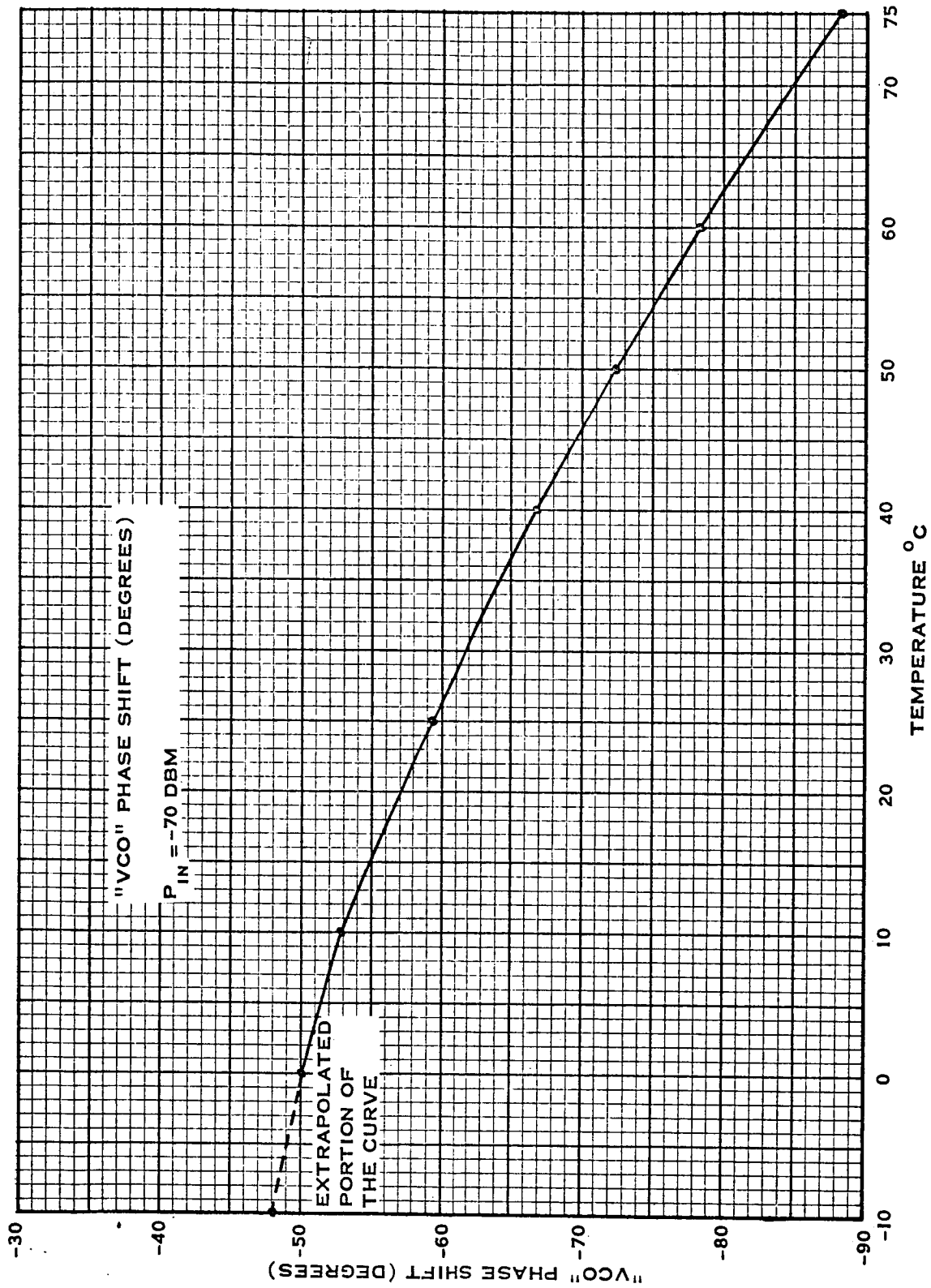


Figure 3.1.1-2 "VCO" Phase Shift Vs. Temperature of the Entire Transponder.

26

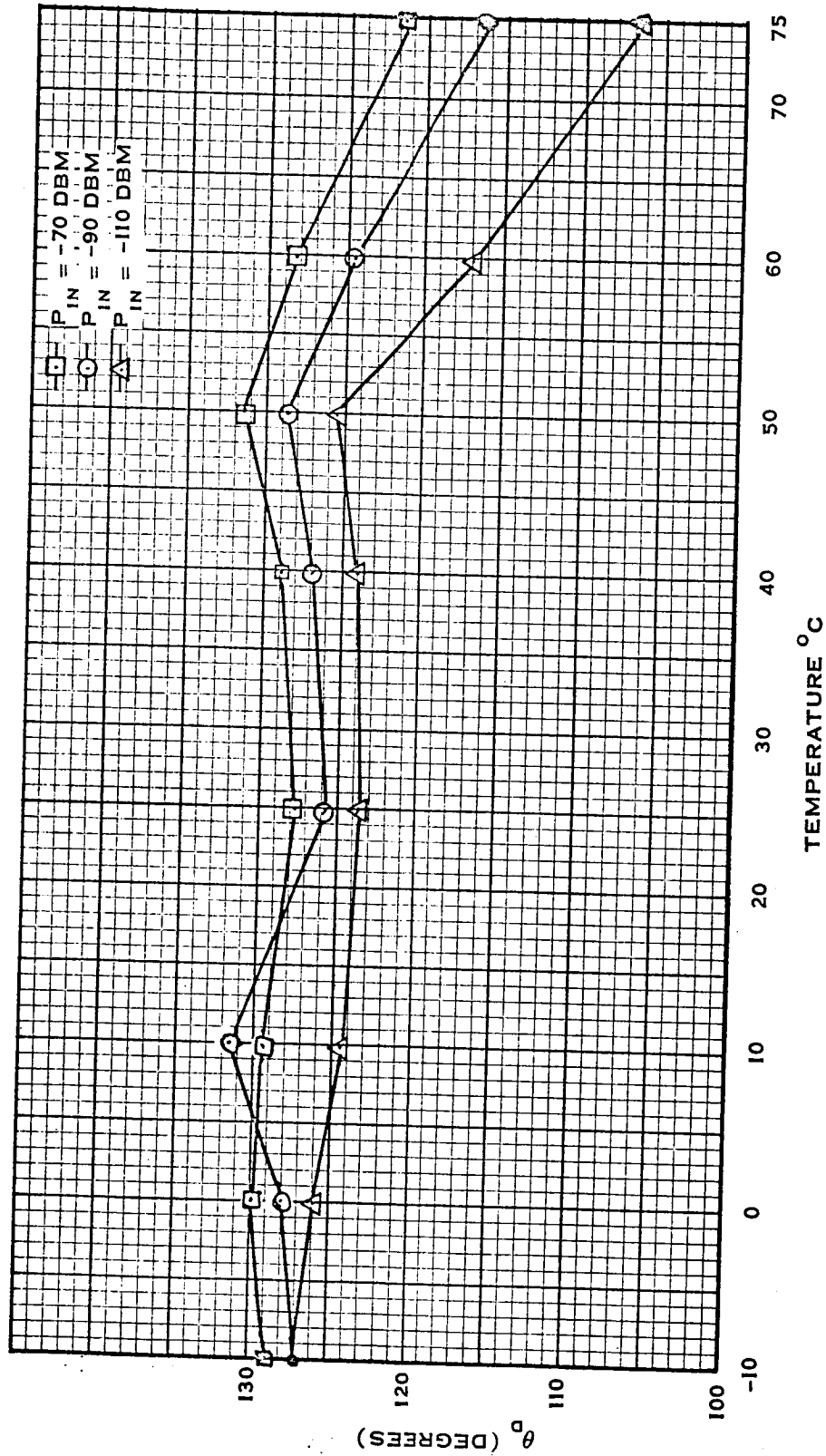


Figure 3.1.1-3 Ranging Delay Vs. Temperature of the Entire Transponder.

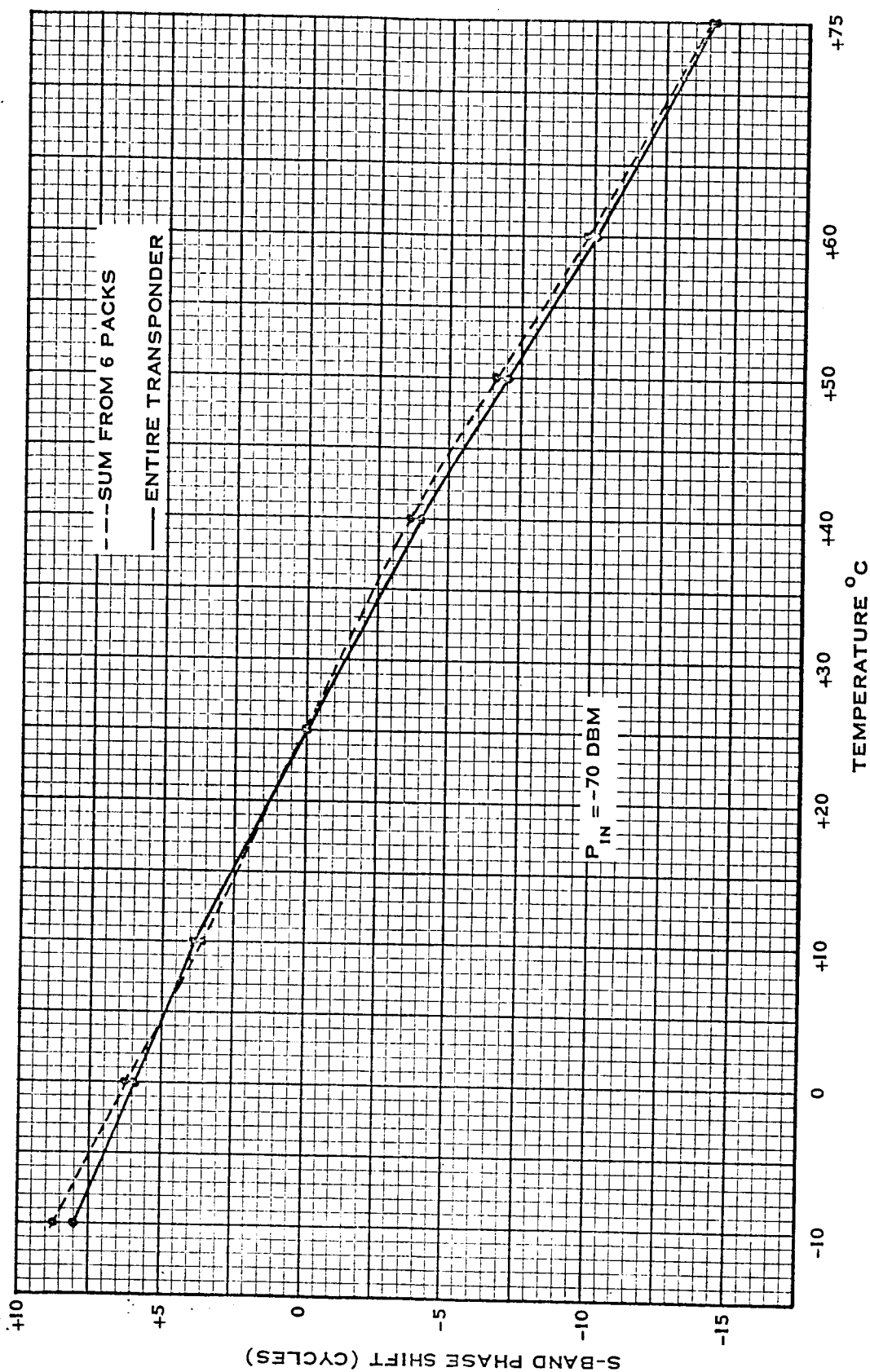


Figure 3.1.1-4 Comparison of S-Band Phase Shift Vs. Temperature Between the Entire Transponder and the Sum of the Phase Shift from the Six Packs.

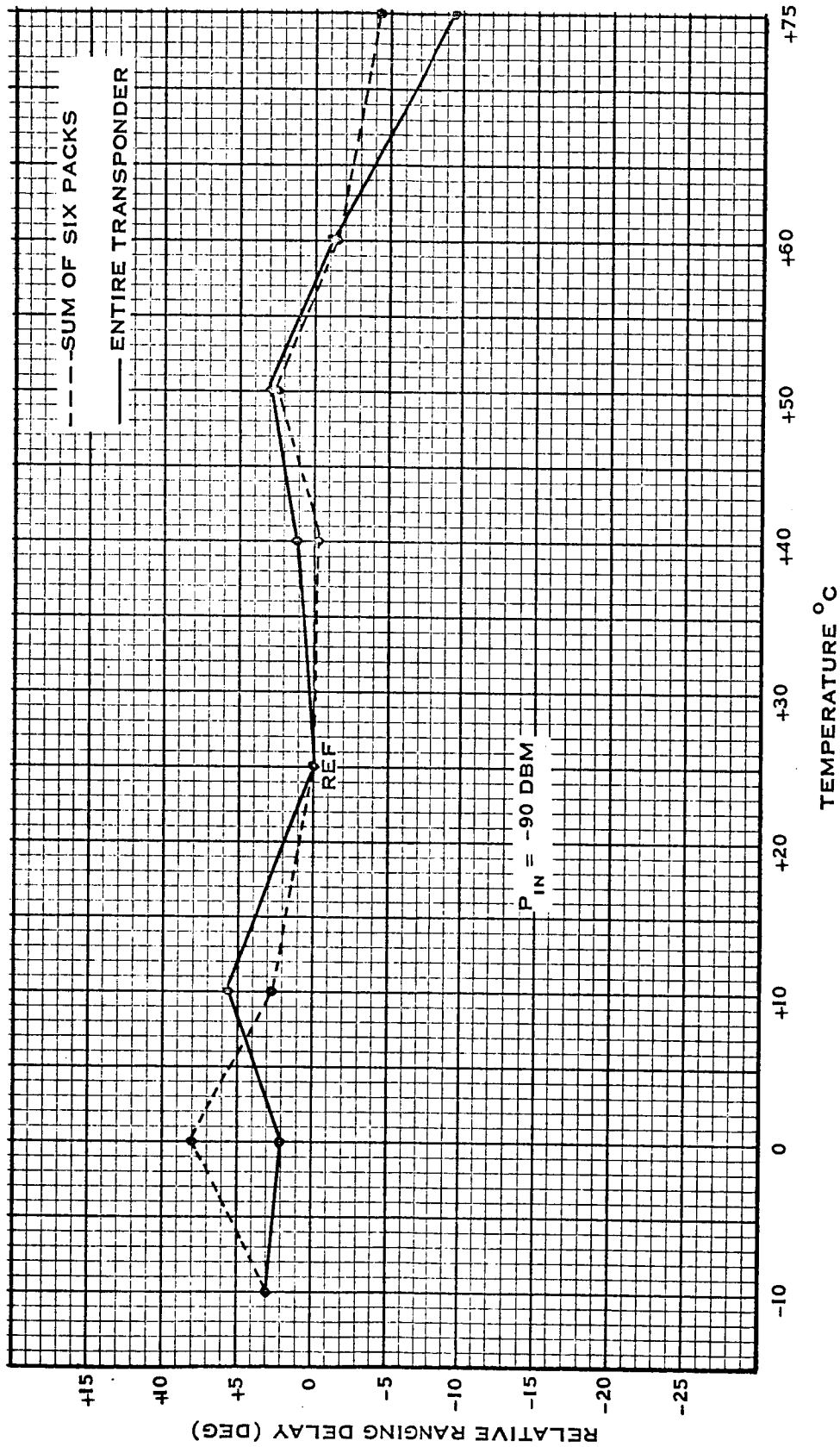


Figure 3.1.1.1-5 Comparison of Relative Ranging Delay vs. Temperature Between the Entire Transponder and the Sum of the Delay from the Six Packs.

since there is good correlation between the data from the entire transponder and the sum from the six packs, that the delay variations are a result of many cancelling effects.

Ranging delay was also noticed to vary as a function of input RF attenuation. In most cases, the delay becomes shorter as the input RF level is decreased. This is probably the result of the reduction in the 498 KHz signal content as the S/N ratio is decreased. Separate ranging delay tests show that the ranging delay is apparently reduced by attenuating the input to the Video Amplifier (see Figure 3.2.2-8).

S-Band and VCO phase shifts were also measured as a function of input RF power to the transponder. Regardless of which part of the transponder was being temperature tested, this plot remained essentially constant. The results were an almost linear response of about $+2.5^\circ$ of S-Band shift per DB of RF input attenuation. The S-Band phase shift divided by 120 approximately equals the VCO phase shift. This indicates that nearly all of the S-Band phase shift resulting from input RF power changes was caused by the receiver portion of the transponder.

Each time the temperature of the test environment was changed, a minimum of one hour was allowed for stabilization. In thirty minutes, essentially complete stabilization was noticed to have occurred.

3.1.2 Six Packs Evaluation Tests

Figures 3.1.2-1, 3.1.2-4, and 3.1.2-7 show the change in S-Band phase as a function of individual six pack temperature changes. Figure 3.1.2-1 indicates that the direction of phase change caused by the Receiver, Six Pack No. 1 undergoing temperature testing is opposite to that of the other

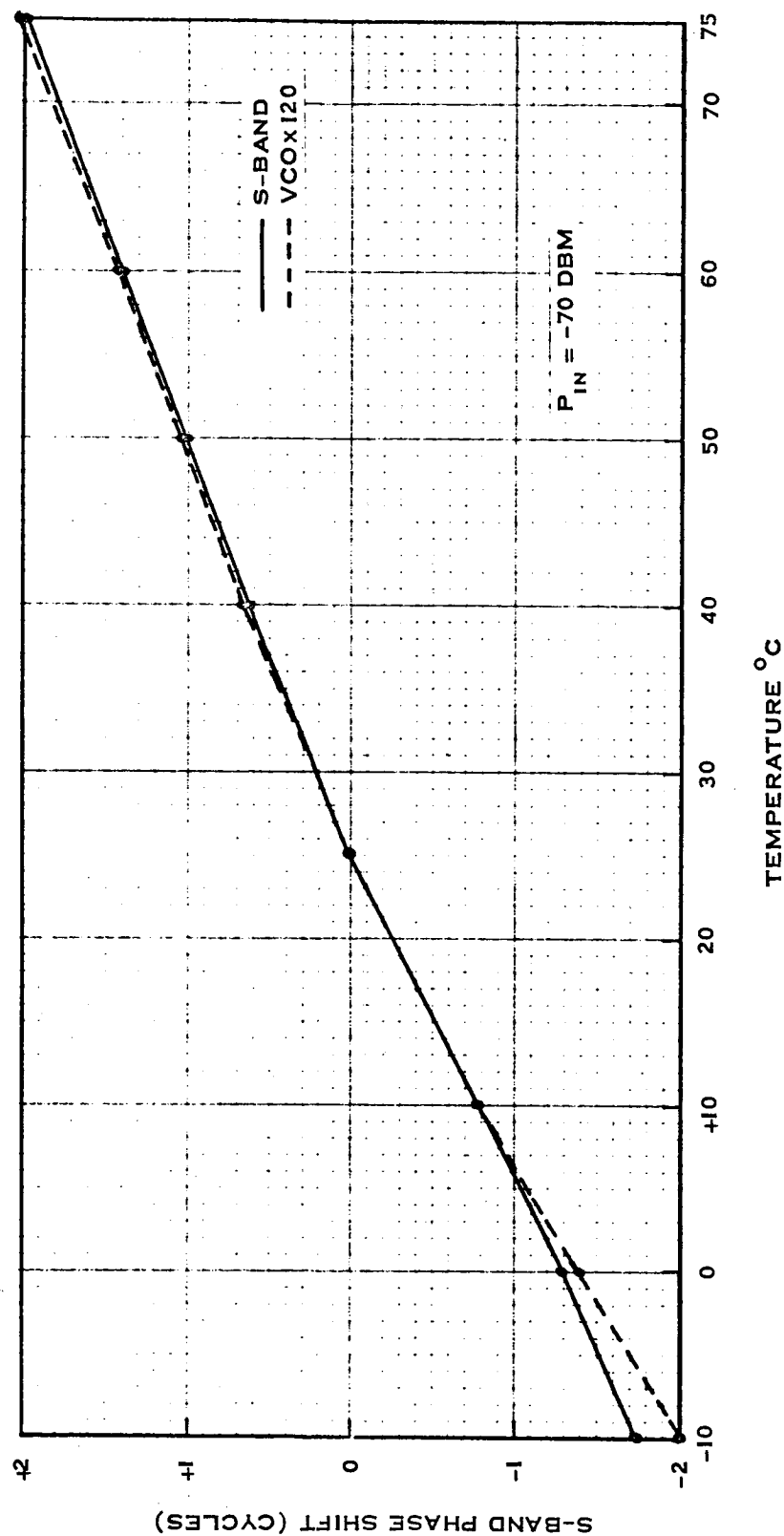


Figure 3.1.2-1 S-Band Phase Shift vs. Temperature of the Receiver, Six Pack No. 1, Only.
Included in It are the Following Modules:

- Preslector
- Mixer-Preamplifier
- 47.8 MHz IF
- 9.56 MHz IF
- X36 Multiplier.

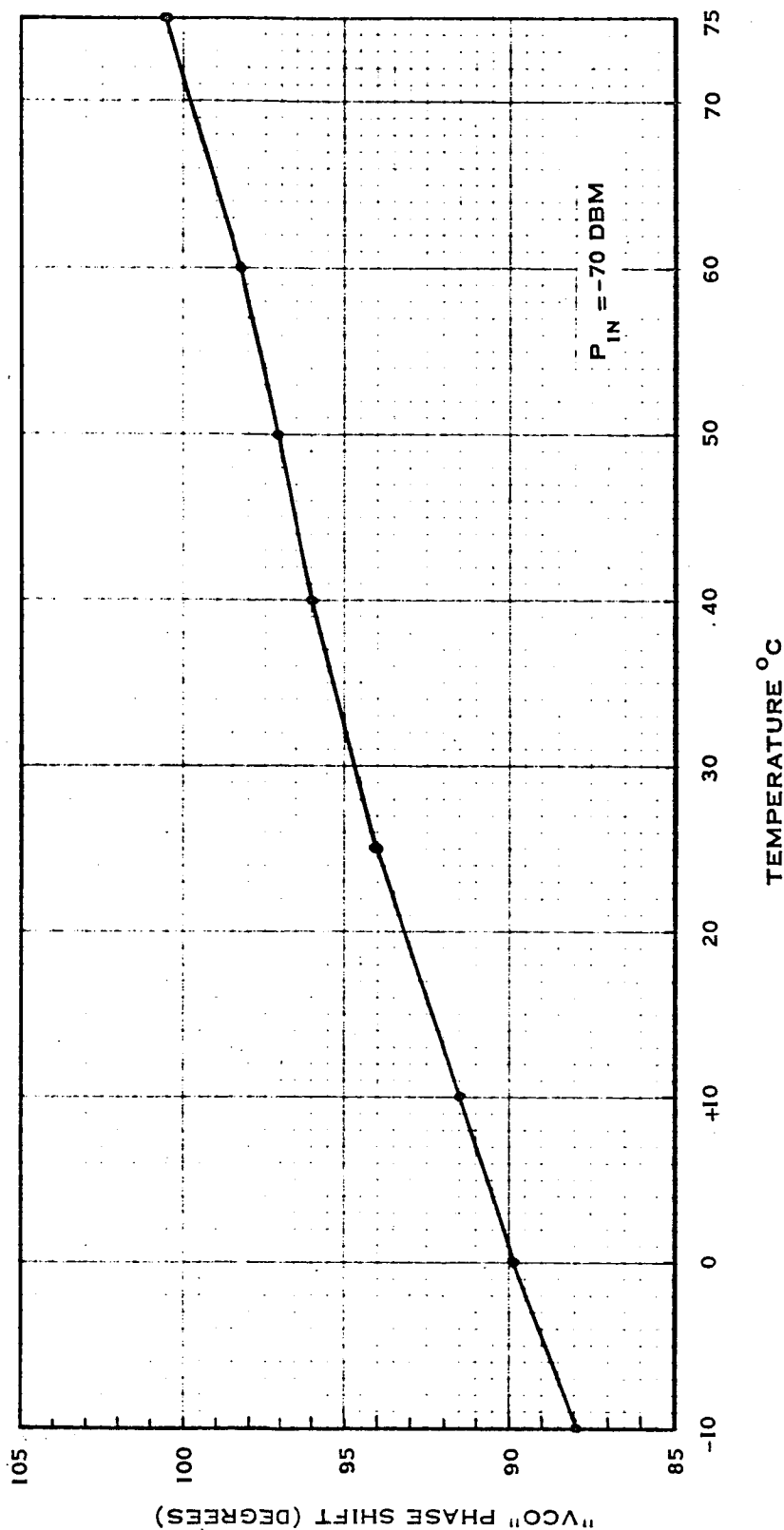


Figure 3.1.2-2 "VCO" Phase Shift vs Temperature of the Receiver, Six Pack No. 1, Only.
Included in It are the Following Modules:

- Preslector
- Mixer-Preamplifier
- 47.8 MHz IF
- 9.56 MHz IF
- X36 Multiplier.

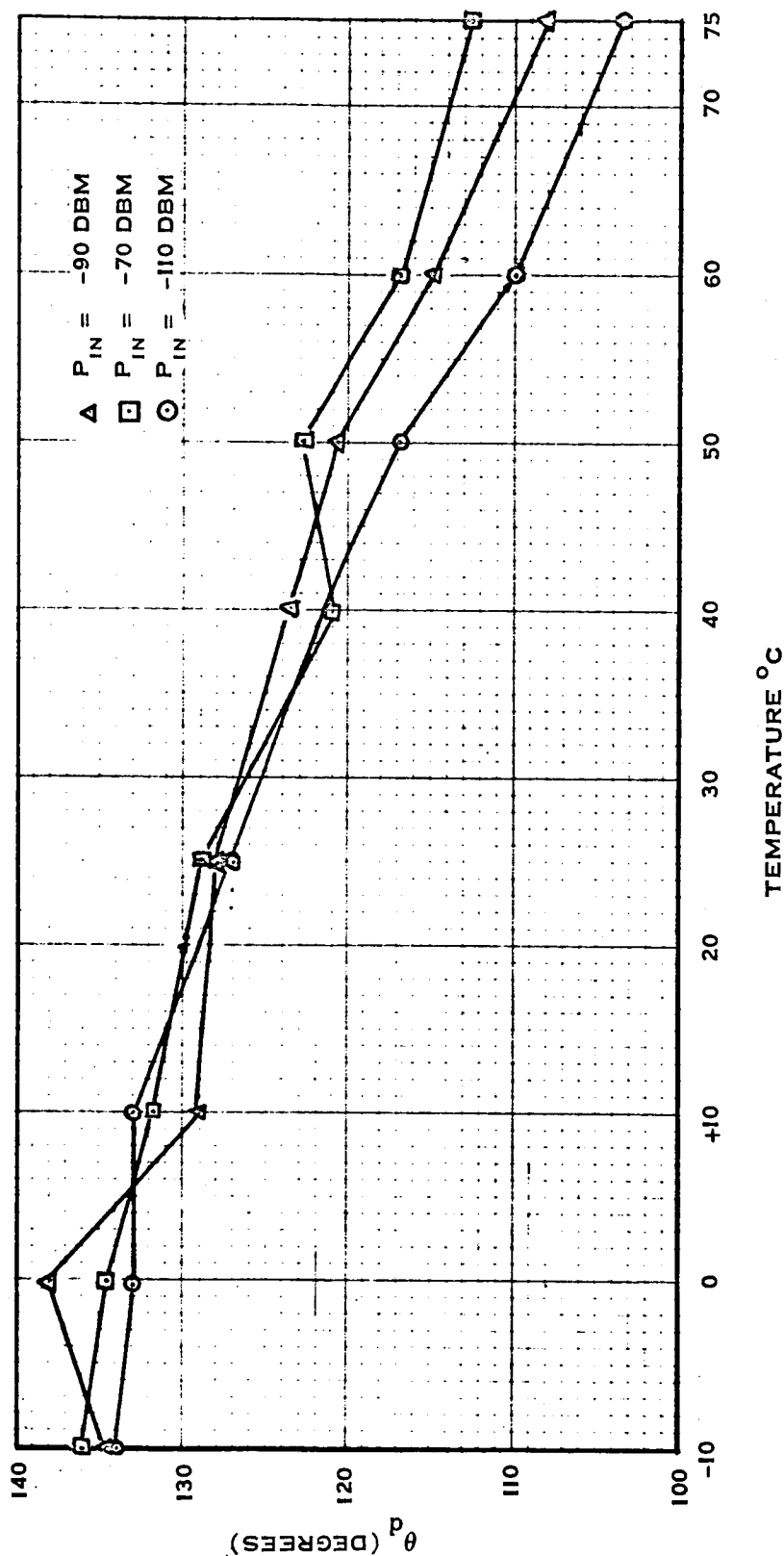


Figure 3.1.2-3 Ranging Delay vs. Temperature of the Receiver, Six Pack No. 1, Only.
Included in It are the Following Modules:

- Preselector
- Mixer-Preamplifier
- 47.8 MHz IF
- 9.56 MHz IF
- X36 Multiplier.

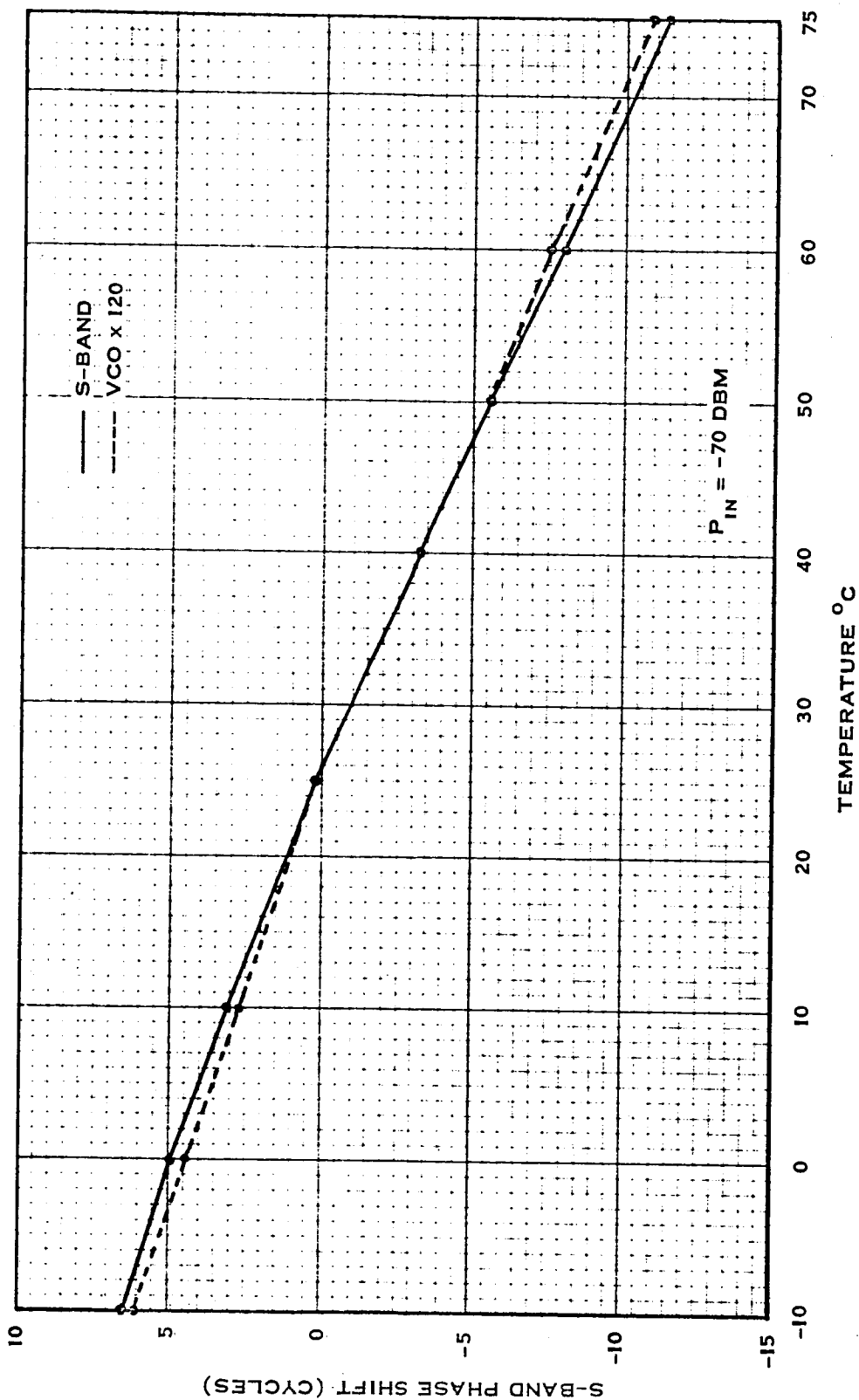


Figure 3.1.2-4 S-Band Phase Shift vs. Temperature of the Receiver, Six Pack No. 2, Only.
Included in It are the Following Modules:

- AGC Detector
- Phase Detector
- VCO
- Frequency Divider
- Isolation Amplifier
- Video Amplifier.

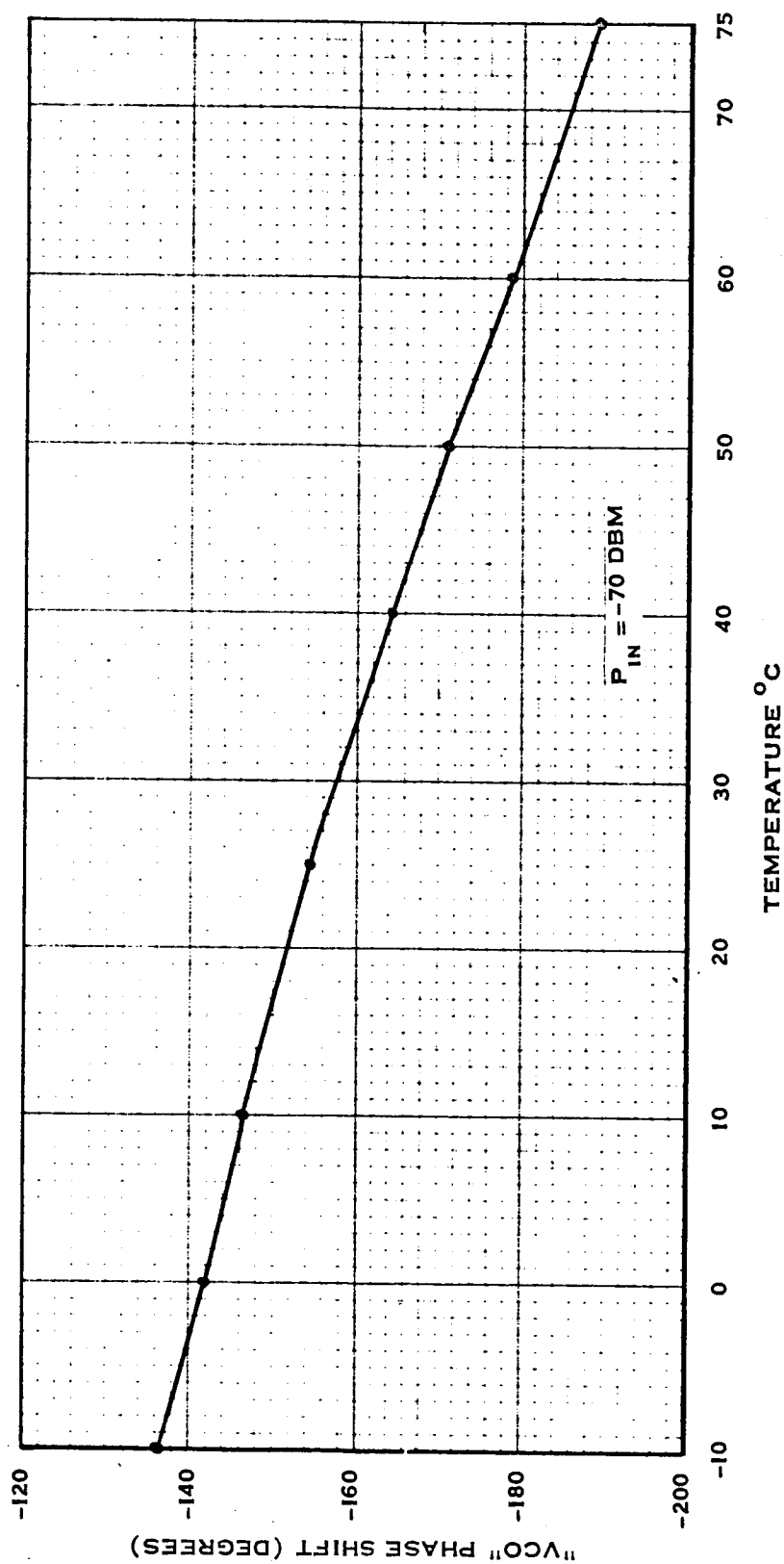


Figure 3.1.2-5 "VCO" Phase Shift vs. Temperature of the Receiver, Six Pack No. 2, Only.
Included in it are the Following Modules:

- AGC Detector
- Phase Detector
- VCO
- Frequency Divider
- Isolation Amplifier
- Video Amplifier.

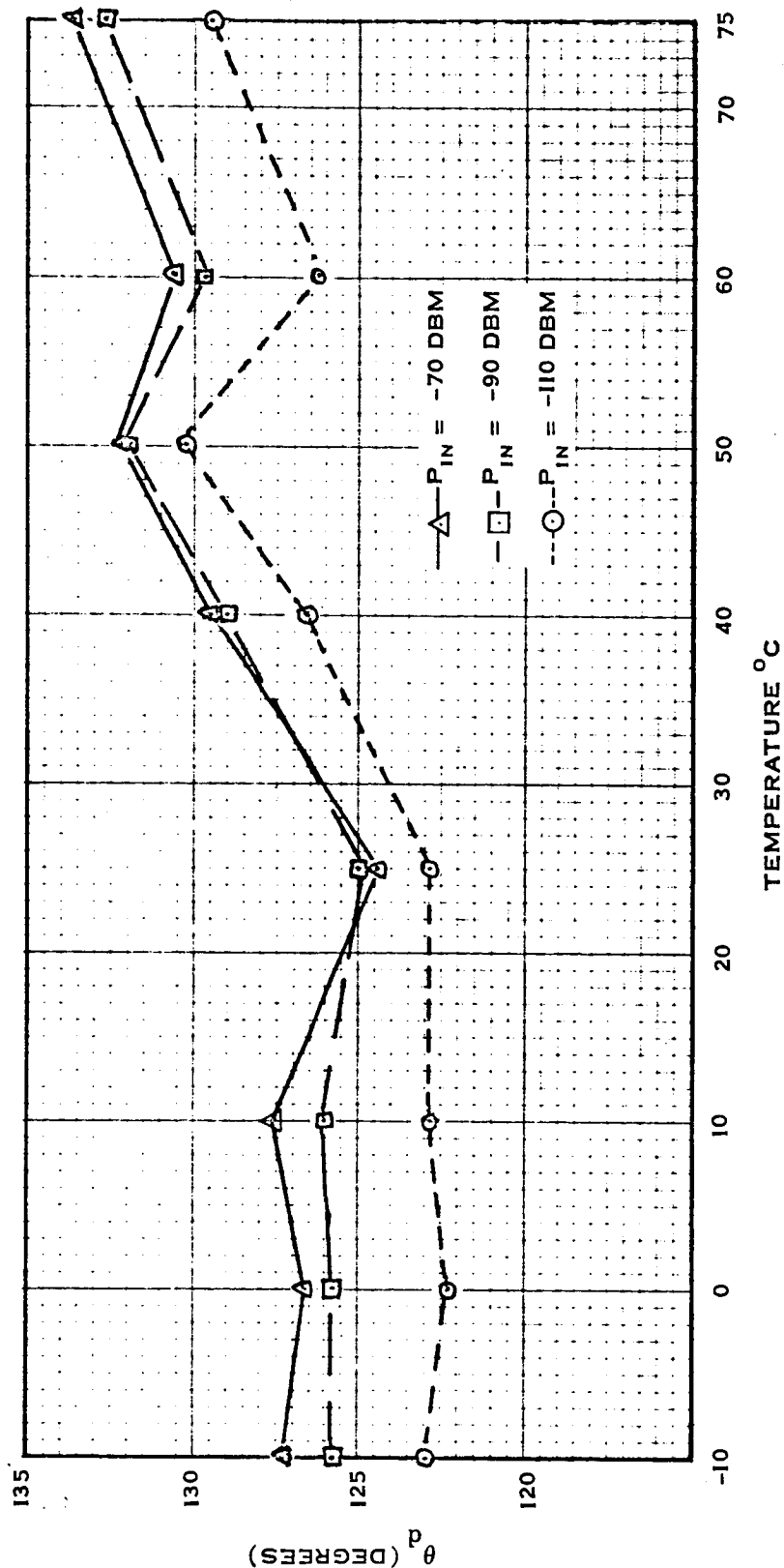


Figure 3.1.2-6 Ranging Delay vs. Temperature of the Receiver, Six Pack No. 2, Only.
Included in It are the Following Modules:

- AGC Detector
- Phase Detector
- VCO
- Frequency Divider
- Isolation Amplifier
- Video Amplifier.

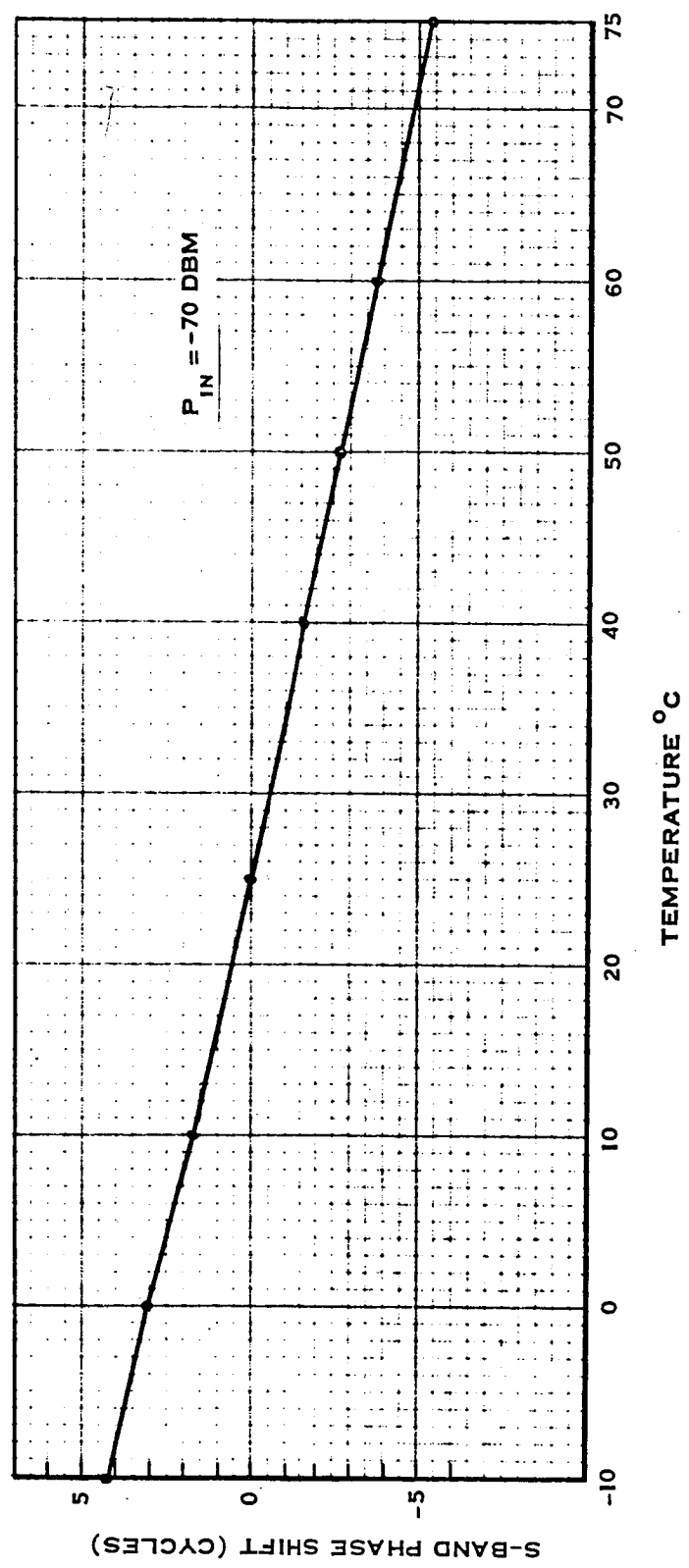


Figure 3.1.2-7 S-Band Phase Shift vs. Temperature of the Exciter Six Pack.
Included in it are the Following Modules:

- Auxiliary Oscillator
- X30 Multiplier.

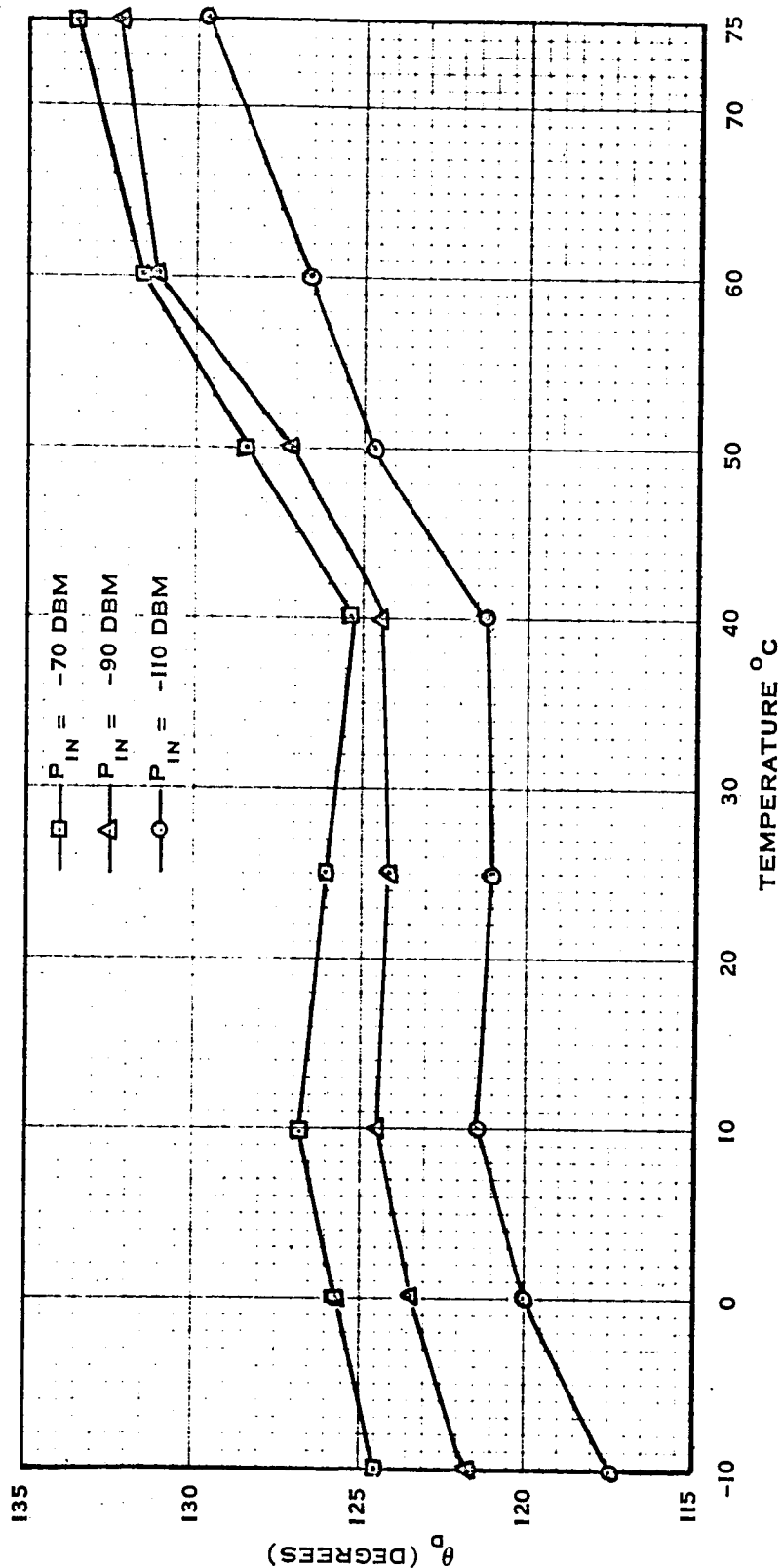


Figure 3.1.2-8 Ranging Delay vs. Temperature of the Exciter Six Pack .
Included in It are the Following Modules:

- Auxiliary Oscillator
- X30 Multiplier.

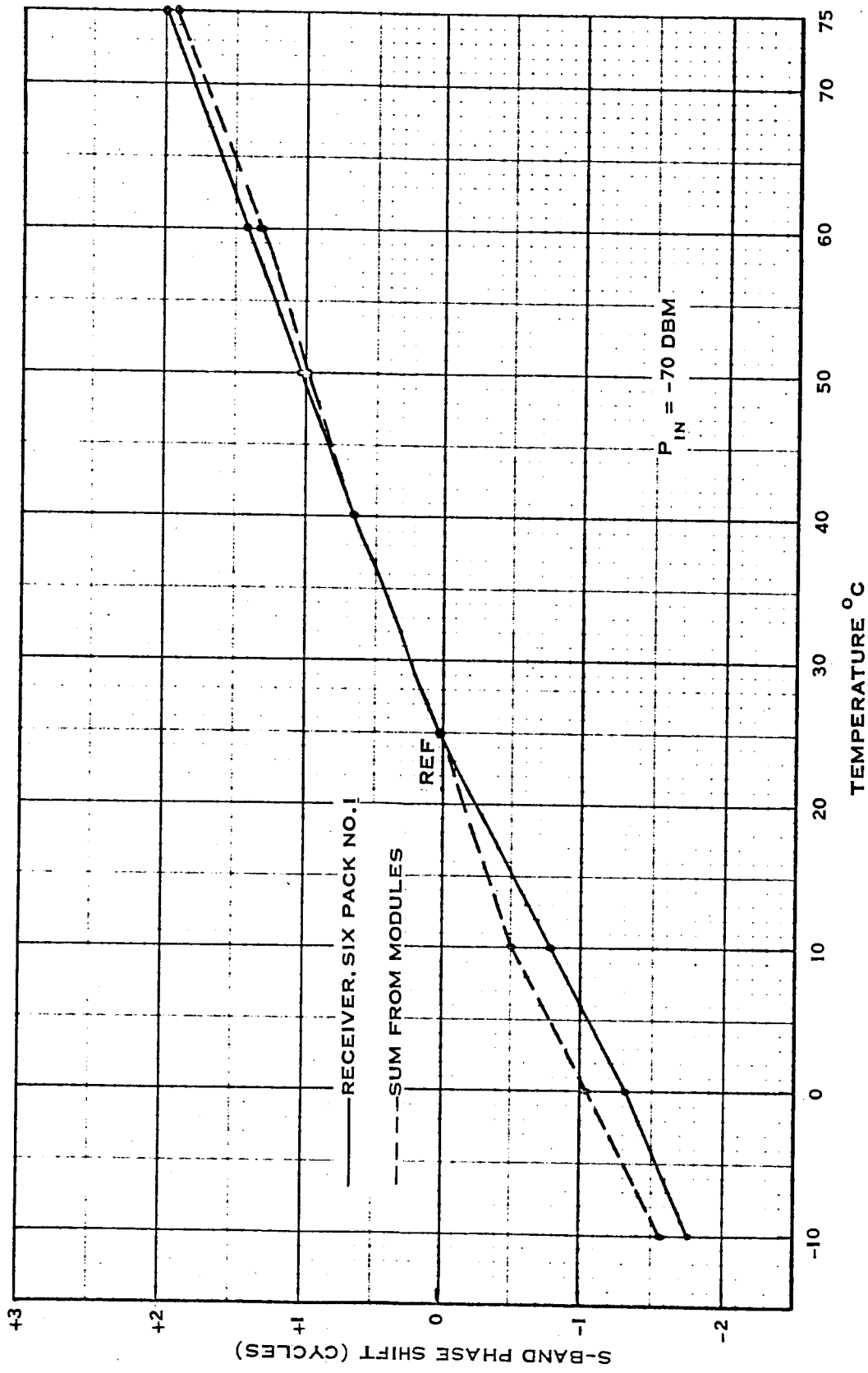


Figure 3.1.2-9 Comparison of S-Band Phase Shift vs Temperature Between the Receiver, Six Pack No. 1, and the Sum of the Phase Shift from its Modules.

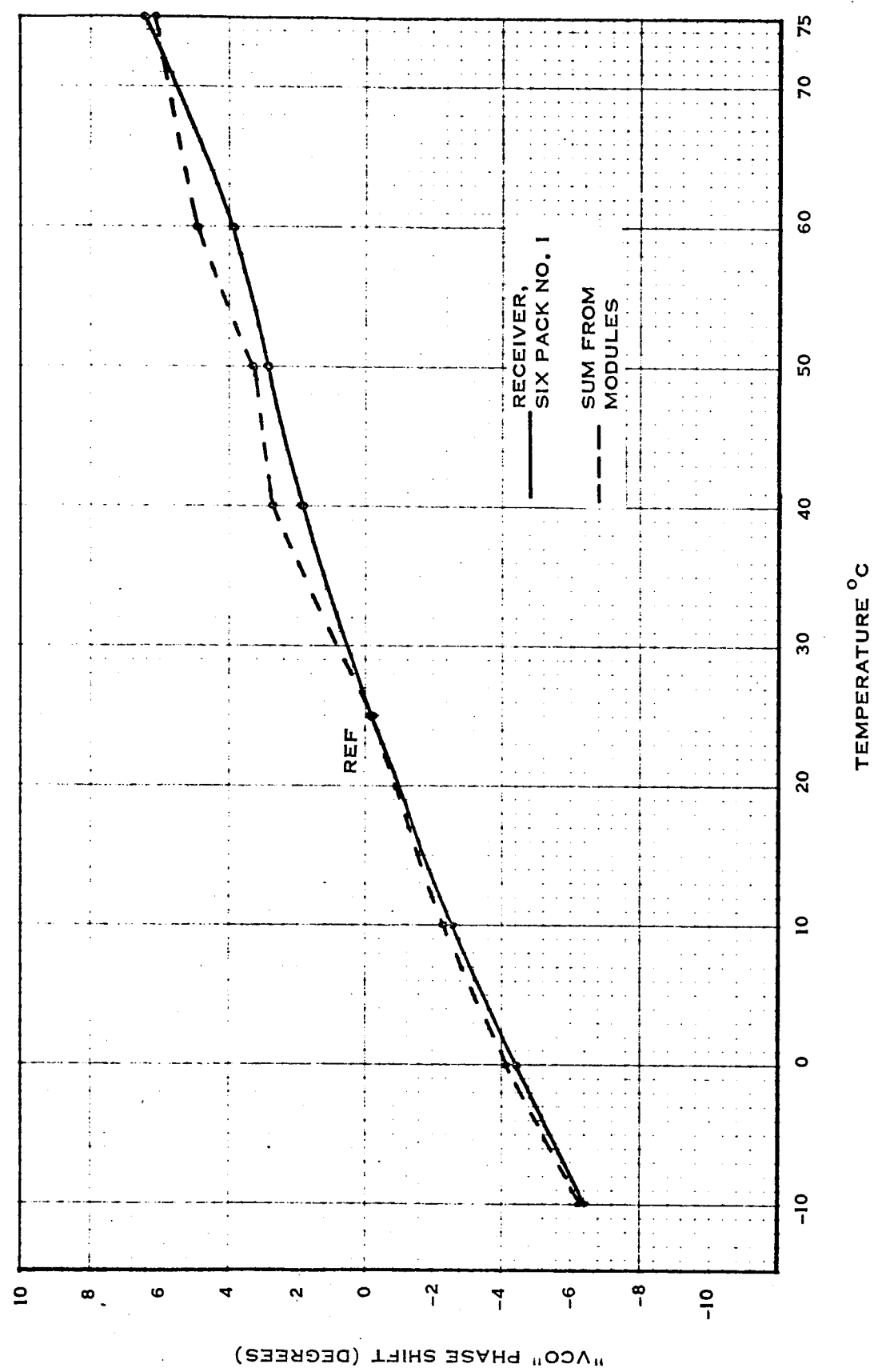


Figure 3.1.2-10 Comparison of "VCO" Phase Shift vs. Temperature Between the Receiver, Six Pack No. 1, and the Sum of the Phase Shift from its Modules.

$P_{in} = -70 \text{ DBM}$

40

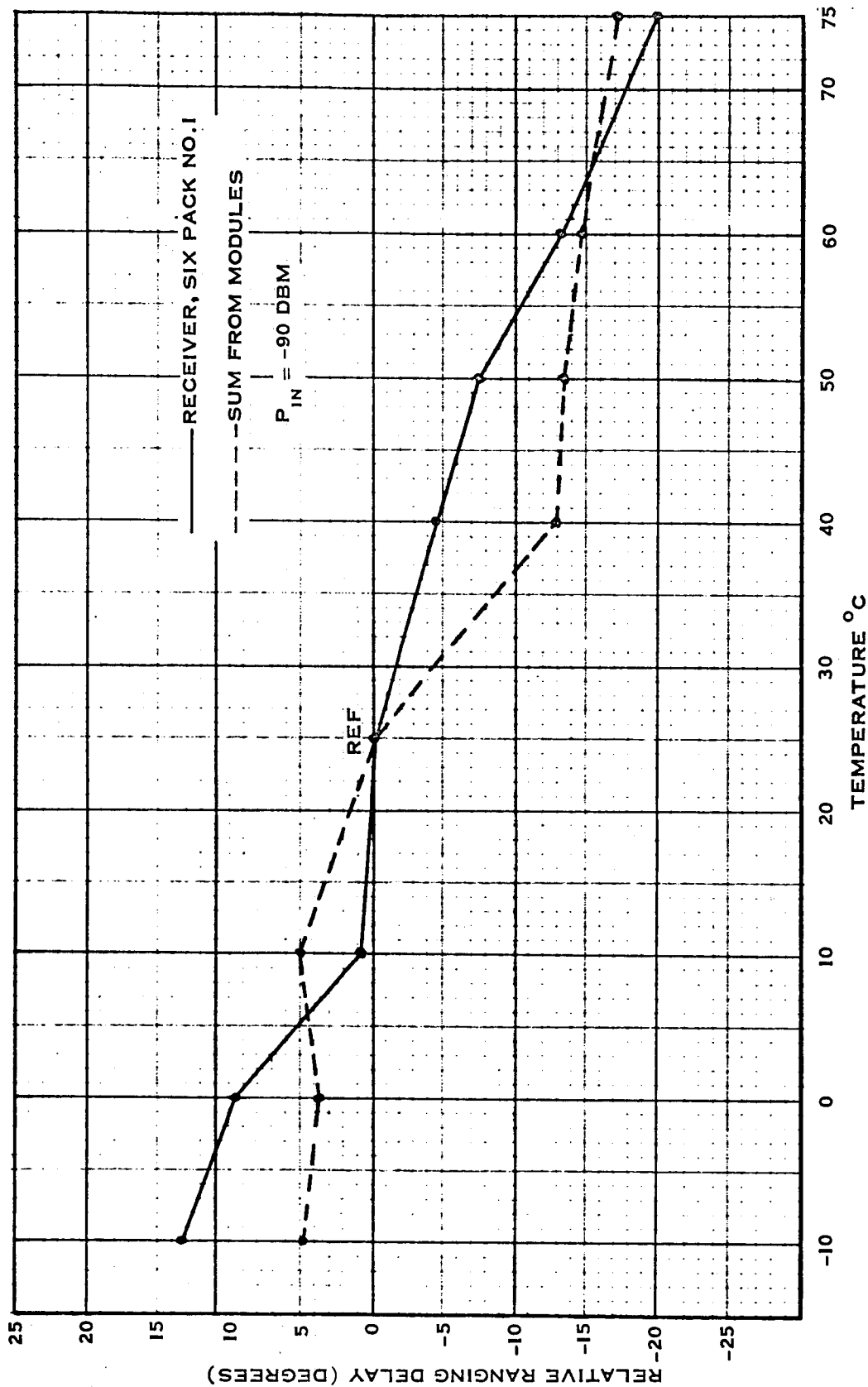


Figure 3.1.2-11 Comparison of Relative Ranging Delay vs. Temperature Between the Receiver, Six Pack No. 1, and the Sum of the Delay from its Modules.

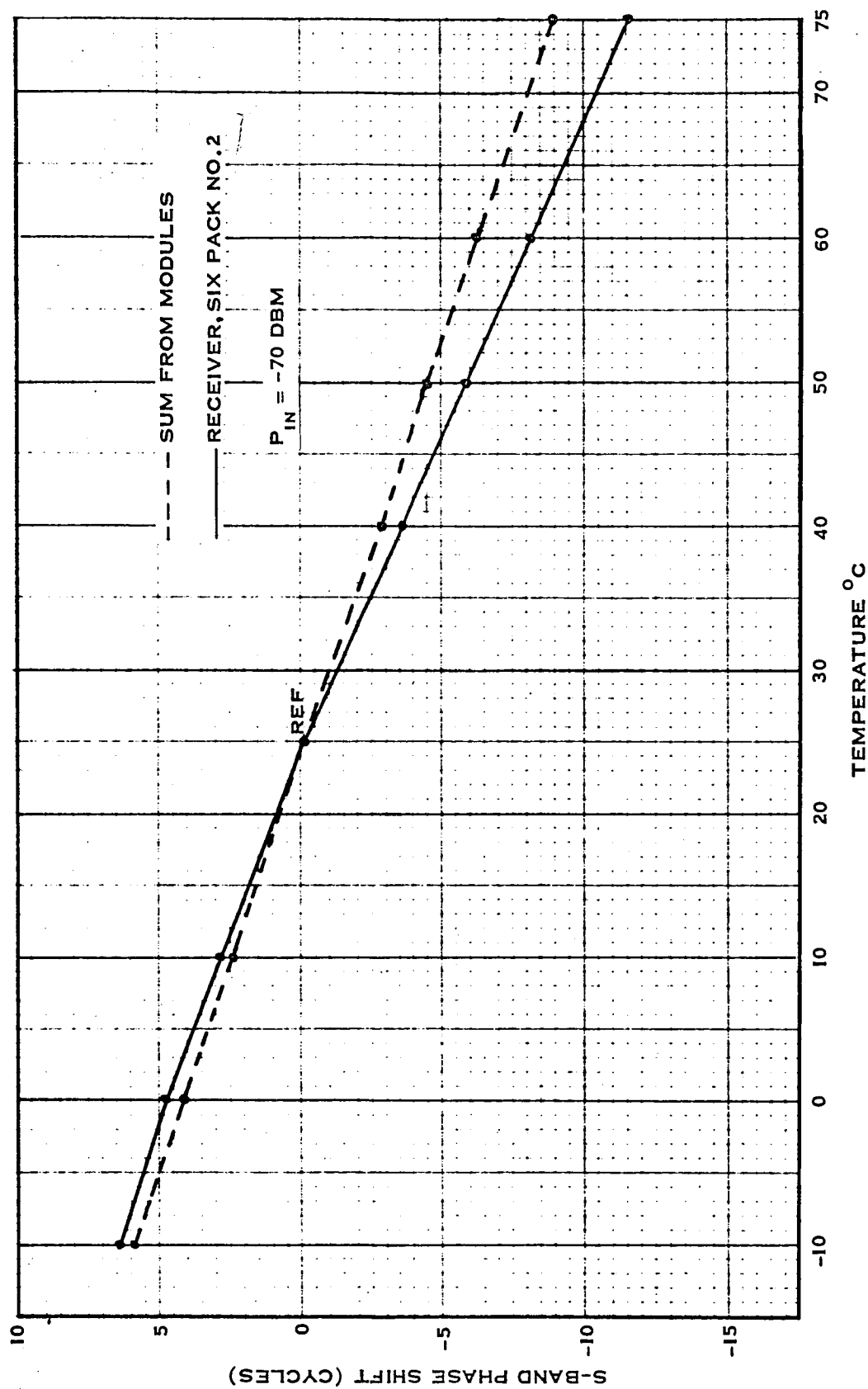


Figure 3.1.2-12 Comparison of S-Band Phase Shift vs. Temperature Between the Receiver, Six Pack No. 2, and the Sum of the Phase Shift from its Modules.

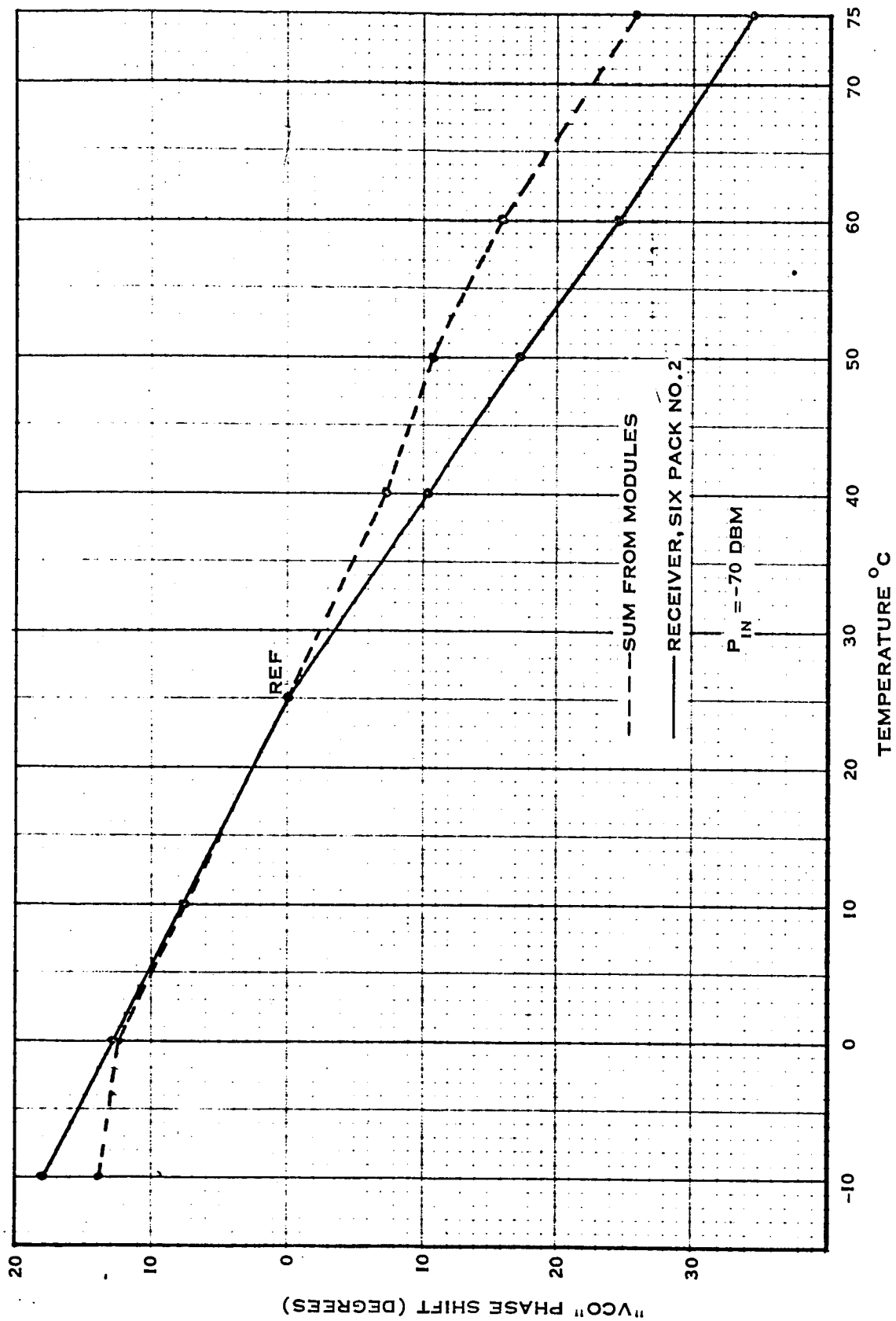


Figure 3.1.2-13 Comparison of "VCO" Phase Shift vs. Temperature Between the Receiver, Six Pack No. 2, and the Sum of the Phase Shift from its Modules.

43

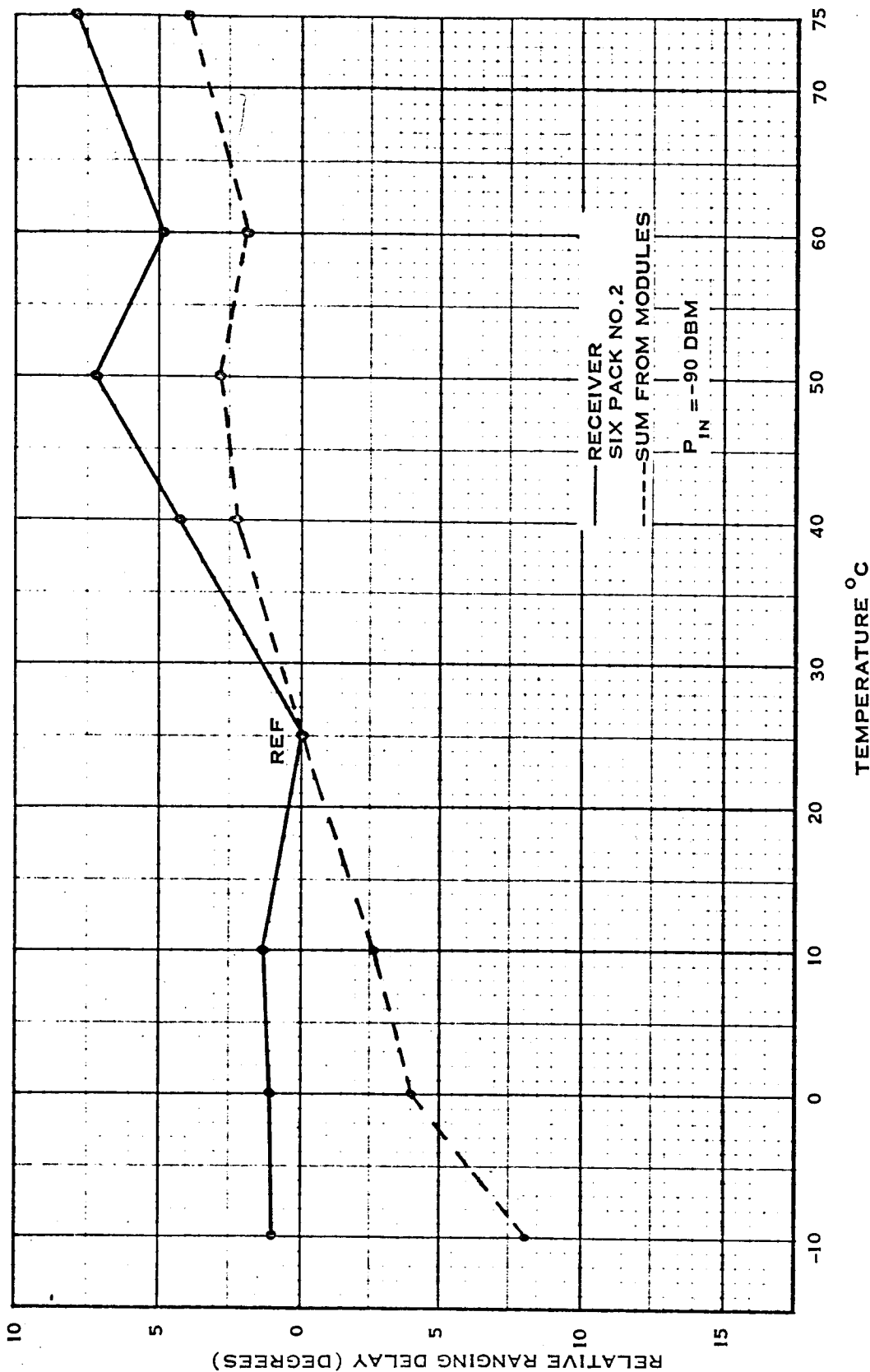


Figure 3.1.2-14 Comparison of Relative Ranging Delay vs Temperature between the Receiver, Six Pack No. 2, and the Sum of the Delay from its Modules.

44

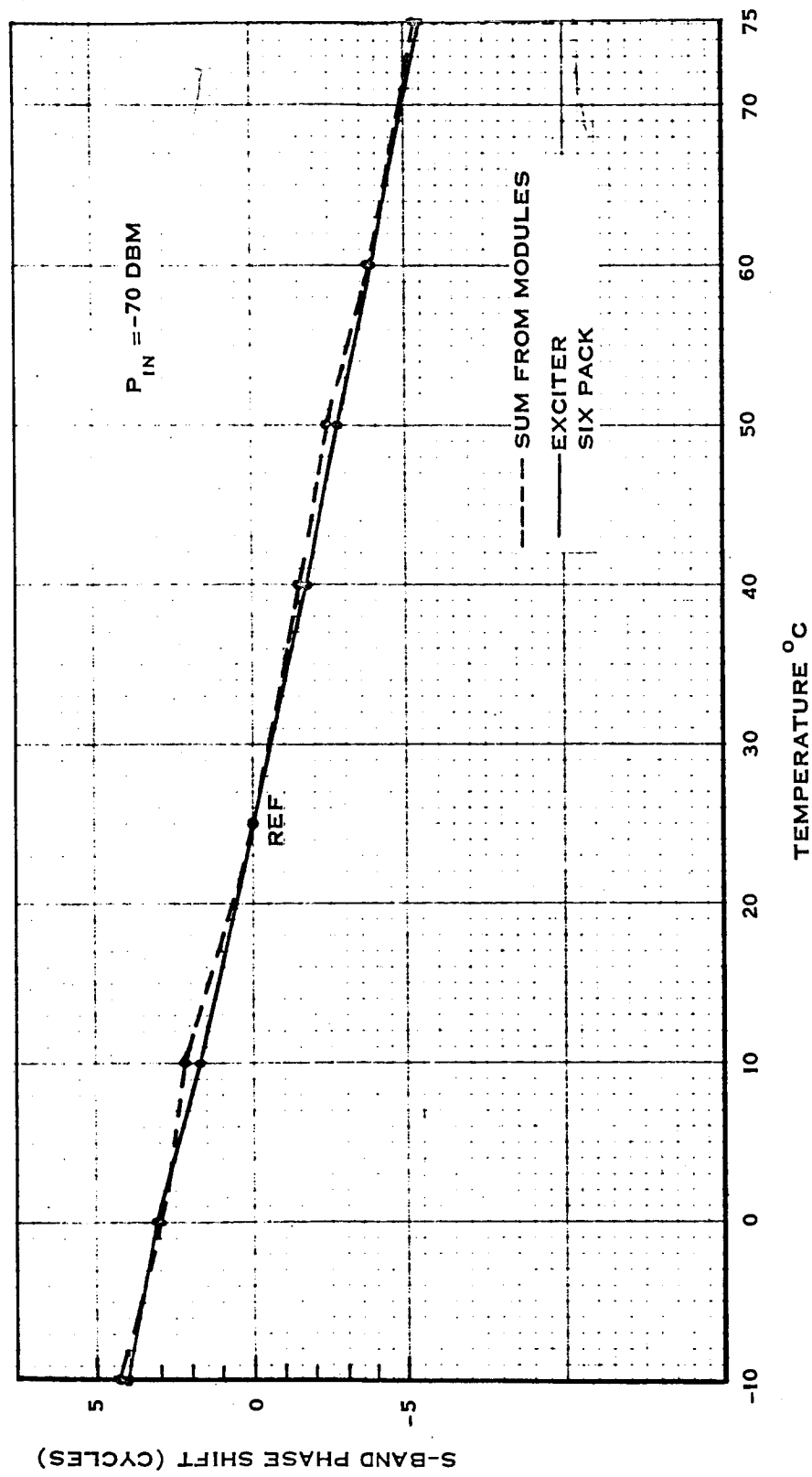


Figure 3.1.2-15 Comparison of S-Band Phase Shift vs. Temperature Between the Exciter Six Pack and the Sum of the Phase Shift From its Modules.

45

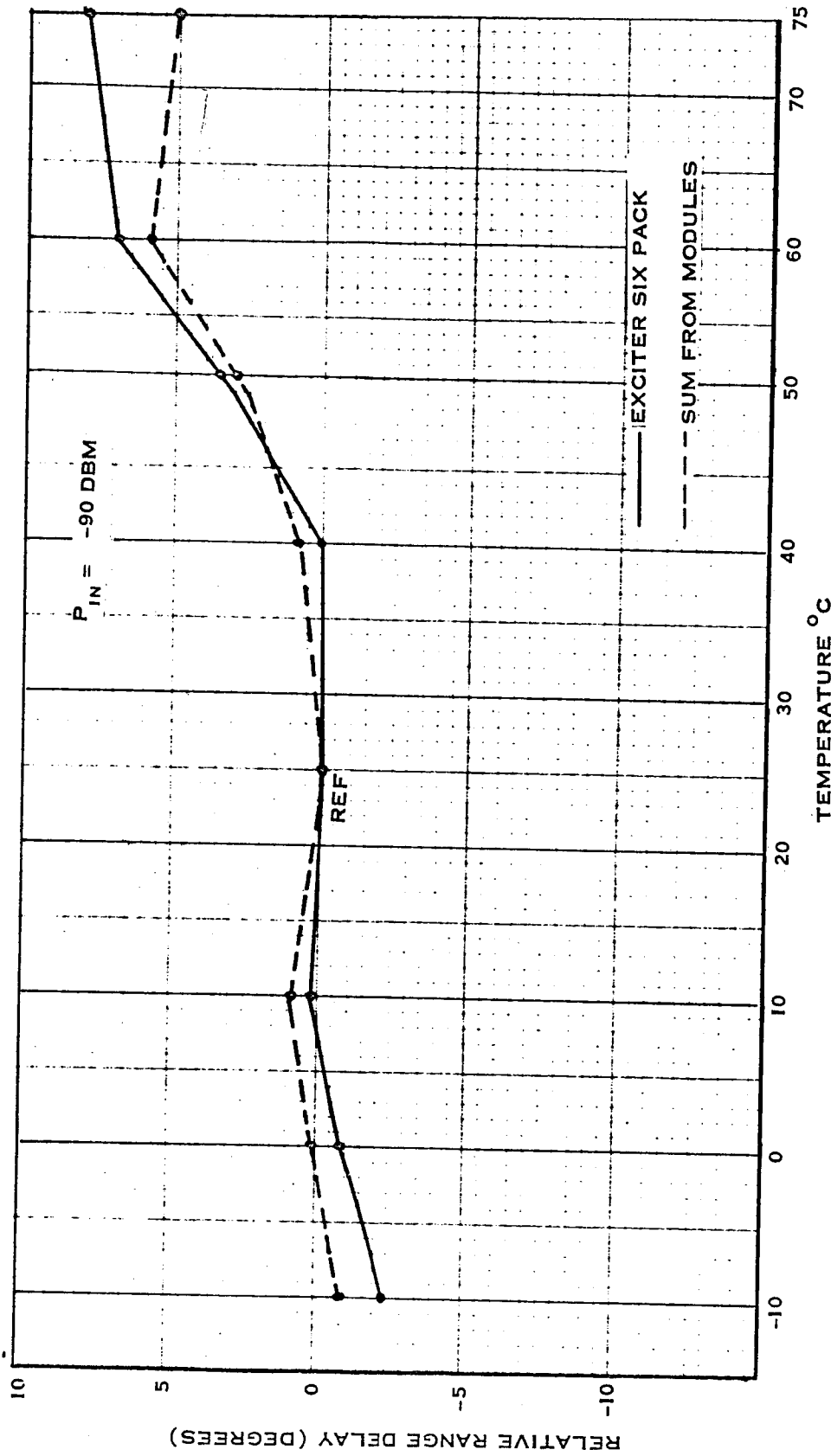


Figure 3.1.2-16 Comparison of Relative Ranging Delay Vs Temperature Between the Exciter Six Pack And the Delay From its Modules.

two six packs. However, its contribution to phase shift is small, only +4.55 cycles total, compared with the contribution of the other six packs, -17.78 cycles for the Receiver, Six Pack No. 2 and -9.48 cycles for the Exciter Six Pack.

Figures 3.1.2-2 and 3.1.2-5 show the VCO phase shift as a function of the receiver temperature. The total deviation indicated in these graphs will equal the S-Band phase shift for the respective six pack when multiplied by $120/360^\circ$. This is natural since the VCO phase shift represents which portion of the S-Band phase shift was caused by the receiver, and the receiver was the only portion undergoing temperature test at this time. There is no VCO phase shift for the Exciter Six Pack because the receiver didn't contribute any of the S-Band phase shift at that time.

Figures 3.1.2-9 through 3.1.2-16 show comparisons between data measured, while individual six packs were in the oven and the sum of the data measured while the respective six pack's modules were in the oven. The sum of the data from the modules correlates fairly well with the data from the six packs. The variations are believed to be due mainly to interaction effects between modules when the individual six packs were being tested.

Again, each time the temperature of the test environment was changed, stabilization was essentially complete in thirty minutes and a minimum of an hour was allowed.

3.1.3 Modules Evaluation Tests

The graphs in this section are presented in a similar manner to those in the previous section, that is the S-Band phase variation first, the VCO phase variation next, and then the ranging delay variation. The main difference is that a separate set of graphs was not made for each module. Rather, the modules were grouped for convenience and comparison between modules. The order of presentation then is a set of S-Band, VCO, and

ranging comparison graphs of the modules for each of the three six packs.

Figures 3.1.3-1, 3.1.3-4, and 3.1.3-7 show the S-Band phase variation associated with the temperature change of each module of the transponder. The X36 Multiplier is responsible for nearly all of the S-Band shift of the Receiver, Six Pack No. 1, except the X36 Multiplier will appear at S-Band in the ratio of 240/221. Phase shifts originating in the X36 Multiplier will appear at S-Band in the ratio of from 240/221 to (36) (240/221) depending on where in that module the phase shift occurs. (See Appendix V and Figure A.5-1). Note that the phase shift caused by the X36 Multiplier is opposite in slope to that of the entire transponder. This agrees with the data taken for the Receiver, Six Pack No. 1 (Figure 3.1.2-1).

The VCO Module caused most of the S-Band phase shift for the entire transponder varying a total of 12.96 cycles. This is because phase shifts appearing at the output of the VCO Module are directly multiplied by 120 before appearing at S-Band. The contribution to S-Band phase shift caused by the Frequency Divider is believed to be due to input impedance changes effecting the phase at the output of the VCO Module. Again, these changes are multiplied directly by 120.

The two modules of the Exciter Six Pack contribute about equally to the S-Band phase shift. Phase shifts originating in these modules appear at S-Band in a ratio of from 1:1 to 120:1 depending on where in the modules the phase shift occurred.

The VCO phase shift for the modules of the receiver six packs (Figures 3.1.3-2 and 3.1.3-5) agree closely to the S-Band phase shift for those modules when multiplied by 120. The modules of the exciter didn't effect the receiver phase shift and so no graphs of VCO phase shift are in that group.

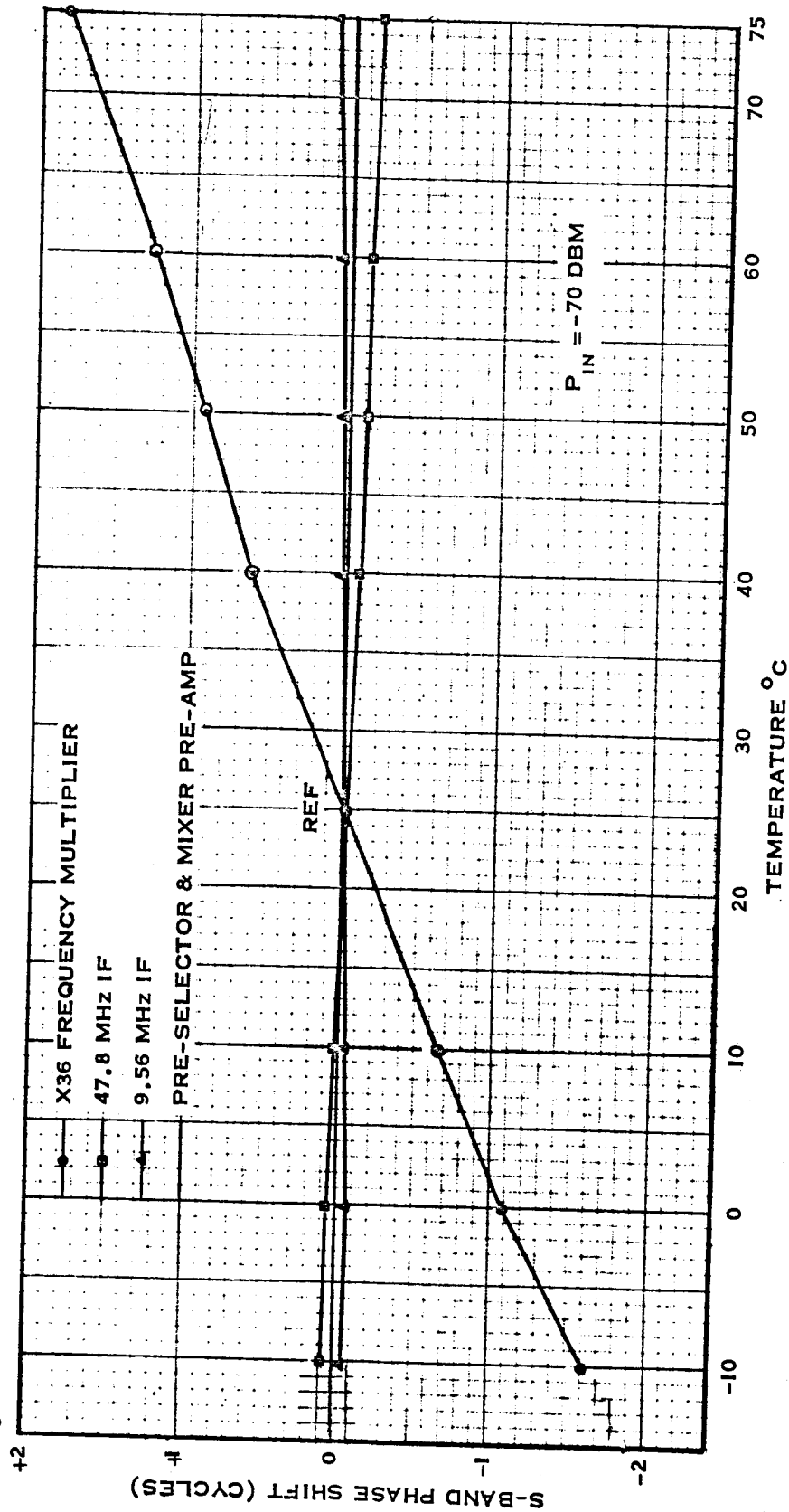


Figure 3.1.3-1 Comparison of S-Band Phase Shift Vs Temperature Between The Modules of The Receiver, Six Pack No. 1.

49

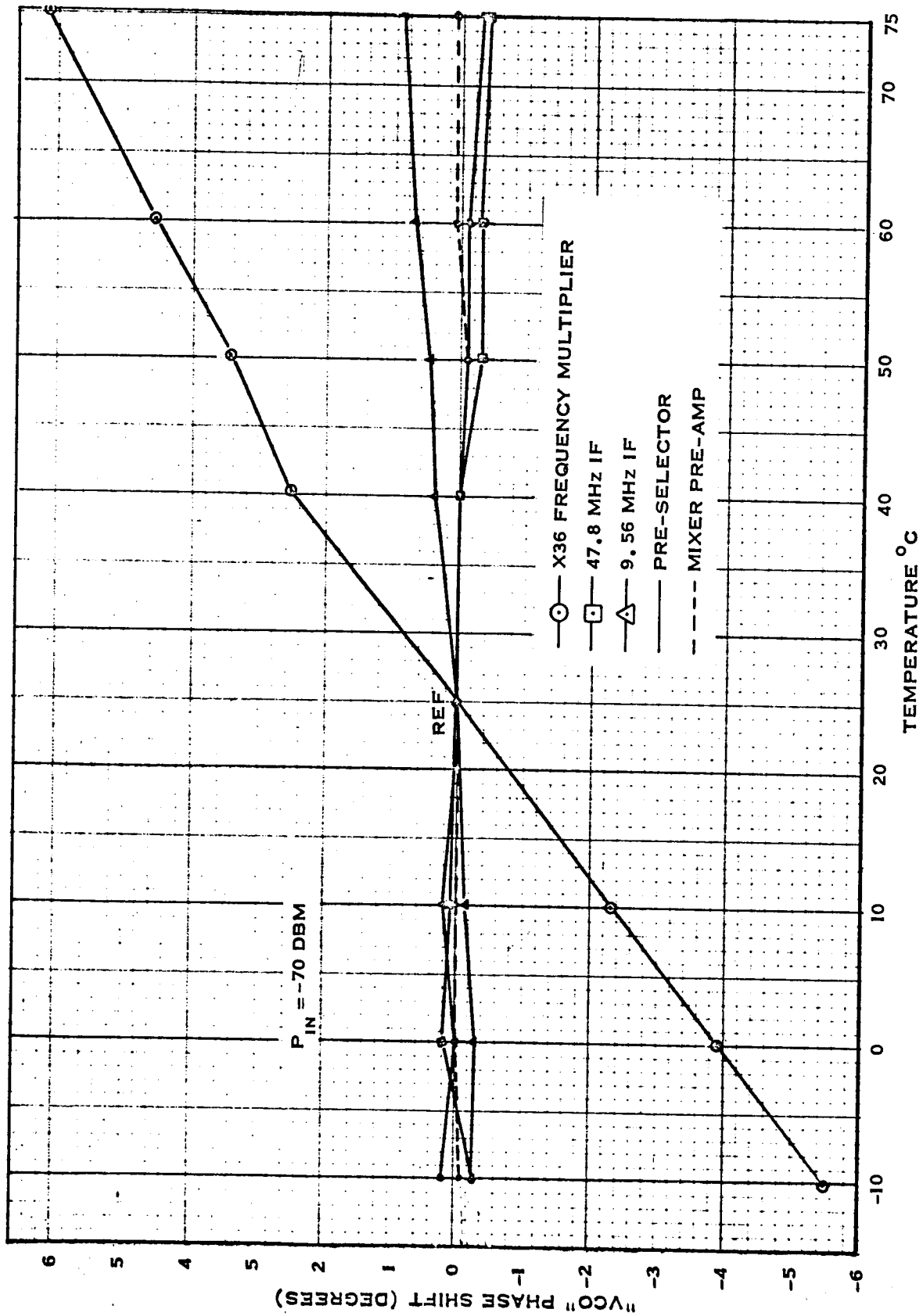


Figure 3.1.3-2 Comparison of "VCO" Phase Shift Vs Temperature Between the Modules of the Receiver, Six Pack No. 1.

50

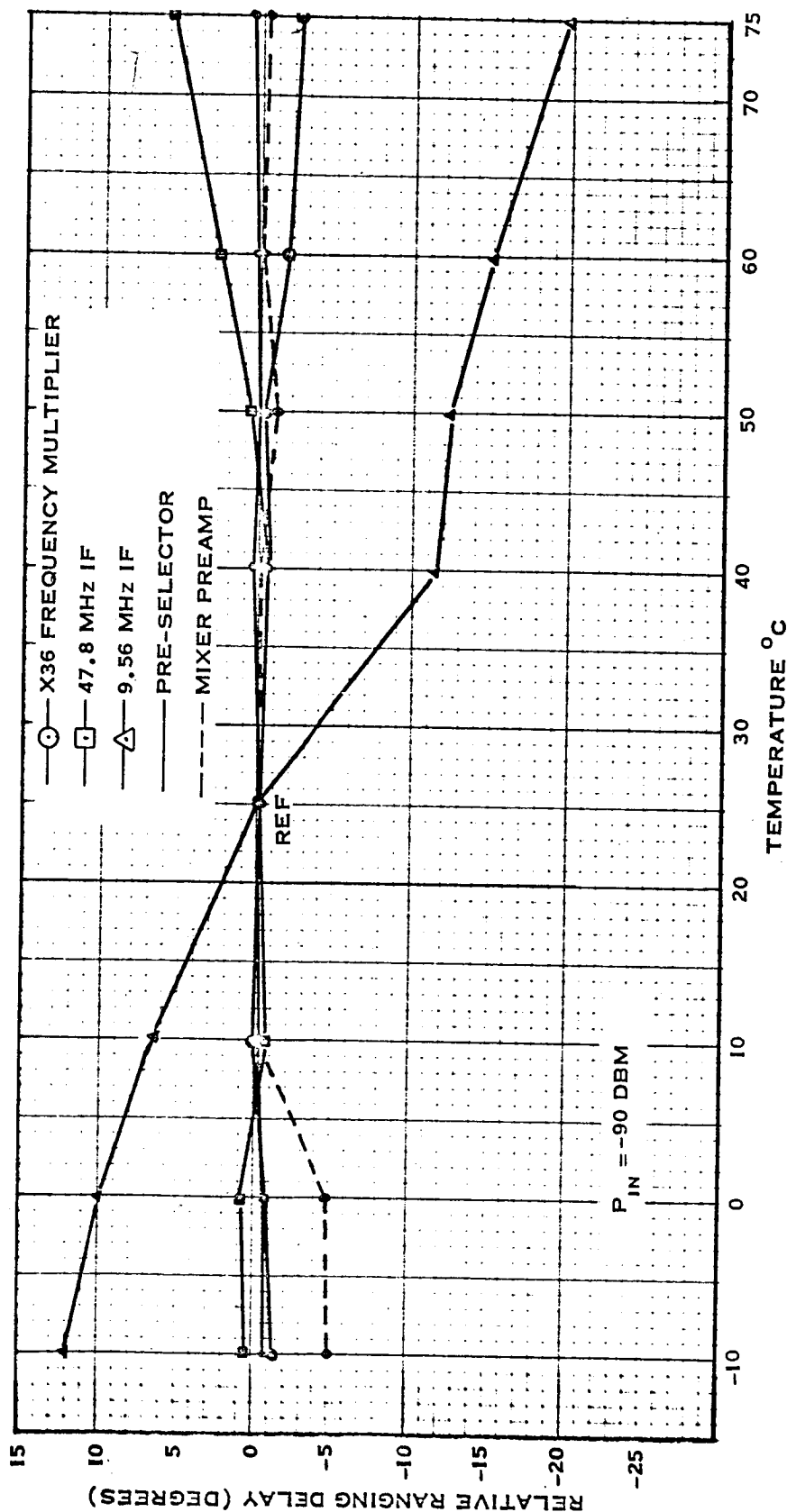


Figure 3.1.3-3 Comparison of Relative Ranging Delay Vs Temperature Between the Modules of the Receiver, Six Pack No. 1.

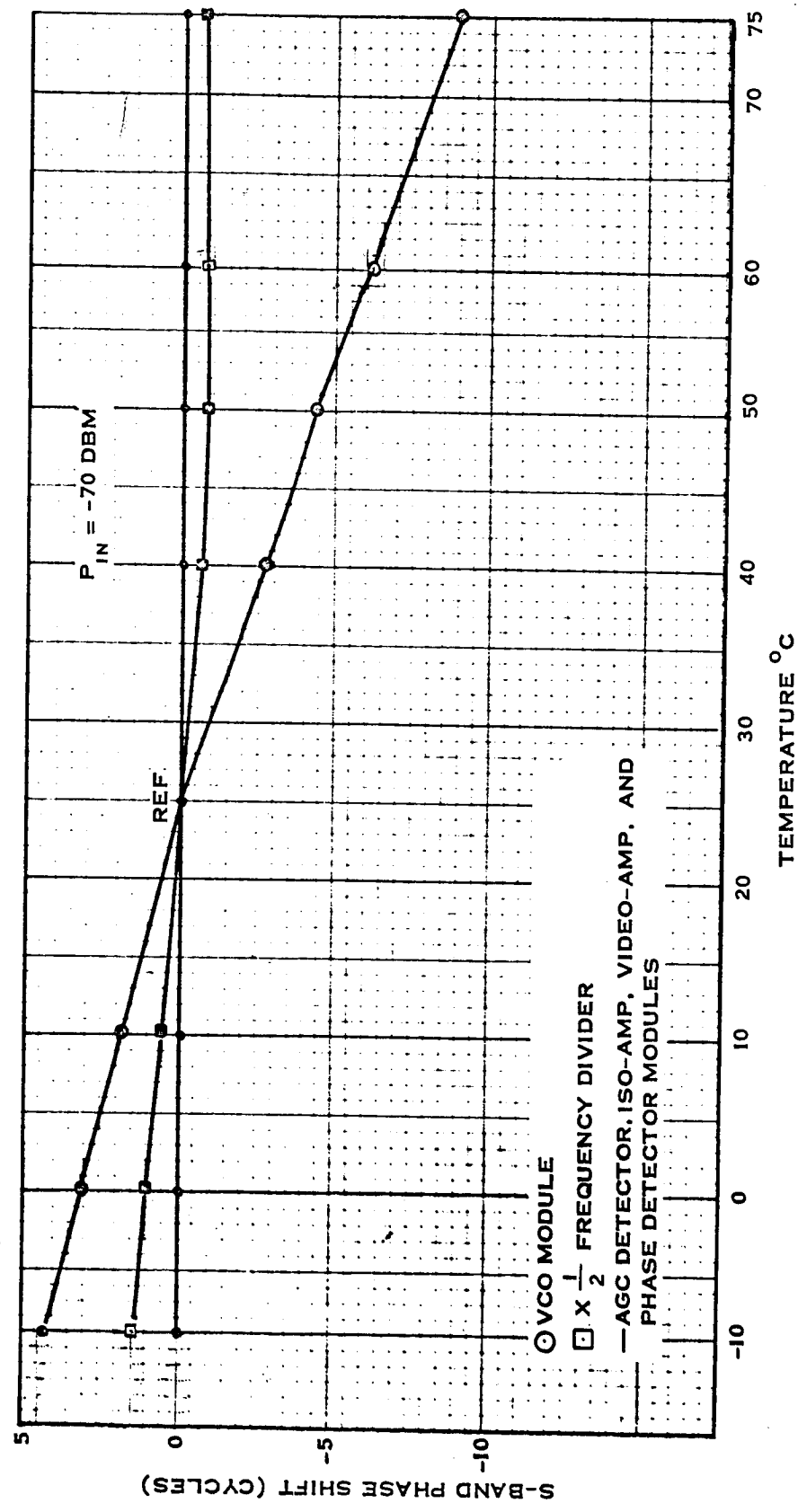


Figure 3.1.3-4 Comparison of S-Band Phase Shift Vs Temperature Between the Modules of the Receiver, Six Pack No. 2.

TR-DA1522A

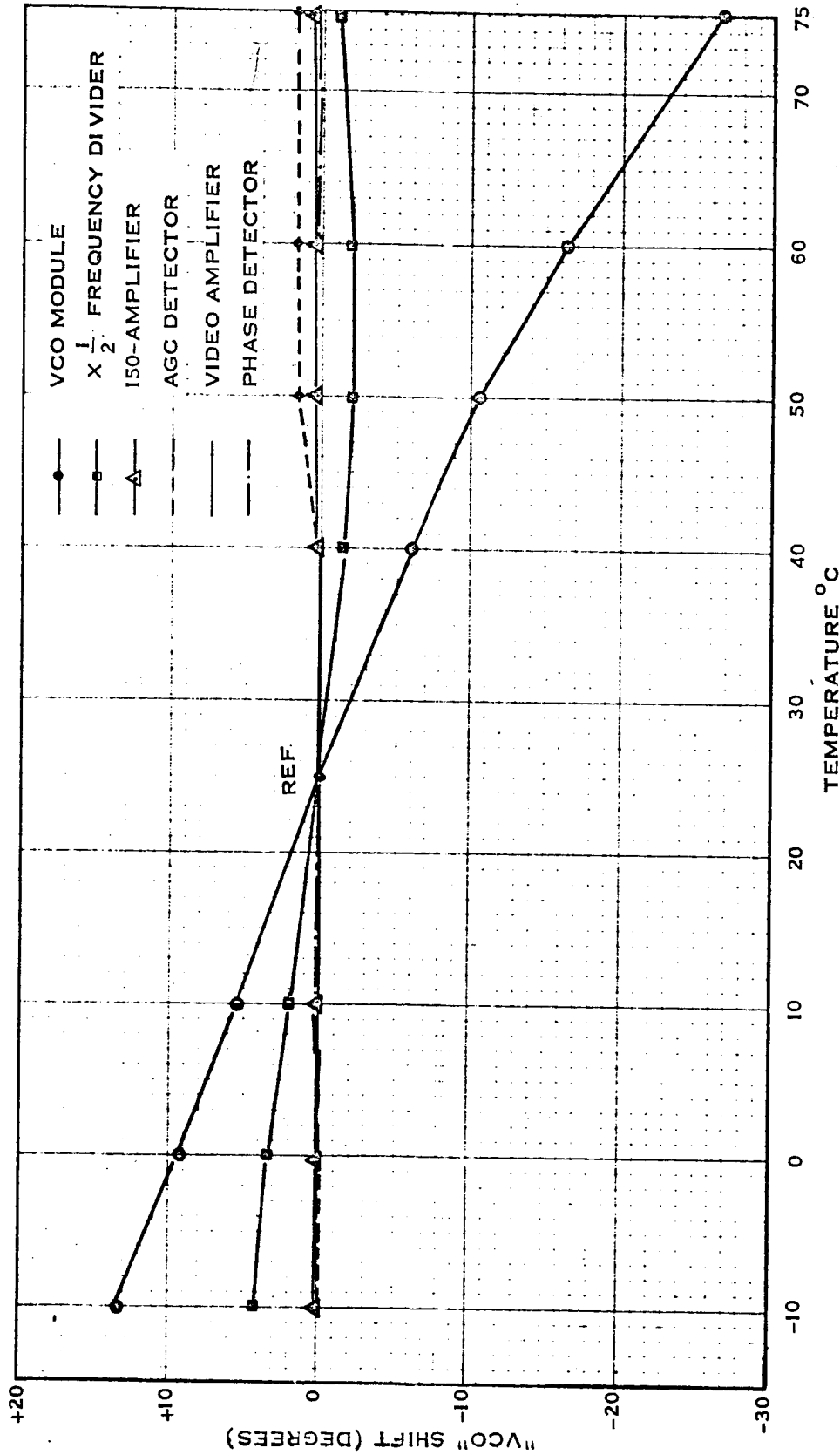


Figure 3.1.3-5 Comparison of "VCO" Phase Shift vs. Temperature between the Modules of the Receiver, Six Pack No. 2.

Comparing the ranging delay variation graphs (Figure 3.1.3-3, 3.1.3-6, and 3.1.3-8) with the S-Band phase shift graphs for these modules (Figures 3.1.3-1, 3.1.3-4, and 3.1.3-7) it can be seen that there was no smooth relationship between the way the S-band shifted with temperature and the way the ranging delay varied. Most of the delay variation for the transponder was caused by the 9.56 MHz I.F. Module, which isn't in the ranging loop. However, because of an unusual effect of the ranging phase detector, carrier shifts occurring in this module result in significant video phase shifts (see Section 4.1.2).

The Isolation Amplifier caused most of the ranging delay variation in the Receiver, Six Pack No. 2. This variation was due to the same effect as observed in the 9.56 MHz I.F. Amplifier. This effect is the result of a shift in phase between the signal and the reference at the ranging detector.

The contribution to ranging delay variation caused by the Frequency Divider is due to this same ranging detector effect. This indicates again that most of the ranging delay variation is caused by the unusual operating characteristics of the ranging phase detector.

The only module which apparently had a significant contribution due to group delay was the X30 Multiplier.

Figures 3.1.3-9 through 3.1.3-19 are S-Band phase and ranging delay graphs of specific module tests. They are presented to give a better view of the phase shift and delay variations caused by those modules which had significant effects. The S-Band graphs are usually shown on a larger scale than the combination graphs noted previously. The ranging delay graphs show the effect of R. F. power level changes into the transponder during the testing

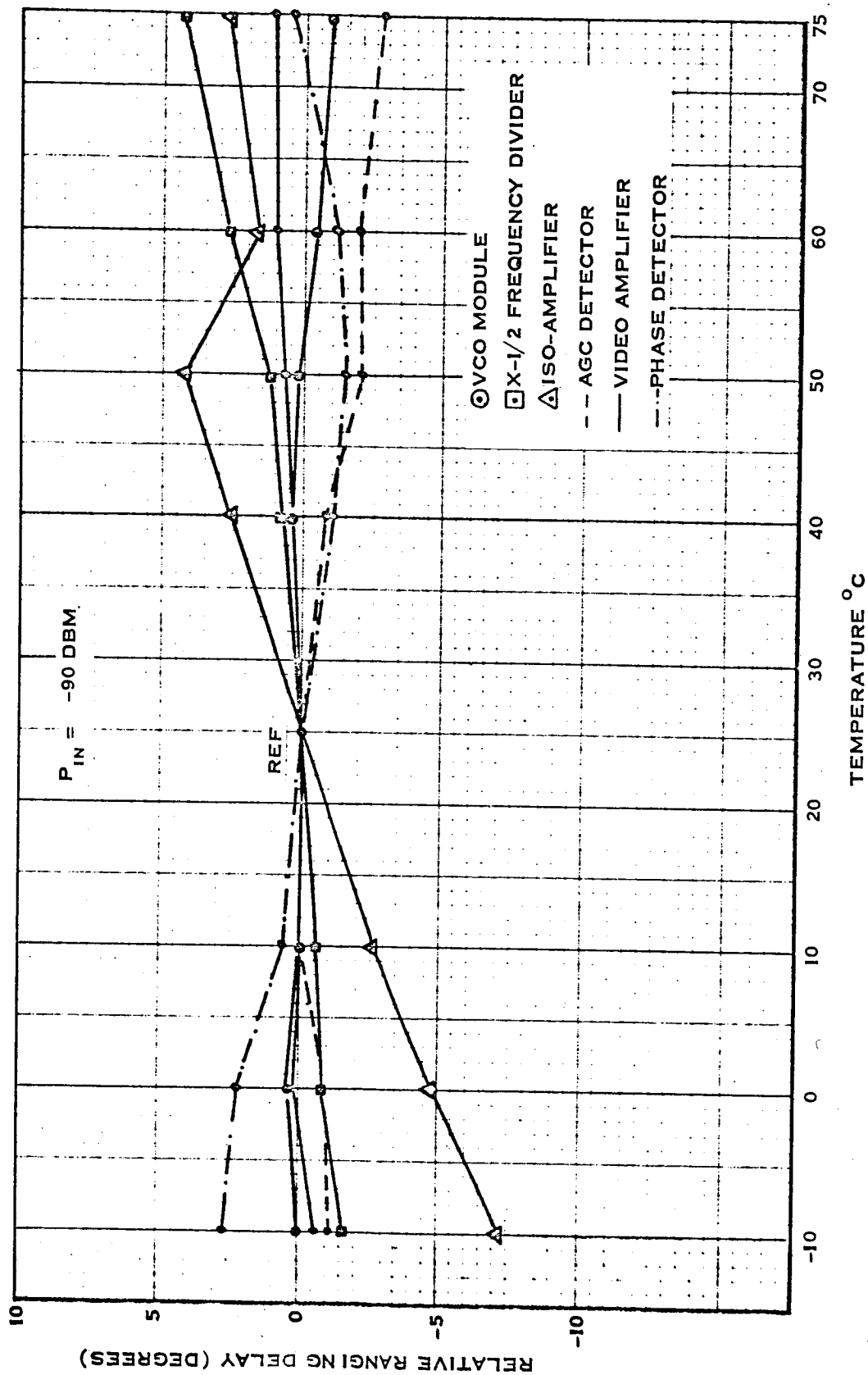


Figure 3.1.3-6 Comparison of Relative Ranging Delay Vs Temperature Between The Modules of the Receiver, Six Pack No. 2.

55

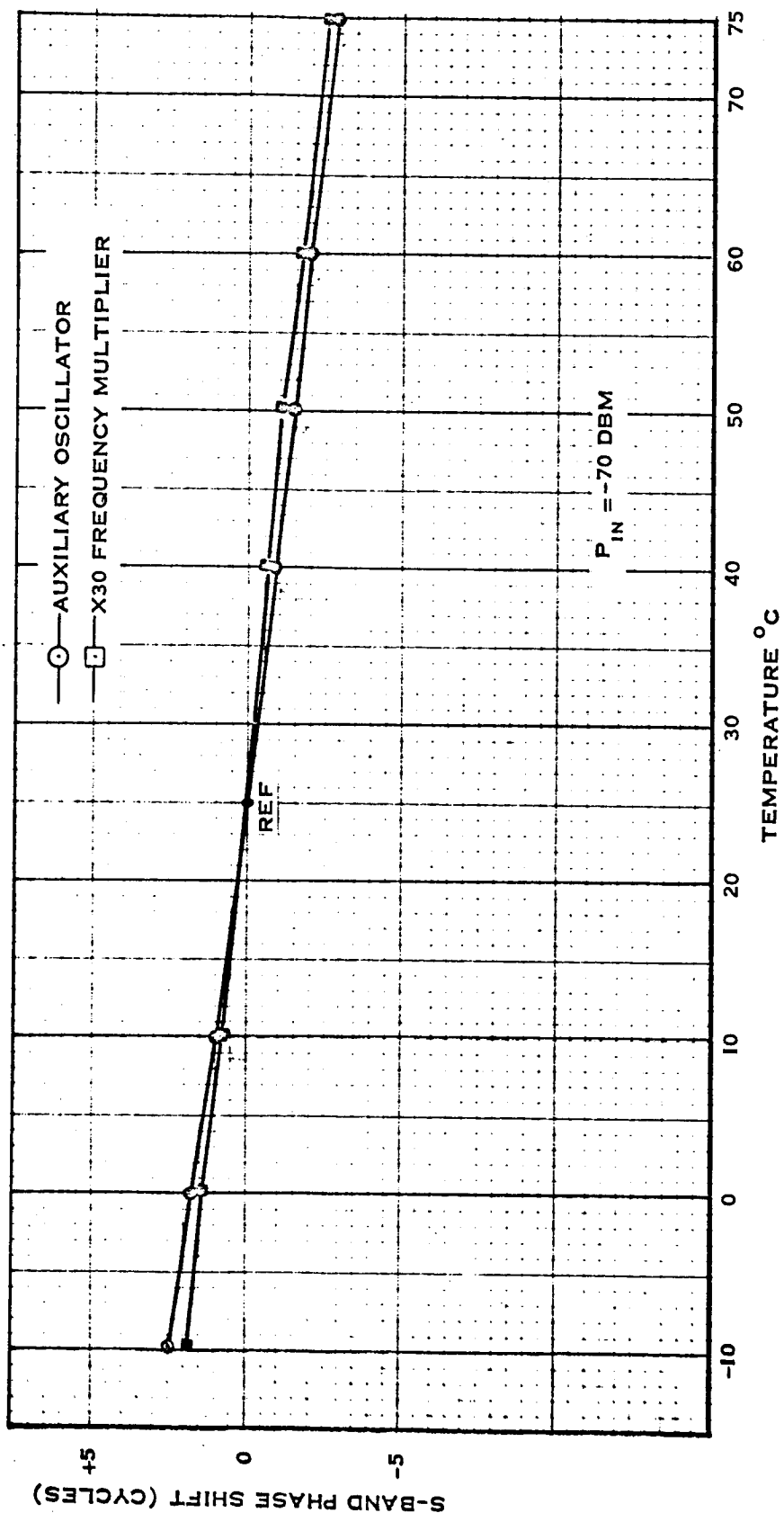


Figure 3.1.3-7 Comparison of S-Band Phase Shift vs Temperature Between the Modules of the Exciter Six Pack.

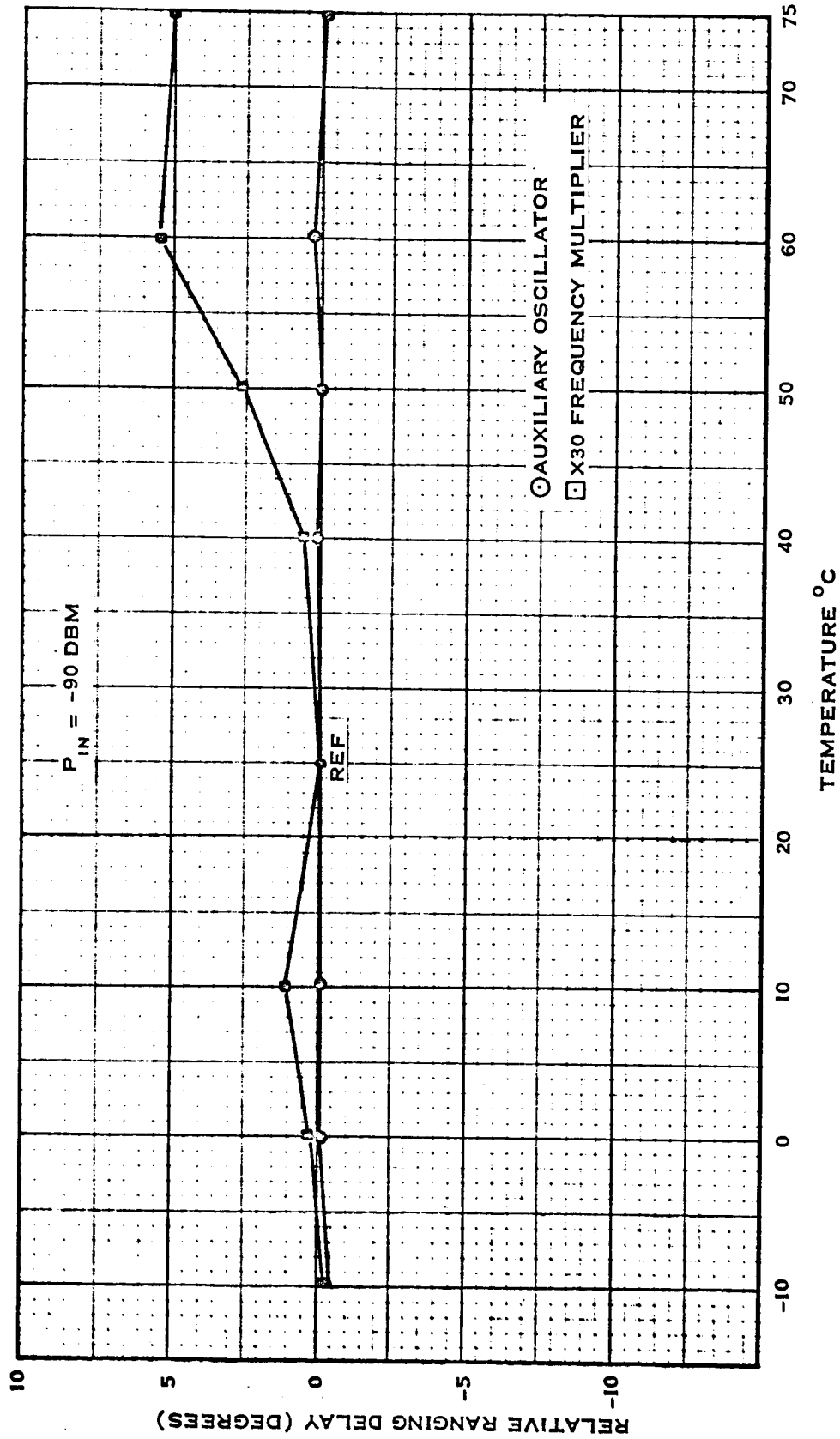


Figure 3.1.3-8 Comparison of Relative Ranging Delay vs. Temperature Between the Modules of the Exciter 6 Pack.

57

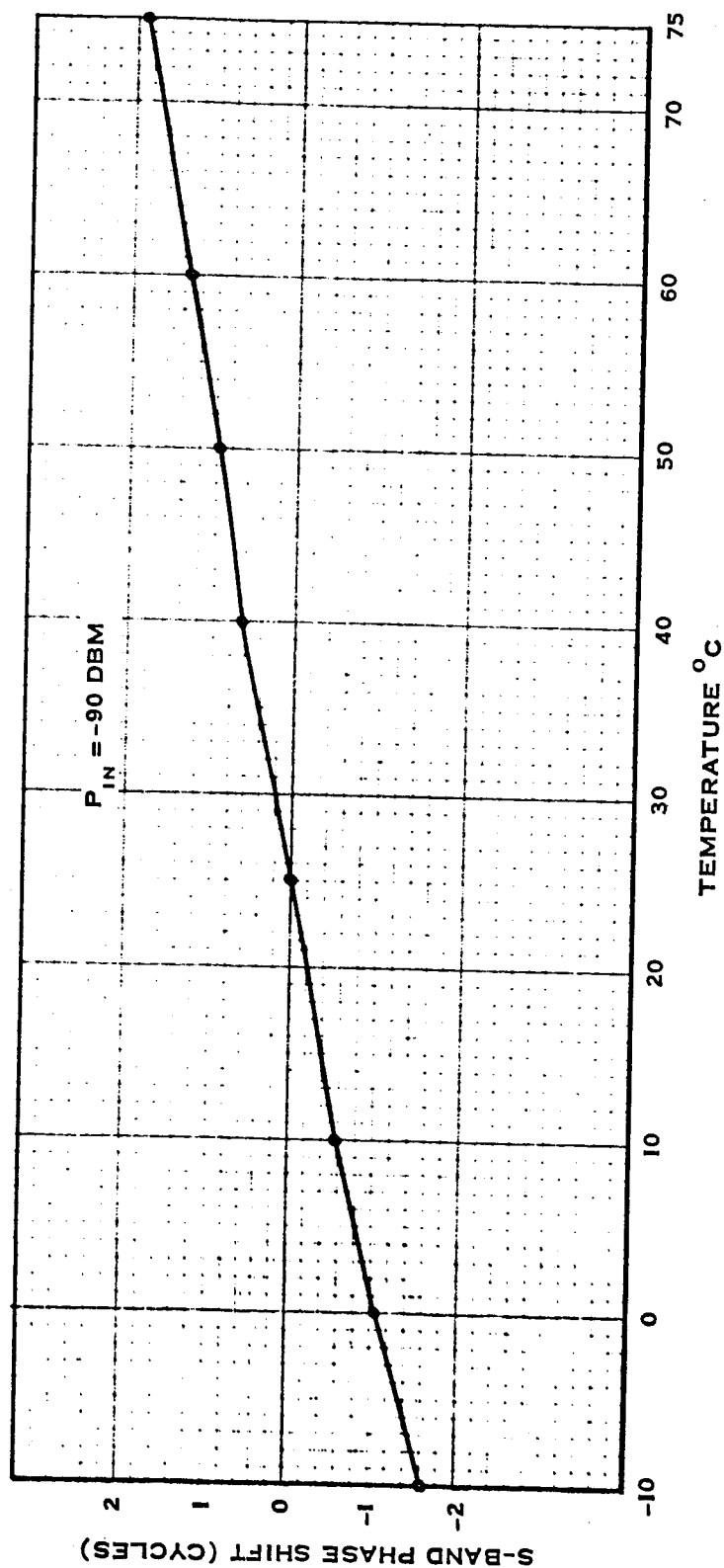


Figure 3.1.3-9 S-Band Phase Shift vs. Temperature of the X36 Frequency Multiplier Module.

58

TR-DA1522A

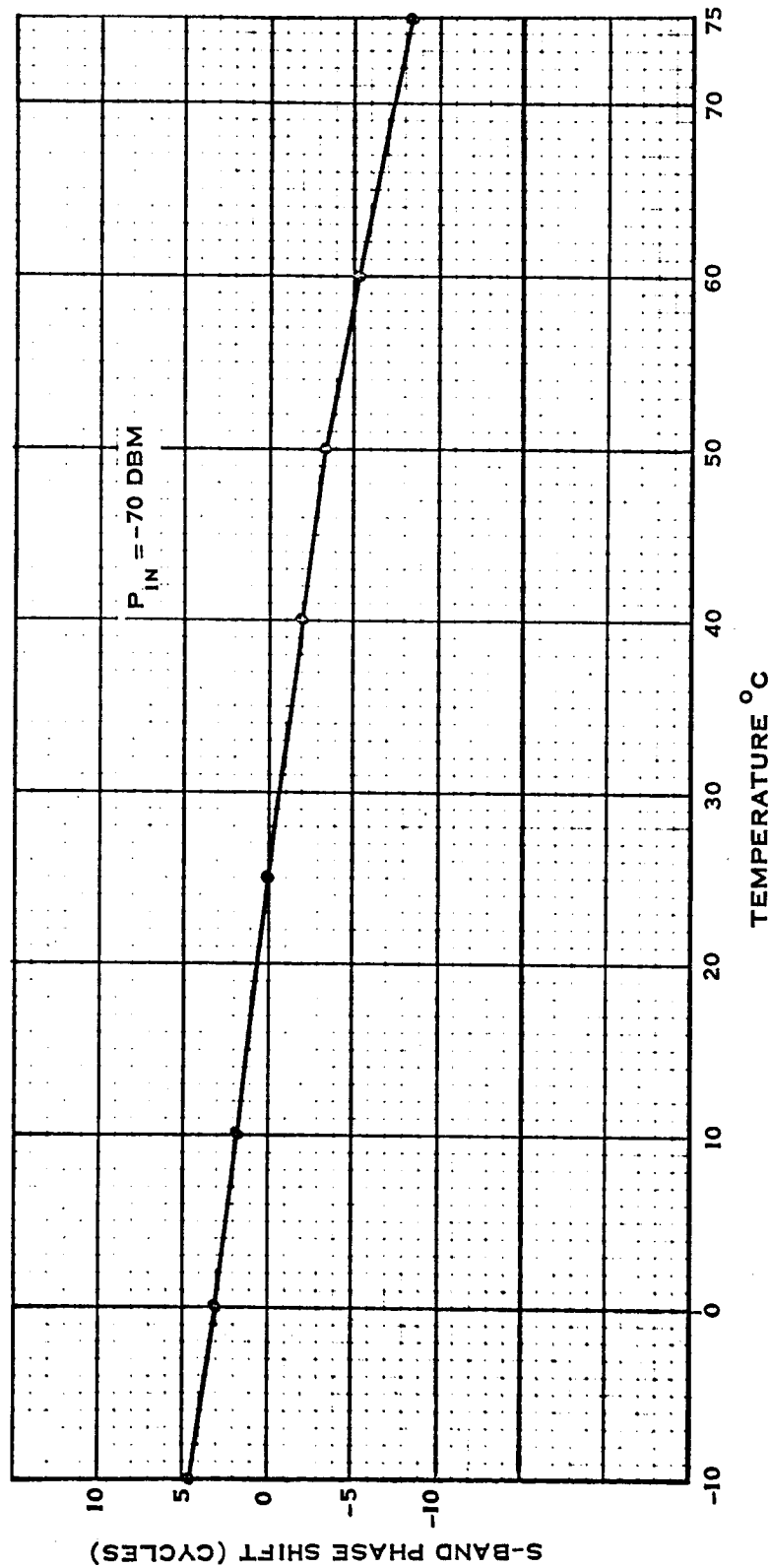


Figure 3.1.3-10 S-Band Phase Shift vs. Temperature of the VCO Module.

59

TR-DA1522A

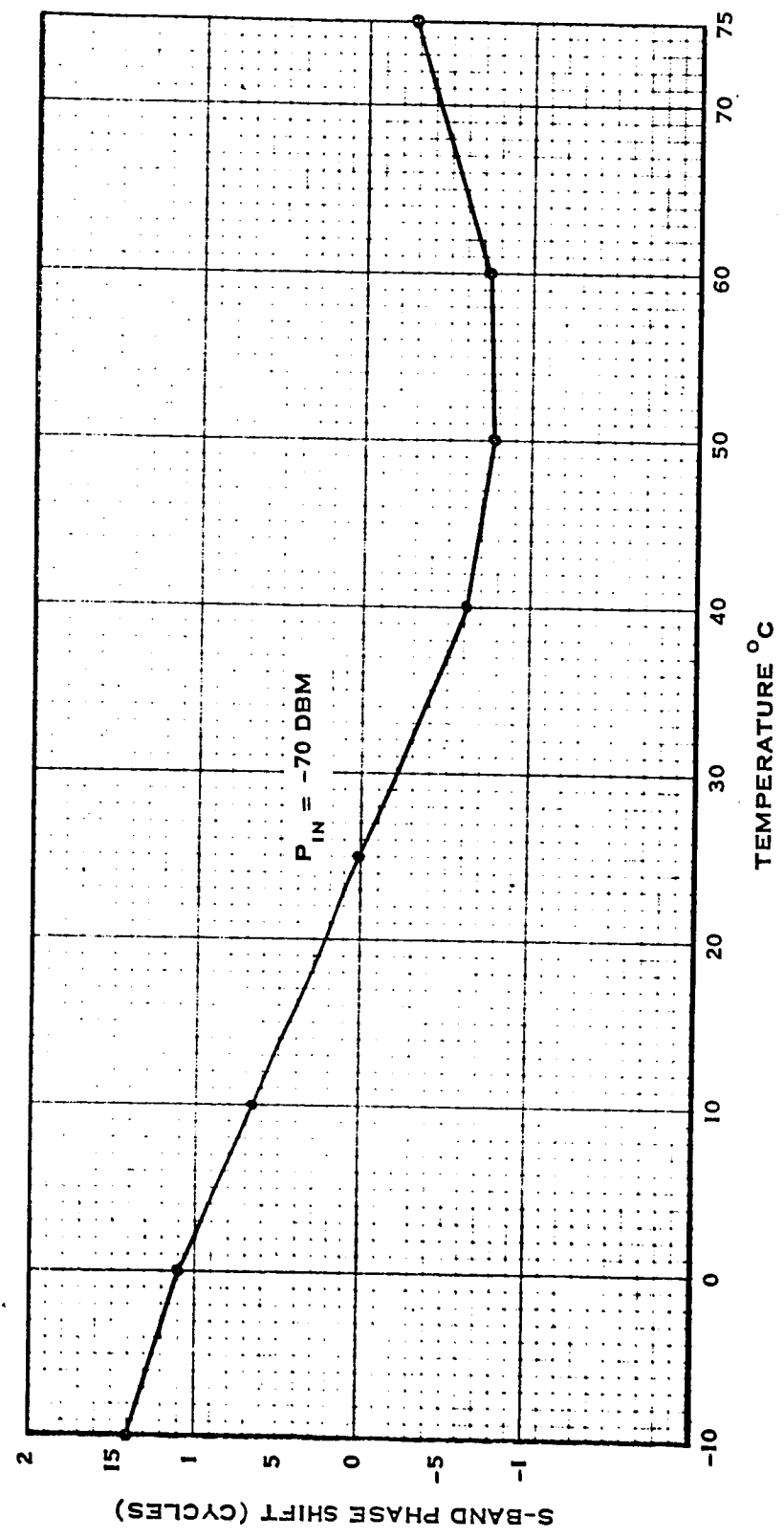


Figure 3.1.3-11 S-Band Phase Shift vs. Temperature of the Frequency Divider Module.

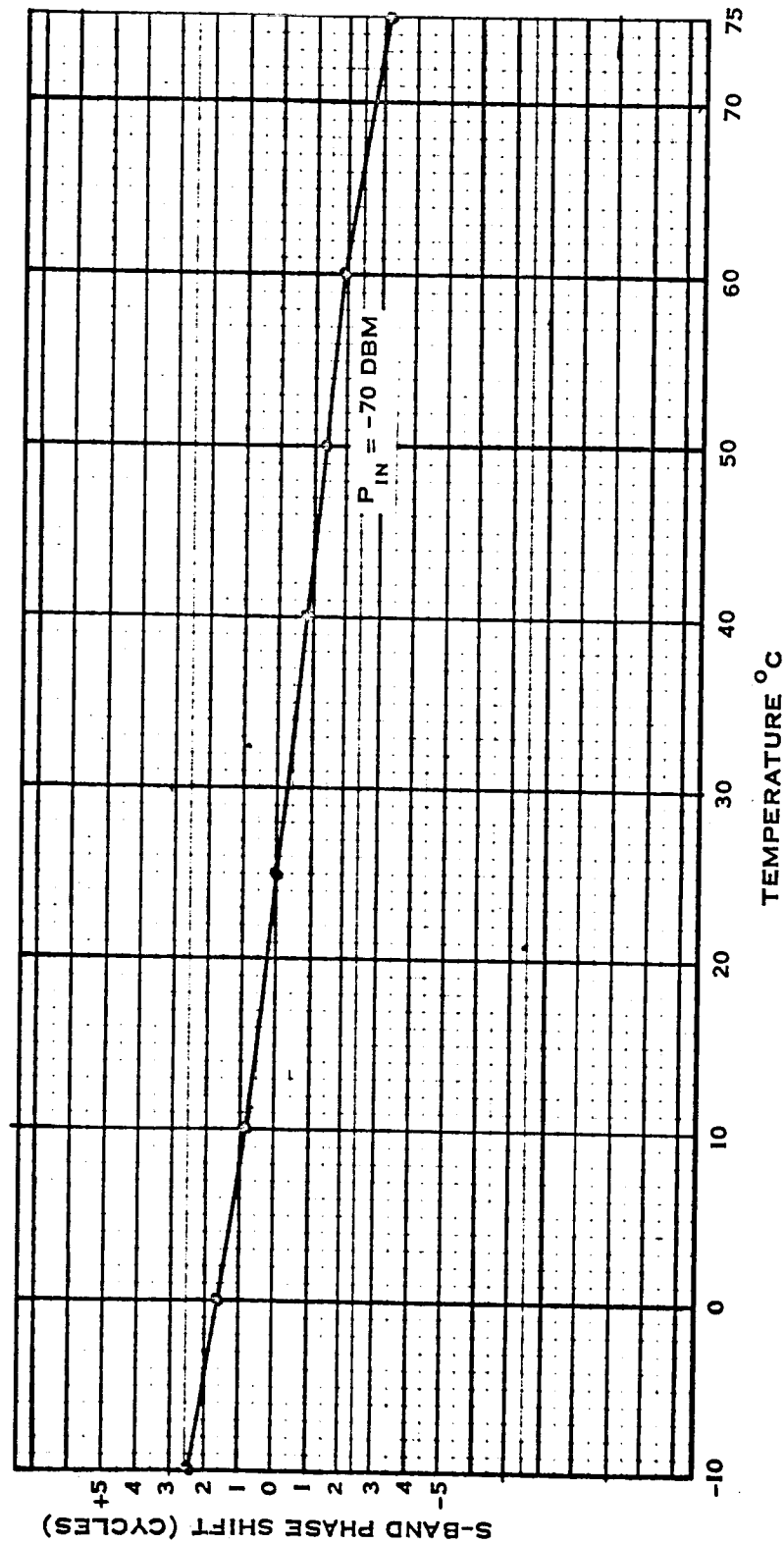


Figure 3.1.3-12 S-Band Phase Shift vs. Temperature of the Auxiliary Oscillator Module.

61

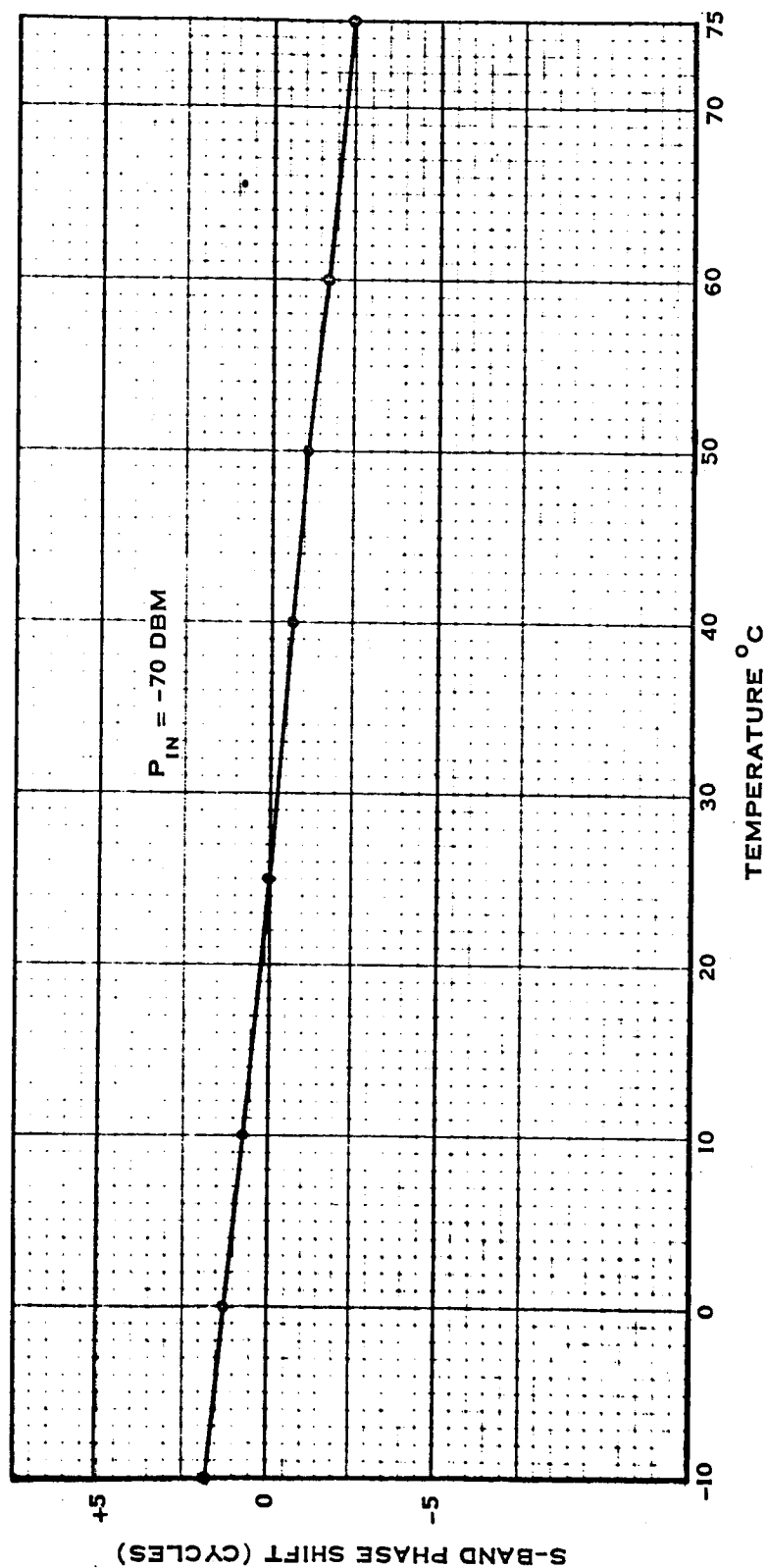


Figure 3.1.3-13 S-Band Phase Shift vs. Temperature of the X30 Frequency Multiplier Module.

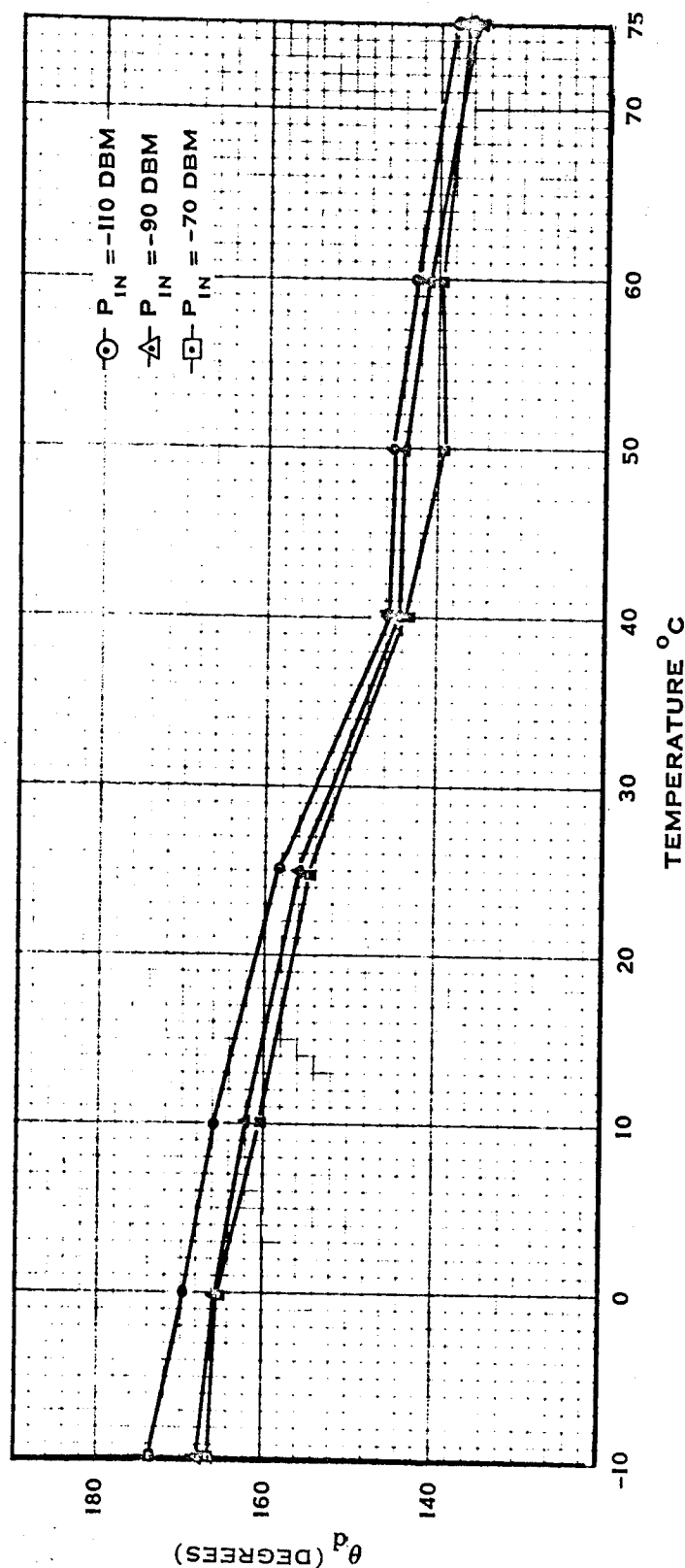


Figure 3.1.3-14 Ranging Delay vs. Temperature of 9.56 MC I.F. Amplifier Module.

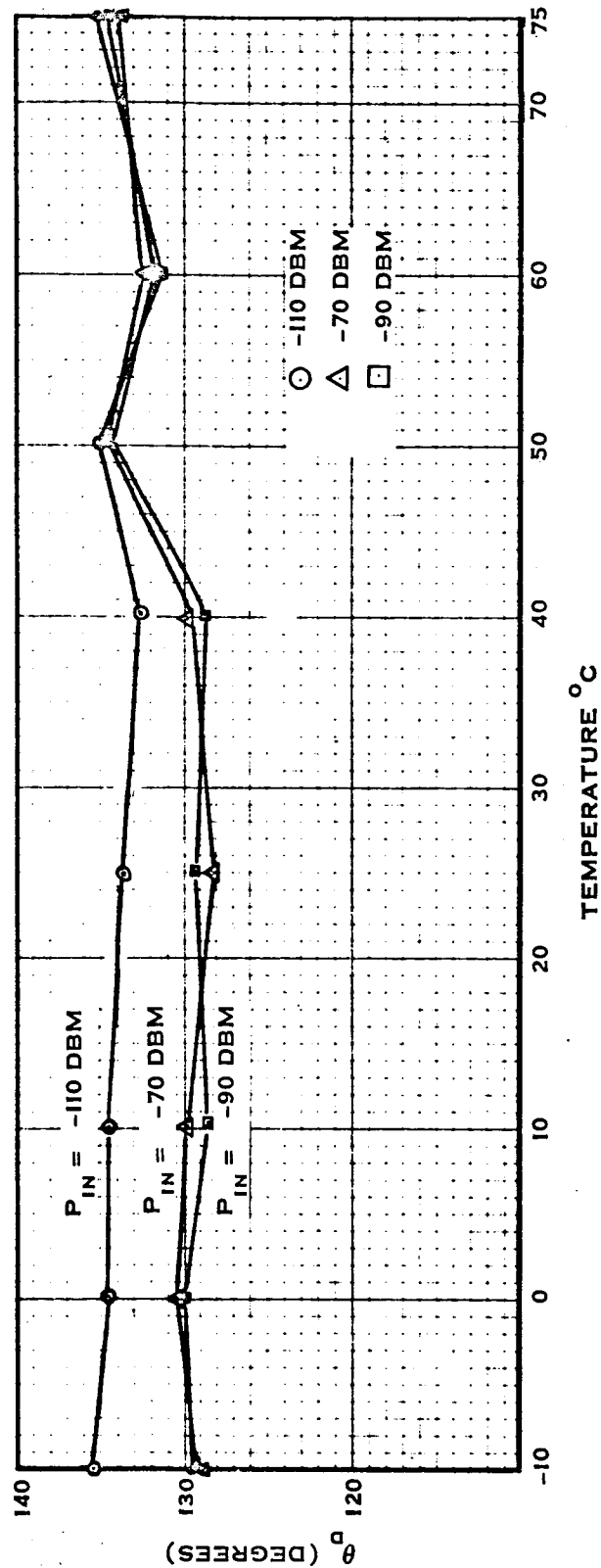


Figure 3.1.3-15 Ranging Delay vs. Temperature of the 47.8 MC I.F. Amplifier Module.

64

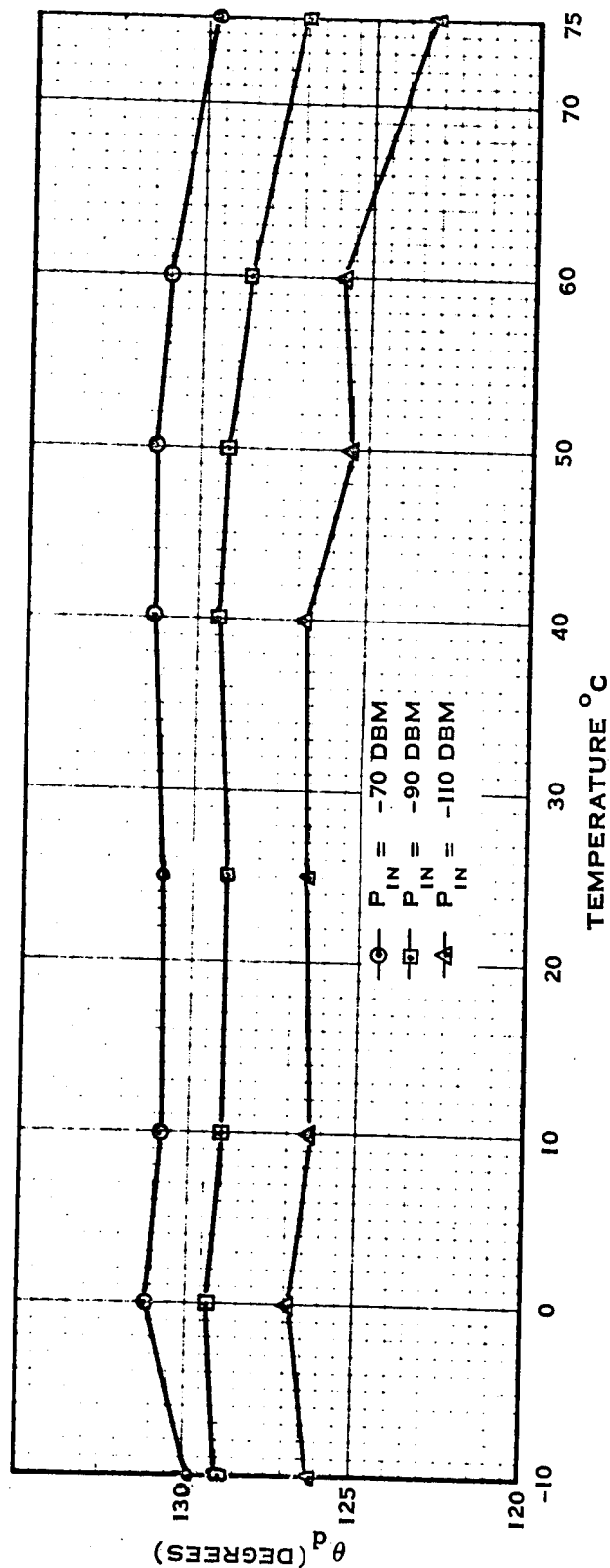


Figure 3.1.3-16 Ranging Delay vs. Temperature of the VCO Module.

65

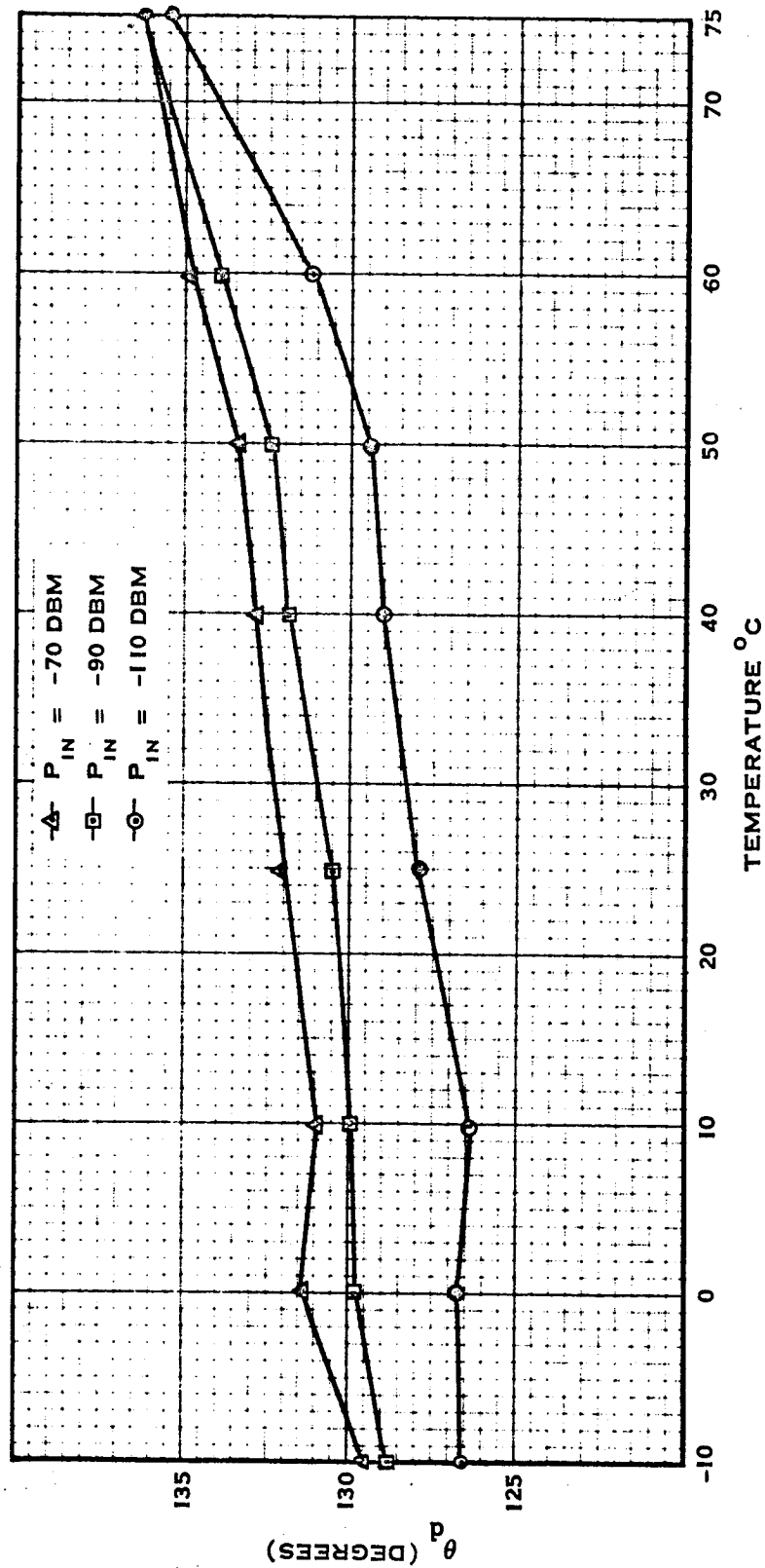


Figure 3.1.3-17 Ranging Delay vs. Temperature of the Frequency Divider Module.

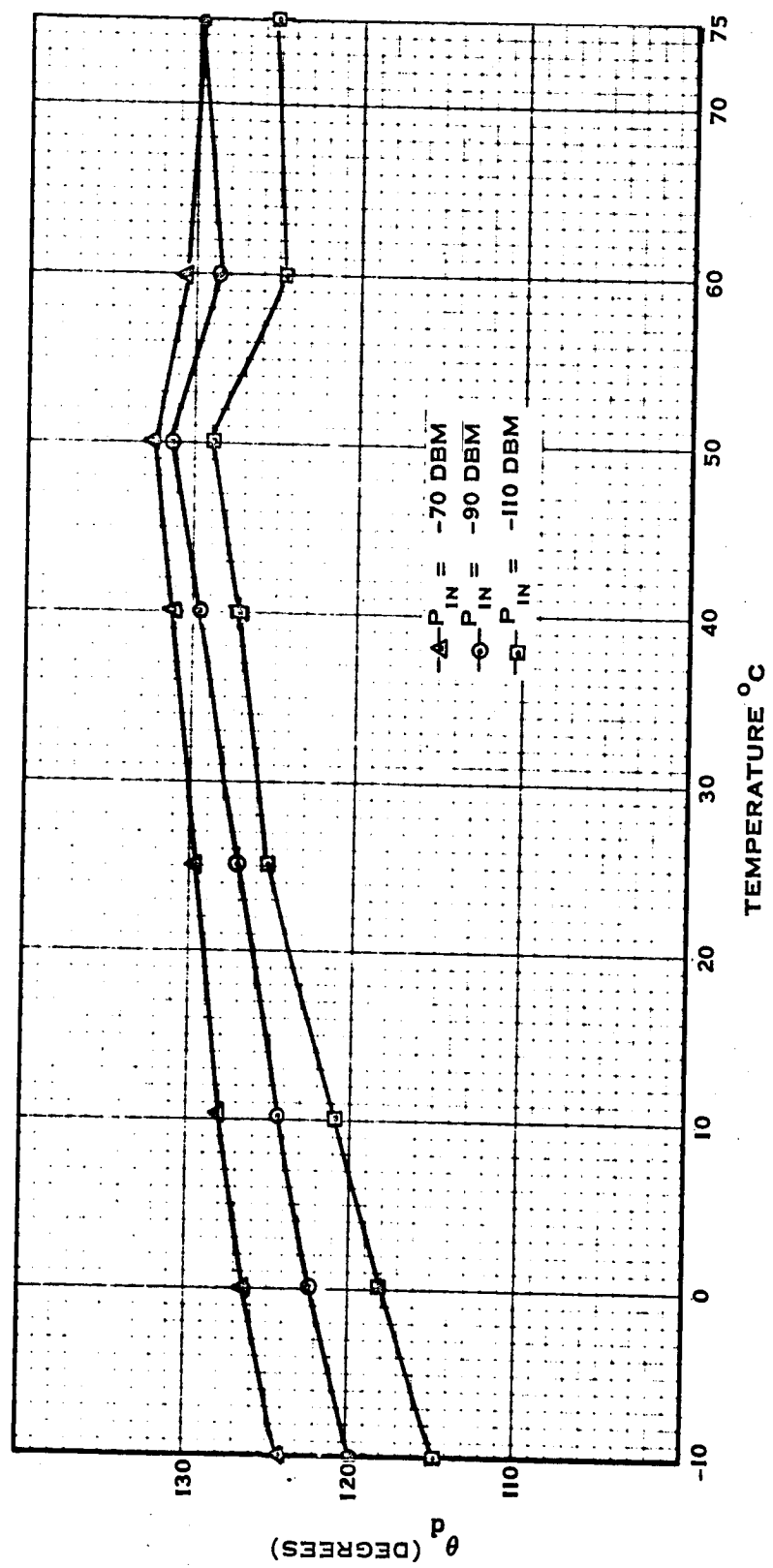


Figure 3.1.3-18 Ranging Delay vs. Temperature of the Isolation Amplifier Module.

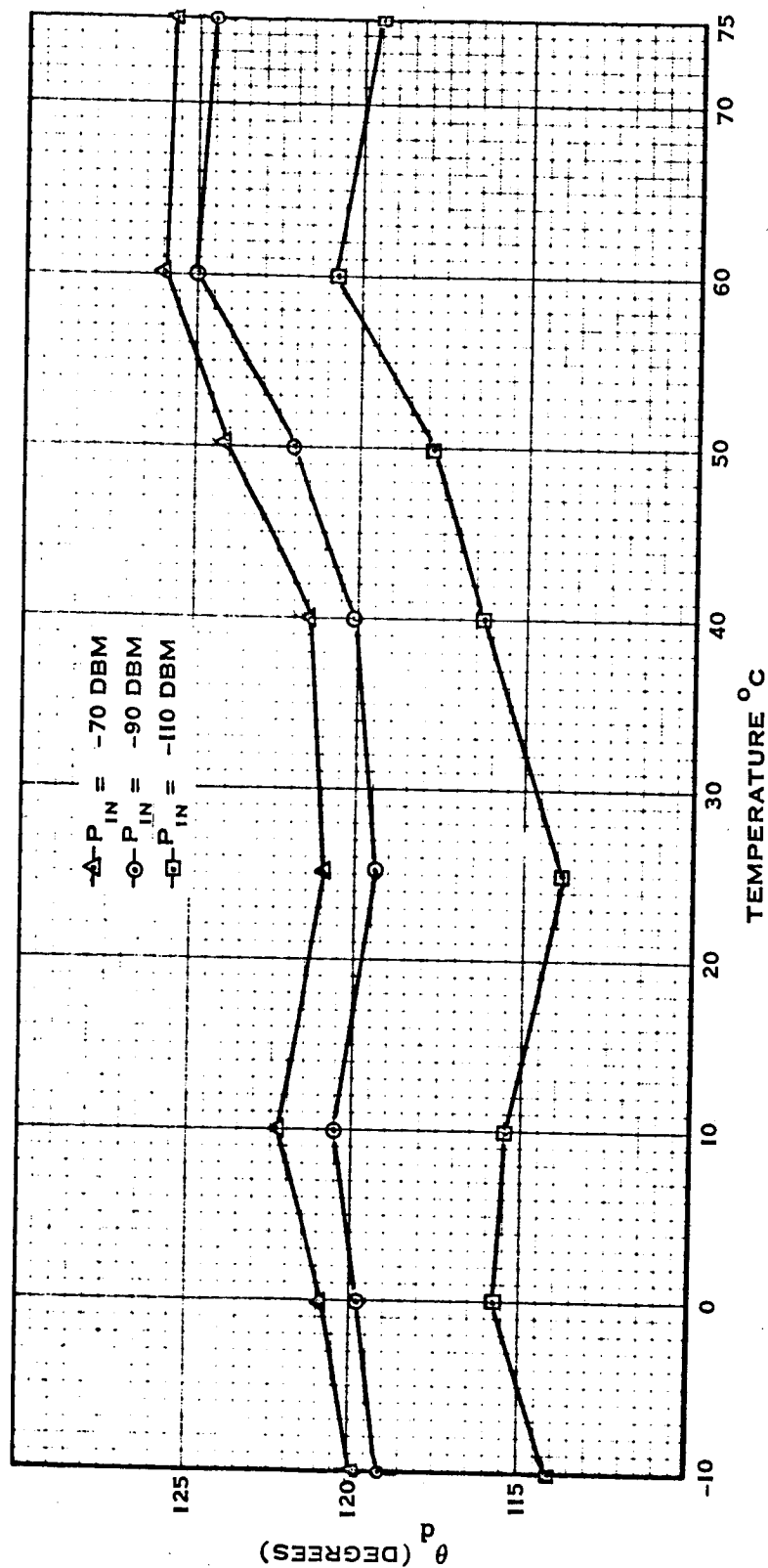


Figure 3.1.3-19 Ranging Delay vs. Temperature of the X30 Frequency Multiplier Module.

of those modules which contributed most to ranging delay variations. These graphs are useful for more closely observing the major S-Band and phase delay contributions.

Stabilization was noticed to be essentially complete after twenty minutes from the time of temperature change. As a result of the faster stabilization for the modules, only a minimum of forty five minutes was allowed between temperature points.

3.2 DIAGNOSTIC TESTS

In order to better understand the effects producing ranging delay variations, several tests were made in addition to the evaluation tests in the previous section. These additional tests, described in this section, were tests made on modules removed from the transponder system. They show the characteristics of some of the modules which produced the most delay variations.

3.2.1 Module Tests

The first module to be investigated separate from the transponder system was the 9.56 MHz I.F. Module. The block diagram showing the setup for the testing done on this module is shown in Figure 3.2.1-10. As can be seen, the crystal filter was disconnected from the module to allow measurements to be made with and without the crystal filter.

Figures 3.2.1-1 through 3.2.1-5 show the phase and amplitude as a function of temperature. The phase variation with temperature for both the linear and limited outputs of the 9.56 MHz I.F. Module differed only slightly between the crystal filter connected and disconnected.

However, the absolute phase shift through the I.F. Module was changed considerably with the crystal filter added. The linear to limited phase shown in Figure 3.2.1-4 shows about a 50° variation with temperature. This means, since the transponder receiver locks to the limited output, that the AGC detector becomes rather badly misaligned as the transponder changes temperature. The specification for linear to limited phase shift over temperature is $\pm 15^\circ$.

Figure 3.2.1-5 shows that the gain roll off for the linear and the limited output of the 9.56 MHz I.F. occur at opposite temperature limits.

The amplitude and phase response of the 9.56 MHz I.F. Module shown in Figures 3.2.1-6 through 3.2.1-9 were obtained with the test setup shown in Figure 3.2.1-10. These measurements were made at room temperature. The graphs indicate that the phase and amplitude response of the 9.56 MHz I.F. is normally almost entirely determined by the very narrow band crystal filter.

Phase and amplitude response measurements were made of the I.F. stages of the 9.56 MHz Isolation Amplifier. In order to facilitate this test, a few minor changes had to be made to the module. Figure 3.2.1-12 indicates the changes made for the phase measurement. Fifty ohms were added to the emitter of the emitter follower so that a small sample of the signal could be monitored for this measurement. This prevented the phase meter from loading this stage. The signal then had to be amplified to permit phase measurement with the Wiltron.

Being a high impedance meter, the Boonton RF voltmeter was used to monitor the output of the emitter follower directly, Figure 3.2.1-14. This permitted an absolute gain measurement of the I.F. stages of the 9.56 MHz Isolation Amplifier. The results of these tests are shown in Figures 3.2.1-11 and 3.2.1-13. Note that although the amplitude response changes only slightly with temperature, the nominal gain varies by about 17 DB.

Figures 3.2.1-15 through 3.2.1-21 show the phase and amplitude characteristics of the Frequency Divider Module. Although considerable phase variation occurs with temperature, the phase relation between the three outputs of this module remain essentially constant which should mean that the reference to all the detectors maintains alignment. Actually, although not shown on the graphs, there was a variation of from 2° to 5° between J_3 and J_4 over temperature. This slight misalignment of the ranging phase detector accounts for some of the ranging delay variation with temperature.

71

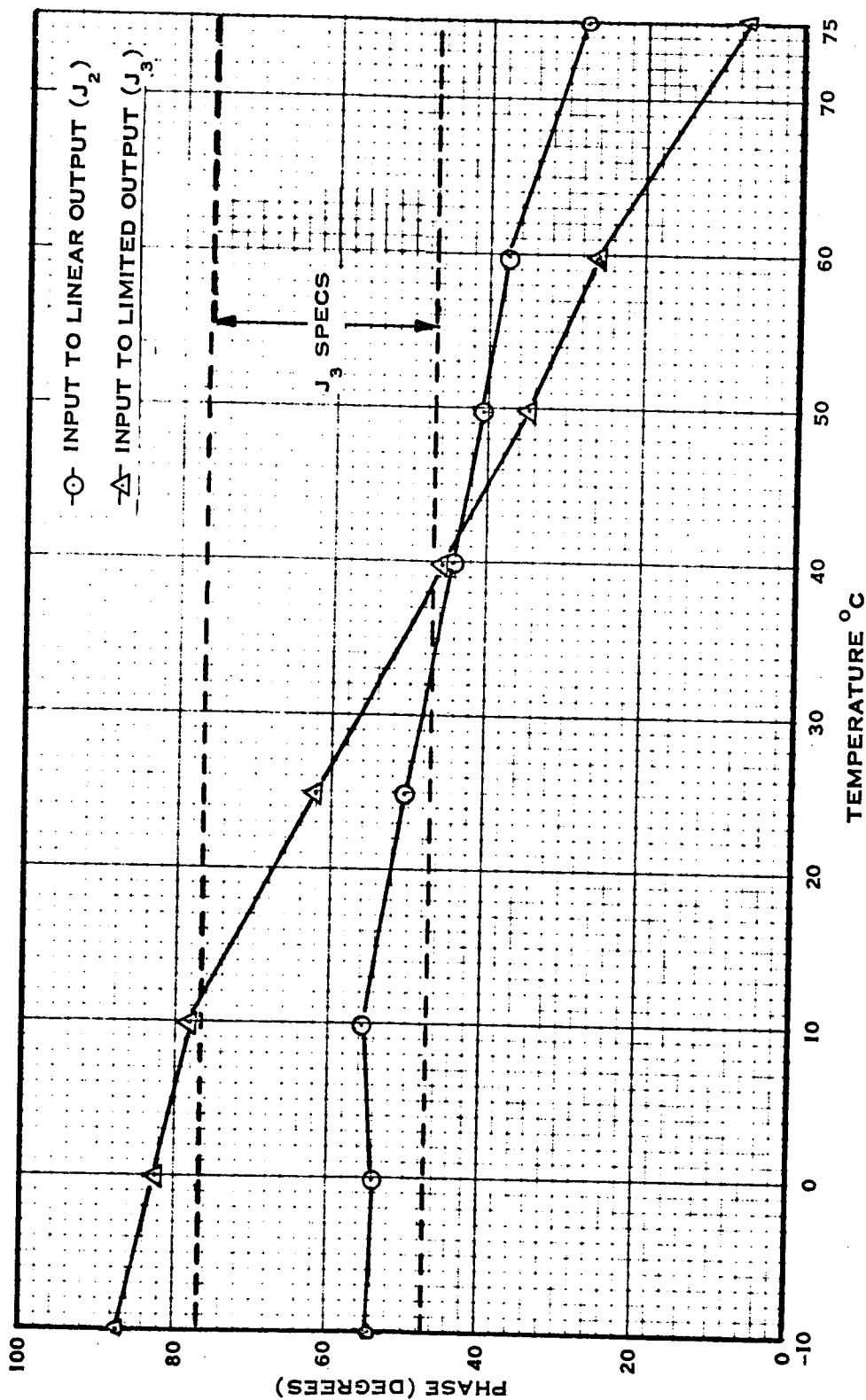


Figure 3.2.1-1 Phase vs. Figure Temperature Response of the 9.56 MHz I.F. Module with the Crystal Filter Connected.

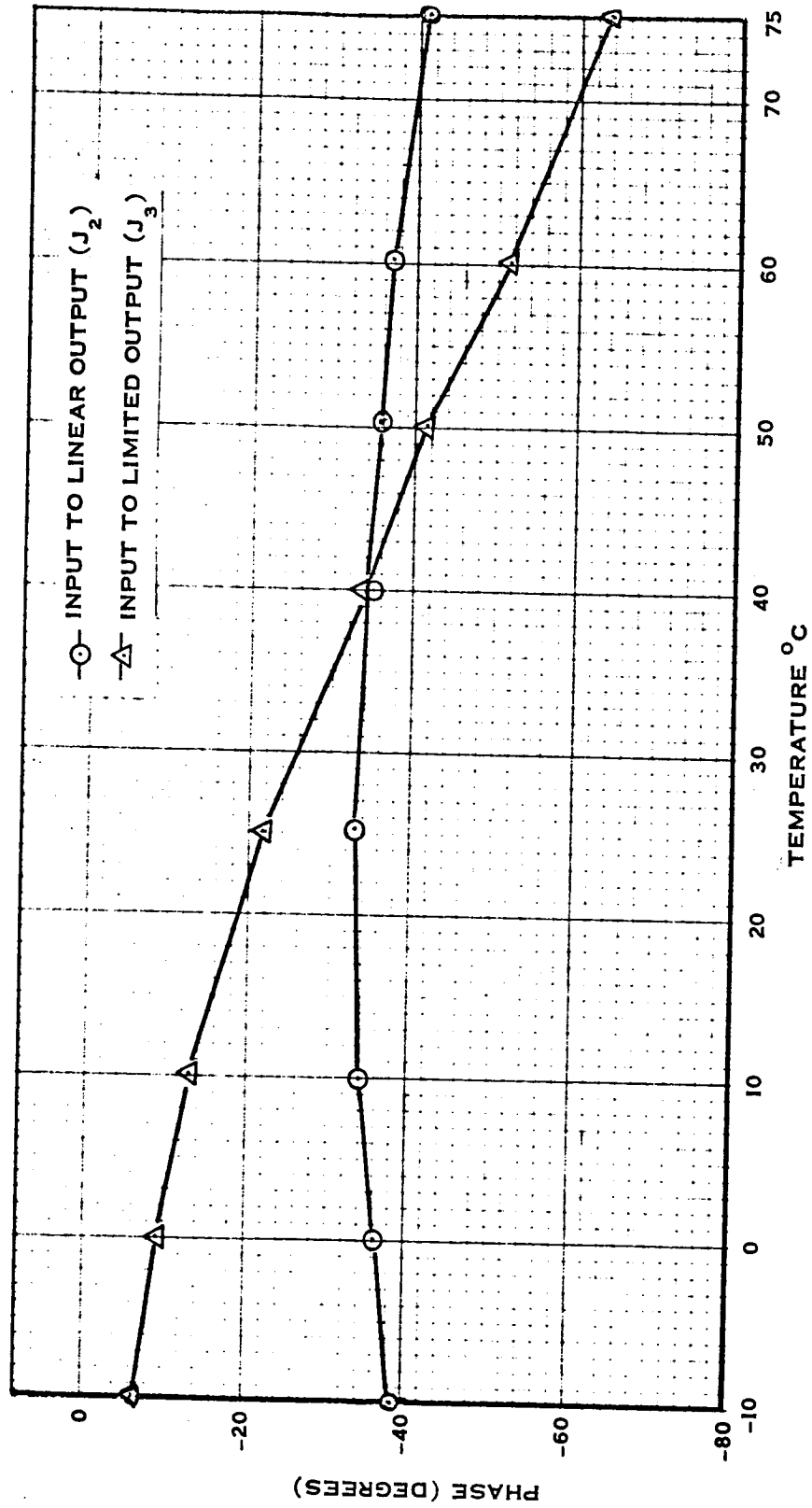


Figure 3.2.1-2 Phase vs. Temperature Response of the 9.56 MHz I.F. Module with the Crystal Filter Disconnected.

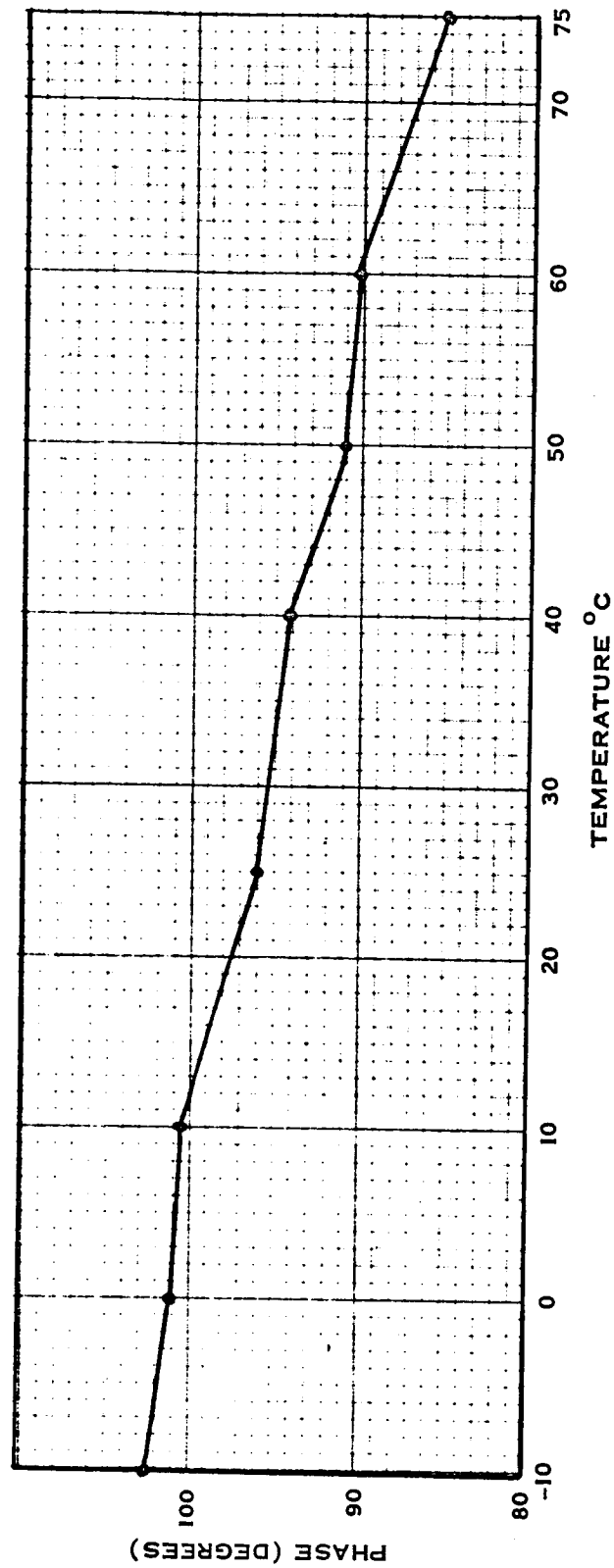


Figure 3.2.1-3 Phase vs. Temperature Response of the 9.56 MHz Crystal Filter.

3-59

74

TR-DA1522A

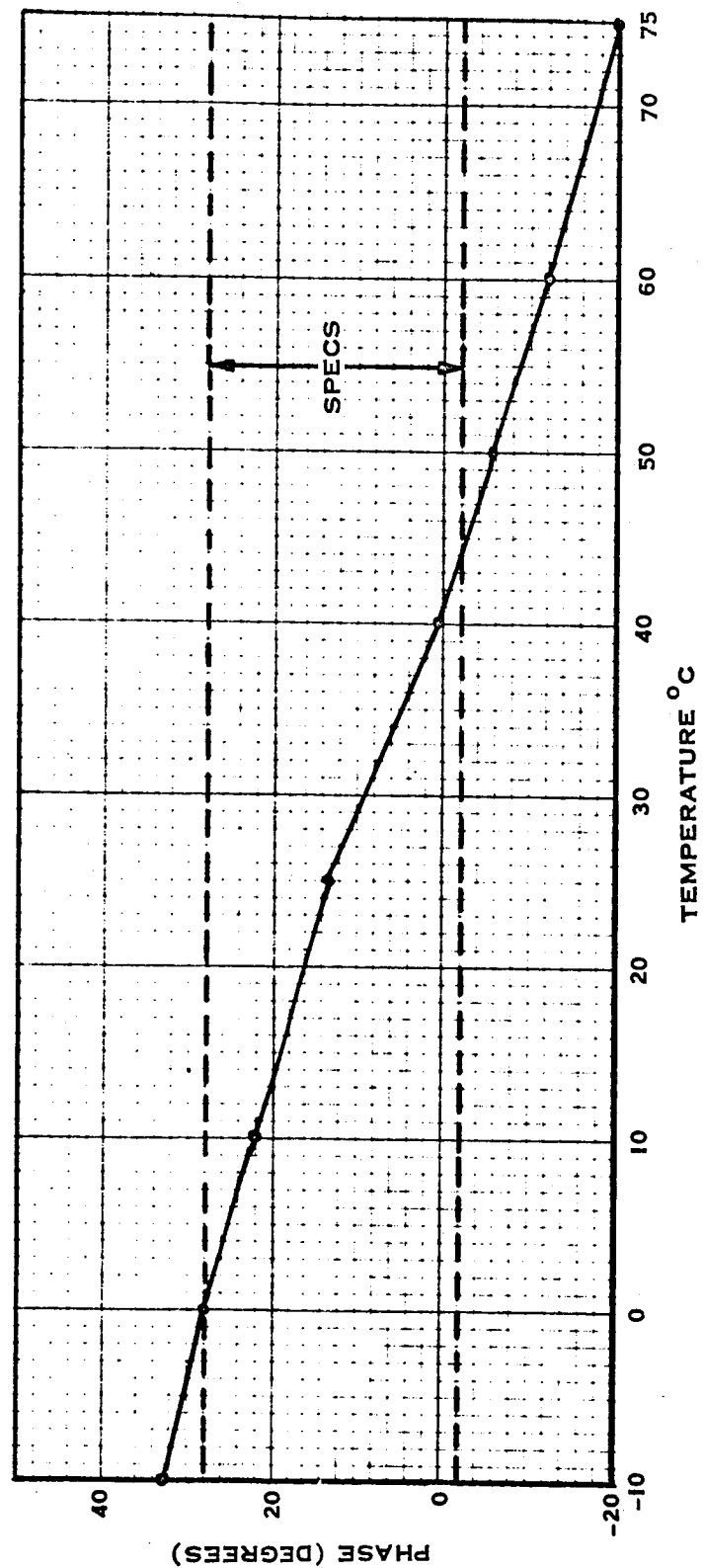


Figure 3.2.1-4 Linear (J_2) to Limited (J_3) Output Phase vs. Temperature Response of the 9.56 MHz IF Module.

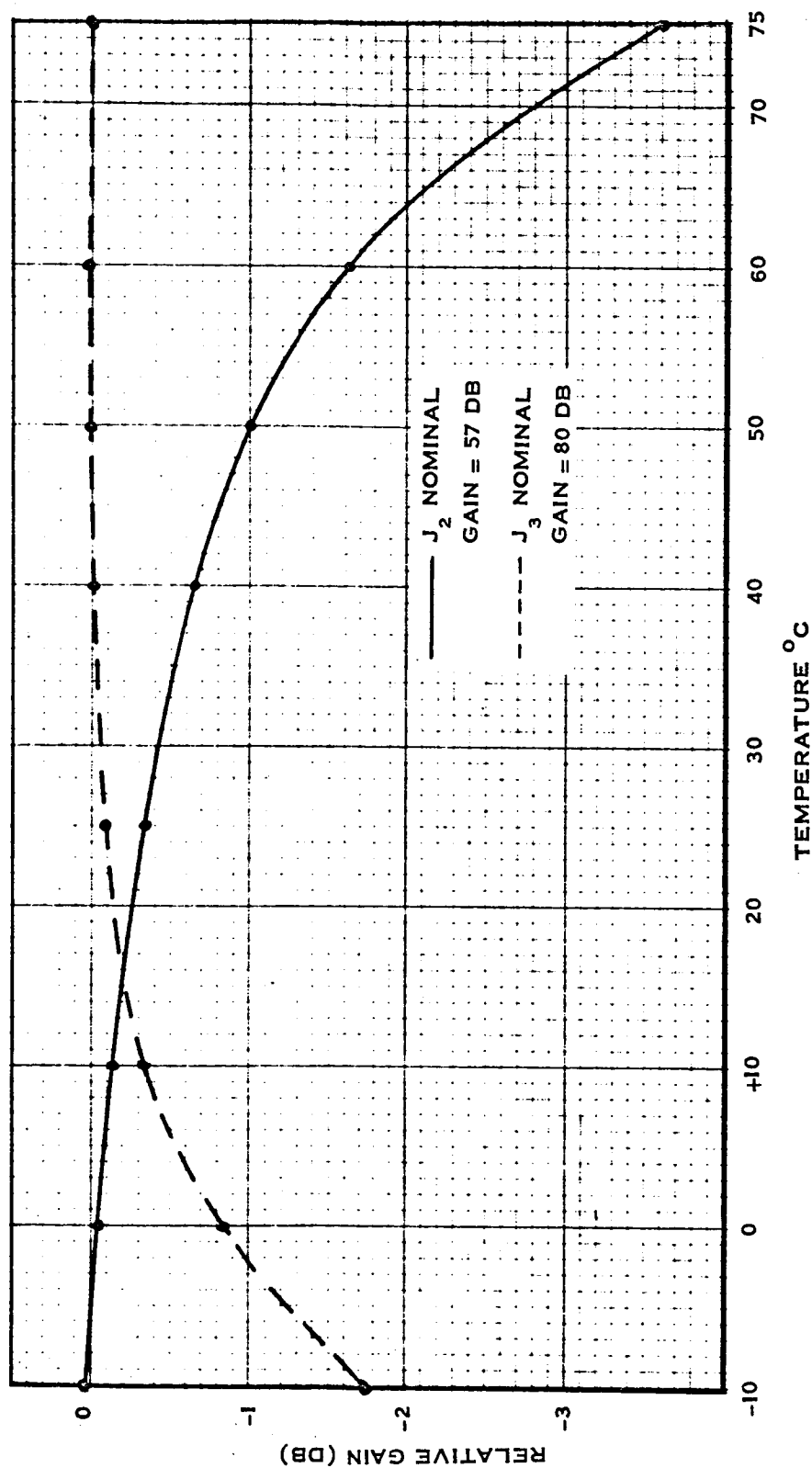


Figure 3.2.1-5 Gain vs. Temperature Response of the 9.56 MHz I.F. Module.

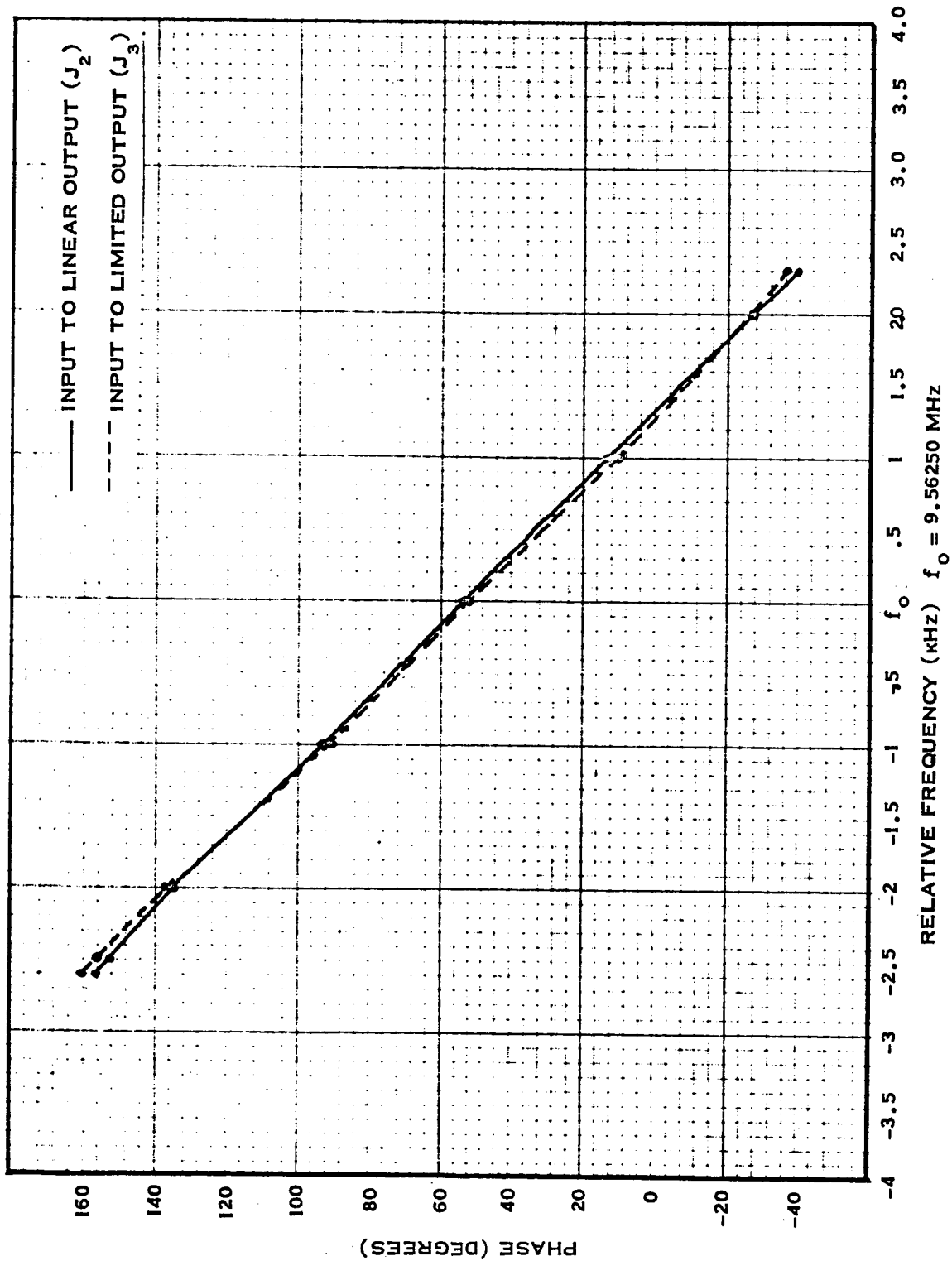


Figure 3.2.1-6 Phase Response of the 9.56 MHz I.F. Module with the Crystal Filter Connected.

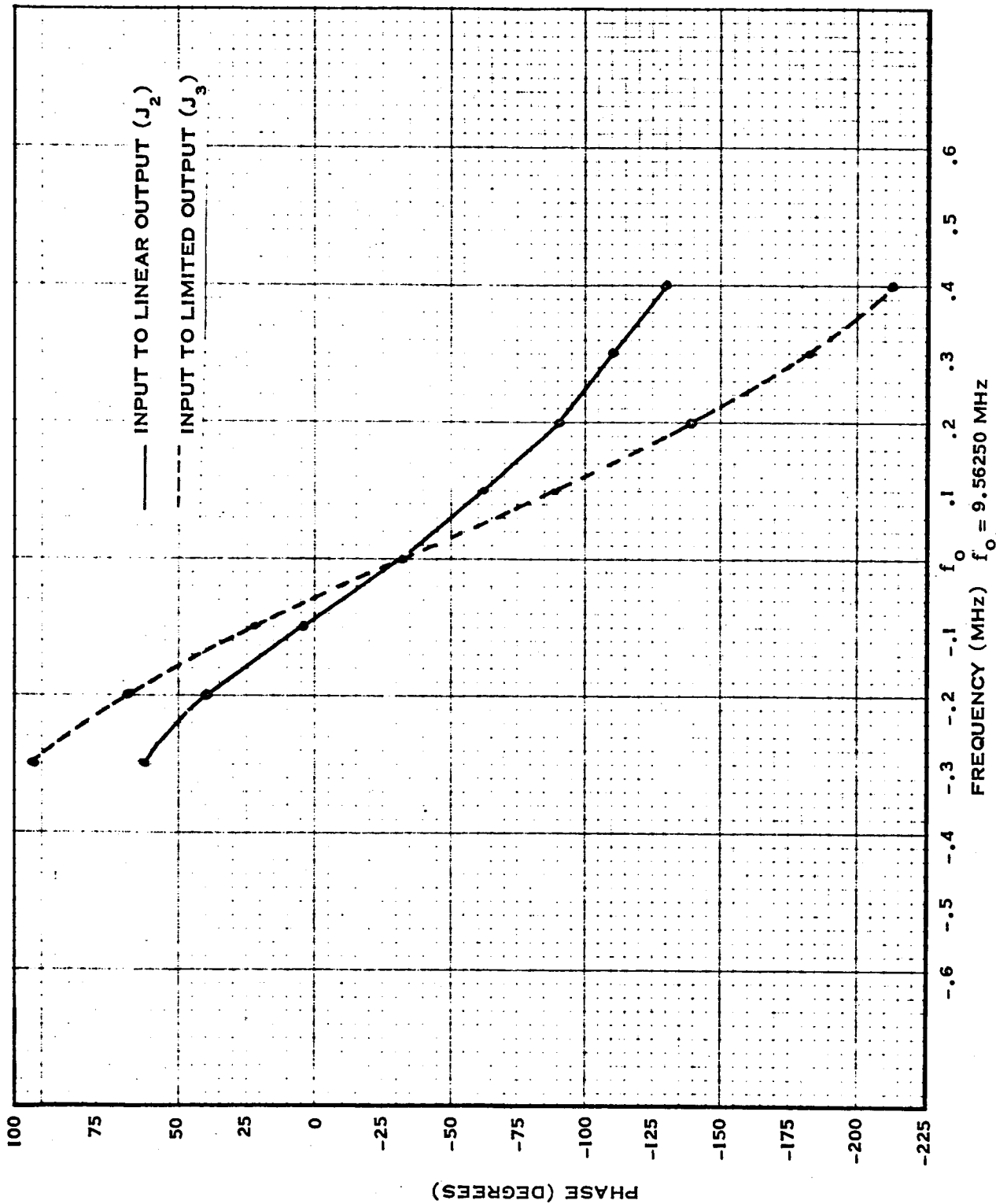


Figure 3.2.1-7 Phase Response of the 9.56 MHz I.F. Module with the Crystal Filter Disconnected.

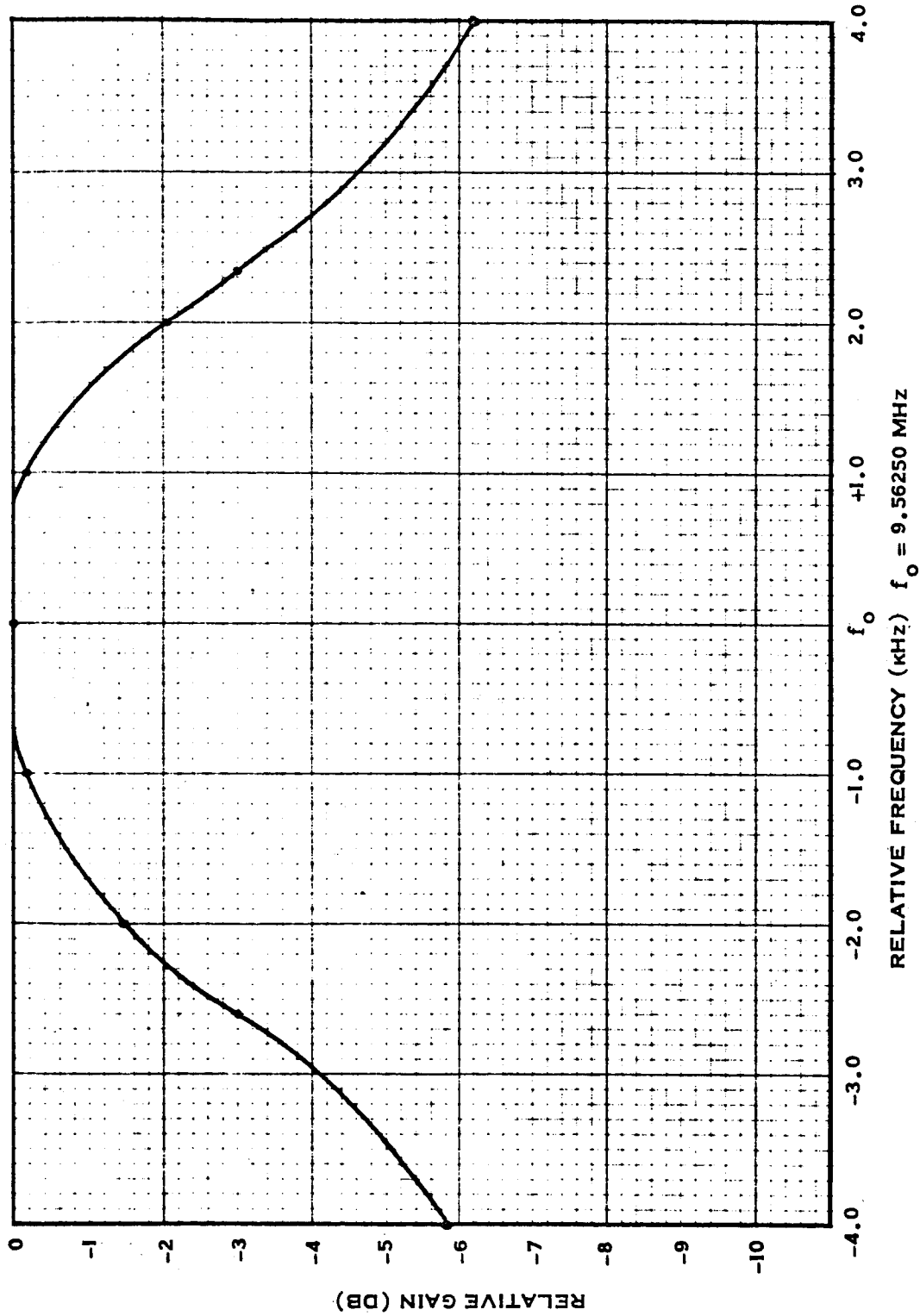


Figure 3.2.1-8 Amplitude Response of the 9.56 MHz I.F. Module with the Crystal Filter Connected.
The Measurement Was Made At J2.

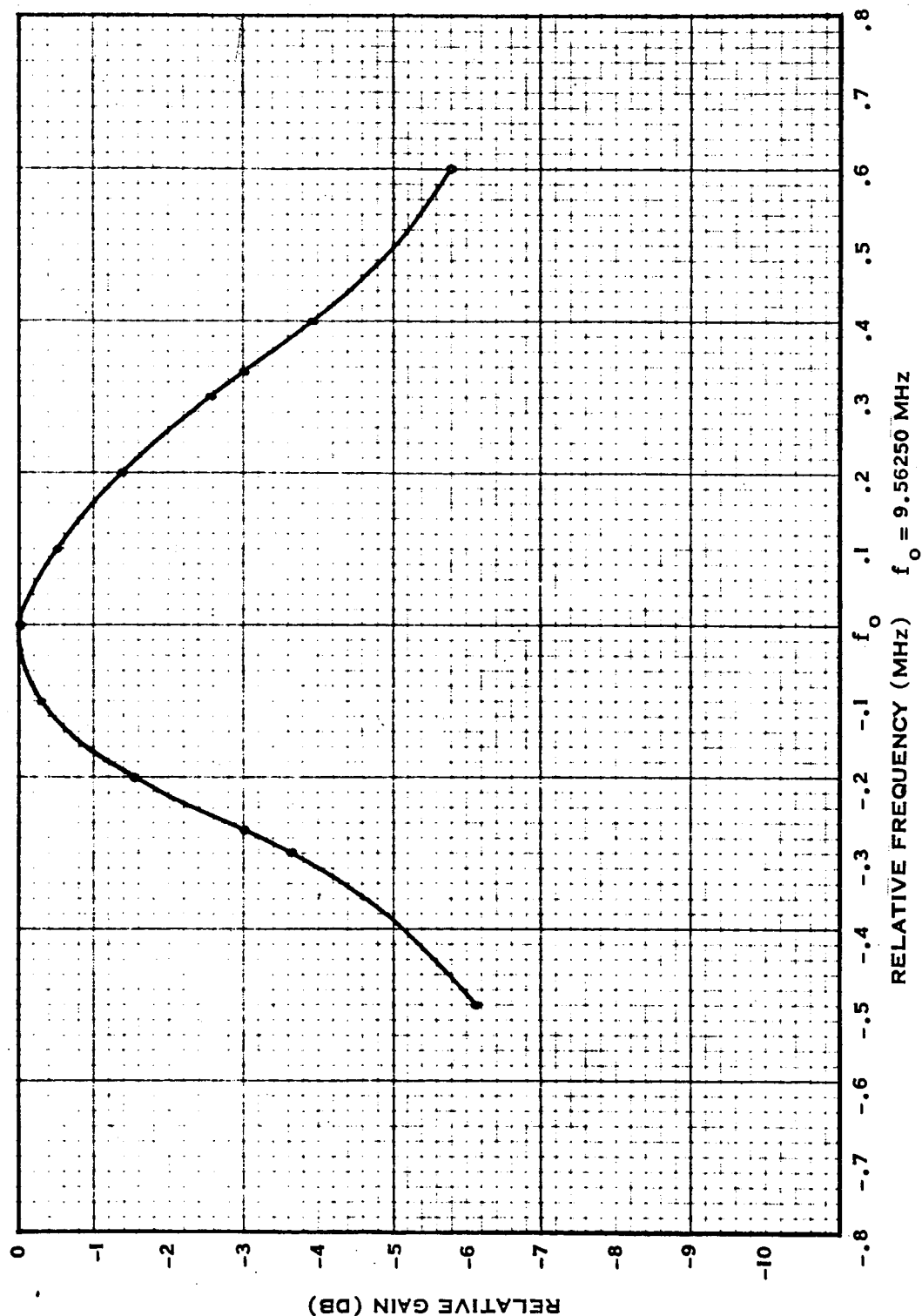
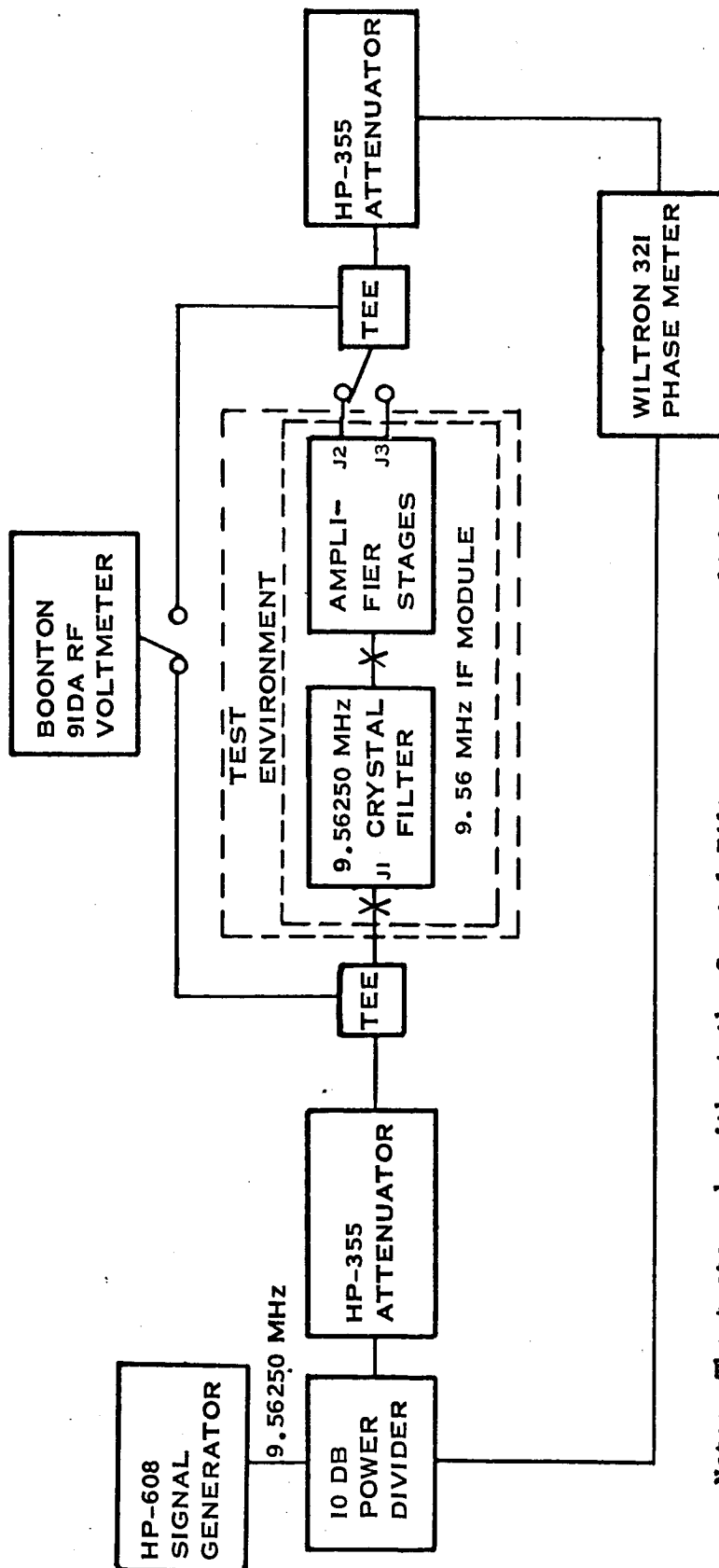


Figure 3.2.1-9 Amplitude Response of the 9.56 MHz I.F. Module with the Crystal Filter Disconnected. The measurement was made at J2.



Note: The tests made without the Crystal Filter were accomplished by disconnecting and removing the Crystal Filter, and temporarily connecting the input directly to the tie point inside the Amplifier enclosure.

Figure 3.2.1-10 Block Diagram of the Test Setup for the Phase and Amplitude Response of the 9.56 MHz IF With and Without the Crystal Filter Connected

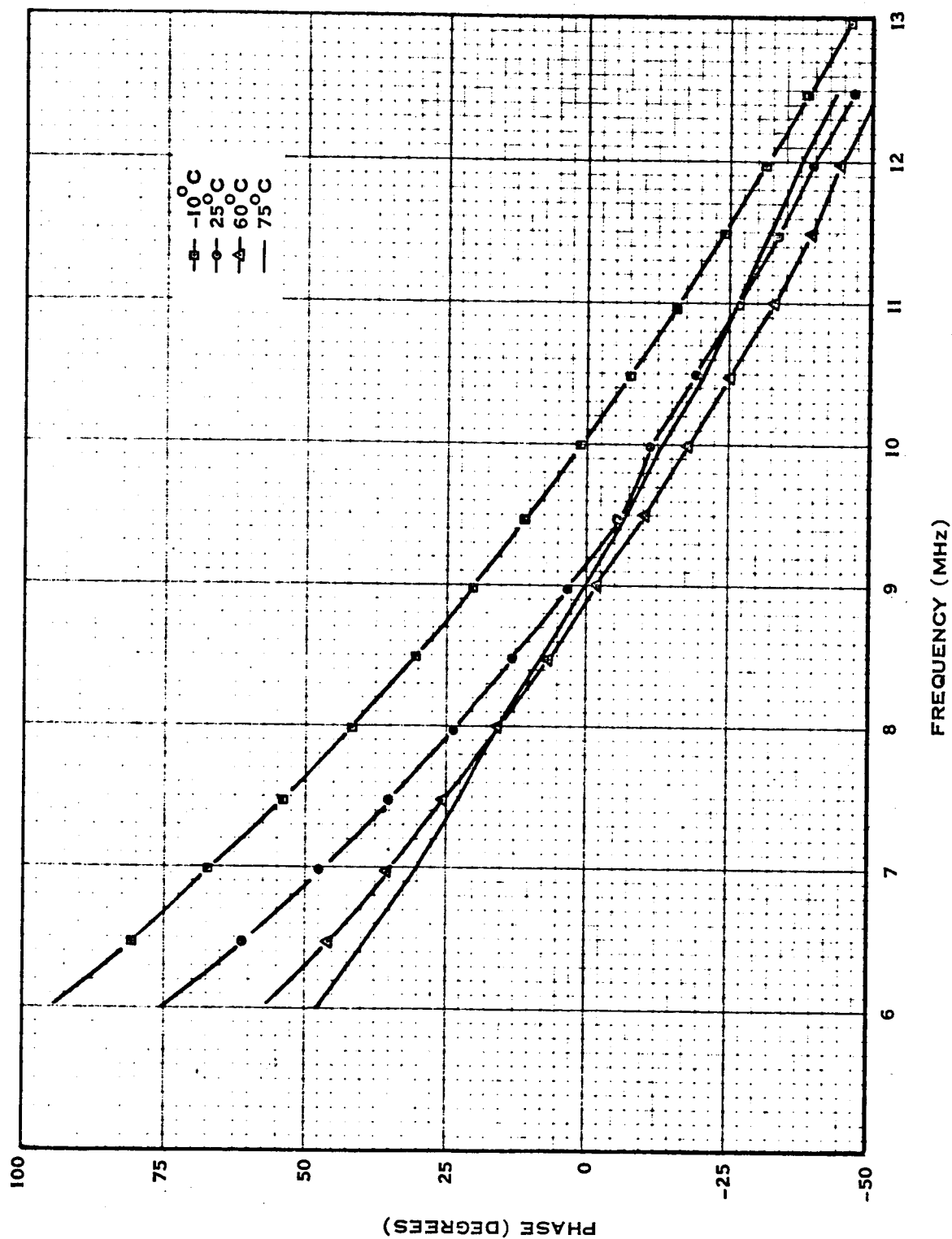


Figure 3.2.1-11 Phase Response of the 9.56 MHz Stages of the 9.56 MHz Isolation Amplifier at Several Temperatures.

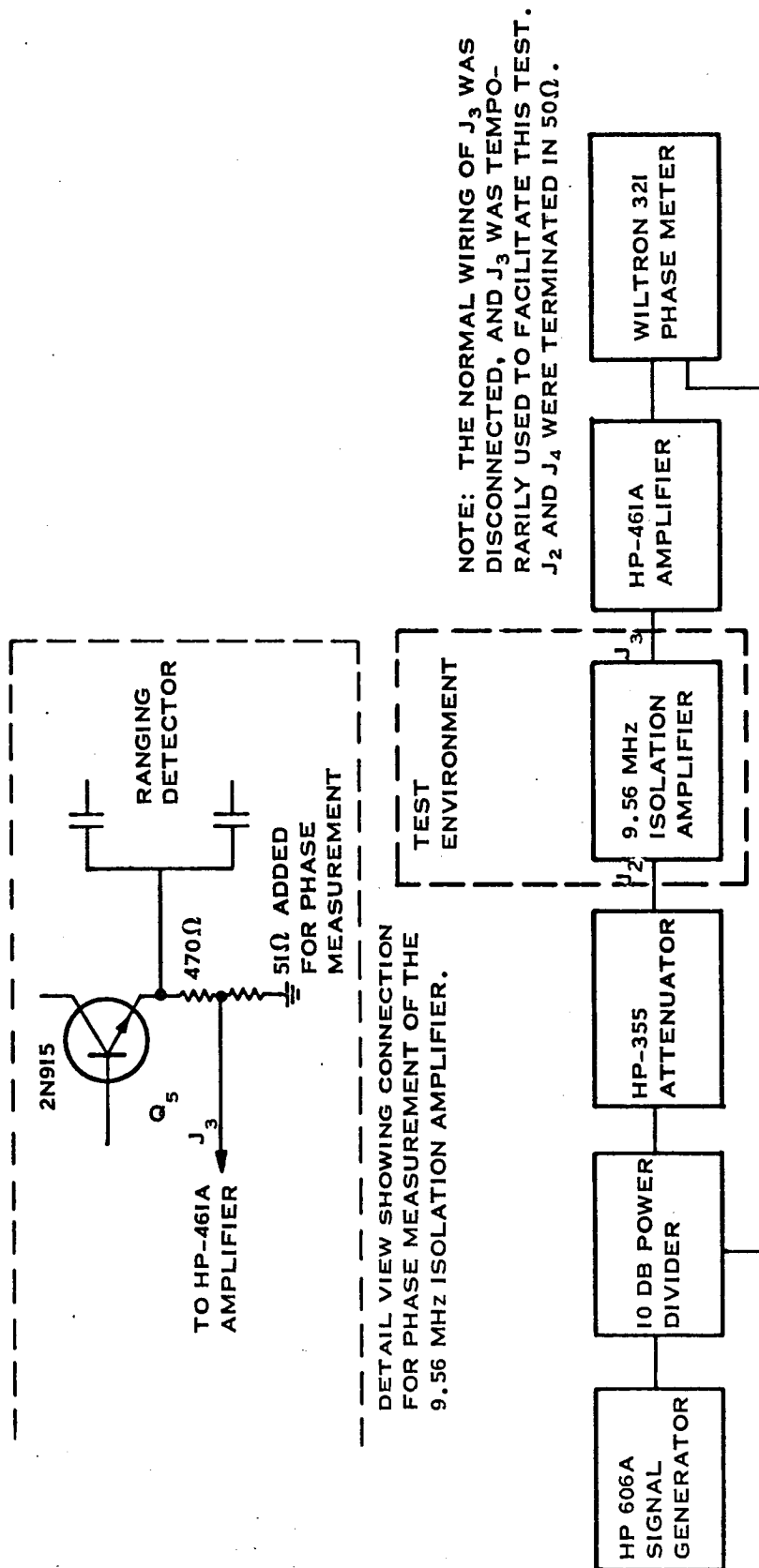


Figure 3.2.1-12 Block Diagram of the Test Setup for the Phase Response of the 9.56 MHz Stages of the 9.56 MHz Isolation Amplifier.

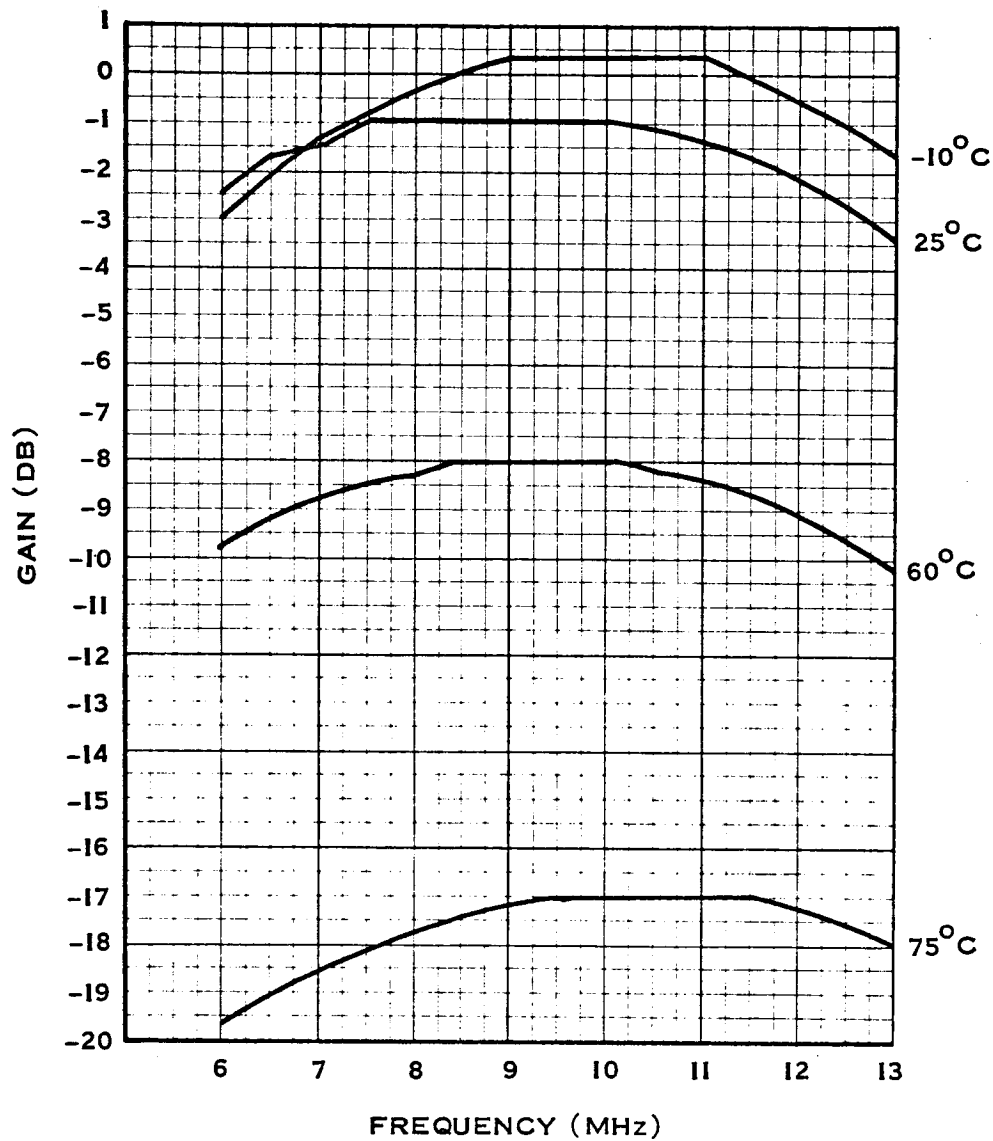


Figure 3.2.1-13 Amplitude Response of the 9.56 MHz Stages of the 9.56 MHz Isolation Amplifier at Several Temperatures.

The Gain Specification is ± 3 db Over the Temperature Range of -10°C to $+75^{\circ}\text{C}$.

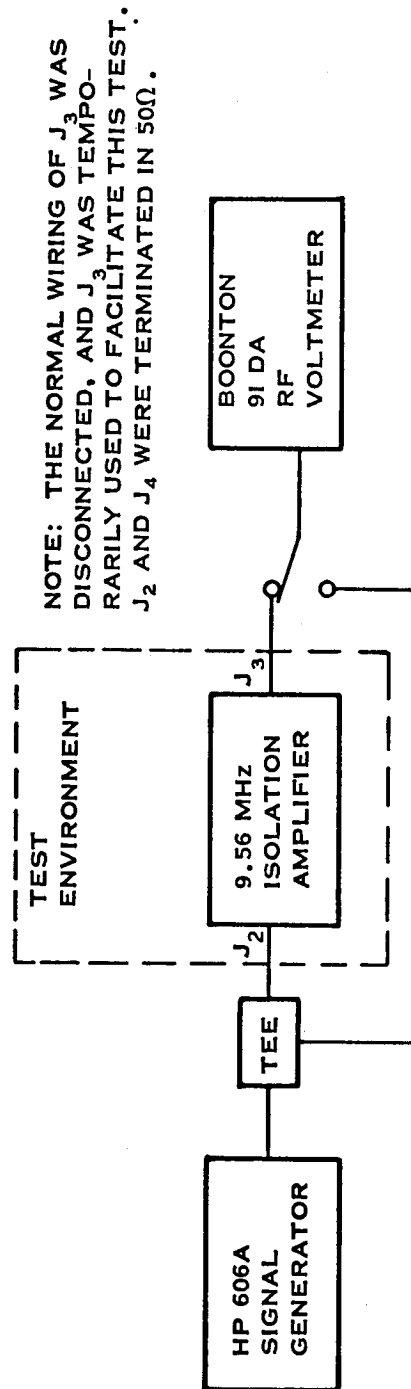
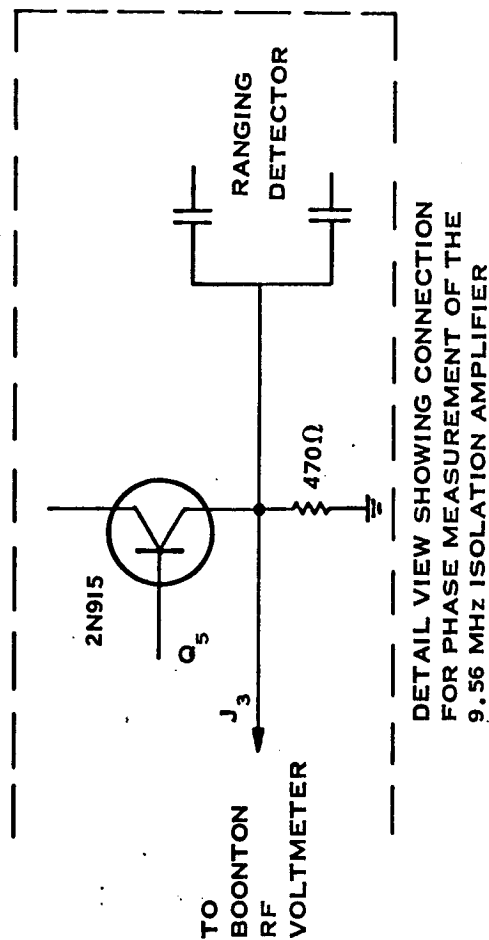


Figure 3.2.1-14 Block Diagram of the Test Setup for the Amplitude Response of the 9.56 MHz Stages of the 9.56 MHz Isolation Amplifier.

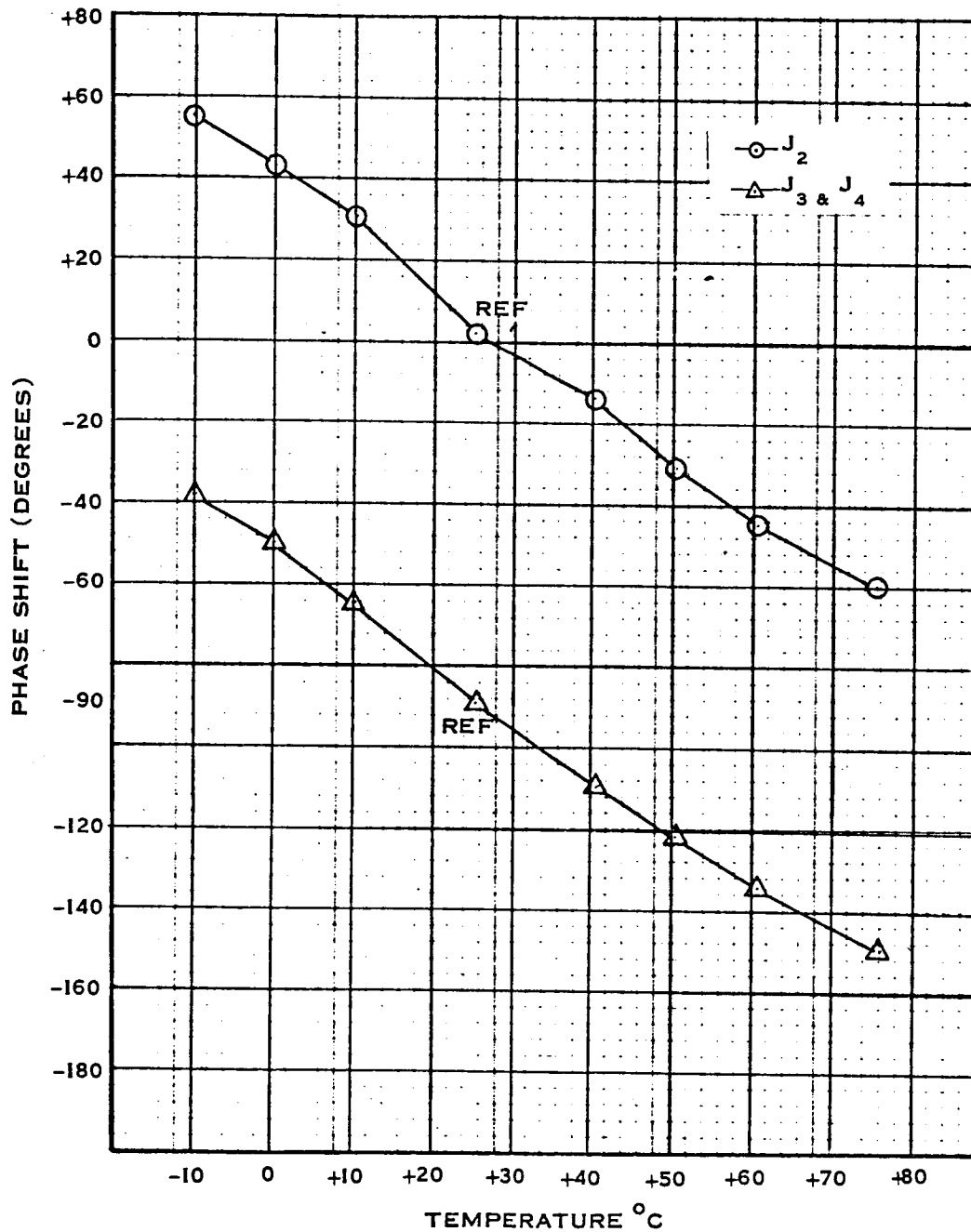


Figure 3.2.1-15 Phase Shift vs. Temperature Response of the Frequency Divider Module.

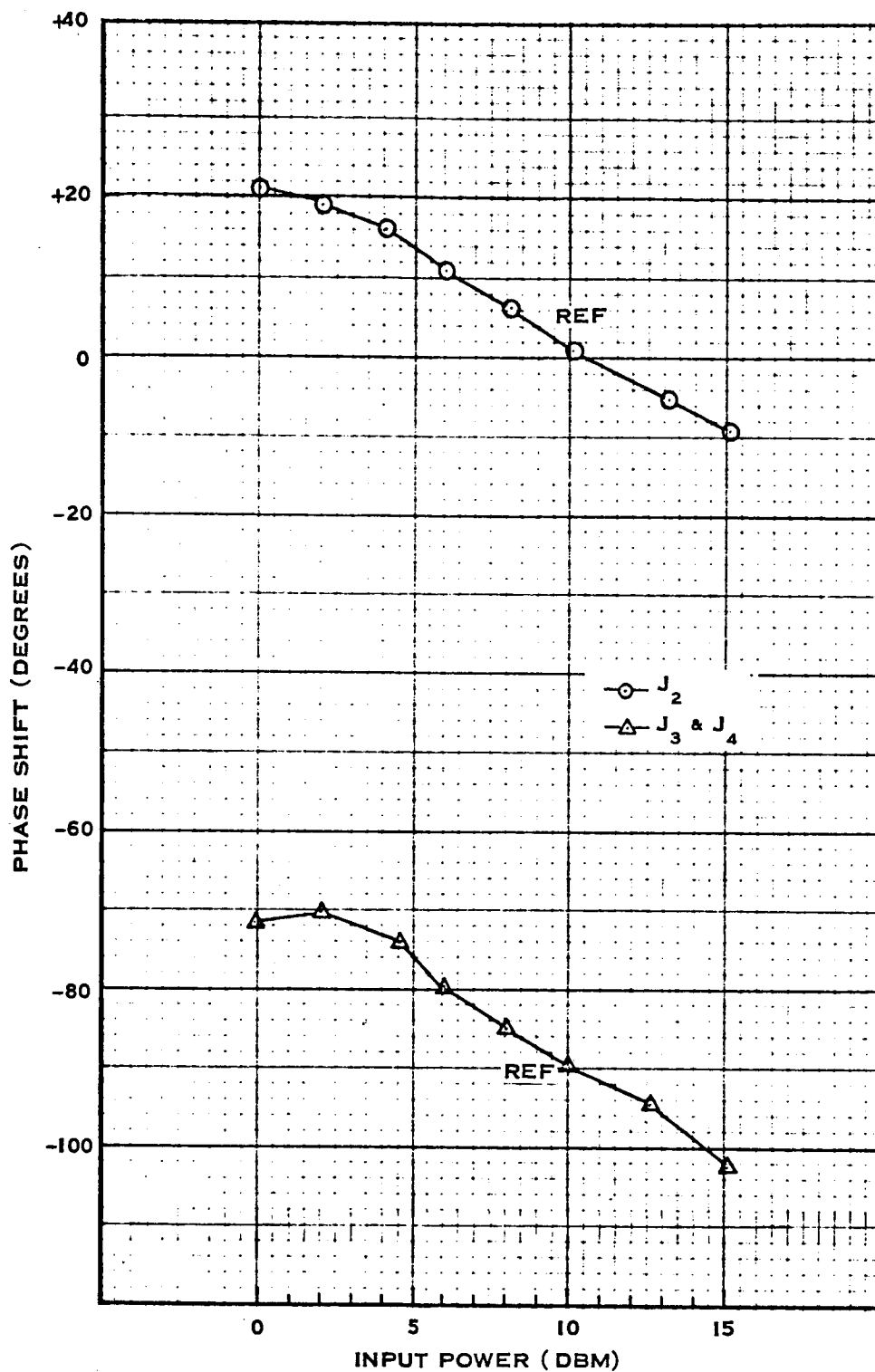


Figure 3.2.1-16 Phase Shift vs. Input Power Response of the Frequency Divider Module.

87

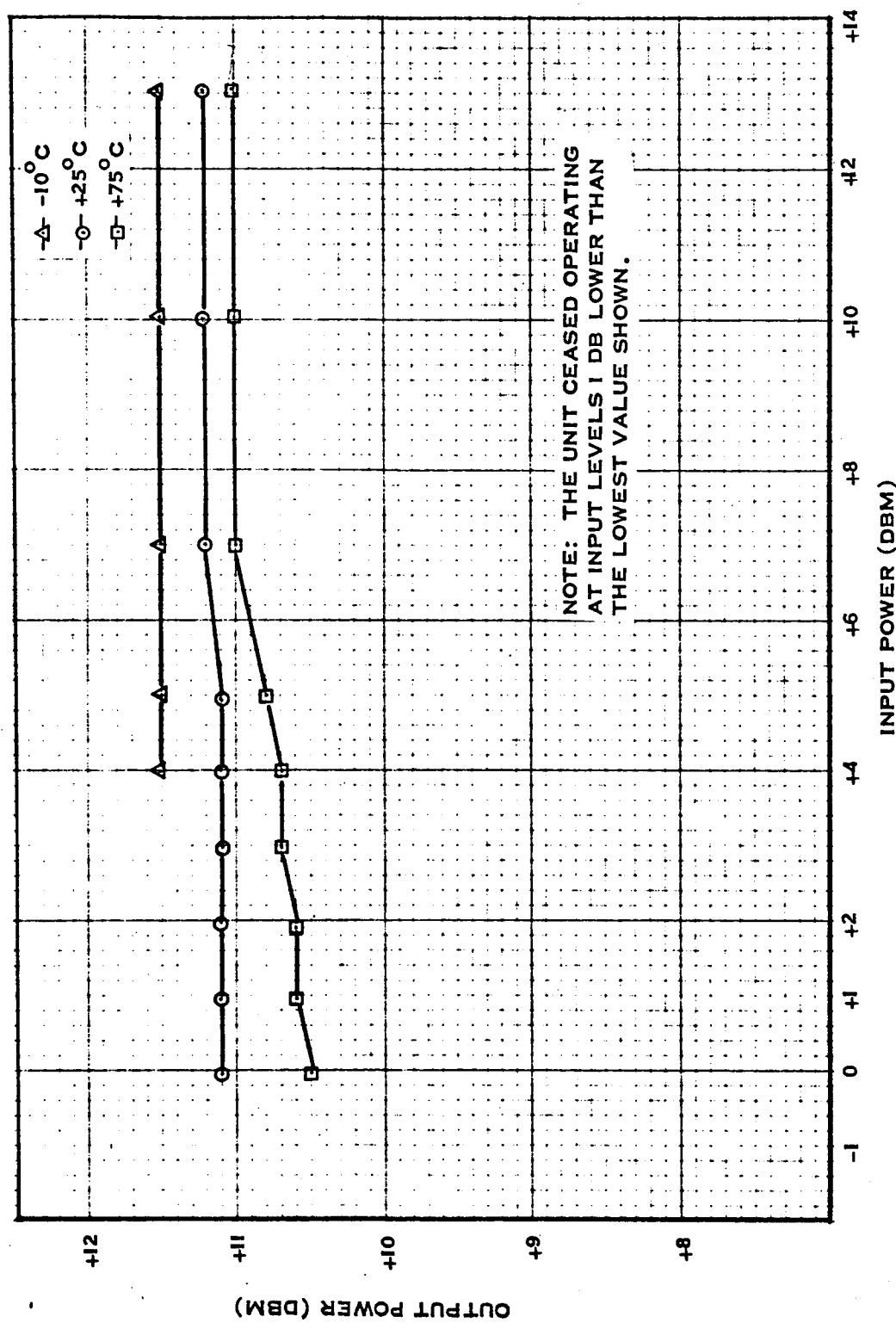


Figure 3.2.1-17 Power Output vs. Power Input of the Frequency Divider Module at the J2 Output ..

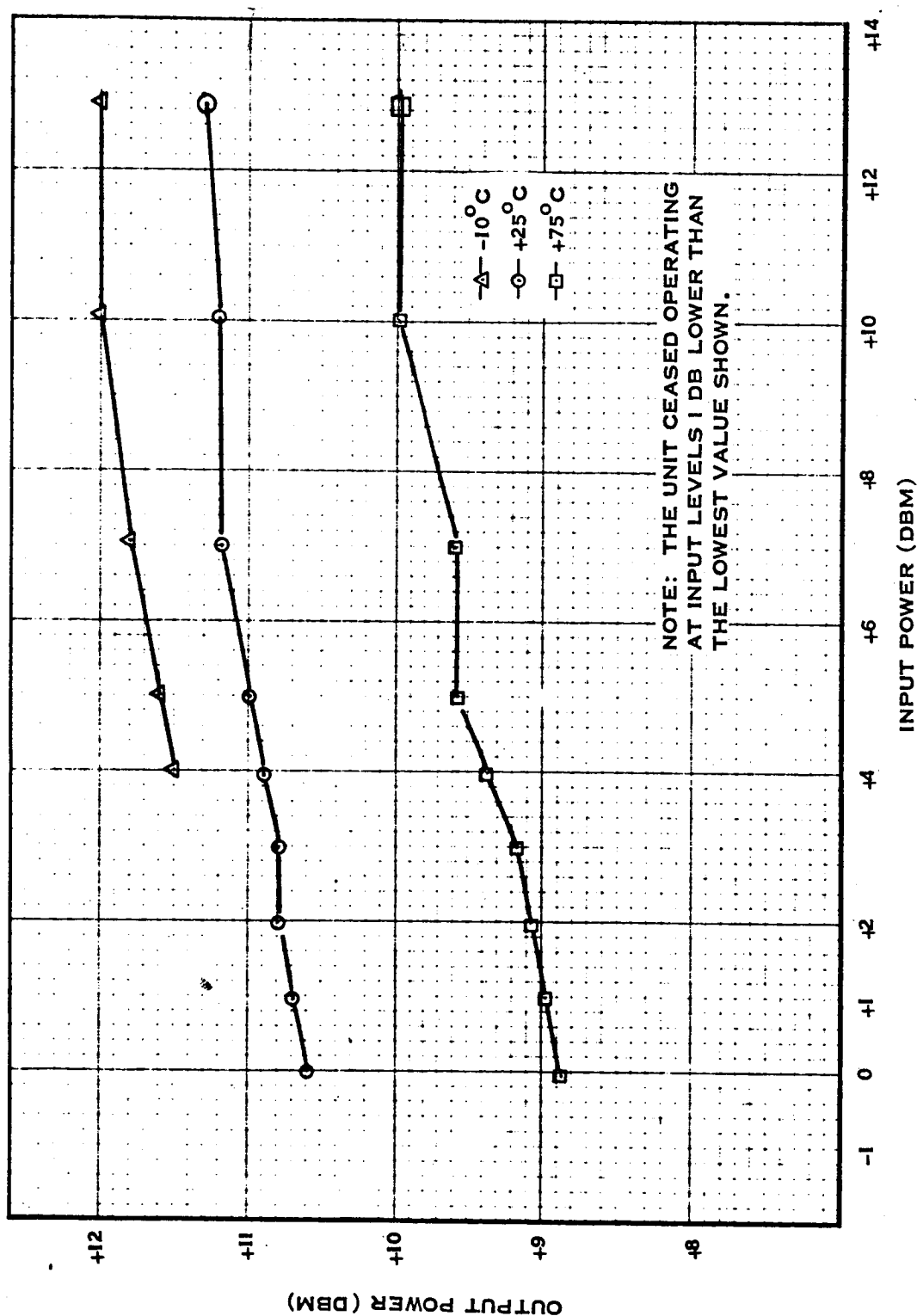


Figure 3.2.1-18 Power Output vs Power Input of the Frequency Divider Module at the J3 Output .

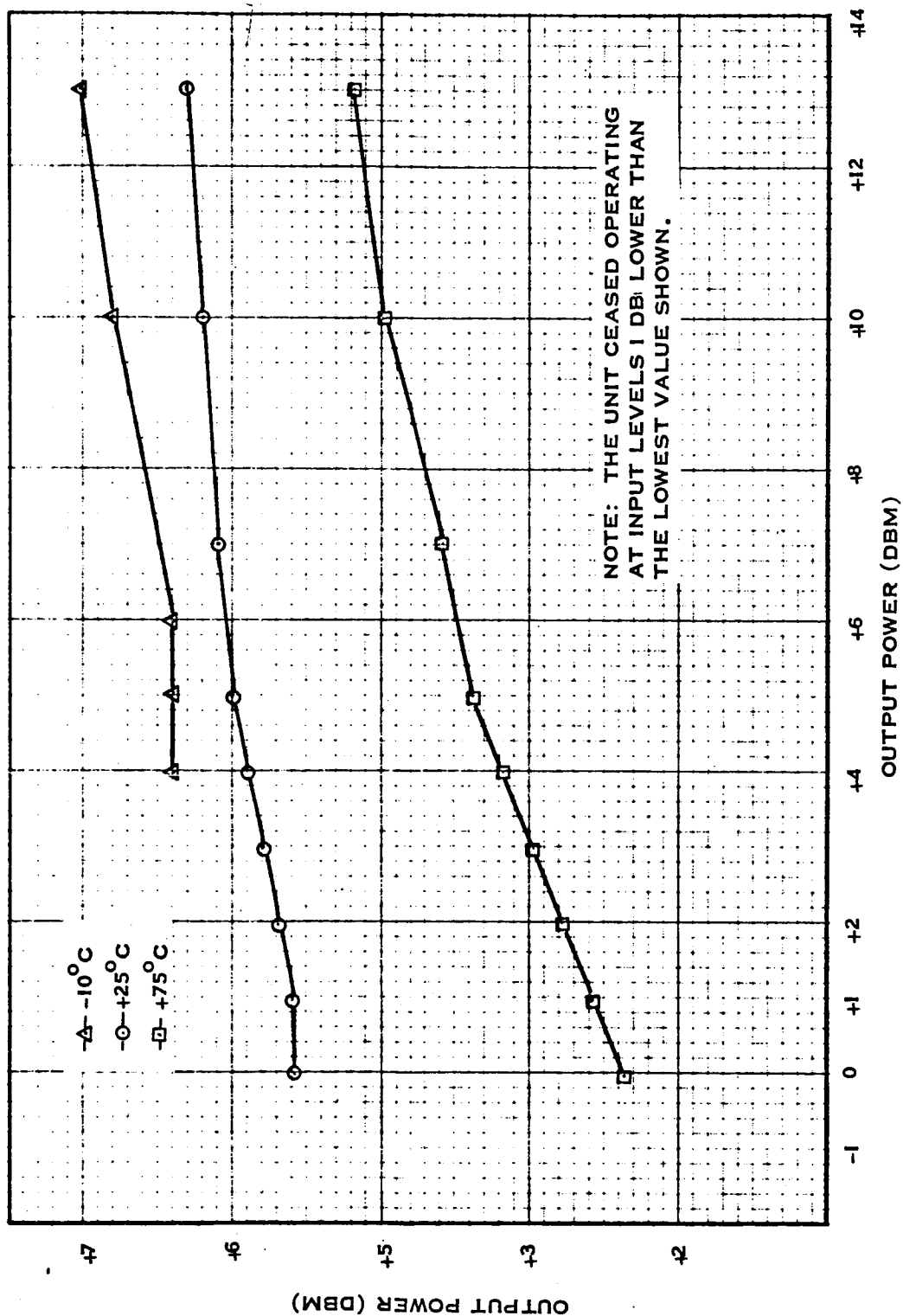


Figure 3.2.1-19 Power Output vs Power Input of the Frequency Divider Module at the J4 Output.

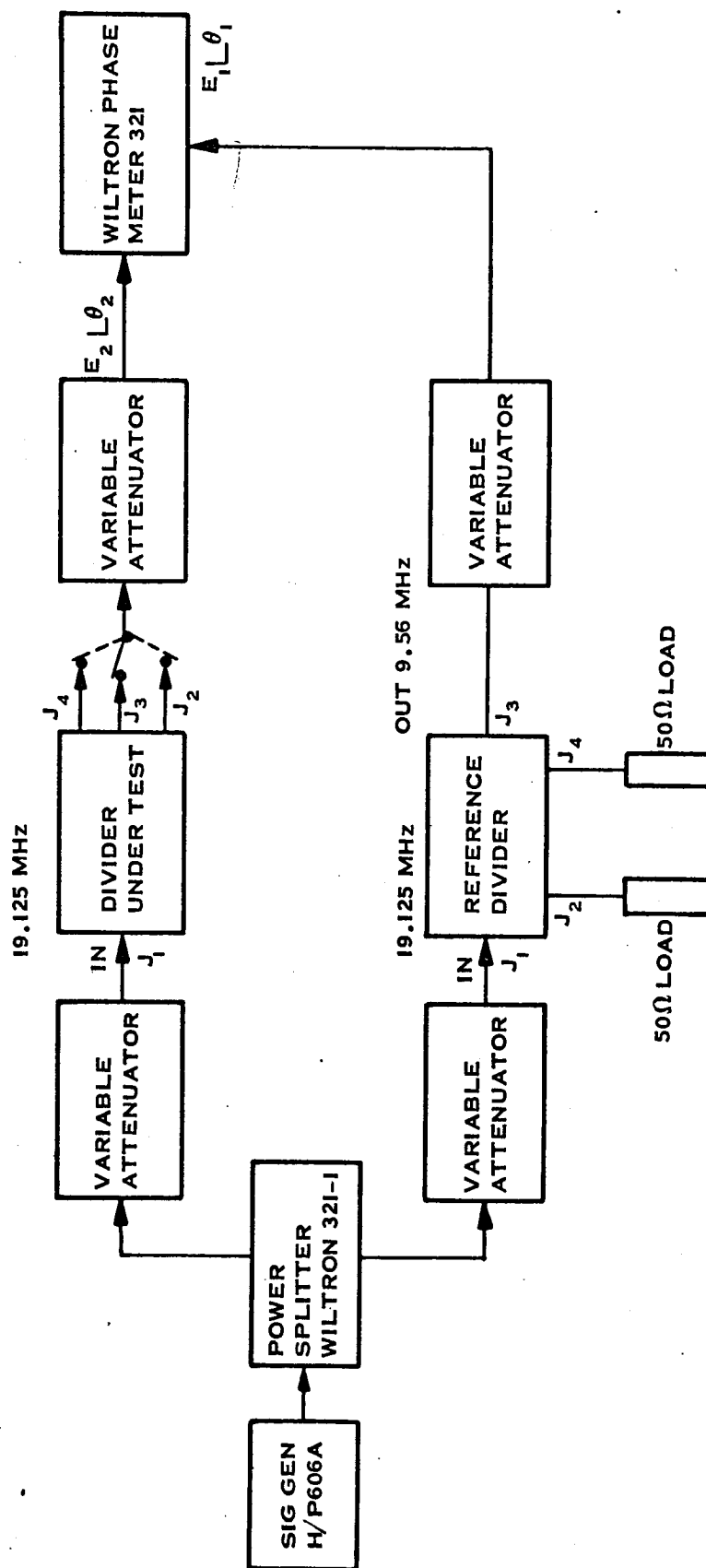
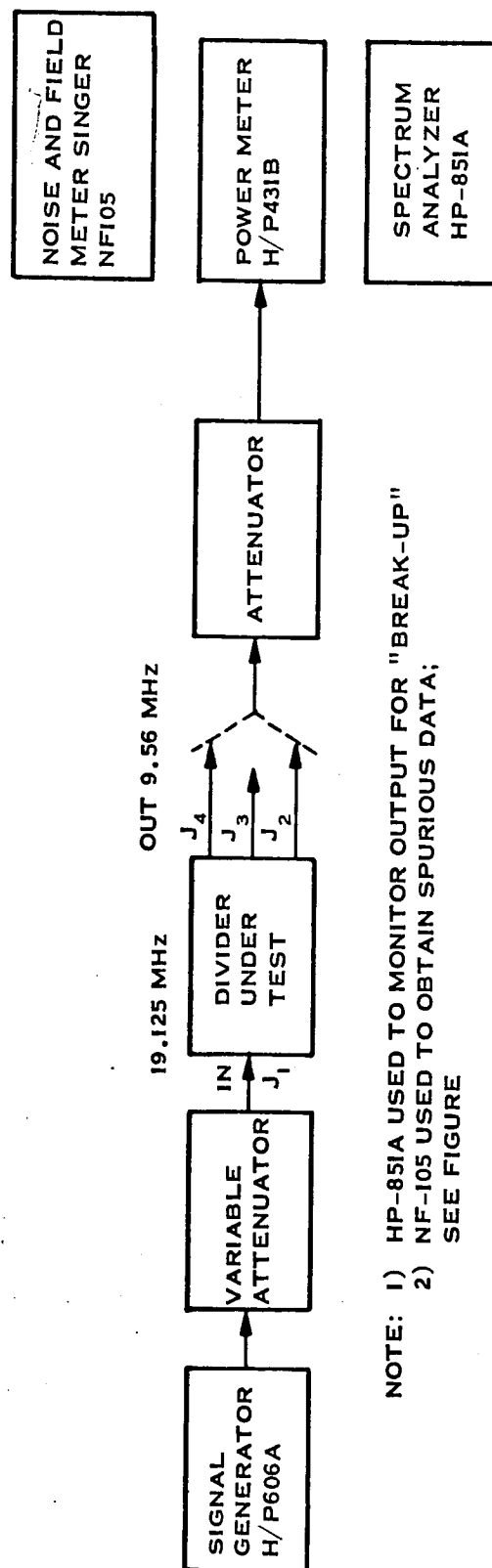


Figure 3.2.1-20 Phase Measurement Test Set Up Block Diagram



NOTE: 1) HP-851A USED TO MONITOR OUTPUT FOR "BREAK-UP"
 2) NF-105 USED TO OBTAIN SPURIOUS DATA;
 SEE FIGURE

Figure 3.2.1-21 Power Measurement Test Set Up
 Block Diagram

Output power is shown as a function of input power for the three Frequency Divider outputs in Figures 3.2.1-17 through 3.2.1-19. The test setup for the measurements made on the Frequency Divider is shown in Figures 3.2.1-20 and 3.2.1-21.

3.2.2 Special Tests

Tests were made to see what effect reflections from the 9.56 MHz Crystal Filter had on the signal from the 47.8 MHz I.F. output to the Isolation Amplifier. Figures 3.2.2-1 through 3.2.2-7 are all associated with these tests. Figures 3.2.2-1 and 3.2.2-2 show the amplitude and phase response measured by the test setup shown in Figure 3.2.2-3. These graphs are plotted with an unusual frequency scale to show a detailed view of small frequency deviations and at the same time permit plotting of large frequency deviations. These figures indicate that with ample isolation between the 47.8 MHz I.F. and the 9.56 MHz Crystal Filter, very little amplitude and phase variation would be observed in the ranging channel. Table 3.2.2-1 was made from the graphs of Figures 3.2.2-1 and 3.2.2-2 by considering a modulation frequency of 500 kHz.

Figure 3.2.2-4 shows the results of the test made in Figure 3.2.2-5. This test was a normal ranging delay test of the transponder with the phase of the reference to the ranging phase detector as the independent parameter. Figure 3.2.2-4 shows that the slope of the curve of ranging delay vs reference phase can be greatly reduced by isolating the 9.56 MHz crystal filter from the 47.8 MHz I.F. output to the Isolation Amplifier between an isolated and non-isolated 9.56 MHz crystal filter.

Figures 3.2.2-8 through 3.2.2-10 show the effects on ranging delay due to miscellaneous factors. Figure 3.2.2-8 shows the effect on ranging delay due to diminishing the signal level to various modules. It should be noted that in modules such as the Video Amplifier, the attenuator reduces signal and noise together thus maintaining a constant signal to noise ratio. Temperature variation of the transponder may change the signal to

noise level in some of the modules and therefore change the shape of some of these curves in actual operation. The signal level input to the modules shown is not expected to change nearly as much as the variations used in this test.

Figure 3.2.2-9 shows ranging delay variation as a function of several unrelated factors. Modulation level of the up-link signal is seen to have little effect on ranging delay. Power supply variations on the other hand have a significant effect. During all testing here, the transponder power supply voltages were monitored and observed to be very well regulated. However, this test shows the importance of well regulated supplies being used in the space craft. The SPE offset curve was measured by changing the test transmitter frequency to obtain a SPE. Because of this change in frequency, the curve shown is not just an effect of SPE as would occur if the transponder VCO crystal changed nominal frequency with temperature, due to the phase characteristic of the crystal filter.

Figures 3.2.2-11 through 3.2.2-18 are concerned with spurious levels within certain modules. Figures 3.2.2-11 through 3.2.2-14 are shown mostly to illustrate the effect of the $f/4$ harmonic of the VCO frequency when it is generated in the Frequency Divider module. It can be seen that when generated, the $f/4$ harmonic goes right through the video amplifier with considerable amplitude. The important thing to note from the spectrum pictures is that the magnitude of the $f/4$ harmonic was within the JPL specification limits for the Frequency Divider module. It was discovered that careful tuning would eliminate this harmonic. It was noted that the ranging delay vs ranging detector reference phase (Figure 3.2.2-4) showed an increase in slope of 1.5 times with the $f/4$ harmonic being generated (this result is not graphed). Thus, the importance of tuning the Frequency Divider not to within spurious specification, but for the elimination of any $f/4$ harmonics can be seen.

Figures 3.2.2-16 through 3.2.2-18 show the output spectrum of the Frequency Divider with the $f/4$ harmonic eliminated. Figure 3.2.2-15 is a time waveform of the video signal at the output of the Isolation Amplifier when the Frequency Divider was not generating a $f/4$ harmonic. Note here the large 9.56 MHz component of the video waveform even during normal operation of the transponder.

Figure 3.2.2-19 is presented as extra useful information. It shows how the harmonic content of the 9.56 MHz I.F. varies as a function of reduced input signal.

A 400 MHz spurious (not shown) was also observed but did not appear to affect the various test results. A slight power supply voltage reduction was noticed to eliminate this spurious.

95

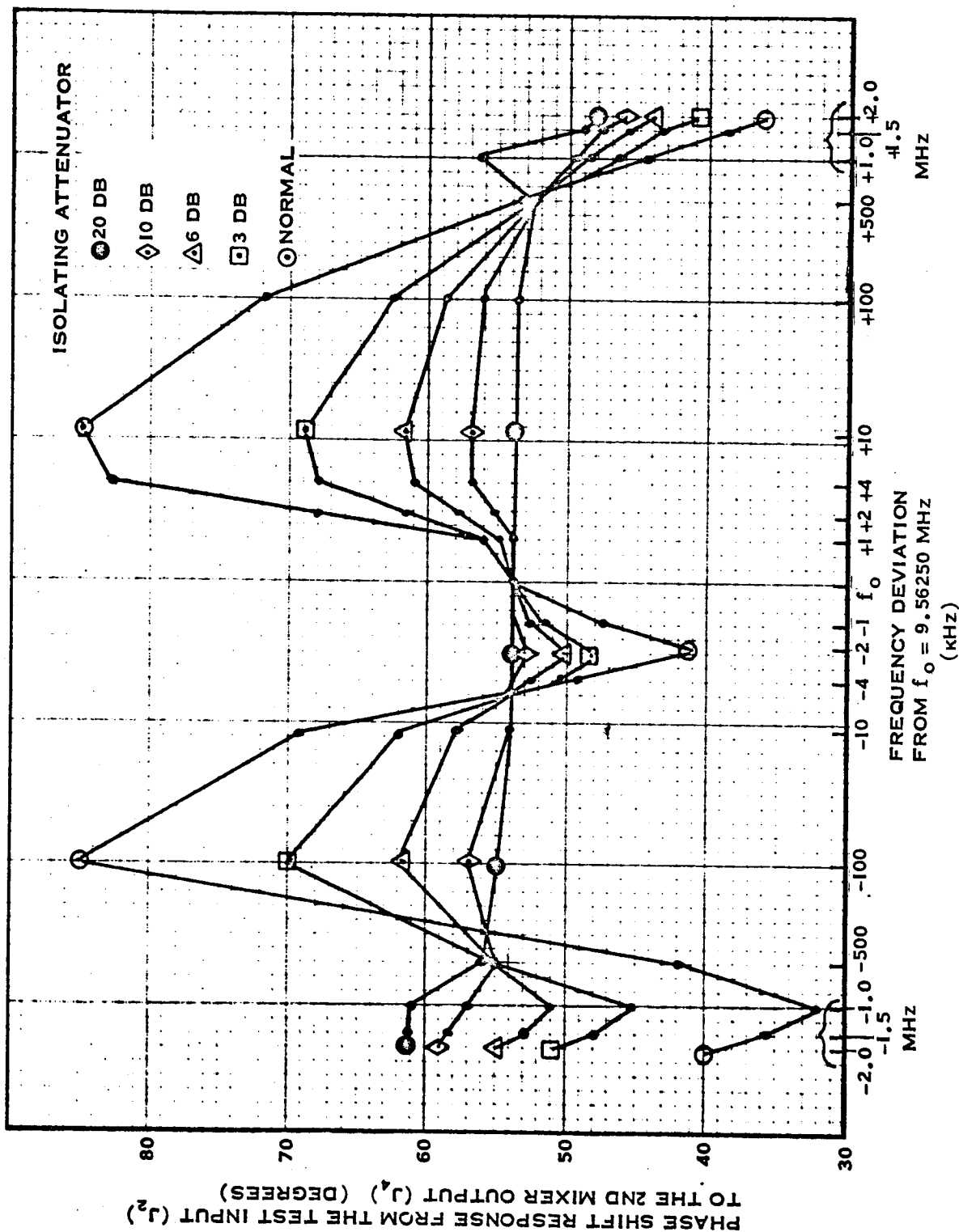


Figure 3.2.2-1 Phase Shift Response at the 2nd Mixer Output as a Function of Crystal Filter Driving Point Impedance Interaction.

96

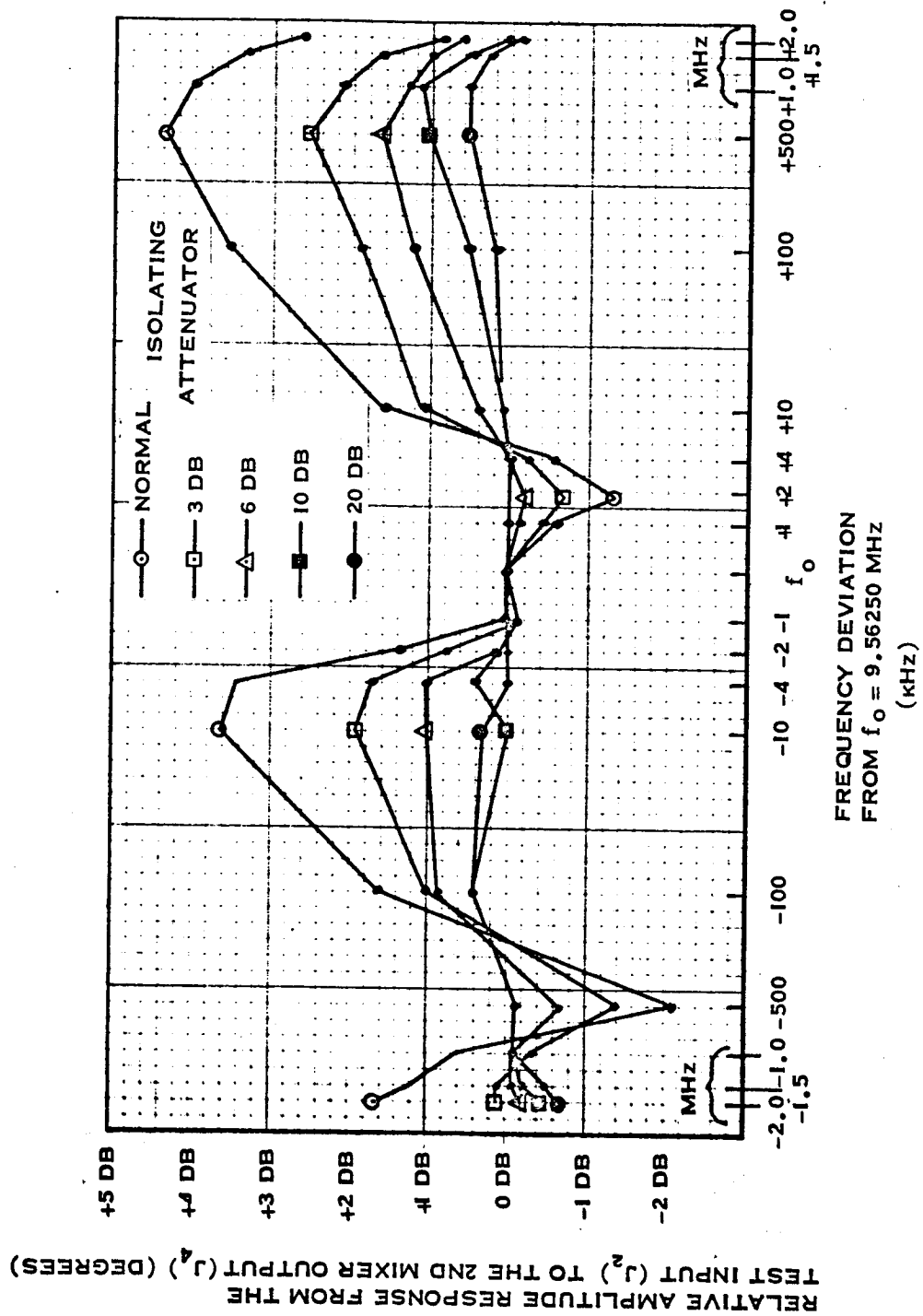


Figure 3.2.2-2 Amplitude Response at the 2nd Mixer Output as a Function of Crystal Filter Driving Point Impedance Interaction.

97

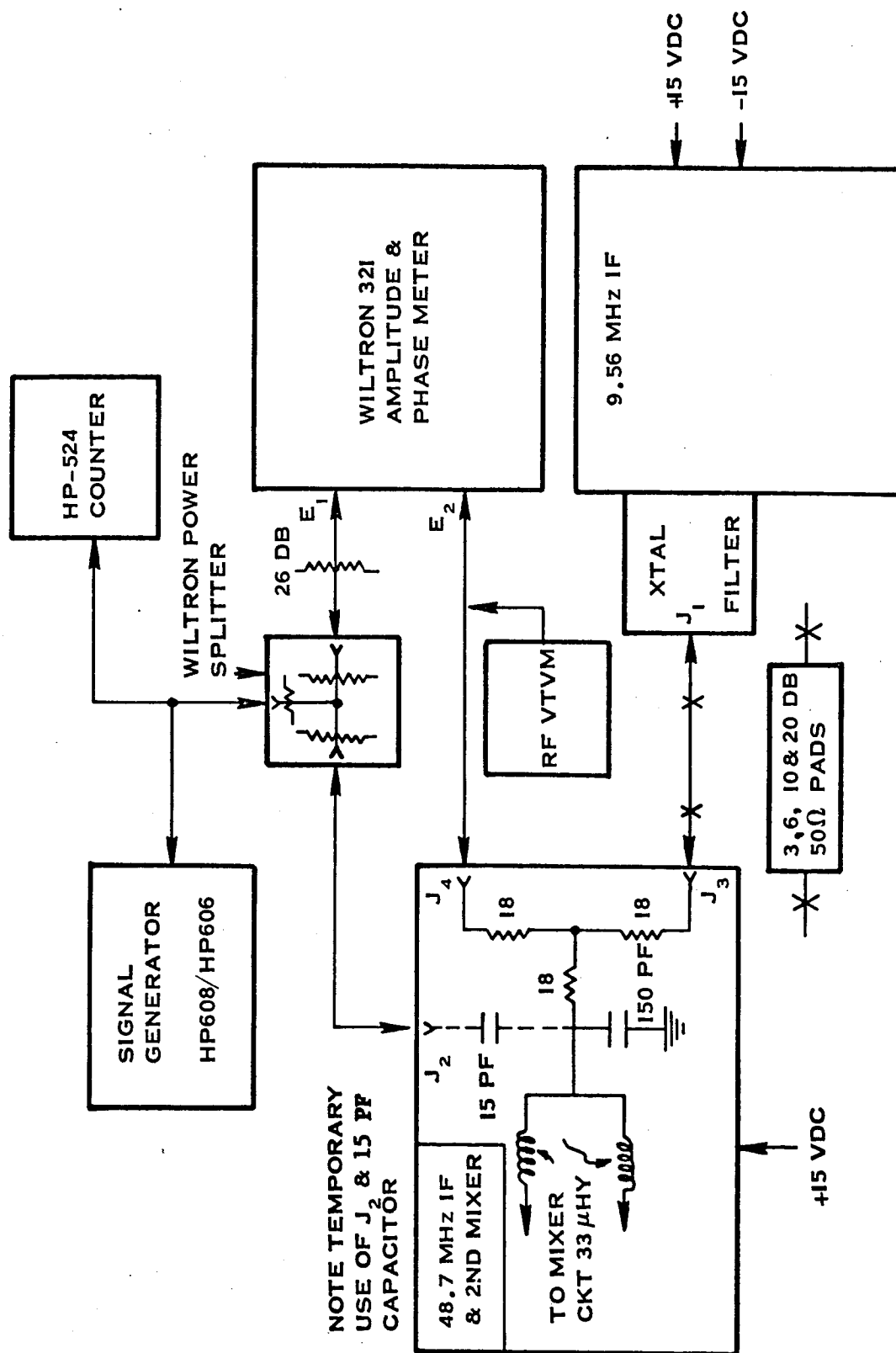


Figure 3.2.2-3 Phase and Relative Amplitude, 2nd Mixer to the ISO Amp Input

TABLE 3.2.2-1

EXPECTED RANGING SIGNAL SPECTRUM DISTORTION
DUE TO CRYSTAL FILTER INTERACTION

<u>SIDEBAND FREQUENCY</u>	<u>AMPLITUDE (db)</u>	<u>PHASE (Deg)</u>
$f_o - 4 f_m$	+1.6	-14
$f_o - 3 f_m$	+1.2	-18
$f_o - 2 f_m$	+0.6	-22
$f_o - f_m$	-2.1	-10
f_o	0.0	0
$f_o + f_m$	+4.3	0
$f_o + 2 f_m$	+4.0	-9
$f_o + 3 f_m$	+3.3	-15
$f_o + 4 f_m$	+2.6	-18

NOTES:

1. f_m = ranging modulation frequency
2. f_o = 9.56250 MHz
3. The AMPLITUDE and PHASE values shown above were taken directly from Figures 3.2.2-1 and 2. The ranging spectrum is altered from normal values by the values shown.

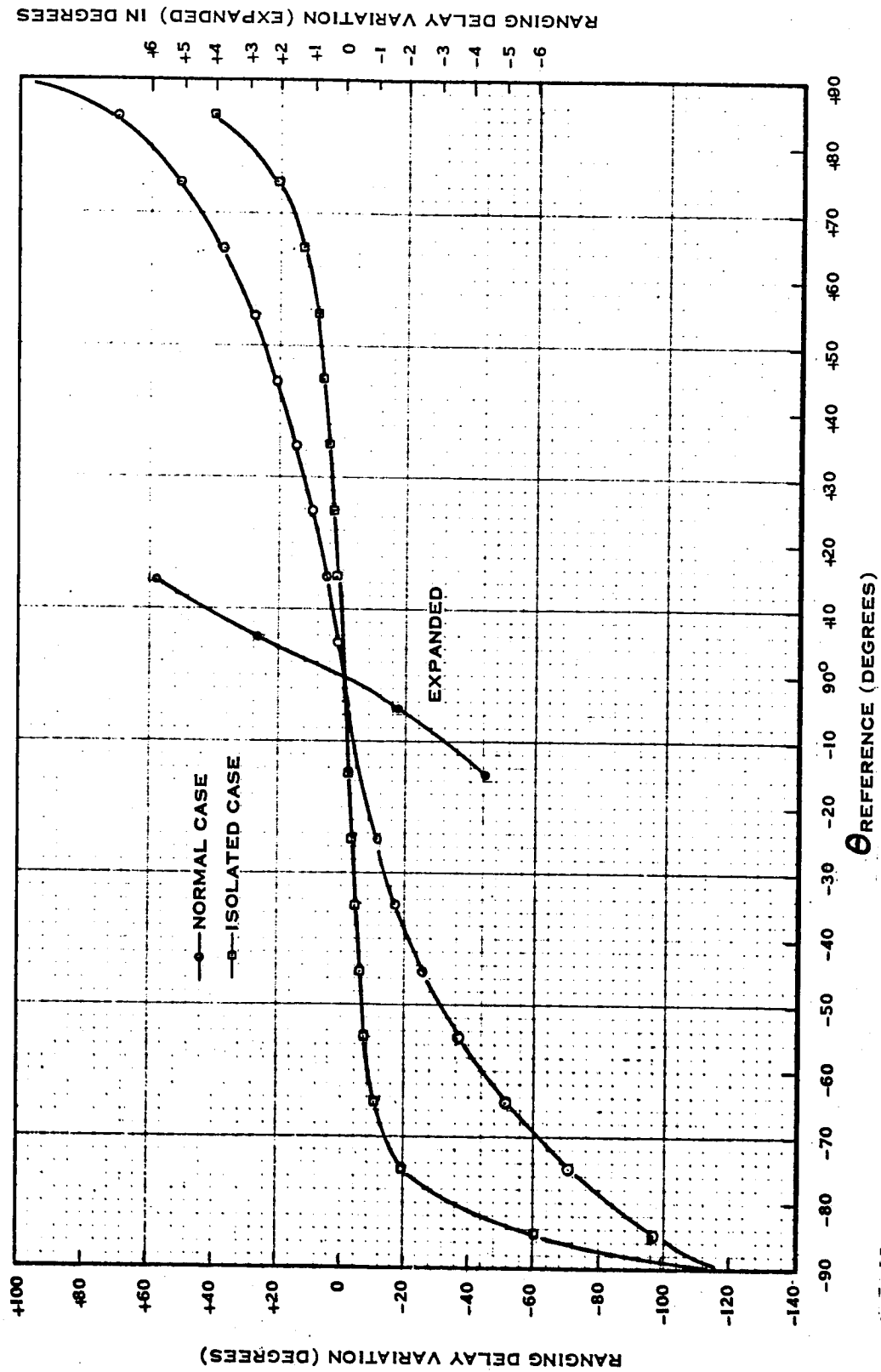


Figure 3.2.2-4 Ranging Delay Variation vs. Phase Shift of the Reference to the Ranging Phase Detector.

100

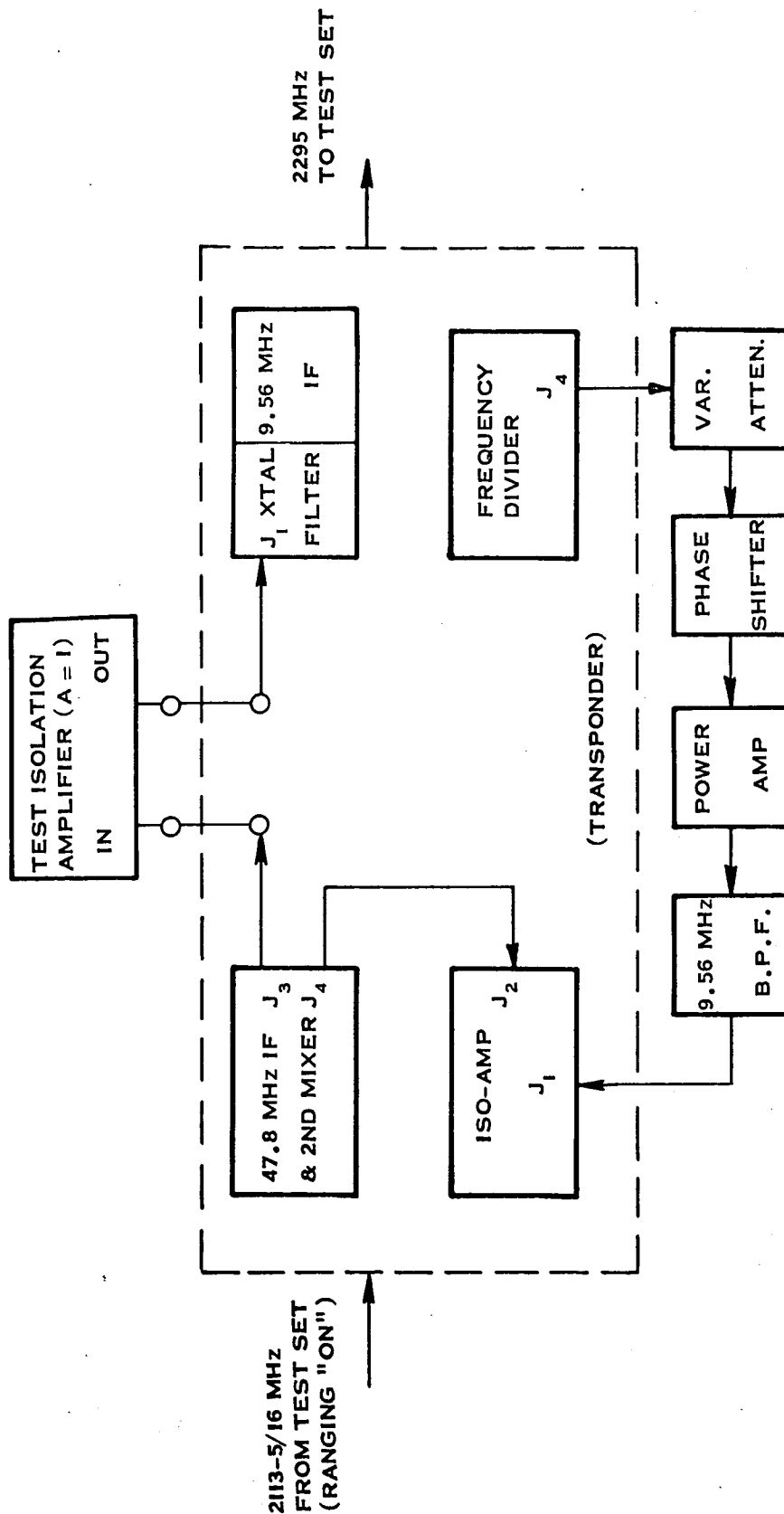
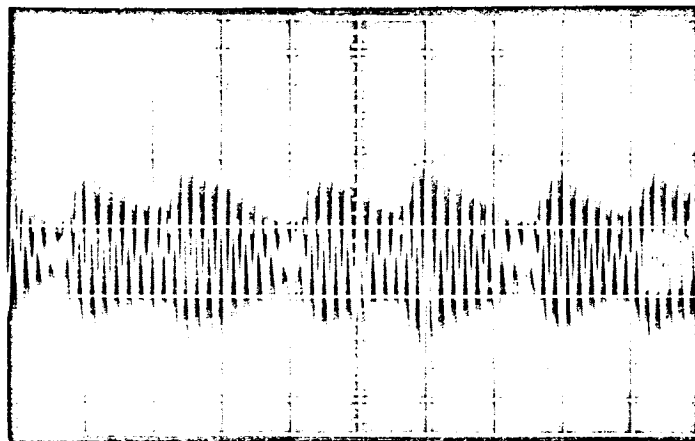
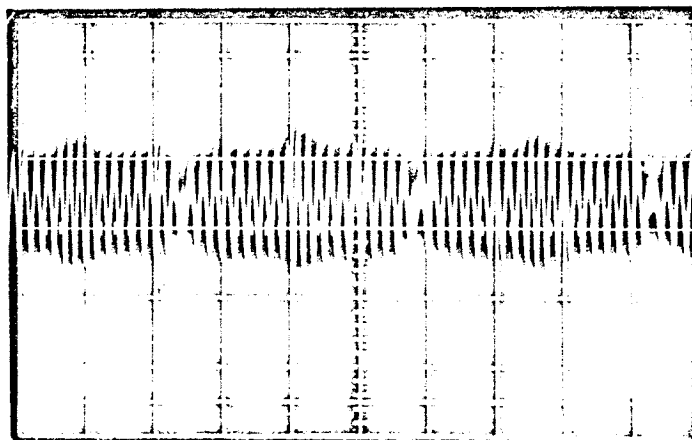


Figure 3.2.2-5 Ranging Delay Variation vs. Reference Phase Shift Test Block Diagram



SCALE: 498 KHz \approx 17 MINOR DIVISIONS

Figure 3.2.2-6a Normal 9.56 MHz Ranging Signal



SCALE: 498 KHz \approx 17 MINOR DIVISIONS

Figure 3.2.2-6b 9.56 MHz Ranging Signal with Crystal Filter
Isolated by 20 db Pad

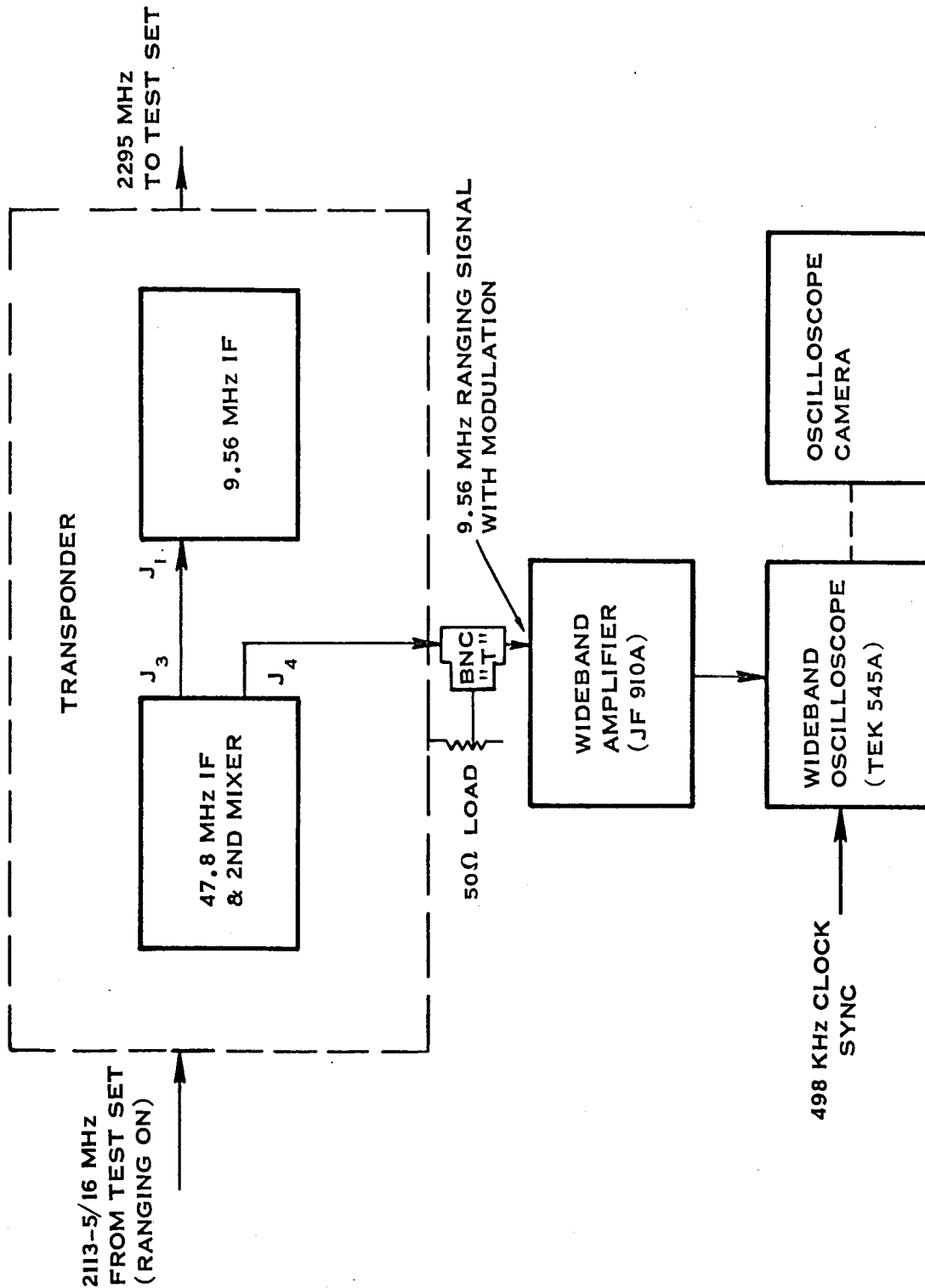


Figure 3.2.2-7 Crystal Filter Interaction Waveform Photograph Test Set Up

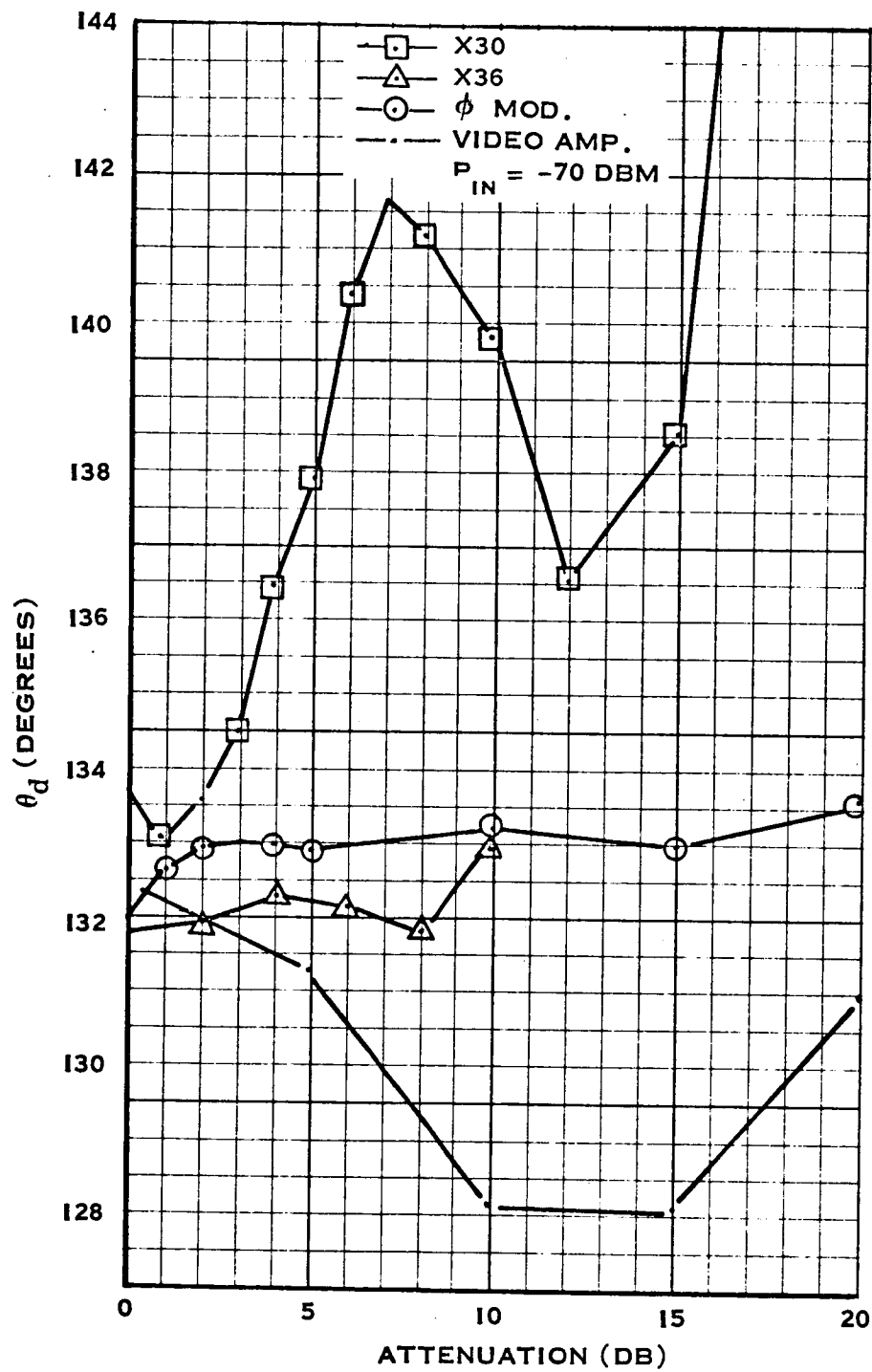


Figure 3.2.2-8 Ranging Phase Delay vs Attenuation of the Normal Power Levels to The Modules Indicated.

104

TR-DA1522A

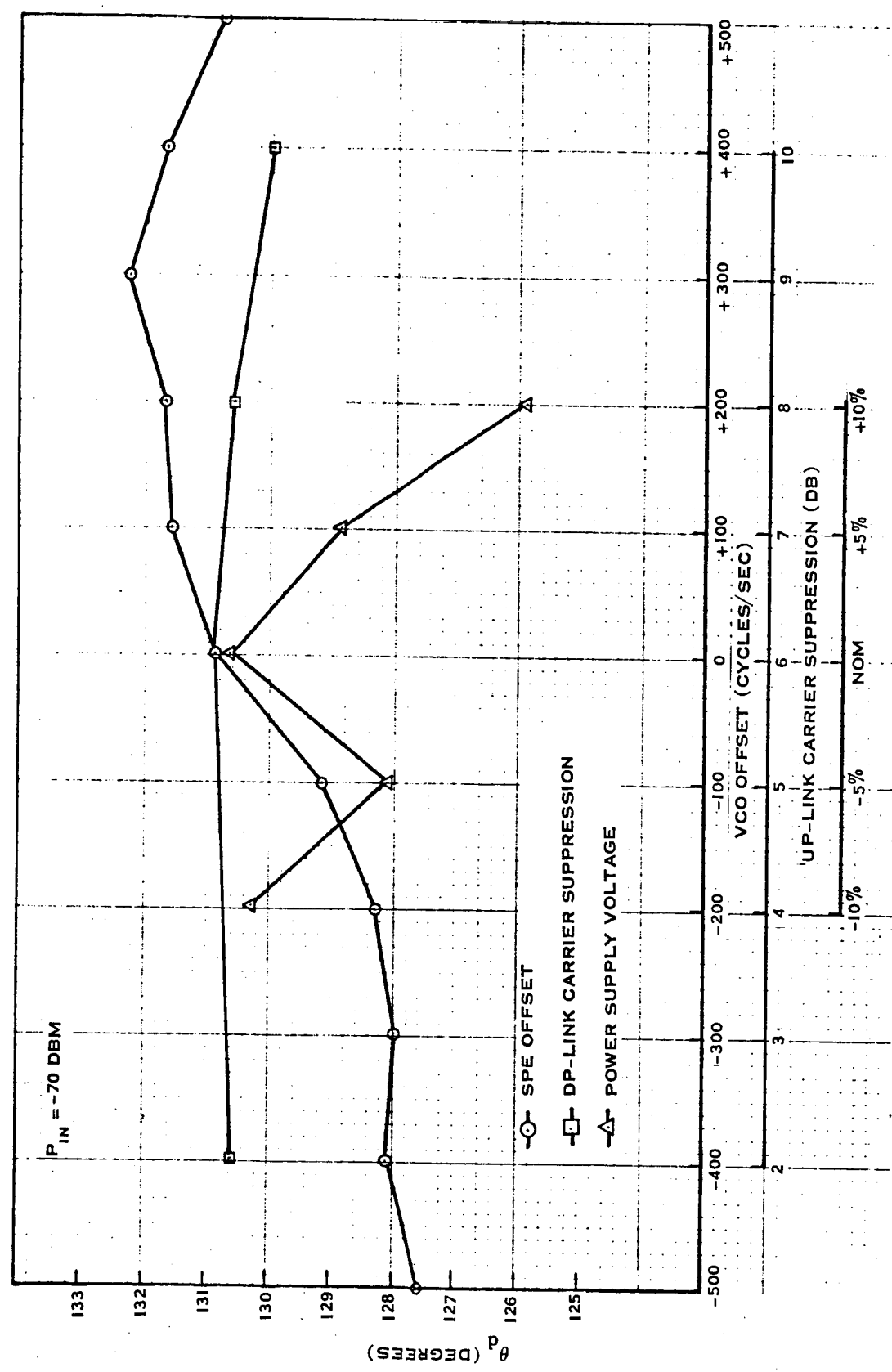


Figure 3.2.2-9 Ranging Phase Delay Versus Selected Parameters .

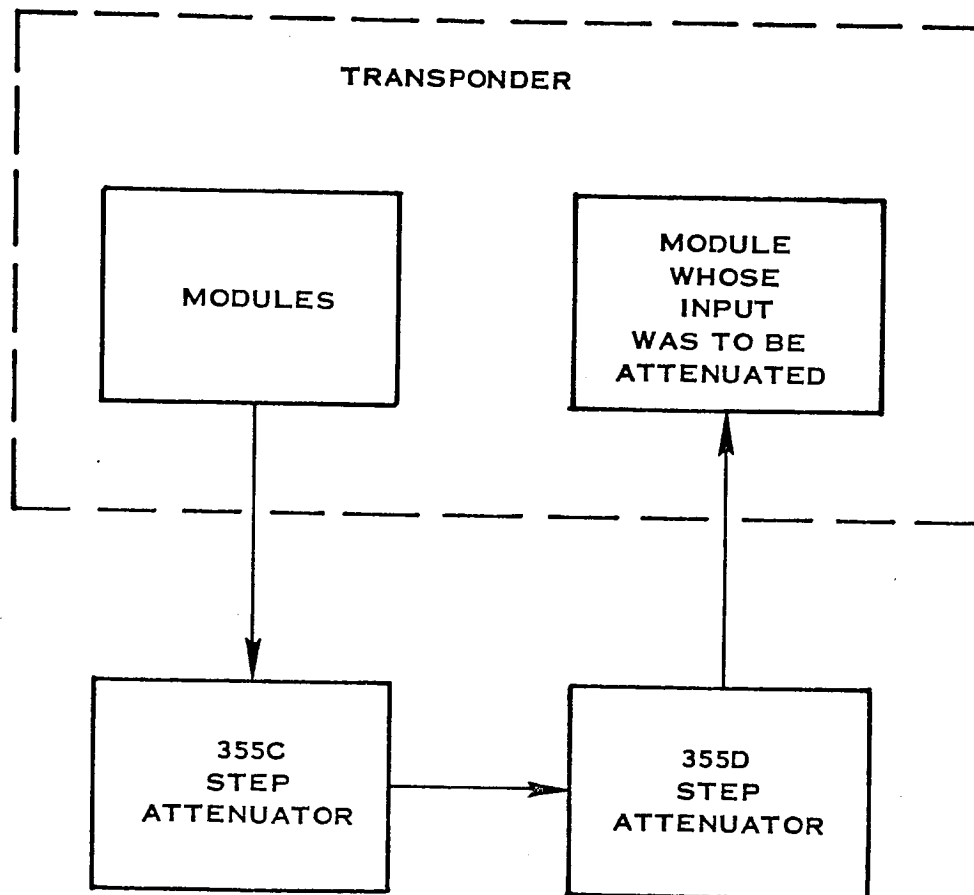


Figure 3.2.2-10 Method of attenuating the Input to Modules to Determine Delay vs Input to Various Modules

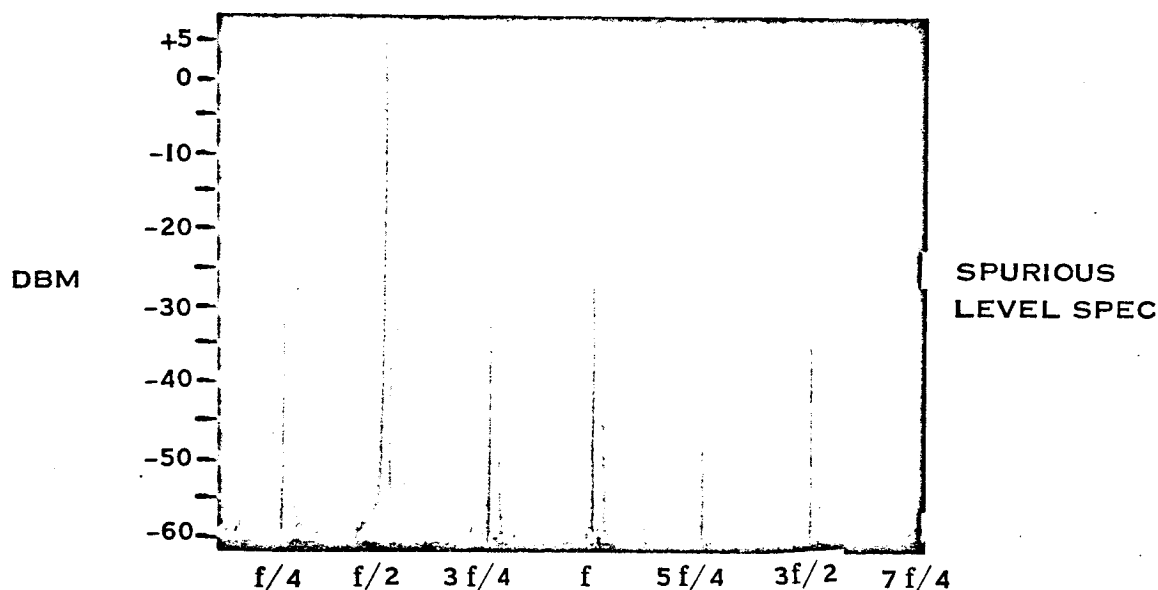


Figure 3.2.2-11 Spectrum of $X_{1/2}$ output to Ranging Phase Detector Due to improper alignment of the Frequency Divider. Note the presence of $\frac{1}{2}F$ harmonics. The harmonic content, although troublesome, met JPL Specs. ($F = 19.125$ MHz)

Note 1: The alignment condition became evident after changing the number of turns of one of the toroids in the divider, so as to achieve stable divider action over the required temperature range. The unit was subsequently aligned so that the $f/4$ harmonics were absent.

Note 2: All the data shown in this report is for the properly aligned case, except where so noted.

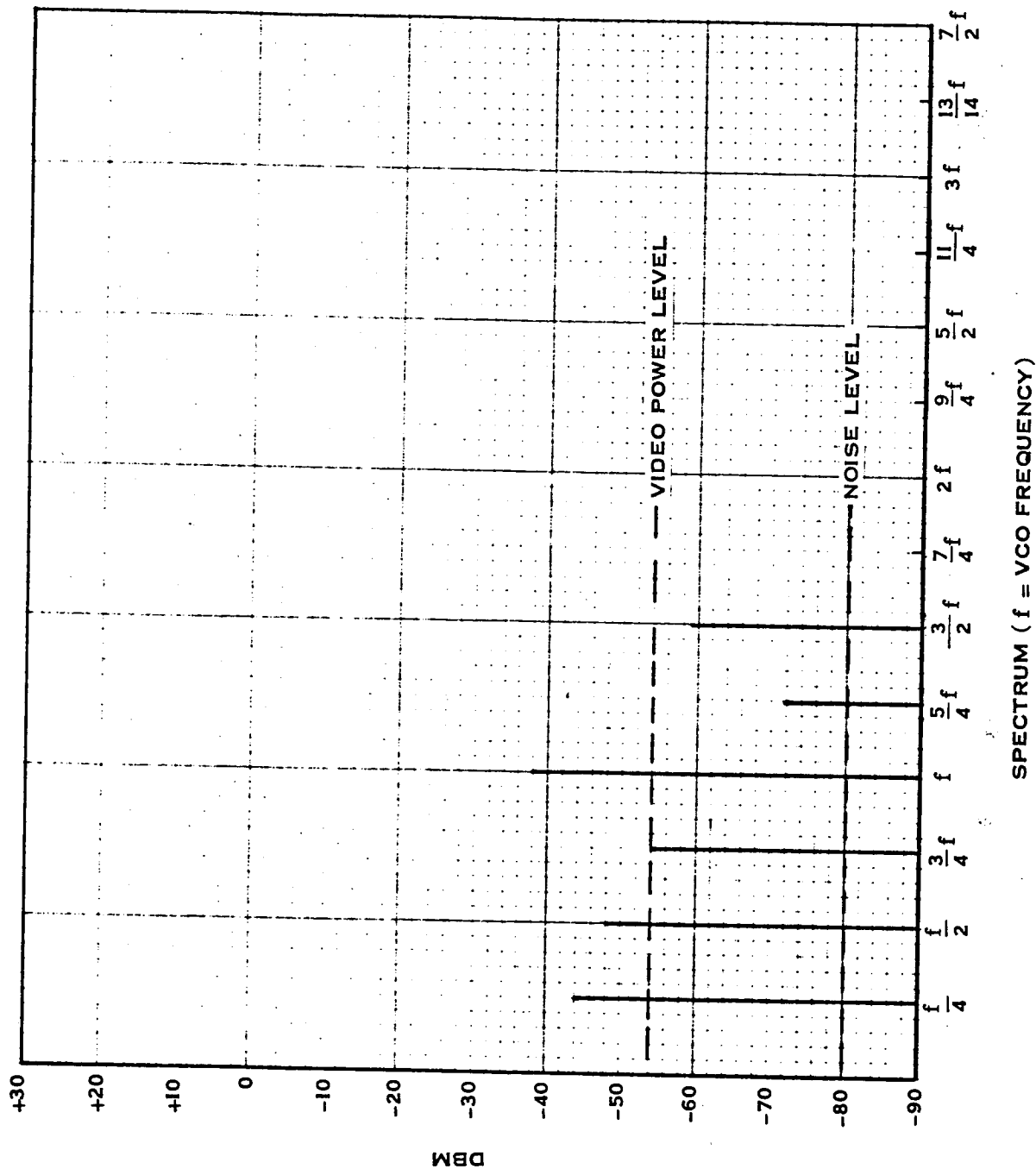


Figure 3.2.2-12 Ranging Phase Detector Output Ranging; Signal Off.

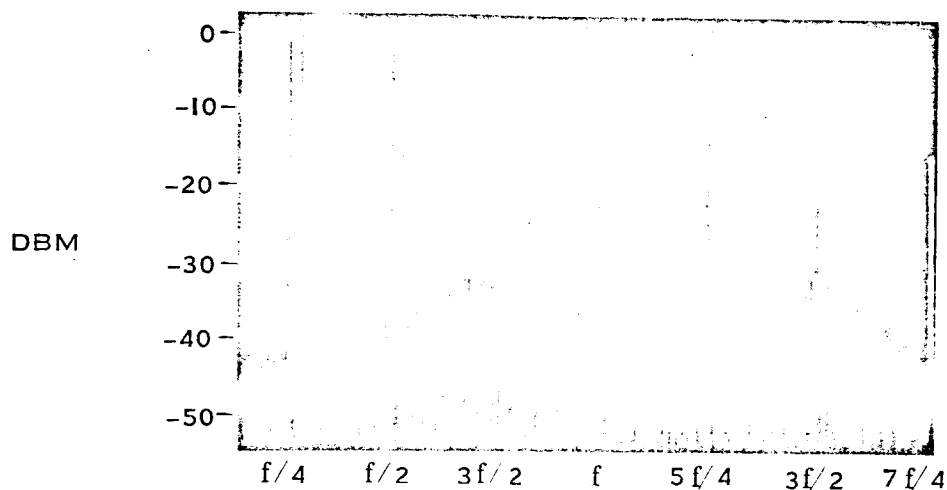


Figure 3.2.2-13a Video Amplifier Spectrum with Transponder Locked to Test Set but no Modulation; $X_{1/2}$ Improperly aligned

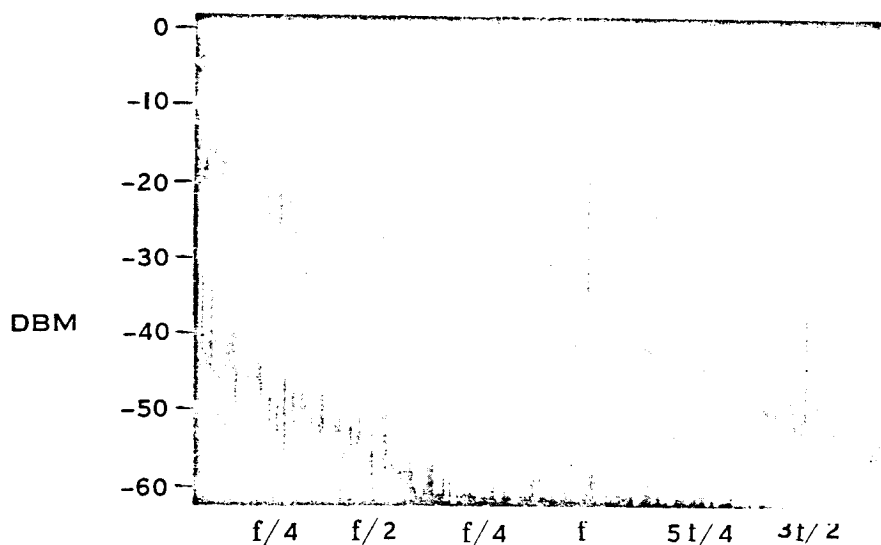


Figure 3.2.2-13b Same as above but with 9.56 MHz Filter Inserted in REF to ISO AMP in Transponder.

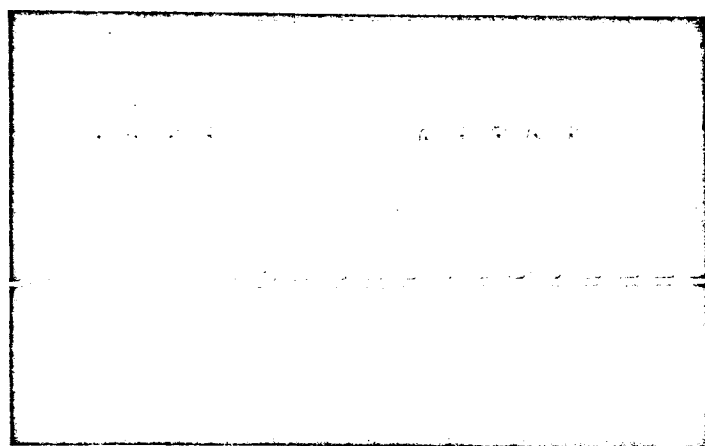


Figure 3.2.2-14a Output of Video Amplifier. Scope Synced to 498 KHz Clock from Code Monitor Panel. $P_{in} = -70$ dbm, with $P_s = 9$ db. The $X\frac{1}{2}$ was Improperly Aligned; Note 4.78 MHz Content.

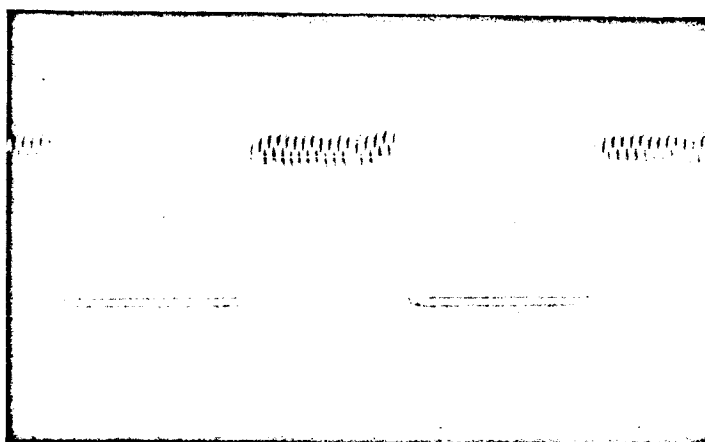


Figure 3.2.2-14b Same as above, but with 9.56 MHz B.P.F. in the Reference Leg of the Ranging Phase Detector.

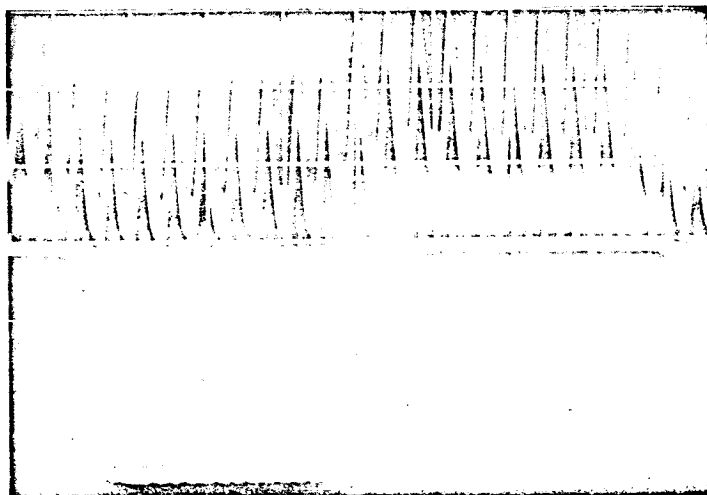


Figure 3.2.2-15 Upper Trace: Input to the Video Ampl.
Lower Trace: Output of the Video Ampl.
Condition: Normal

Note: The Photos are Intended to Show the Large 9.56 MHz Content Which is Normally Present at the Input to the Video Amplifier ($X\frac{1}{2}$ Properly Aligned).

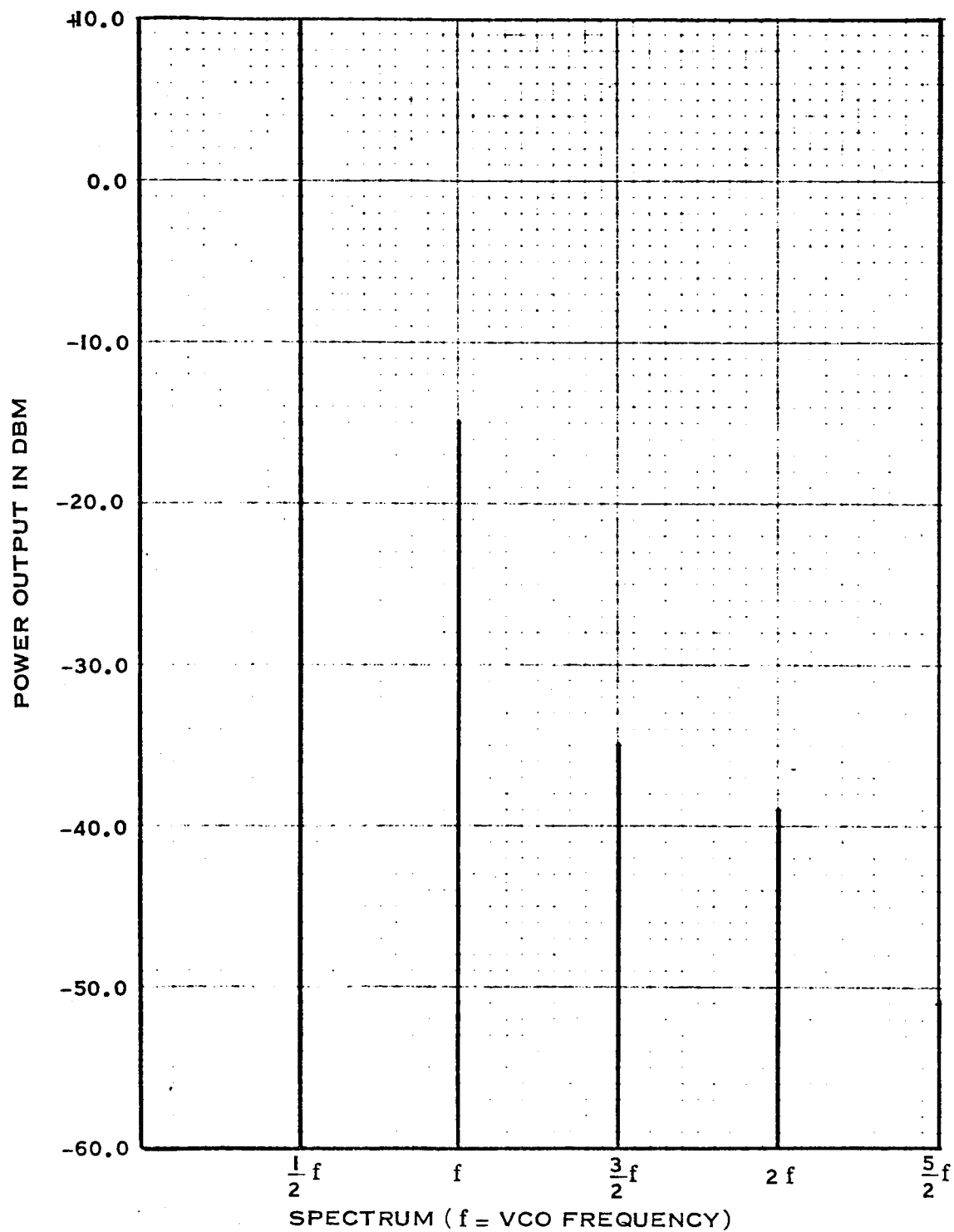


Figure 3.2.2-16 Frequency Divider. Frequency Spectrum For J₂ Output (AGC).

112

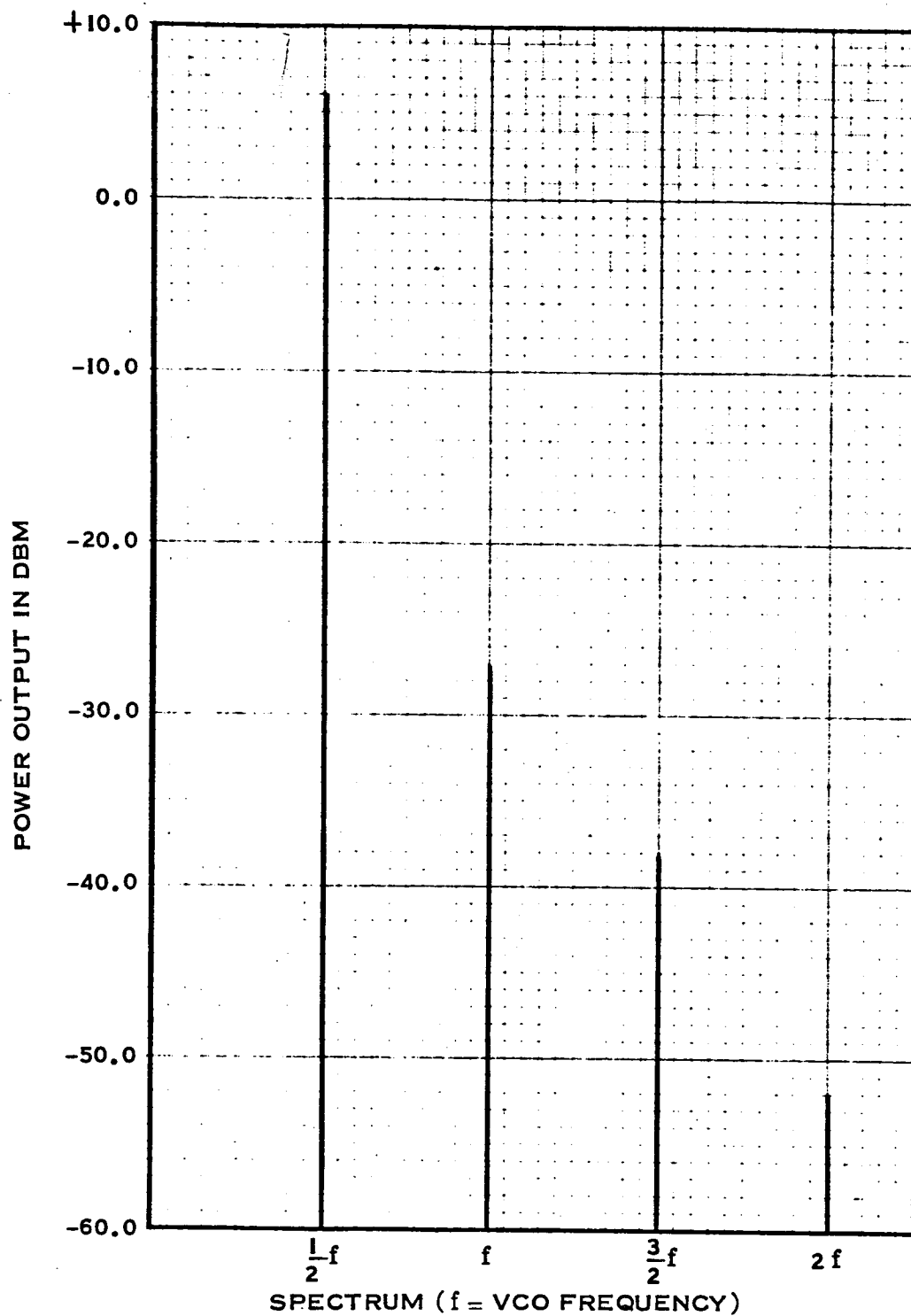


Figure 3.2.2-17

Frequency Divider. Frequency Spectrum For J₃ Output (Ø DET) .

113

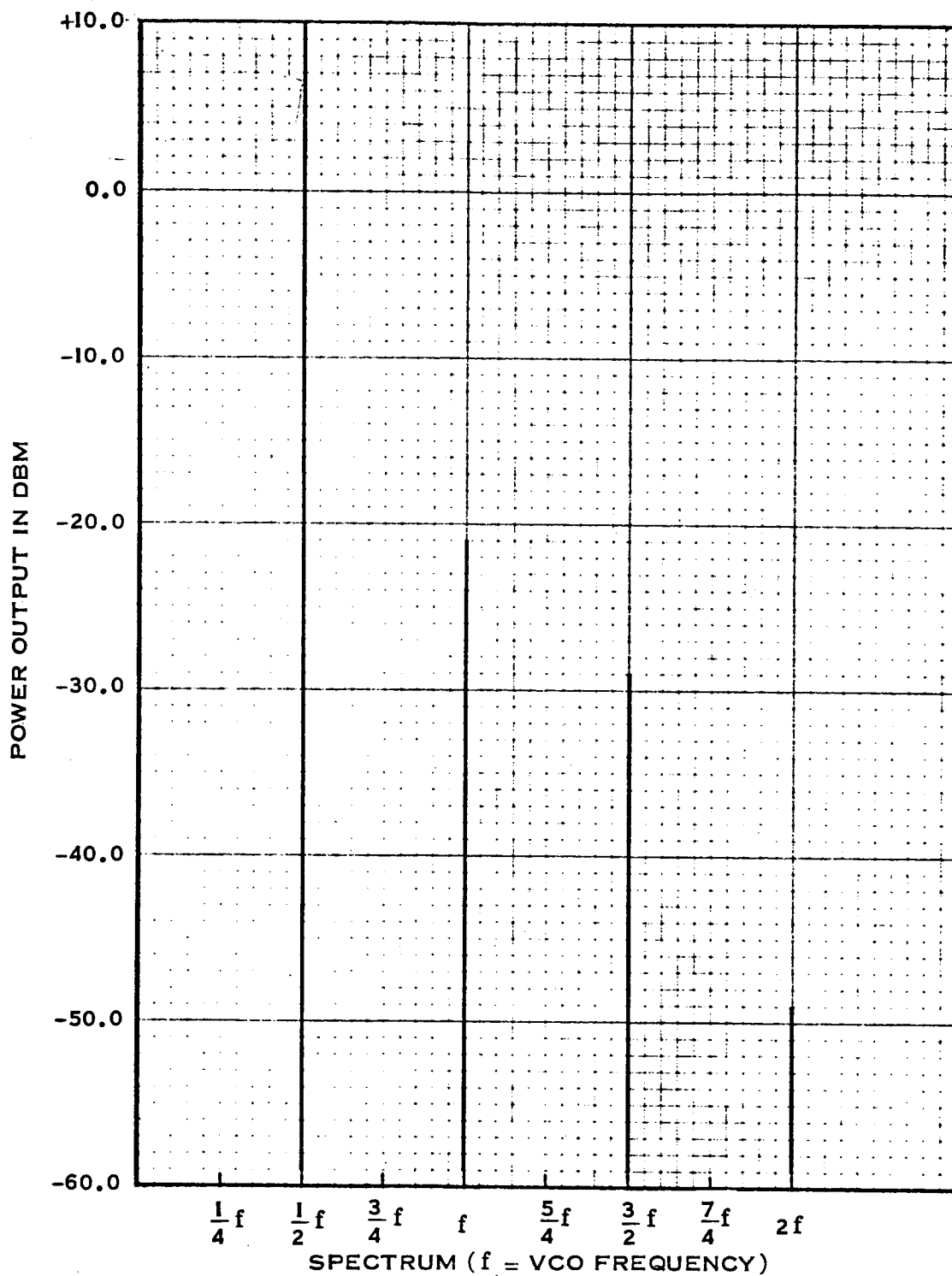


Figure 3.2.2-18 Frequency Divider. Frequency Spectrum For J_4 Output (ISO AMP).

114

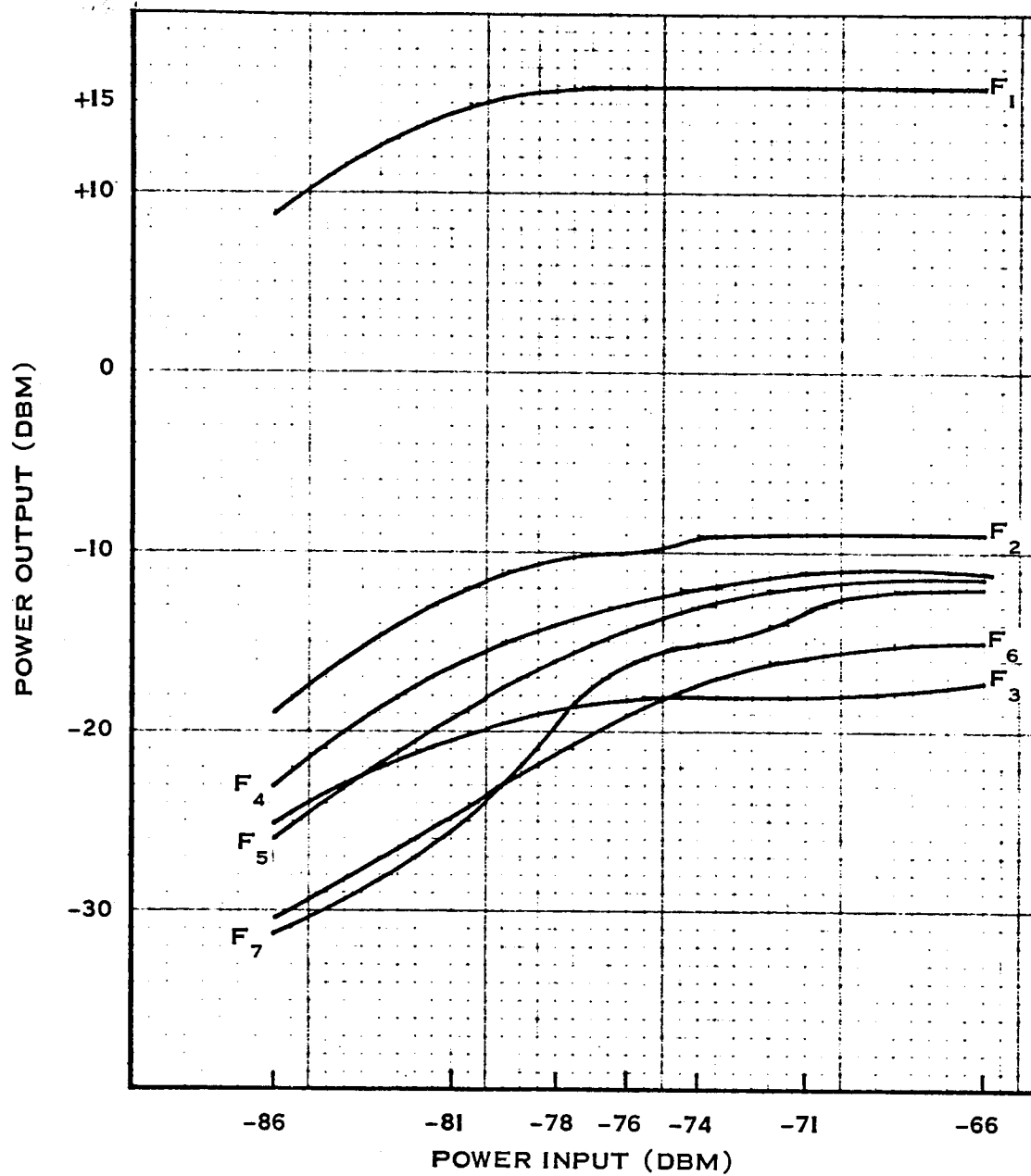


Figure 3.2.2-19 Power Output vs Power Input of the Fundamental and Harmonics of the 9.56 MHz I.F. Amplifier Module.

SECTION 4

ANALYSIS AND STUDY

4.0 GENERAL

The principal goal of the analysis and study effort was to relate the ranging delay and S-band phase temperature data to transponder circuit functions. In addition to this, a study was made to determine the optimum transmit-to-receive frequency ratio, from the transponder viewpoint, for the proposed change in the DSIF band occupancy.

4.1 RANGING DELAY AND RANGING DELAY VARIATION

The various measurements made in the program, combined with the analysis efforts indicate that:

- a. Group delay in RF stages due to bandpass interstage coupling networks, and phase shift of the fundamental component of the 498 KHz square wave in video stages, is responsible for almost all of the measured ranging delay time in the transponder. These are normal, unavoidable delay phenomenon and result mainly from bandwidth limiting requirements.
- b. Ranging delay variations measured in the JPL transponder are produced principally in the demodulation process, and are caused by variations in the reference phase relative to the carrier. This phenomenon can be corrected to acceptable limits.

The delay produced by interconnecting coaxial cables and module wiring is in the order of tenths of a nanosecond per inch, and hence are not considered significant for analytical purposes. The delay due to the active elements such as transistors and diodes is in the order of tenths of a nanosecond per unit.

A functional block diagram of the ranging loop is shown in Figure 4.1-1. A summary of the measured and the expected ranging delay and ranging delay variation data is presented in Figure 4.1-2.

116

TR-DA1522 A

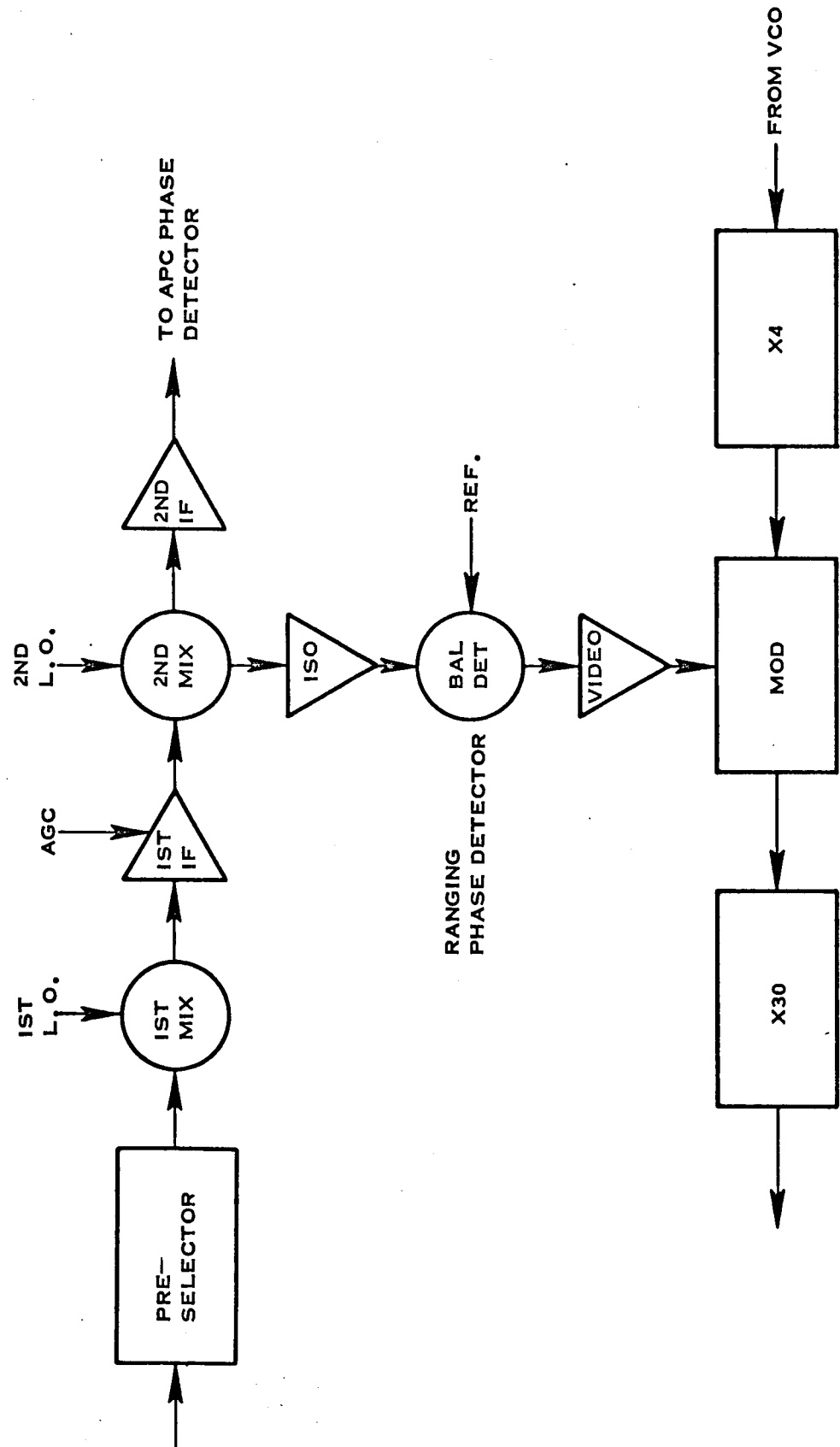


Figure 4.1-1 Ranging Channel Loop Functional Block Diagram

TABLE 4.1-2
RANGING DELAY AND RANGING DELAY VARIATION SUMMARY (1)
Using the Results of the S-Band/"VOC"/Ranging Phase Vs. Temperature Tests

Six Pack No.	MODULE, OR MODULE GROUP	Measured Overall S-Band Carrier Phase Shift		Module Carrier Phase Shift		EXPECTED DELAY VARIATION						Measured Delay Variation	Expected Delay (Nominal)	Expected Transit Delay (Nominal)	
		(CYCLES)		(DEGREES)		Due to Carrier Phase Shift		Due to Group Delay		Total					
						- ΔT	+ ΔT	- ΔT	+ ΔT		- ΔT				+ ΔT
NAME		- ΔT (2)	+ ΔT(2)	- ΔT	+ΔT	(N SEC)		(N SEC)		(N SEC)		- ΔT	+ ΔT	(N SEC)	
Receiver Six Pack No. 1	1. Preselector	<±0.01	<±0.01	<±3	<±3	0.0	0.0	0.0	0.0	0.0	0.0	-3.9	+0.6	(N SEC)	
	2. Mixer-Preamp1	<±0.01	<±0.01	<±3	<±3	0.0	0.0	<±0.1	<±0.1	0.0	0.0	-5.0	-2.8	40	
	3. 47.8 MHz I.F. & 2nd MIX	+0.09	-0.14	+29.8	-46.4	0.0	0.0	+0.8	1.8	+0.8	+1.8	-1.1	+30.6	118	
	4. 9.56 MHz I.F. (6)	-0.05	+0.15	+16.5	-49.7	+36.3	-173.0	N.A.	N.A.	+36.3	-173.0	+66.3	-110	99	
	5. X36 Multiplier	-1.60	+1.87	+530	-620	±0.25	±0.25	N.A.	N.A.	±0.25	±0.25	+5.0	+5.6	N.A.	
Receiver Six Pack No. 2	6. AGC Detector	<±0.01	<±0.01	N.A.	N.A.	0.0	0.0	N.A.	N.A.	N.A.	0.0	-6.7	-15.0	N.A.	
	7. Phase Detector	<±0.01	<±0.01	<±3	<±3	0.0	0.0	N.A.	N.A.	N.A.	0.0	+14.5	+2.2	N.A.	
	8. VCO & X3 Mult.	+4.41	-8.55	+13.2	-25.7	+3.9	-19.0	N.A.	N.A.	N.A.	+3.9	-19.0	0.0	N.A.	
	9. Freq. Divider (7)	+1.41	-0.77	+46 (4)	-60 (4)	-4.9 (5)	+12.3 (5)	N.A.	N.A.	N.A.	-4.9	+12.3	-9.5	+27.2	N.A.
	10. Isolation Ampl.	<±0.01	<±0.01	+16.6 (6)	-3.2 (4)	-30.7	+8.4	-0.5	<-0.1	-31.2	+8.4	-40.0	+15.0	167	1.0
Exciter Six Pack	11. Video Ampl.	<±0.01	<±0.01	N.A.	N.A.	N.A.	N.A.	(10)	(10)	(10)	(10)	-3.4	+6.1	85	0.6
	12. AUX-OSC, MOD, & X4	+2.39	-2.74	+28.8	-32.4	0.0	0.0	+4.4	+5.5	+4.4	+5.5	-2.2	-0.6	139	0.4
	13. X30 Multiplier	+1.88	-2.50	+677	-900	0.0	0.0	+1.8	+3.2	+1.8	+3.2	-1.7	+28.4	265	0.9
	Receiver, Six Pack No. 1	-1.67	+1.98	N.A.	N.A.	+36.3 (8)	-173.0 (8)	+0.8 (8)	+1.8 (8)	+37.1 (8)	-171.2 (8)	+35.6	-101	257 (8)	1.7 (8)
	Receiver, Six Pack No. 2	+6.38	-11.40	N.A.	N.A.	-31.7 (8)	+1.7 (8)	-0.5 (8)	0.0 (8)	-32.2 (8)	+1.7 (8)	+5.6	+43.9	252 (8)	1.6 (8)
	Exciter, Six Pack	+4.15	-5.33	N.A.	N.A.	0.0 (8)	0.0 (8)	+6.2 (8)	+8.7 (8)	+6.2 (8)	+8.7 (8)	-12.2	+44.5	404 (8)	1.3 (8)
	Transponder	+8.00	-14.20	N.A.	N.A.	+4.6 (9)	-171.3 (9)	+6.5 (9)	+10.5 (9)	+11.1 (9)	-160.8 (9)	-5.0	-62.8	913 (9)	4.6 (9)

NOTES:

1. Pin = -90 dbm
2. -ΔT Data is the Difference Between +25°C and -10°C Data
+ΔT Data is the Difference Between +25°C and +75°C Data
3. Phase Shift of Carrier at Output of Module Under Test (See Sec. 4.1.1)
4. Diagnostic Test Data
5. θ (J3-J4): -2° @ -ΔT
+5° @ +ΔT
6. Input to "Limited" (J3) Output
7. Input to "APC Phase Detector" (J3) Output
8. Summation of Pertinent Module Data
9. Summation of Six - Pack Data
10. Not Computed

4.1.1 Ranging Delay and Ranging Delay Variation, Due to Interstage Coupling Networks

A module-to-module analysis was performed in order to obtain calculated values for nominal ranging delay, and ranging delay variation due to interstage coupling networks so that expected and measured data at normal operating temperatures and temperature varying conditions could be compared directly when possible. The overall transponder expected ranging delay and ranging delay variation due to interstage coupling networks is then taken to be equal to the sum of the individual module values. Three simplifying assumptions are used in the analysis:

- a. The interstages are either of three types; 1-pole bandpass or low pass, or 2-pole Butterworth bandpass
- b. Similar interstage types in each module can be grouped together as m identical n -poles.
- c. The ranging signal is not coded. (Measured ranging delay change from code ON to code OFF was -25 nanosecond at $P_{IN} = -90$ dbm).

In computing the expected nominal ranging delay for each module, the pertinent data was obtained from the "Transponder Parameter Summary" given in Table 4.1.1-1.

The expected ranging delay variation due to interstage coupling networks was computed on the basis of group delay variations in RF stages. This was done by relating carrier phase shifts in the interstage to circuit detuning, and then relating group delay variations to the circuit detuning. Thus a relationship was established between measured carrier phase variations and expected ranging delay variation.

Expressions were derived for nominal group delay and group delay variations as a function of circuit detuning. These are presented in Appendix I and were used in the calculations which follow.

Table 4.1.1-1
TRANSPONDER PARAMETER SUMMARY

MODULE	ACTIVE ELEMENT	INTERSTAGE		TOTAL BANDWIDTH	Bandwidth per Stage (B _n)
		Type (n-pole)	No. (m)		
RANGING LOOP					
Preselector	None	5-Pole Cavity	1	30 MHz ⁽¹⁾	30 MHz
Mixer Preampl.	4 Transistors 1 Diode Pair (Mixer)	2-pole	3	8.1 MHz ⁽²⁾	11.4 MHz
47.8 IF & 2nd Mixer	8 Transistors 1 Diode Pair (Mixer)	2-pole	4	12.0 MHz ⁽²⁾	18.2 MHz
Isolation Ampl.	7 Transistors 1 Diode Pair (Detector)	1-Pole	4	8.0 MHz ⁽⁶⁾	18.2 MHz
		1-Pole	2	2.1 MHz ⁽⁴⁾	3.28 MHz
Video Ampl.	4 Transistors 2 Diode Pairs (Lims.)	1-Pole	4	3.3 MHz	7.50 MHz
Aux-Osc, Mod.&X4	2 Transistors 1 Diode Pair (Mult.)	2-pole	2	(5)	6.45 MHz
X30 Multiplier	4 Transistors 1 Diode Pair (Mult.) 2 Diodes (Mults.)	2-pole Cavity	1	2.5 MHz ^{(5) (2)}	(3)
		1-pole	4		22.7 MHz ⁽⁴⁾
		2-pole	3		6.45 MHz ⁽⁴⁾
		OTHER			
9.56 MHz IF (J3 Output)	7 Transistors	2-Pole X-TAL Filter	1	4.90 KHz	4.90 KHz
		2-Pole	5	600 MHz	968 MHz
X36 Multiplier	2 Transistors 1 Diode Pair (Mult.) 2 Diodes (Mults.)	2-pole Cavity	1	(3)	(3)
		1-pole	3		(3)
		2-pole	2		(3)
AGC Detector					
Phase Detector					
VCO & X3 Multiplier (J4 Output)	4 Transistors	1-pole	1	(3)	(3)
		2-pole	4		(3)
Frequency Divider (J3 Output)	3 Transistors 1 Diode Pair (Mult.)	1-pole	2	(3)	(3)
		2-pole	3		(3)
Aux. Osc., Mod. & X4	1 Transistor 2 Diode Pairs (Switches)	2-pole	2	(3)	(3)

- NOTES: 1. Specification value
 2. JPL - supplied data for S/N 4 transponder, dated 1964.
 3. Data not known
 4. Interior engineering report values
 5. Composite Aux-Osc And X30 value
 6. Extrapolated value

All other data is contained in this report.

Refer to Figure A.1-1 which is a plot of phase shift and fractional change in group delay vs relative detuning, for one-pole and two-pole Butterworth bandpass interstage coupling networks.

Tank circuit overall temperature coefficients can also be deduced from carrier phase shift data through the formulas presented at the end of Appendix I. This could not be done however, in the allotted budget.

The results of the computations which follow are tabulated in the "Ranging Delay and Ranging Delay Variation Summary" given in Table 4.1-2.

Preselector

1. $\tau_d \triangleq \frac{\Delta}{d\phi} = \text{phase slope at } \omega_0$

Using the Bode approximation for phase slope,

$$\tau_d \approx \frac{\Delta\phi}{\Delta\omega} = \frac{(5)(-\frac{\pi}{2} \text{ rad})}{(2\pi)(30 \times 10^6 \text{ rad/sec})}$$

$$\tau_d \approx 40 \text{ nsec}$$

2. This simplified model does not show the change in phase slope for deviations from band center which actually are present in a Butterworth filter, so that delay variations cannot be shown from this model. However, the variations should be nil, since the carrier phase shift over the temperature range is nil.

Mixer-Preamplifier

$$\begin{aligned}
 1. \quad \tau_d &= m\tau_n = \text{total nominal expected group delay} \\
 &= (\text{no. of interstages})(\text{delay per interstage}) \\
 \tau_d &= 3\tau_2 = 3\left(\frac{2\sqrt{2}}{2\pi B_2}\right) \text{ sec}
 \end{aligned}$$

where B_2 is the bandwidth per 2-pole interstage in hertz.

$$\tau_d = 3\left(\frac{\sqrt{2}}{\pi \times 11.4 \times 10^{-6}}\right) = 3(39.4 \times 10^{-9}) = 118 \text{ nsec}$$

$$2. \quad \Delta\tau_d = m\Delta\tau_n = m(\tau_n)(\Delta_n) = \text{total expected group delay variation}$$

$$\approx (3)(\tau_2)(\Delta_2) = \tau_d(+1/2 \phi_2^2)$$

where ϕ_2 is the carrier phase shift per 2-pole interstage, in radians.

$$\phi_2 = \frac{\Delta\theta(\tau)}{m} = \frac{\text{total carrier phase shift due to temperature}}{\text{No. of interstages}}$$

$$\therefore \Delta\tau_d \approx +(\tau_d)\left[1/2\left(\frac{\Delta\theta}{m}\right)^2\right]$$

Since

$$\Delta\theta < \pm (2\pi)(0.01)\left(\frac{221}{240}\right) \text{ rad}$$

$$\Delta\tau_d < + (118)\left(\frac{1}{2}\right)\left(\frac{5.77 \times 10^{-2}}{3}\right)^2 = +0.10 \text{ nsec.}$$

47.8 MHz IF

$$1. \quad \tau_d = 4\tau_2 = 4\left(\frac{0.45}{18.2 \times 10^{-6}}\right) \text{ sec}$$

$$= 4(24.7 \times 10^{-9}) = 99 \text{ nsec}$$

$$2. \quad \Delta\tau_d(-\Delta\tau) = +(99 \text{ nsec})\left(\frac{1}{2}\right)\left(\frac{+29.8}{-57.3}\right)^2$$

$$= +0.8 \text{ nsec}$$

where $-\Delta\tau$ signifies that the carrier phase shift, and hence the group delay variation, occurs in the temperature range below $+25^\circ\text{C}$.

$$\Delta\tau_d(+\Delta\tau) = \left[\Delta\tau_d(-\Delta\tau)\right]\left[\frac{\Delta\theta(+\Delta\tau)}{\Delta\theta(-\Delta\tau)}\right]^2$$

$$= +(0.8 \text{ nsec})\left(\frac{-46.4}{+29.8}\right)^2 = +1.8 \text{ nsec}$$

Isolation Amplifier

$$1. \quad \tau_d = (\tau_d)_{\text{RF}} + (\tau_d)_{\text{vid}}$$

$$(\tau_d)_{\text{RF}} = 4\tau_1 = 4\left(\frac{2}{2\pi B_1}\right) \text{ sec}$$

$$= 4\left(\frac{0.318}{18.2 \times 10^{-6}}\right) = 4(17.5 \times 10^{-9}) = 70 \text{ nsec}$$

$$(\tau_d)_{\text{vid}} = (m)(320 \frac{\text{nsec}}{\text{rad}})(\Delta\theta_1)$$

= total delay of fundamental component (i.e., 498 KHz)

$$\Delta\theta_1 = \tan^{-1} \left(\frac{498 \text{ KHz}}{f_1} \right) \text{ rad}$$

= phase delay of fundamental per interstage

$$\approx \frac{498 \text{ KHz}}{f_1} = \frac{498 \times 10^3}{3.28 \times 10^6} = 0.152 \text{ rad}$$

$$(\tau_d)_{\text{vid}} = (2) \left(320 \frac{\text{nsec}}{\text{rad}} \right) (0.152 \text{ rad}) = 97 \text{ nsec}$$

$$\tau_d = (70 + 97) = 167 \text{ nsec}$$

$$2. \quad \Delta\tau_d = (\Delta\tau_d)_{\text{RF}} + (\Delta\tau_d)_{\text{vid}}$$

But due to lack of phase shift versus temperature data on the video portion, only the delay variation $(\Delta\tau_d)_{\text{RF}}$ was computed.

$$\Delta\tau_d(-\Delta\tau) = -(70 \text{ nsec}) \left(\frac{\frac{+16.6}{57.3}}{4} \right)^2$$

$$= -0.5 \text{ nsec}$$

$$\Delta\tau_d(+\Delta\tau) = -(0.5 \text{ nsec}) \left(\frac{-3.2}{+16.6} \right)^2$$

$$= -0.05 \text{ nsec}$$

Video Amplifier

$$1. \tau_d = (m) \left(320 \frac{\text{nsec}}{\text{rad}} \right) (\Delta\theta_1)$$

$$\approx (4) \left(320 \frac{\text{nsec}}{\text{rad}} \right) \left(\frac{498 \times 10^3}{7.50 \times 10^6} \right)$$

$$\approx (4) (21.3 \text{ nsec}) = 85 \text{ nsec}$$

2. $\Delta\tau_d$ was not computed, due to lack of phase shift versus temperature data.

Auxiliary Oscillator

$$1. \tau_d = 2\tau_2 = 2 \left(\frac{0.450}{6.45 \times 10^6} \right) \text{ sec}$$

$$= 2(69.6 \times 10^{-9}) = 139 \text{ nsec}$$

$$2. \Delta\tau_d(-\Delta\tau) = +(139 \text{ nsec}) \left(\frac{1}{2} \right) \left(\frac{+28.8}{57.3} \right)^2$$

$$= +4.4 \text{ nsec}$$

$$\Delta\tau_d(+\Delta\tau) = +(4.4 \text{ nsec}) \left(\frac{-32.4}{+28.8} \right)^2$$

$$= +5.5 \text{ nsec}$$

X30 Multiplier

$$1. \tau_d = (\tau_d)_{1\text{-poles}} + (\tau_d)_{2\text{-poles}}$$

$$(\tau_d)_{1\text{-poles}} = 4\tau_1 = 4 \left(\frac{0.318}{22.7 \times 10^6} \right) \text{ sec}$$

$$= 4(14.0 \times 10^{-9}) = 56 \text{ nsec}$$

$$\begin{aligned}
 (\tau_d)_{2\text{-poles}} &= 3\tau_2 = 3\left(\frac{0.450}{6.45 \times 10^6}\right) \text{ sec} \\
 &= 3(69.7 \times 10^{-9}) = 209 \text{ nsec}
 \end{aligned}$$

$$\tau_d = (56 + 209) = 265 \text{ nsec}$$

$$2. \quad \Delta\tau_d \approx (\Delta\tau_d)_{2\text{-poles}}$$

$$\begin{aligned}
 \Delta\tau_d(-\Delta\tau) &= +(209 \text{ nsec})\left(\frac{1}{2}\right)\left(\frac{+\frac{677}{30 \times 57.3}}{3}\right)^2 \\
 &= +1.8 \text{ nsec}
 \end{aligned}$$

$$\begin{aligned}
 \Delta\tau_d(+\Delta\tau) &= +(1.8 \text{ nsec})\left(\frac{-900}{+677}\right)^2 \\
 &= +3.2 \text{ nsec}
 \end{aligned}$$

The expected total nominal ranging delay due to interstage coupling networks is 913 nsec. Adding about 5 nsec for all the active elements brings the final total to 918 nsec. That this figure is higher than the measured value by about 17% is not too surprising, since the second assumption at the beginning of this section would tend to cause a cumulative error on the increased delay side. This follows from the fact that the narrowest interstage dominates the overall bandwidth of a group of similar interstages, and that all but the narrowest interstage is then over-charged in the group delay.

However, this effect is somewhat compensated by two cavity filters (see Figure 4.1.1-1) which were neglected in these calculations, due lack of data.

The expected $-\Delta\tau$ and $\Delta\tau$ ranging delay variations due to RF interstages is +6.5 and +10.5 nsec, respectively.

Comparing these figures to the measured values indicates that the nominal group delay is due to the interstage coupling networks, but that the measured variations under temperature are mostly caused by other factors. See Table 4.1-2 for complete details.

4.1.2 Delay Variation Produced in the Demodulation Process

As mentioned previously, ranging delay variations in the JPL transponder are produced principally in the demodulation process, and are caused by variations of the reference phase relative to the carrier in the ranging phase detector.

4.1.2.1 Description of the Phenomenon

The phenomenon is described in the sequence outlined as follows:

1. Figure A.3-4
Schematic diagram of the ranging phase detector; for reference purposes.
2. Figure 4.1-1
Ranging channel loop functional block diagram; for reference purposes.
3. Figure A.5-2
Transponder phase detector(s) block diagram; useful for describing the phase relationship between reference and carrier in the ranging phase detector.
4. Figure 3.2.2-4
Graph of ranging delay versus reference phase shift; this is the chief exhibit in describing the ranging delay variation phenomenon. The phase slope, with and without the effects of crystal filter interaction are as follows:

$$\bullet \left(\frac{\Delta \theta_d}{\Delta \theta_{ref}} \right)_{norm} = 0.44 \text{ deg/deg}$$

$$\bullet \left(\frac{\Delta \theta_d}{\Delta \theta_{ref}} \right)_{iso-amp} = 0.12 \text{ deg/deg}$$

5. Figure 3.2.2-6a and 6b

Photographs of the ranging signal in the time domain show the distortion of the ranging signal caused by the crystal filter.

6. Figure 3.2.2-3

The cut-out section of the second mixer schematic diagram shows that the crystal filter input impedance can effect the ranging signal; the isolating pads are not adequate to prevent the interaction effect.

7. Figures 3.2.2-1 and 2, and Table 3.2.2-1

These figures and the accompanying table show the amplitude and phase distortion in the frequency domain, caused by the crystal filter.

Figure 3.2.2-4 shows that a significant reduction in susceptibility to ranging delay variation can be obtained by effectively isolating the crystal filter input impedance from the second mixer output that feeds the ranging loop.

A limited effort was made to explain the ranging delay variation produced in the ranging phase detector due to reference phase shift relative to the carrier. The results of these studies are outlined as follows:

1. Appendix II.

This is a mathematical model of the demodulation of a sinusoidal carrier which is phase modulated by a symmetrical trapezoidal modulating waveform. The carrier frequency relative to the frequency of the modulating signal is infinite. The results show that for any peak phase deviation or any slope, the phase of the fundamental component of the demodulated signal is invariant. More importantly, it shows that the phase of fundamental component of the demodulated signal has only two discrete values, 0 and 180 degrees, relative to the modulating signal. The curve shape

shown in Figure 3.2.2-4 is not predicted in this model.

2. Appendix III.1

The mathematical model described in the preceding paragraph was augmented so as to include a complex amplitude modulating waveform superimposed on the trapezoidal phase modulated carrier. The periodicity of the complex A.M. is assumed to be the same as the modulating signal. The results show that the variation of the reference phase can produce the type of curves shown in Figure 3.2.2-4, providing that there is a large fundamental component of A.M. and that there is an appreciable phase difference between the A.M. and P.M. waveforms. The A.M. component on the ranging signal due to crystal filter interaction shown in Figure 3.2.2-6a appears to contain a large second harmonic content, indicating that the A.M. content may not be responsible for the large ranging variations shown in Figure 3.2.2-4.

3. Appendix III.2

The fact that the 498 KHz ranging frequency is appreciable with respect to the 9.56 MHz RF frequency was considered, with the result that reference phase variations relative to the ranging signal carrier phase do produce small ranging variations. Figure A.3-3 illustrates how this can happen, in a qualitative way. From the figures it appears that the ultimate value of slope, for small reference variations is

$$\bullet \left(\frac{\Delta \theta_d}{\Delta \theta_{ref}} \right)_{ult} \approx 0.05 \text{ deg/deg}$$

Further effort on this concept could easily lead to a curve similar to the ones shown in Figure 3.2.2-4, thus defining the limiting ranging delay variation susceptibility to reference phase variations. The concept of ranging delay variations in the demodulation process illustrated in Figure A.3-3 appear to be equally applicable to the mixing processes shown in the

ranging loop functional block diagram, Figure 4.1-1. Even if true, the effect would be quite small, since the two LO injection frequencies are 6 and 72 times higher than the 9.56 KHz reference frequency.

This concludes the description of the ranging delay variation phenomenon that is attributable to the demodulation process.

4.1.2.2 Causes of Reference Phase Shift

The causes of reference phase shift relative to the carrier are listed as follows, in the order of importance as indicated by measurement data:

1. 9.56 MHz IF; input to limited output:

The phase variation over the temperature range is about 76 degrees; Figure A.5-2 shows that a phase shift in the 9.56 MHz IF causes the reference phase to shift in a 1 to 1 manner.

Figure 3.1.3-14 shows that the greatest ranging delay variation, 177 nsec, occurred when the 9.56 MHz IF was subjected to temperature variations.

2. Isolation Amplifier:

Figure 3.2.1-11 shows that the carrier phase shift over temperature is about 20 degrees. Figure A.5-2 shows that this is equivalent to a negative reference phase shift relative to the carrier. The measured ranging delay variation is about 64 nsec.

3. Frequency Divider:

The phase shift between the output to the ranging phase detector and the APC phase detector causes the reference phase of the ranging phase detector relative to the ranging carrier to shift in a 1 to 1 manner; see Figure A.5-2.

4. VCO Crystal:

The frequency versus temperature characteristic of the VCO quartz crystal is responsible for causing an SPE versus temperature variation. The result is that the ranging phase detector reference relative to the carrier is affected on a 1-1 basis; see Figure A.5-2. This effect is discussed in Section 4.2.2.

5. The crystal filter:

The phase versus frequency slope is sufficiently steep so that variations in S-band input frequency can cause the reference to shift noticeably; the phase slope is approximately 0.04 deg/hertz. This effect is discussed in Section 4.2.2.

6. APC Phase Detector Slope:

The conversion factor K_D of static phase error (SPE) to error voltage is a function of the S/N. Since the APC loop actuating error is a fixed value under locked conditions, the phase error must follow any change in K_D , on a 1-1 basis. The net effect then is a variation in ranging phase detector alignment, and hence a variation in ranging delay.

This concludes the section on the causes of reference phase shift relative to the carrier in the ranging phase detector.

4.2 TRANSPONDER PHASE RELATIONSHIPS

This section concludes the analytical efforts which were made in predicting and explaining the results of the S-Band/"VCO"/ranging phase versus temperature test measurement program.

4.2.1 General Transponder Phase Relationships

The block diagram shown in Figure A.5-1 was created in order to facilitate the effort. This block diagram depicts the pertinent APC loop "locked" phase relationships. It takes into account module input-to-output phase shifts, which may be thought of as being functions of temperature, time, or input S-Band frequency.

The equations derived in A.5-2 using this basic block diagram, predict transient as well as steady state performance. The equations were used primarily to predict the direction of, and in a qualitative sense the magnitude of, the steady state value of the measured S-Band phase variations versus temperature. The APC loop mixing and frequency multiplying processes can, and do, alter the S-Band phase deviations as compared to the module (or module group) input-to-output values.

An example of how the equations of A.5-2 were used is as follows:

1. The steady state performance to step inputs is found by use of the final value theorem of Laplace Transformation Theory; i.e.:

$$\lim_{t \rightarrow \infty} \theta_{vco}(t) = \lim_{s \rightarrow 0} s \theta_{vco}(s)$$

where $\theta_{vco}(s)$ = equation A.5.2.6

$$\therefore \theta_{vco} \text{ steady state} = \frac{0}{110\frac{1}{2}}$$

2. Let θ be evaluated for the 9.56 MHz I.F., for example:

where θ = equation A.5.2.4

$$\therefore \theta_{\text{vco}} \text{ steady state} = \frac{-\theta_{9.56}}{110\frac{1}{2}}$$

3. Finally, from equation A.5.2.7:

$$(\theta_s)_{\text{out}} = 120 \theta_{\text{vco}} = - \left(\frac{240}{221} \right) \theta_{9.56}$$

Thus it is apparent that the module input-to-output phase variation, $\theta_{9.56}$, will be modified in reaching the S-Band output by a $-(240/221)$ factor. Since the module phase deviation is expected to go negative with increasing temperature, the S-Band phase will go positive with increasing temperature. In addition, the magnitude of the shift is expected to be a small fraction of a cycle. These observations are borne out by actual measurement (see Figure 3.1.3-1).

This method of predicting the S-Band phase variations is accurate to the extent that interfacing driving point impedances do not vary. An example of this is the apparent effect of the Frequency Divider input impedance variation under temperature and power input varying conditions. The curve of phase shift versus temperature and input power, Figures 3.2.1-15 and 3.2.1-16, along with the calculated multiplication factor, $+(240/221)$, predict only a fraction of a cycle of deviation at S-Band, compared to the measured value of about 2.3 cycles. See Figure 3.1.3-11; note that the phase shift curve is not monotonic, like all of the others.

The only other example of the failure of the analysis given in A.5-2 to explain measured S-Band phase variations is the test results of the VCO module. The phase varied opposite to the expected direction, and the magnitude was much greater than expected (13 cycles). A list of possible

explanations include the following, in order of expected importance:

1. The last isolation amplifier of the VCO shown in Figure 3.0-1, which is not taken into account in Figure A.5-1 and the derived equations, is responsible for much of the S-Band phase deviation, since its phase deviation is multiplied by 120 times.
2. The output power of the JPL VCO module is known to vary by about 3 db over temperature. This coupled with the fact that the input stage of the frequency divider is normally driven in a limiting condition, and that the tuning is effected by the input level, leads to the conclusion that the input impedance of the Frequency Divider is being varied by the VCO module. The variation in impedance varies the carrier phase angle at that point, which then is multiplied by 120 times in reaching the S-Band output. This interface problem, along with the VCO last isolation amplifier phase shift, is believed mainly responsible for the large variation measured.
3. Either or both of the two X3 multipliers and/or the other isolation amplifiers (see Figure 3.0-1) could be providing a positive phase shift with increased temperature; this is not thought to be the case.

The two exceptional cases need further tests to determine the facts.

4.2.2 Ranging Delay Variation Caused by the VCO Crystal Temperature Characteristic

As mentioned in Section 4.1.2.2.4, the frequency versus temperature characteristic of the VCO quartz crystal causes a variation in the relative phase between reference and carrier in the ranging phase detector. This in turn causes a variation in the ranging delay as a function of temperature.

Figure 4.2.2.1 shows the expected ranging delay variation as a function of temperature, due to this effect. The following steps show how the curve was obtained (Note: brackets are used exclusively to indicate functional dependence).

1. $\Delta\theta_{\text{ref}} = -\theta_{\text{SPE}}$ (See Figure A.5-2)
2. $\theta_{\text{SPE}} = V_{\text{SPE}}/K_D$
3. $V_i(T) \triangleq$ Hypothetical internally generated bias voltage which is equivalent to the frequency pulling effect of temperature
4. $V_{\text{SPE}} = -V_i(T)$
= APC loop correction voltage
5. $V_i(T) = V_{\text{VCO}}[f_{\text{VCO}}(T)]$
 - $f_{\text{VCO}}(T)$ = VCO frequency versus temperature characteristic curve; Figure 4.6-2 of "Interim Engineering Report"

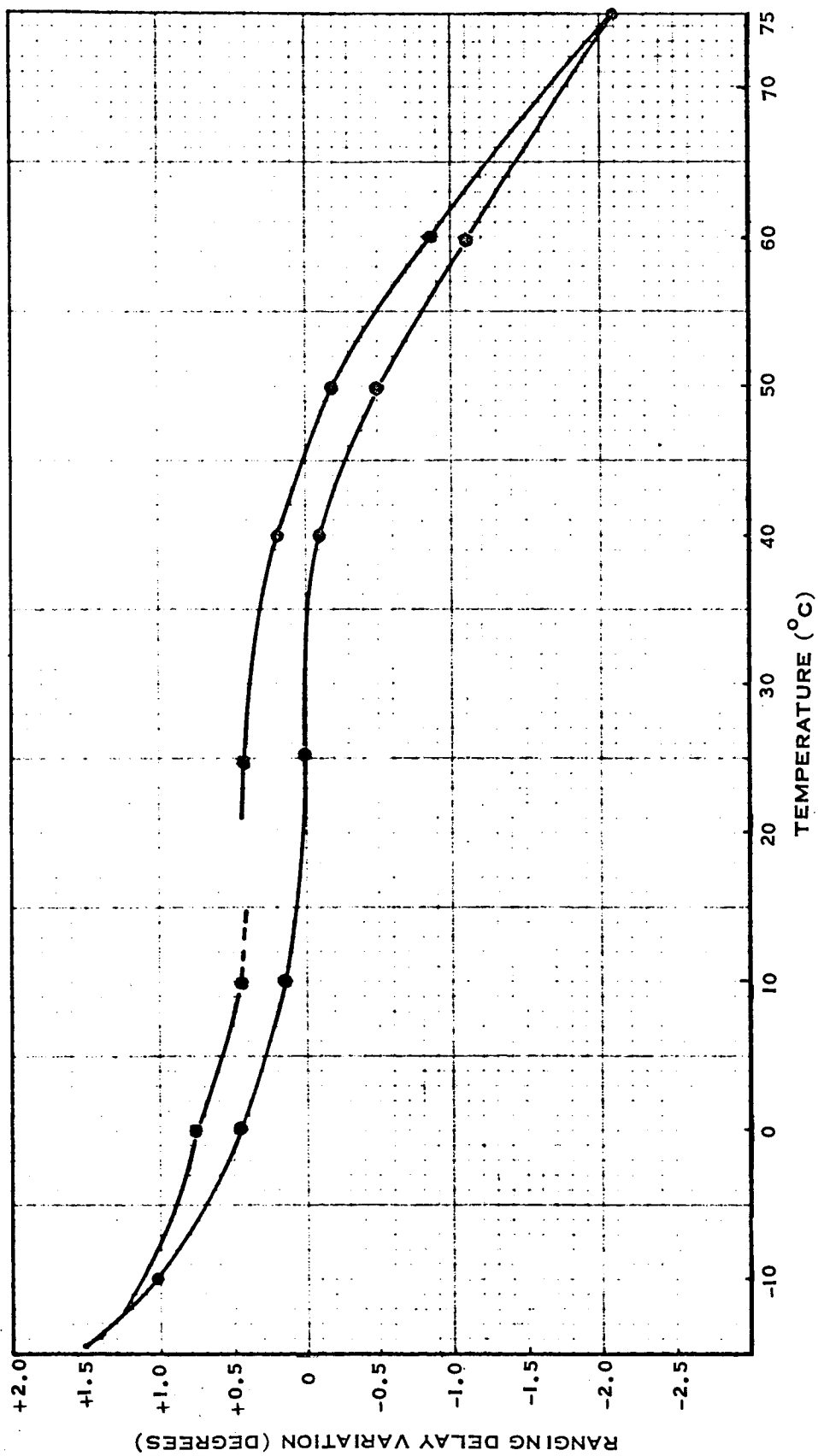


Figure 4.2.2-1 Expected Ranging Delay Variation vs. Temperature of the VCO Module
Calculated from $\Delta\theta_D$ vs. $\Delta\theta_{ref}$, Figure 3.2.2-4, by Substituting.

$$\Delta\theta_{ref} = -\theta_{spe}(T)$$

- $V_{VCO}(f_{VCO})$ = Inverse of the VCO frequency versus bias voltage curve; from data taken during this program, but not appearing in this report.

$$6. \Delta\theta_{ref} = \frac{1}{K_D} \times V_{VCO}[f_{VCO}(T)]$$

$$7. \Delta\theta_d = f(\Delta\theta_{ref}) \quad (\text{Figure 3.2.2-4})$$

The curve, Figure 4.2.2.1, is hence obtained by determining the parameters in the given sequence, until the $\Delta\theta_{ref}$ parameter is obtained. Then the ranging delay variation curve, Figure 3.2.2-4, is used to compute $\Delta\theta_d$.

The curve shows an expected ranging delay variation of about 3.1 degrees, or 17.3 n sec, as opposed to the measured variation of about 13.3 n sec. Note that Figure 4.2.2-1 predicts a small hysteresis effect.

4.2.3 "Cog" Phase Steps

At the beginning of the S-band /"VCO"/ ranging phase versus temperature testing program, it was noticed that the measured "VCO" phase (i.e., the VCO output signal relative to the corresponding signal in the reference transponder) would take discrete phase steps whenever the ranging channel was turned "on." These "Cogs" are explained as follows:

1. Reference to Figure A.5-2 shows that the APC loop is controlled at its phase detector; hence one cycle "slipped" here should result in one "cog" of "VCO" phase jump.
2. The magnitude of one "cog" is computed by noting that the APC converts an incremental phase change in θ_{VCO} , as defined in Figure A.5-2, by 111 times at one input to the APC phase detector, and by $1/2$ times at the other input. Hence, for a one cycle or 360 degree advance of the upper input relative to the lower one

$$+ 111(\Delta\theta_o) - \left[+ \frac{1}{2}(\Delta\theta_o) \right] = 360^\circ$$

$$\therefore \Delta\theta_o = \frac{360^\circ}{110\frac{1}{2}} = 3.26^\circ \triangleq 1 \text{ "cog."}$$

3. A half "cog" is theoretically possible, since the Frequency Divider has two stable modes. Its output waveform relative to the input drive signal has been observed to take either of two phases, 180 degrees apart, due to a momentary interruption of the input drive.
4. The "VCO Loop" shown in Figure A.5-3 is very sensitive to VCO bias voltage transients having fast rise times relative to the loop filter response time (see Figure A.5-5). From this Figure, a step input results in a "VCO" phase overshoot which is approximately 3.2×10^3 times the steady state value. From equation A.5.3.2, the steady state value is

$$(\Delta\theta_{VCO})_{S.S.} = \frac{V_1}{(110\frac{1}{2})(K_D)}$$

The amplitude of V_i that will cause the SPE to reach a 90 degree "knee" of the phase detector defines the stable limit of V_i . The incremental variation in the "VCO" phase for this condition is:

$$(\Delta\theta_{VCO})_{\max} = \frac{(\pi/2)}{110\frac{1}{2}} .$$

The final result is hence

$$(\Delta\theta_{VCO})_{\max} = \frac{(\pi/2)}{(110\frac{1}{2})} = (3.2 \times 10^3) \left[\frac{V_i}{(110\frac{1}{2})(20)} \right]$$

$$(V_i)_{\max} = \frac{10\pi}{3.2 \times 10^3} \approx 10 \text{ millivolts peak.}$$

5. The transient created in the +15 volt test power supply and its associated leads was found to produce the "cog" phase steps, whenever the ranging channel was turned "on," but not "off."
6. Switching the ranging channel "on" involves only applying D.C. power to the Isolation Amplifier module.
7. Both transponders were affected about equally, since the power supplies were common. The measured "cogs" were predominantly about 1.6 degrees, which is the equivalent of one-half of an expected "cog".
8. When the transponders were connected to separate power supplies, only the test transponder was affected. The phase jumps were in the order of 30 to 60 degrees, or the equivalent of many "cogs."
9. Power supply isolating tests revealed that only the VCO module was affected, and that isolating it eliminated the phase jumps altogether. Heavier transients were additionally applied to the remainder of the transponder without any sign of "cogs."

The conclusions drawn from these observations are as follows:

1. Power supply transients are suspected of upsetting the VCO via the frequency pulling varicap. The biasing of this varicap should be transient-free. Further effort is required, however, to verify that only the varicap biasing is affected.
2. The Frequency Divider can switch between the two bi-stable modes in the APC loop "pulling in" process.

4.3 FREQUENCY RATIO STUDY

The results of this effort indicate a usable ratio of the transponder transmit-to-receive frequency as follows:

$$\frac{\text{Transmit Frequency}}{\text{Receive Frequency}} = \frac{f_d}{f_\mu} = r = \frac{80}{63}.$$

The objective of this study was to develop an analytical approach and to use it to select an optimum value of r . It is apparent that a particular set of constraints, when applied to the frequency relationships in a given order will produce a value of r which is optimum in a particular sense.

The sections which follow present the analytical approach and the results of applying one particular set of constraints in a given order.

The basic transponder configuration analyzed is presented in Figure 4.3-1, and the significant results are presented in block diagram form in Figure 4.3.-2.

General Discussion

The relationships presented in Section 4.3.1 comprise an independent set of basic equations which govern the transponder frequency relationships. These relationships were used to derive the working formulas presented in Section 4.3.2, and used throughout the analysis which is presented in Appendix VI. The analysis is presented in outline form.

The constraints which were applied in the analysis reflect the desire to change the existing S-band transponder configuration as little as possible, particularly the APC loop mixer signs.

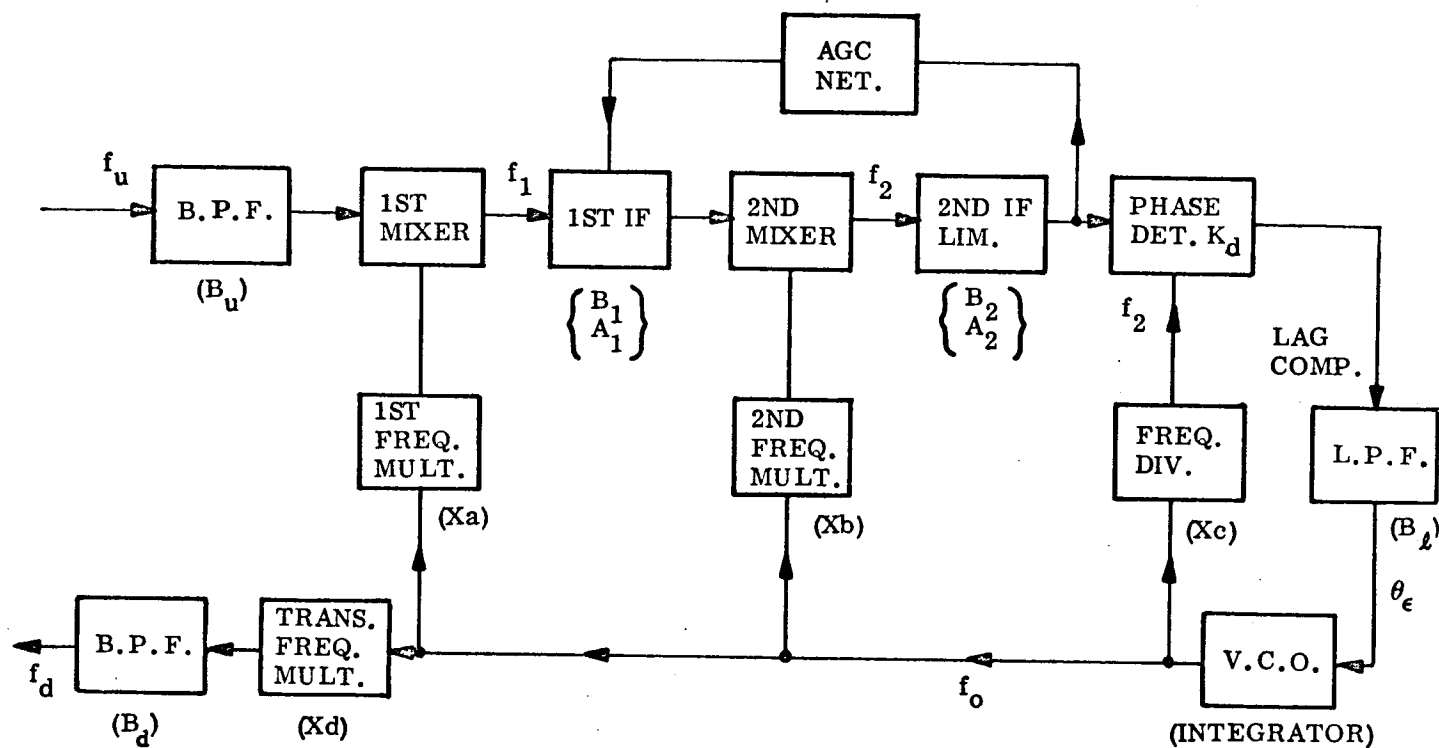


Figure 4.3.-1 Basic Configuration

4.3.1 Basic Frequency Relationships*

4.3.1.1 $r \stackrel{\Delta}{=} f_d/f_\mu$

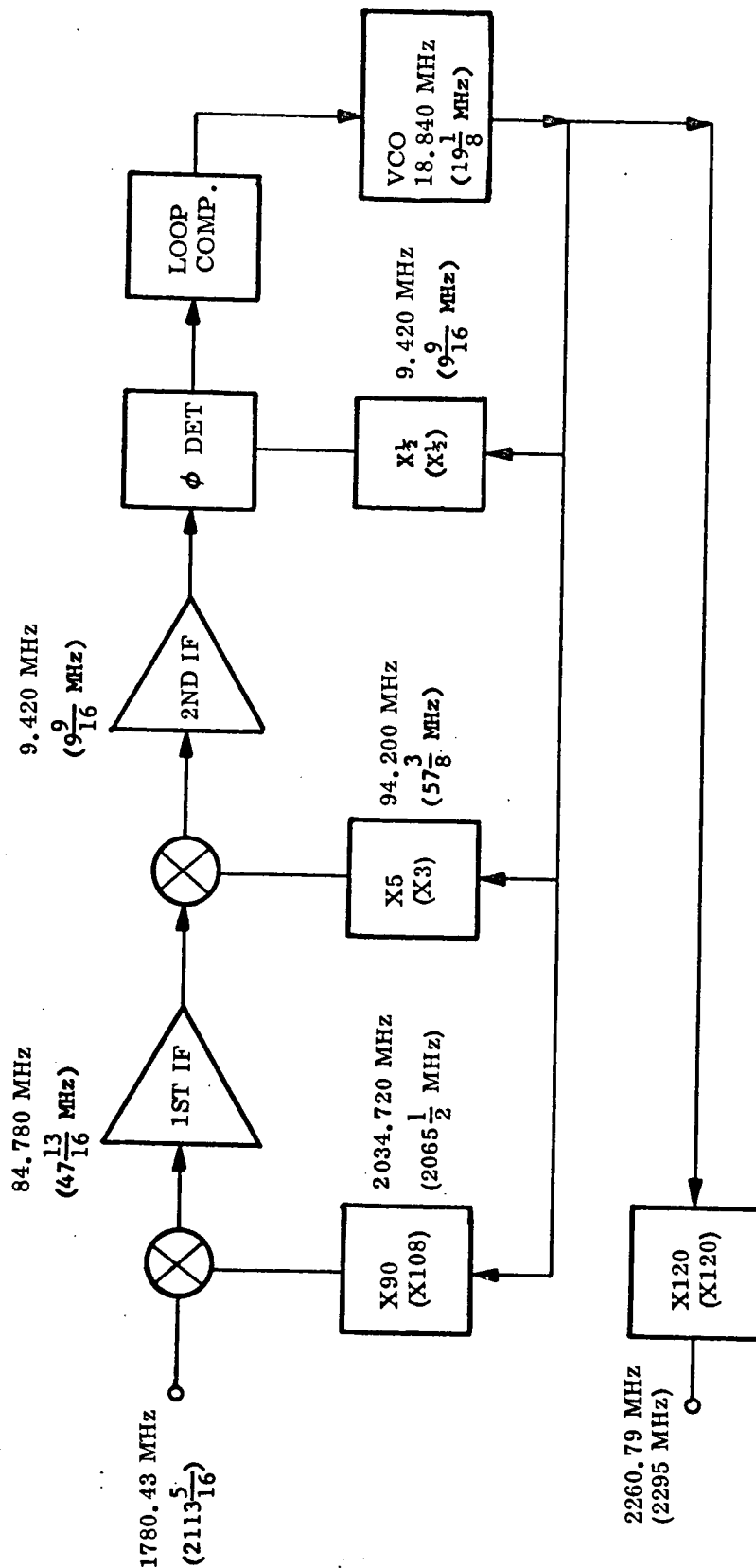
$$4.3.1.2 \quad f_{\mu} = af_0 \pm f_1$$

4.3.1.3 $f_1 = bf_0 \pm f_2$

4.3.1.4 $f_2 = cf_0$

4.3.1.5 $f_d = df_o$

*All frequencies and multiplication factors are positive quantities.



NOTE: Values shown in parenthesis are present S-band values.

Figure 4.3-2 Resultant Transponder

4.3.2 Derived Formulas

The following formulas are obtained by straightforward algebraic means, from the basic frequency relationships given in Section 4.3.1.

$$4.3.2.1 \quad f_u/f_o = [a \pm (b \pm c)]^*$$

$$4.3.2.2 \quad f_u/f_2 = [a \pm (b \pm c)]/c$$

$$4.3.2.3 \quad f_u/f_1 = [a \pm (b \pm c)]/(b \pm c)$$

$$4.3.2.4 \quad f_1/f_o = (b \pm c)$$

$$4.3.2.5 \quad f_1/f_2 = (b \pm c)/c$$

$$4.3.2.6 \quad f_2/f_o = c$$

$$4.3.2.7 \quad f_d/f_o = d$$

$$4.3.2.8 \quad f_d/f_2 = d/c$$

$$4.3.2.9 \quad f_d/f_1 = d/(b \pm c)$$

$$4.3.2.10 \quad f_d/f_u = d/[a \pm (b \pm c)] \triangleq r$$

Sign choices:	1.	+c	$f_1 > bf_o$
	2.	-c	$f_1 < bf_o$
	3.	+(b±c)	$f_u > af_o$
	4.	-(b±c)	$f_u < af_o$

*Derived by substitution of Equations 4.3.1.3 and 4.3.1.4 into Equation 4.3.1.2.

SECTION 5

VIDEO AMPLIFIER

5.0 GENERAL

The following describes the SRS Video Amplifier which was developed as part of the Phase II effort.

5.1 Functional Description.-

The video amplifier accepts the detected ranging modulation from the isolation amplifier, amplifies the signal to a limited output level, and provides separate outputs (isolated from one another) to each of the two phase modulators. A block diagram of the video amplifier is shown in Figure 5.1-1.

5.2 Specification Requirements.-

The performance requirements for the SRS Video Amplifier module are summarized in Table 5.2-1.

5.3 Problems in Mariner C Design.-

- a. Both output level and pulse symmetry vary excessively with variation in input level.
- b. As a function of temperature, gain variation and pulse asymmetry cause ranging distortion and error.
- c. Rise and fall times are a function of bandwidth.

14/6

TR-DA1522 A

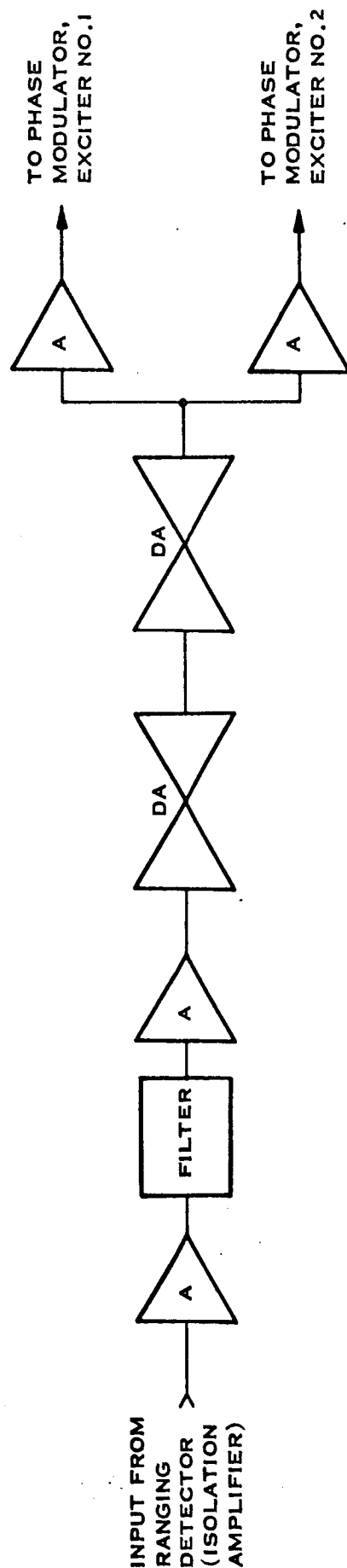


FIGURE 5.1-1 VIDEO AMPLIFIER

- d. Isolation between the two outputs (6 db) is marginal.
- e. Gain is too high both at 9.56 MHz and at 19.1 MHz.
- f. Output impedance is too low and is not controllable.
- g. Insufficient bandwidth results in undesirable ranging errors.

5.4 SRS Module Design.

The video amplifier module has been completely redesigned to overcome the above difficulties. The schematic diagram of the new module is shown in Figure 5.4-1.

The incoming signal is amplified approximately 20 db by the first stage (Q1, 2N917) and then goes through a five-pole Butterworth filter. The 3 db bandwidth of the filter is 40 Hz to 4.0 MHz. The steep attenuation above 4 MHz assures adequate suppression of any components at the second IF, VCO, or first IF frequencies. After the filter, the signal is amplified approximately 20 db by the second stage (Q2, 2N917).

The third stage of amplification is a differential amplifier consisting of a pair of 2N916 transistors (Q3 and Q4), that amplifies linearly at input levels up to -60 dbm, then limits at all higher input levels. The next stage is another differential amplifier (Q5 and Q6, also 2N916's) that limits the output regardless of whether the input to this stage is linear or has already been limited by the first differential amplifier.

The output stage for each of the two outputs is another 2N916 (Q7, Q8) in a common collector configuration. The gain provided at this stage brings the signal up to the required 0 dbm output level. Separation of the output stages of the signals to the two exciters provides 50 db isolation between the two outputs.

148

TABLE 5.2-1

VIDEO AMPLIFIER MODULE DESIGN SPECIFICATIONS

Modulation Frequency	70 Hz to 3.0 MHz
Impedance	
Input	50 \pm 5 ohms resistive
Output	50 \pm 10 ohms resistive
Video Power	
Input	-70 dbm to -5 dbm
Output	0 dbm \pm 1 db
Limiting (for 3 db drop in input power)	1 db max
Rise and Fall Time	80 nsec max
Transient Response (-70 db squarewave)	
Overshoot	5% max
Undershoot	5% max
Gain	
9.56 MHz	25 db max
19.1 MHz	10 db max
Current Drain	50 ma max
Voltage Supply	\pm 15 volts \pm 3%
Power Output Variation	+0.4, -0 db
Temperature	-20°C to +75°C

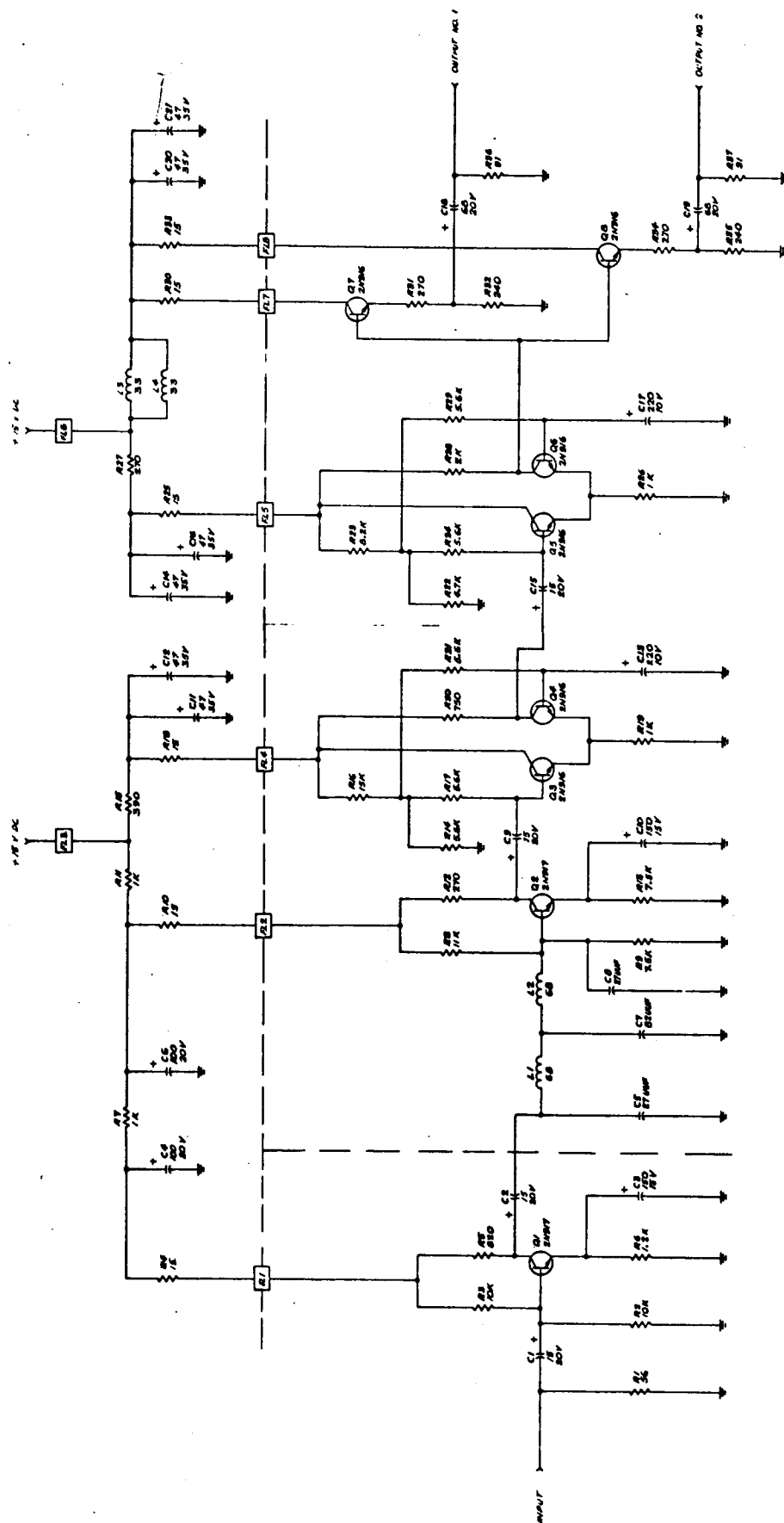


FIGURE 5.4-1 SCHEMATIC DIAGRAM - VIDEO AMPLIFIER

5.5 Test Data.-

Performance of the breadboard video amplifier module is summarized in Table 5.5-1. Figures 5.5-1 and 5.5-2 show representative oscillograph traces from which time delay measurements were made. Figures 5.5-3 and 5.5-4 show output vs input of 9.56 and 19.1 MHz signals, respectively; Figure 5.5-5 shows the module bandpass characteristic. Table 5.5-2 shows the attenuation of 498 kHz harmonics.

5.6 Comparison with Mariner C Module.-

Table 5.6-1 summarizes the significant differences between the Mariner C and the SRS Video Amplifier modules.

TABLE 5.5-1

SRS VIDEO AMPLIFIER BREADBOARD TEST DATA

Current Drain (15 vdc supply)	43 ma
Input Impedance	48 ohms
Output Impedance	50 ohms
Limited Gain (-70 dbm input)	70 db
Linear Gain (-85 dbm input)	85 db
Bandwidth (-85 dbm input)	
Lower 3 db point	40 Hz
Upper 3 db point	3.4 MHz
Rise Time	
-70 dbm input	50 nsec
-55 dbm input	50 nsec
Fall Time	
-70 dbm input	50 nsec
-55 dbm input	50 nsec
Power Output in dbm (-55 dbm input)	
Supply Voltage	-20°C 0°C +25°C +50°C +75°C
14.5 vdc	-.50 0.00 +.25 +.50 +.50
15.0 vdc	-.25 +.25 +.50 +.75 +.75
15.5 vdc	0.00 +.50 +.75 +1.00 +1.00

Limited Output Level (15 vdc supply, +25°C)

<u>Input Level</u>	<u>Power Output</u>
-70 dbm	+50 dbm
-60	+50
-55	+50
-50	+50
-40	+50
-30	+50

TABLE 5.5-1 (Continued)

SRS VIDEO AMPLIFIER BREADBOARD TEST DATA

Time Delay from Input to Output (25°C) - See Figure 5.5-1

<u>Input Level</u>	<u>Rise Time Delay (nsec)</u>	<u>Fall Time Delay (nsec)</u>
-70 dbm	245	240
-60	240	235
-55	240	230
-50	235	230
-40	230	230
-30	200	240

Time Delay from Input to Output (-55 dbm input) - See Figure 5.5-2

<u>Temperature</u>	<u>Rise Time Delay (nsec)</u>	<u>Fall Time Delay (nsec)</u>
-20°C	235	220
0°C	240	220
+25°C	240	230
+50°C	240	230
+75°C	240	250

Note: No change in time delay was observed due to supply voltage variations of ± 0.5 vdc.

9.56 MHz output level (-70 dbm input) -52 dbm (See Figure 5.5-3)
19.1 MHz output level (-70 dbm input) -76 dbm (See Figure 5.5-4)

Linear Frequency Response at -85 dbm input (See Figure 5.5-5)

<u>Frequency</u>	<u>Output (dbm)</u>	<u>Attenuation (db)</u>
30 Hz	-8	-6
40 Hz	-5	-3
60 Hz	-3	-1
100 Hz	-2	0
50 kHz	-2	0
500 kHz	-2	0
1.0 MHz	-2	0
2.0	-2	0
2.8	-3	-1
3.4	-5	-3
4.0	-8	-6

(continued)

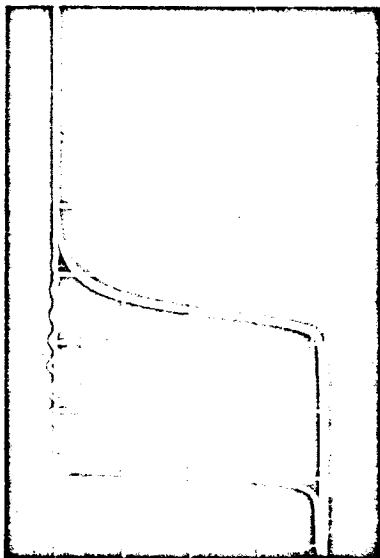
<u>Frequency</u>	<u>Output (dbm)</u>	<u>Attenuation (db)</u>
4.6 MHz	-14	-12
5.0	-19	-17
5.5	-29	-27
6.0	-32	-30
7.0	-43	-41
8.0	-52	-50
9.56	-68	-66

TABLE 5.5-2

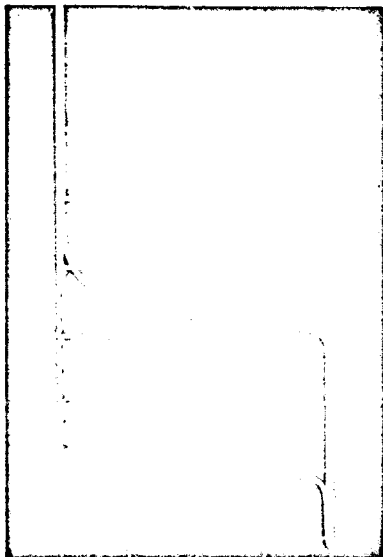
ATTENUATION OF 498 kHz HARMONICS IN DB

498 kHz Input (dbm)	1.0	1.5	2.0	2.5	3.0	3.5	4.0	4.5	5.0	5.5	6.0	6.5	7.0
-70	-30db	-20	-50	-40	-50	-50	-50	-50	-50	-50	-50	-50	-50
-60	-30	-10	-30	-20	-30	-20	-30	-30	-40	-50	-50	-50	-50
-50	-40	-10	-30	-20	-30	-20	-30	-20	-30	-30	-40	-50	-50
-40	-40	-10	-40	-20	-40	-20	-40	-30	-40	-30	-40	-30	-40

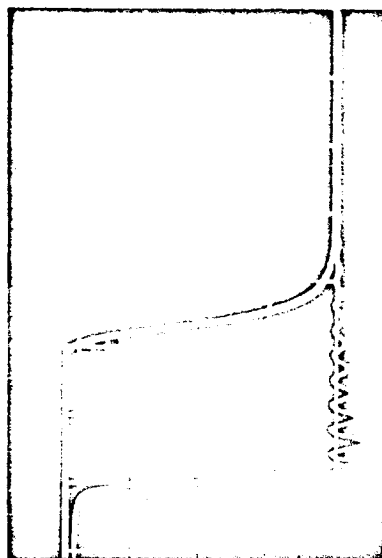
Note: Attenuation is given in db below 0.0 dbm of 498 kHz output, e.g., -50 indicates that attenuation is at least 50 db below 0.0 dbm.



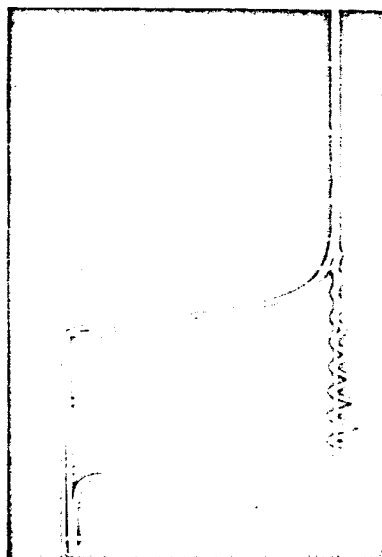
TIME DELAY: 245 NSEC
Figure 1



TIME DELAY: 230 NSEC
Figure 3

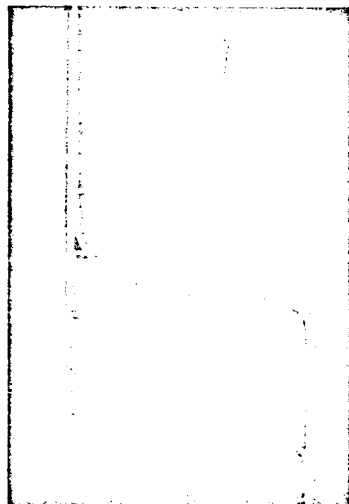


TIME DELAY: 240 NSEC
INPUT LEVEL: -70 DBM
Figure 2

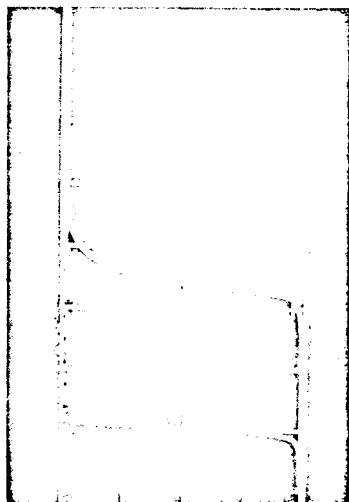


TIME DELAY: 230 NSEC
INPUT LEVEL: -40 DBM
Figure 4

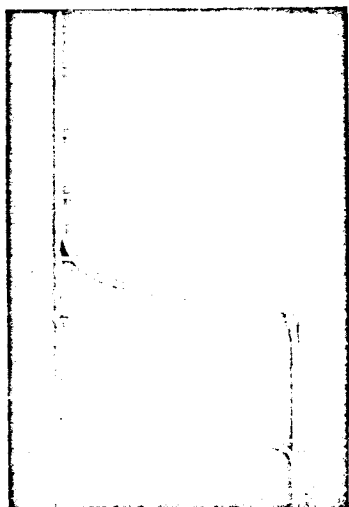
Figure 5.5-1 Response at -70 DBM and -40 DBM Input Levels
SCALE: 0.1 μ sec/cm
TEMPERATURE: +25°C
OUTPUT LEVEL: .5 dbm



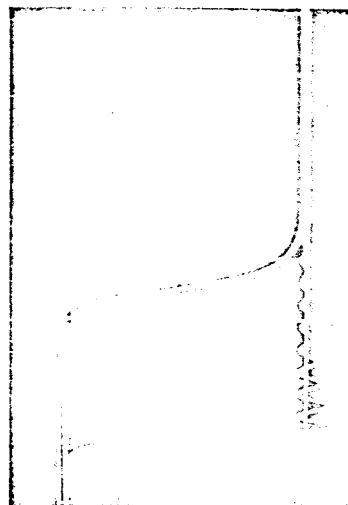
TIME DELAY: 240 NSEC
Figure 2-5



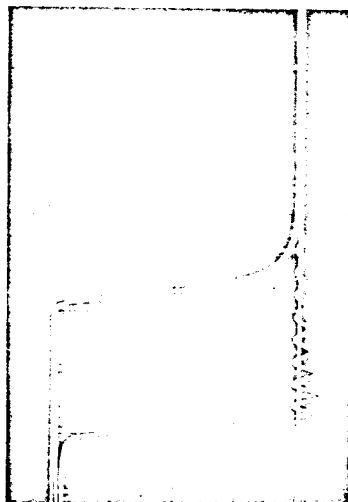
TIME DELAY: 240 NSEC
Figure 2-3



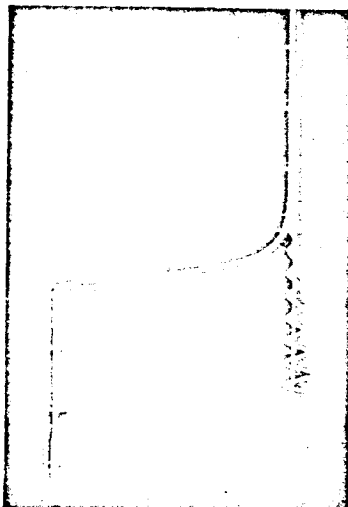
TIME DELAY: 235 NSEC
Figure 2-1



TIME DELAY: 250 NSEC
TEMPERATURE: +75°C
Figure 2-6



TIME DELAY: 230 NSEC
TEMPERATURE: +25°C
Figure 2-4



TIME DELAY: 220 NSEC
TEMPERATURE: -20°C
Figure 2-2

Figure 5.5-2 Response at -20°C, +25°C, and +75°C
SCALE: 0.1 μ sec/cm
INPUT LEVEL: -55 dbm

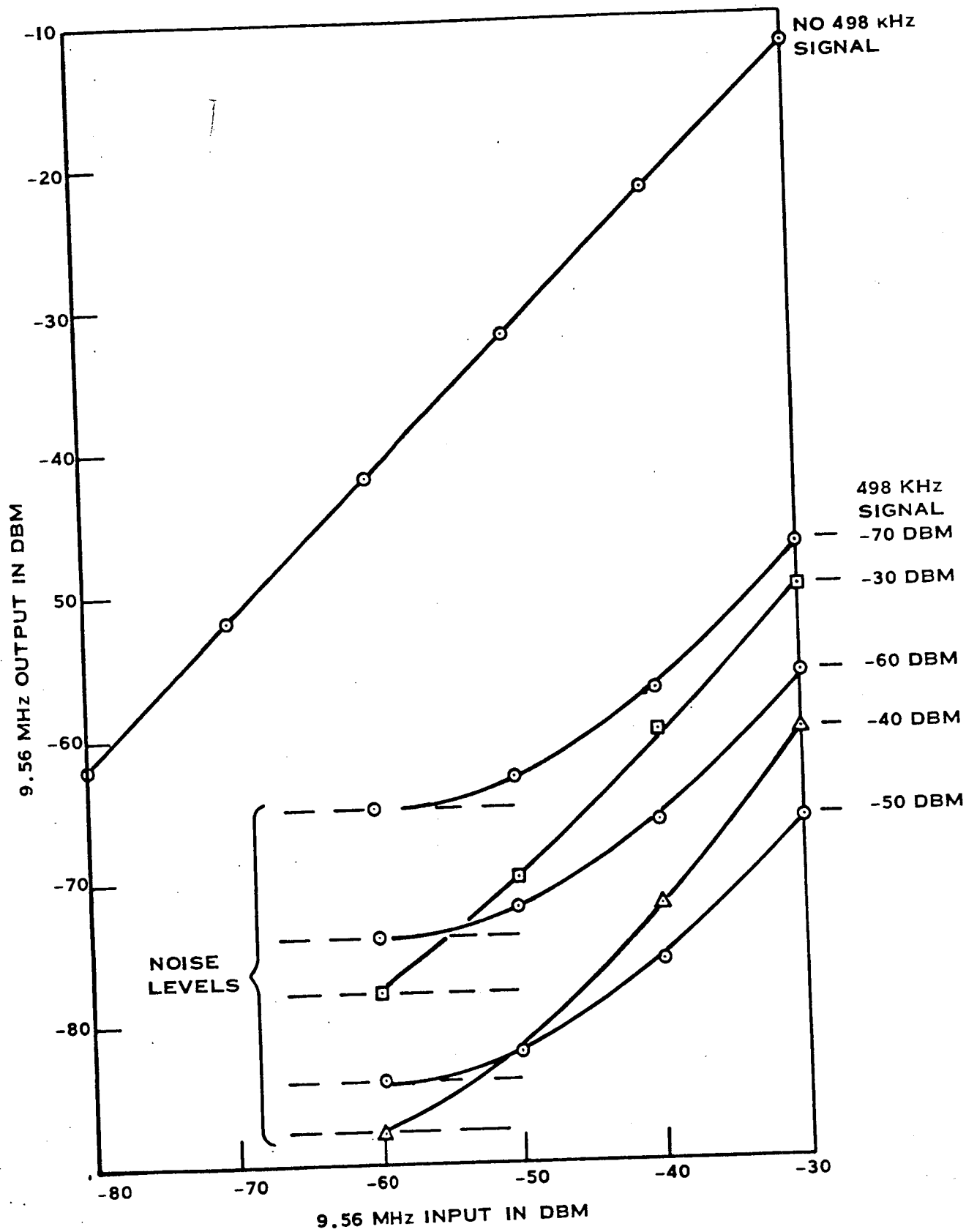


FIGURE 5.5-3 9.56 MHz OUTPUT VS. INPUT

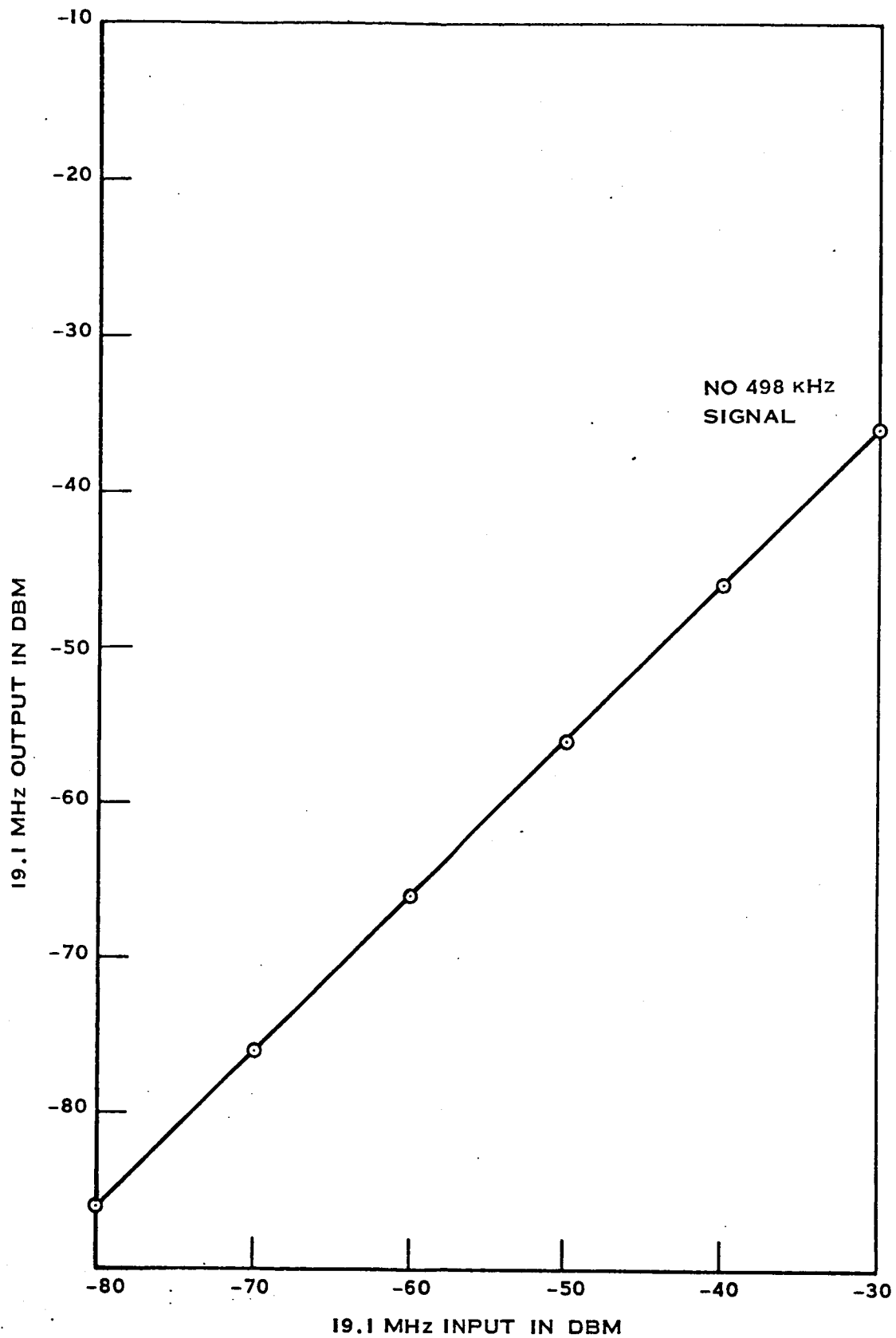


FIGURE 5.5-4 19.1 MHz OUTPUT VS. INPUT

TR-DA1522 A

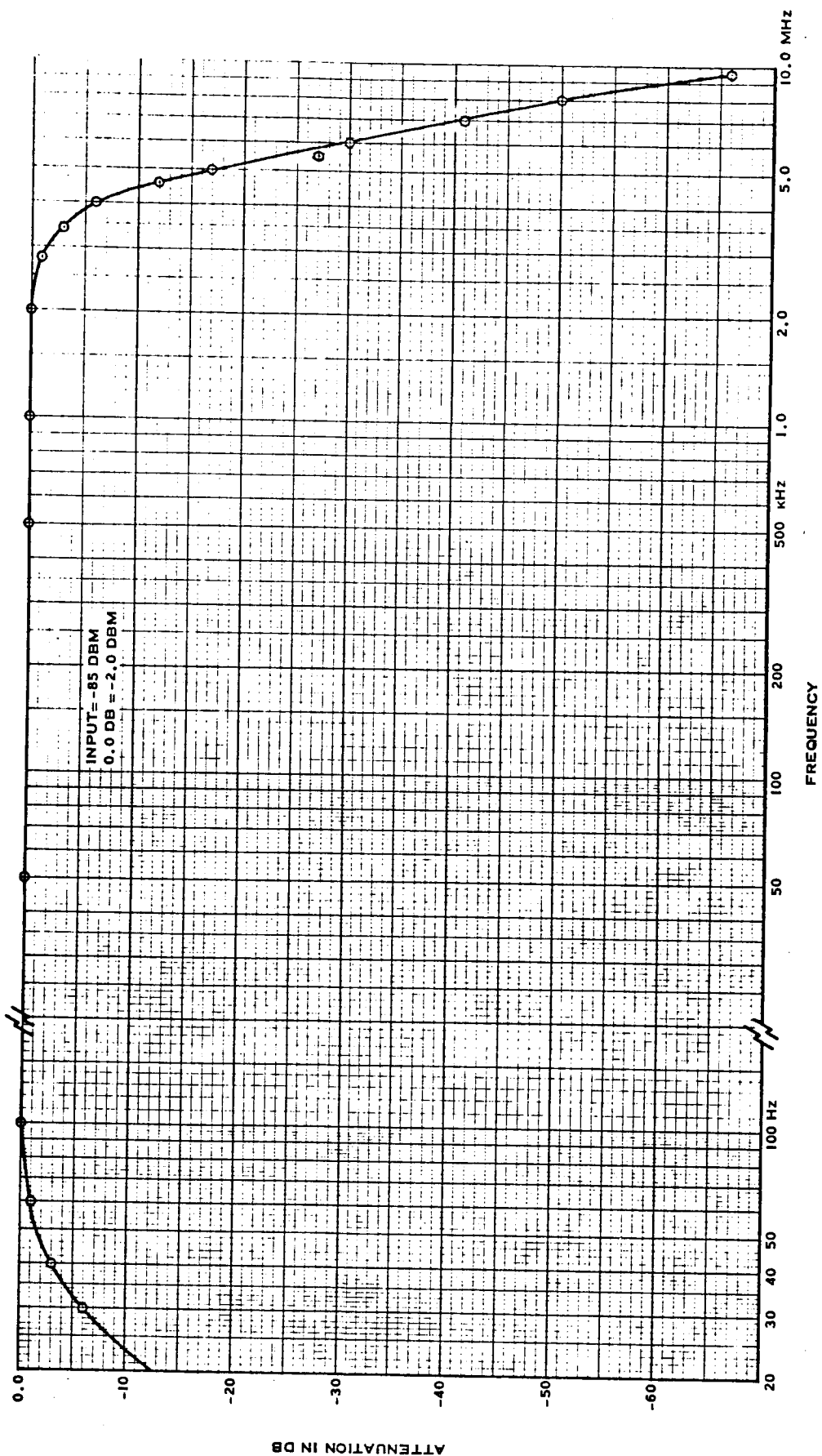


FIGURE 5.5-5 VIDEO AMPLIFIER BANDPASS CHARACTERISTIC

ATTENUATION IN DB

5-14

TABLE 5.6-1

VIDEO AMPLIFIER CHANGES FROM MARINER C

	<u>Mariner C</u>	<u>SRS Version</u>
1. Gain Variation vs Temperature	± 2 db	± 1 db
2. Output Level vs Input Drive (-5 to -70 dbm)	± 1 db	± 0.25 db
3. Pulse Symmetry Variation vs Temperature	50 ns	30 ns
4. Pulse Width Symmetry	500 ns	10 ns
5. Rise & Fall Times (-70 dbm Input)	80 ns R; 90 ns F	50 ns
6. Output Impedance	35 ohms	50 ohms (Adjustable)
7. Isolation Between Outputs	6 db	50 db
8. Bandwidth at -85 dbm Input	1 kHz to 3.3 MHz	40 Hz to 3.4 MHz
9. Gain at 9.56 MHz	34 db	18 db
10. Gain at 19.1 MHz	34 db	-6 db
11. Symmetry Variation vs P.S. Voltage Variations (± 5 volt)	25 ns	Unmeasurable
12. Current Drain	21 ma	43 ma

SECTION 6

CONCLUSIONS AND RECOMMENDATIONS

6.1 DISCUSSION AND REVIEW

The design study of the S-Band Turnaround Ranging Transponder was divided into two parts, Phase I and Phase II. The Phase I effort was directed toward general circuit and system performance improvements, and the Phase II effort was directed towards evaluating the ranging system mainly, and secondly towards evaluating the input-to-output S-Band phase stability over temperature.

Due to the fact that the Phase I effort covered a broad spectrum of topics, no attempt will be made in this section to discuss the conclusions or recommendations resulting from that effort. A brief summary of the design deficiencies and the proposed module and system design changes to correct these deficiencies is presented in the Summary, Section II. For further details, refer to the "Interim Engineering Report", WDL-TR3066.

6.1.1 Ranging System

Table 2.3.1-2 summarizes the ranging delay and ranging delay variation evaluation study. In it is presented measured and expected values, for the Mariner "C" transponder. The expected delay variation performance can be improved greatly, as it will be shown, if the following conditions are met:

1. Crystal filter interaction is eliminated
2. Ranging detector misalignment is held to ± 20 degrees.

<u>$\Delta\theta_{ref}$</u>	<u>ΔT_d</u>
(deg)	(n sec)
-20	-12.3
+20	+14.0

This data, plus the expected total group delay variation obtained from Section 4.1.1 provide the following design goals in ranging delay variation:

<u>Temperature</u> <u>Range</u>	<u>$(\Delta T_d)_{min}$</u> (n sec)	<u>$(\Delta T_d)_{max}$</u> (n sec)
$-\Delta T$	-5.8	+20.5
$+\Delta T$	-1.8	+24.5

Note that now the delay variations due to group delay is now an appreciable factor, compared to that due to misalignment in the ranging detector.

The new maximum expected spread is then about 30.3 n sec, as compared to measured value of 84.3. The improvement is all the more significant in view of the reduction in cancellation effects, not to mention the reduction in ranging signal distortion.

6.1.2 S-Band Phase Shift

The S-Band phase shift can be reduced to about one-half its present value by correcting only the impedance interface problem between the VCO and the Frequency Divider. This can be done by replacing the present VCO output stage and the present Frequency Divider input stages with temperature compensated, broad-band isolation stages. (Note: The preceding statements hinge on the verification of the assumption that an impedance interface problem exists; time and funding did not permit proper investigation of the problem.)

It is estimated that the input-to-output S-Band phase shift can be reduced to about five cycles. This is equivalent to a time delay equal to 2.18 n sec. Use of the S-Band carrier in range measurements is attractive from the standpoint of fine range resolution, but would be complicated by "lost" cycle counts in the mission. "Cogs" would also result in small ranging errors, since the "VCO" phase has 221 equally probable locked states, relative to the input S-Band signal.

6.1.3 Spectrum Analysis

Table A.4-1 lists the expected spectral amplitudes of the ranging signal at the input and the output of the transponder. The values are based on the mathematical model presented in Appendix IV. This analysis was a by-product of the demodulation analysis presented in Appendix II, and was funded on another related program. Measurements indicate that the results are valid for the values of the parameters chosen, and are useful in checking for unwanted variations in the input or output signals of the transponder. Note that the test set output spectrum is non-symmetrical, and that the transponder output spectrum indicates over-deviation, and limited bandwidth as evidenced by the high value of the even sidebands.

6.2 RECOMMENDATIONS FOR FUTURE WORK

In order to achieve the ultimate in performance of the JPL transponder, the following areas are recommended for future effort:

Modules

- Existing Mixer Preamplifier Design lacks gain and stability.
- The Frequency Divider should be redesigned to increase stability and give added filtering to subharmonics.
- Redesign the VCO to provide isolation between frequency divider and auxiliary oscillator outputs, and improve oscillator bias stability.

System

- A transponder detail system analysis should be made to determine optimum gain, bandwidth, and signal/reference level distribution.
- A review should be made to determine the optimum transponder functional configuration.
- Ranging and doppler measurements should be made on the new module designs to verify the expected improvements. It is recommended that modules be tested as is, at first, then updated according to the design recommendations arising out of the Phase II effort, and then given a final test. The tests should be done with a JPL-supplied transponder on an SRS module, SRS six-pack, and a complete SRS transponder basis. This would allow JPL to evaluate and accept only those changes deemed necessary.

The technical know-how and experience exists at Philco-SRS Division for efficiently investigating these areas, due to the invaluable experience derived from the design study program, JPL Contract 951290.

APPENDIX I

**PHASE SHIFT AND GROUP DELAY VS RELATIVE DETUNING
SINGLE AND TRANSITIONAL COUPLED DOUBLE TUNED FILTERS**

APPENDIX I

PHASE SHIFT AND GROUP DELAY VS RELATIVE DETUNING
SINGLE AND TRANSITIONAL COUPLED DOUBLE TUNED FILTERS

$$A.1.1 \text{ Relative detuning} = \frac{\Delta \omega}{B} = \frac{\omega - \omega_0}{B} = \chi$$

$$\Delta \omega = \omega - \omega_0 \stackrel{\Delta}{=} \text{detuning in rad/sec}$$

$$B = \text{filter BW}_{-3\text{db}} \text{ in rad/sec}$$

$$B_1 = \text{BW}_{-3\text{db}} \text{ of 1-pole}$$

$$B_2 = \text{BW}_{-3\text{db}} \text{ of 2-pole, transitionally coupled}$$

$$B_2 = \sqrt{2} B_1 \text{ for two identical 1-poles having } B_1 \\ \text{and transitionally coupled}$$

A.1.2 Phase Shift

$$\phi_1 = \text{phase shift of 1-pole}$$

$$\phi_2 = \text{phase shift of 2-pole}$$

$$\phi_1 = -\tan^{-1}(2\chi)$$

$$\phi_2 = -\tan^{-1}\left(\frac{2\sqrt{2}\chi}{1-4\chi^2}\right)$$

A.1-1

From the preceeding expressions:

χ	ϕ_1 (deg)	ϕ_2 (deg)
0.0	0.0	0.0
0.1	11.3	16.4
0.2	21.8	34.0
0.3	31.0	52.9
0.4	38.7	72.3
0.5	45.0	90.0
0.6	50.1	104.6
0.7	54.4	115.9

This data is plotted in Figure A.1-1.

A.1.3. Group Delay*

$$\tau = - \frac{d\phi}{d\omega} = - \frac{d\phi}{d\chi} \frac{d\chi}{d\omega}$$

$$\tau_1 = - \frac{d\phi_1}{d\chi} \frac{d\chi}{d\omega} = \left(\frac{2}{B_1} \right) \left(\frac{1}{1+4\chi^2} \right)$$

$$\tau_2 = \frac{d\phi_2}{d\chi} \frac{d\chi}{d\omega} \left(\frac{2\sqrt{2}}{B_2} \right) \left(\frac{1+4\chi^2}{1+16\chi^4} \right)$$

*Fagot and Magne, Frequency Modulation Theory.

Pergamon Press, New York, 1961.

Note: This theory is subject to the limitation that the filter bandwidth is large with respect to the modulation spectrum.

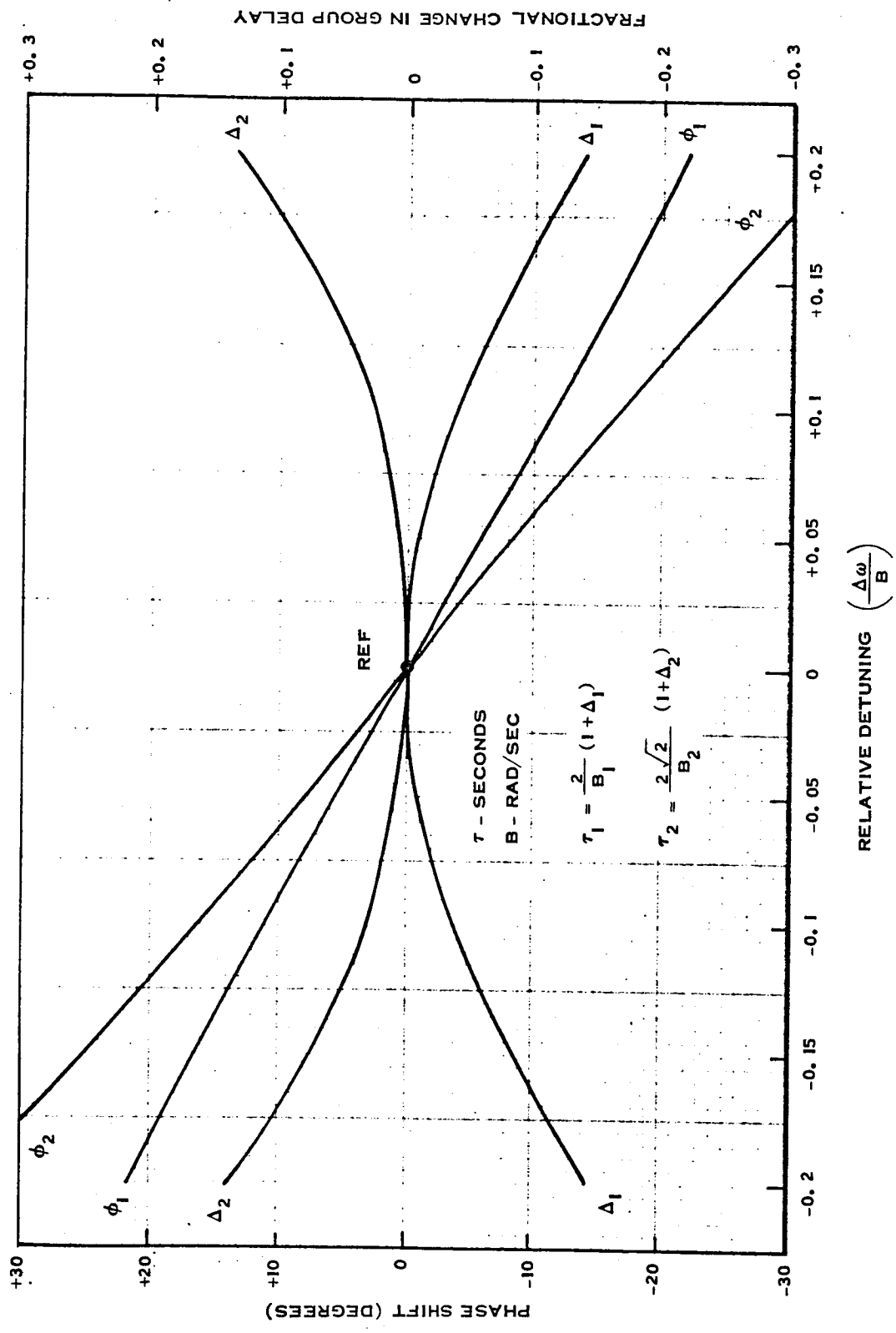


Figure A.1-1 Phase Shift and Fractional Change in Group Delay vs. Relative Detuning for 1-Pole and 2-Pole Bandpass Interstage Coupling Networks.

A.1.3.1 Fractional Change in Group Delay Versus Relative Detuning

Let

$\Delta_1 \triangleq$ fractional change for 1-pole

$\Delta_2 \triangleq$ fractional change for 2-pole

$$\tau_1 = \left(\frac{2}{B_1}\right)(1 + \Delta_1)$$

$$\tau_2 = \left(\frac{2\sqrt{2}}{B_2}\right)(1 + \Delta_2) .$$

Then, solving for Δ_1 and Δ_2

$$1 + \Delta_1 = \frac{1}{1 + 4x^2}$$

$$1 + \Delta_2 = \frac{1 + 4x^2}{1 + 16x^4}$$

$$\Delta_1 = - \frac{4x^2}{1 + 4x^2}$$

$$\Delta_2 = + \frac{4x^2(1 - 4x^2)}{1 + 16x^4} .$$

The expressions for Δ_1 and Δ_2 have been evaluated, and are tabulated in the following table.

χ	$4\chi^2$	$16\chi^4$	$-100\Delta_1$	$+100\Delta_2$
0.00	0.0000	0.0000	0.00	0.00
0.02	0.0016	2.56×10^{-6}	0.16	0.16
0.04	0.0064	4.10×10^{-5}	0.64	0.63
0.06	0.0124	1.54×10^{-4}	1.23	1.21
0.08	0.0264	6.97×10^{-4}	2.56	2.48
0.10	0.0400	1.60×10^{-3}	3.84	3.69
0.12	0.0576	3.32×10^{-3}	5.41	5.10
0.14	0.0784	6.15×10^{-3}	7.21	6.63
0.16	0.1024	0.0104	9.18	8.26
0.18	0.1296	0.0169	11.3	9.83
0.20	0.1600	0.0256	13.4	11.3

This data is plotted in Figure A.1-1.

A.1.3 Group Delay for Small Relative Detuning, χ :

The phase expressions given in Section 2. can be simplified as follows when χ is small

$$\phi_1 \approx -2\chi \text{ radians}$$

$$\phi_2 \approx -2\sqrt{2} \chi \text{ radians.}$$

This results in the following simplified expressions

$$\Delta_1 \approx -\phi_1^2$$

$$\Delta_2 \approx +\frac{1}{2} \phi_2^2$$

$$\tau_1 \approx \frac{2}{B_1} (1 - \phi_1^2)$$

$$\tau_2 \approx \frac{2\sqrt{2}}{B_2} (1 + \frac{1}{2} \phi_2^2).$$

Where the ϕ values are in radians, as noted above.

A.1-5

A.1.4 Circuit Element Stability

$$\omega_o = \frac{1}{\sqrt{L_o C_o}}$$

$$\frac{\Delta\omega}{\omega_o} = \sqrt{L_o C_o} \left(\frac{1}{\sqrt{LC}} - \frac{1}{\sqrt{L_o C_o}} \right)$$

$$= \sqrt{L_o C_o} \left[\frac{1}{\sqrt{(L_o)(1 + \frac{\Delta L}{L_o})(C_o)(1 + \frac{\Delta C}{C_o})}} - \frac{1}{\sqrt{L_o C_o}} \right]$$

$$= \frac{1}{\sqrt{1 + (\frac{\Delta L}{L_o} + \frac{\Delta C}{C_o}) + \frac{\Delta L \Delta C}{L_o C_o}}} - 1$$

$$\frac{\Delta\omega}{\omega_o} \approx -\frac{1}{2} \left(\frac{\Delta L}{L_o} + \frac{\Delta C}{C_o} \right)$$

$$\therefore \frac{\Delta L}{L_o} + \frac{\Delta C}{C_o} = -2 \left(\frac{\Delta\omega}{\omega_o} \right)$$

$$\frac{\Delta\omega}{\omega_o} = \frac{\Delta\omega}{\beta} \times \frac{\beta}{\omega_o}$$

$$\frac{\Delta L}{L_o} + \frac{\Delta C}{C_o} = - \left(\frac{2\beta}{\omega_o} \right) \frac{\Delta\omega}{\beta}$$

To determine the temperature stability coefficient of a 1-pole or transitional 2-pole when the phase versus temperature characteristic is known.

1. Calculate $\frac{2B}{\omega_o}$
2. Obtain $\frac{\Delta\omega}{B}$ from the ϕ vs. $\frac{\Delta\omega}{B}$ graph or the simplified expressions
(Note: $\frac{\Delta\omega}{B} = \chi$)
3. Compute $\frac{\Delta L}{L_o} + \frac{\Delta C}{C_o}$ and divide by the temperature increment

TR-DA1522A

APPENDIX II

DEMODULATION OF A TRAPEZOIDAL PHASE MODULATED CARRIER

APPENDIX II

DEMODULATION OF A TRAPEZOIDAL PHASE MODULATED CARRIER

A.2.1 Definitions

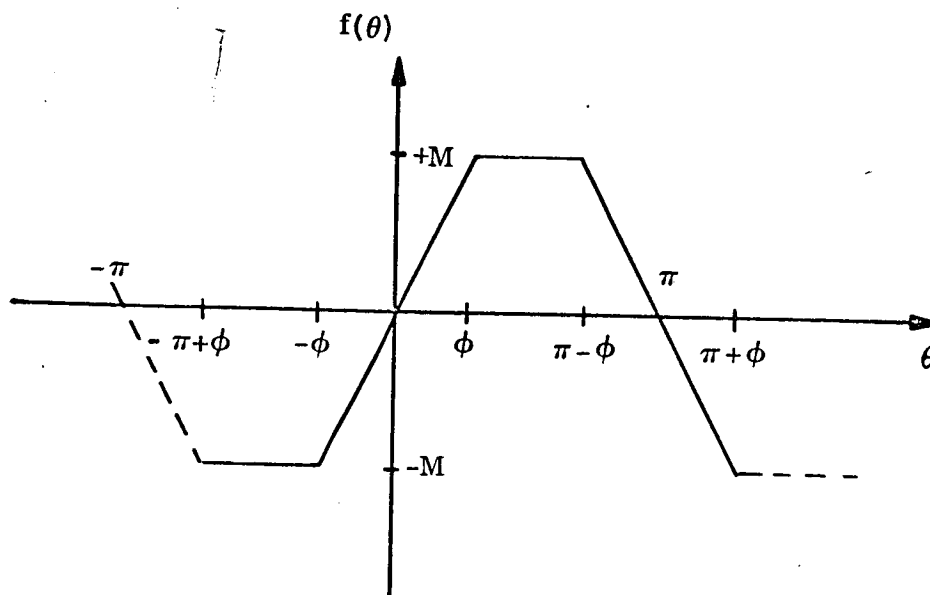
- $\theta = \theta(t) = \omega_m t =$ Modulation phase variable
 $\theta_R =$ reference phase relative to signal carrier
 $M =$ peak amplitude of phase excursion
 $2\phi =$ period of slope, in assumed trapezoidal modulation waveform ($\phi_{\max} = \pi/2$)
 $f(\theta) =$ modulation function
 $\cos[\theta_R + f(\theta)] =$ phase detector function
 $e_o(\theta) =$ video output waveform

Note: The R.F. carrier frequency is considered much greater than the modulation frequency.

A.2.2 Mathematical Model Analyzed

$$e_o(\theta) = K \cos[\theta_R + f(\theta)]$$

$$\begin{aligned}
 f(\theta) &= -M & -\pi + \phi \leq \theta \leq -\phi \\
 &= \frac{M}{\phi} \theta & -\phi \leq \theta \leq +\phi \\
 &= +M & +\phi \leq \theta \leq \pi - \phi \\
 &= -\frac{M}{\phi}(\theta - \pi) & \pi - \phi \leq \theta \leq \pi + \phi
 \end{aligned}$$



A.2.2.1 Fourier Series for $f(\theta)$, the Modulation Function

$$f(\theta) = \frac{A'_0}{2} + \sum_{n=1}^{\infty} A'_n \cos n\theta + B'_n \sin n\theta$$

$$f(\theta) = \sum_{n=1}^{\infty} B'_n \sin n\theta = B'_1 \sin \theta + B'_3 \sin 3\theta + B'_5 \sin 5\theta \dots$$

$$\frac{\pi}{K} B'_n = [1 - (-1)^n] \left(\frac{2M}{n} \right) \left(\frac{\sin n\theta}{n\theta} \right)$$

A.2.2.2 Fourier Analysis of $e_o(\theta)$, the video output waveform:

$$e_o(\theta) = \frac{A_o}{2} + \sum_{n=1}^{\infty} A_n \cos n\theta + B_n \sin n\theta$$

$$\frac{\pi}{K} A_o = \int_{-\pi+\phi}^{+\pi+\phi} e_o(\theta) d\theta$$

$$\frac{\pi}{K} A_n = \int_{-\pi+\phi}^{+\pi+\phi} e_o(\theta) \cos n\theta d\theta$$

$$\frac{\pi}{K} B_n = \int_{-\pi+\phi}^{+\pi+\phi} e_o(\theta) \sin n\theta d\theta$$

$$\frac{\pi}{K} \frac{A_o}{2} = \cos \theta_R \left[(\pi - 2\phi) \cos M + 2\phi \frac{\sin M}{M} \right]$$

$$\frac{\pi}{K} A_n = +[1+(-1)^n](\cos \theta_R) \left\{ \phi \left[\frac{\sin(M+n\phi)}{M+n\phi} + \frac{\sin(M-n\phi)}{M-n\phi} \right] - \frac{2}{n} \cos M \sin n\phi \right\}$$

$$\frac{\pi}{K} B_n = -[1-(-1)^n](\sin \theta_R) \left\{ \frac{2}{n} \sin M \cos n\phi - \phi \left[\frac{\sin(M+n\phi)}{M+n\phi} - \frac{\sin(M-n\phi)}{M-n\phi} \right] \right\}$$

A.2.3 Fourier Coefficients

$$\frac{\pi}{K} A_1 = B_2 = A_3 = B_4 \cdots \equiv 0$$

$$\frac{\pi}{K} B_1 = -2 \sin \theta_R \left\{ 2 \sin M \cos \phi - \phi \left[\frac{\sin(M+\phi)}{M+\phi} - \frac{\sin(M-\phi)}{M-\phi} \right] \right\}$$

$$\frac{\pi}{K} A_2 = +2 \cos \theta_R \left\{ \phi \left[\frac{\sin(M+2\phi)}{M+2\phi} + \frac{\sin(M-2\phi)}{M-2\phi} \right] - \cos M \sin 2\phi \right\}$$

$$\frac{\pi}{K} B_3 = -2 \sin \theta_R \left\{ \frac{2}{3} \sin M \cos 3\phi - \phi \left[\frac{\sin(M+3\phi)}{M+3\phi} - \frac{\sin(M-3\phi)}{M-3\phi} \right] \right\}$$

$$\frac{\pi}{K} A_4 = +2 \cos \theta_R \left\{ \phi \left[\frac{\sin(M+4\phi)}{M+4\phi} + \frac{\sin(M-4\phi)}{M-4\phi} \right] - \frac{1}{2} \cos M \sin 4\phi \right\}$$

•
•
•

A.2.4 Demodulated Output ($\theta = \omega_M t$)

$$\begin{aligned}
 e_o(t) = & \frac{A_o}{2} + B_1 \sin(\omega_M t) + A_2 \cos(2\omega_M t) \\
 & + B_3 \sin(3\omega_M t) + A_4 \cos(4\omega_M t) \\
 & + \dots
 \end{aligned}$$

Note that θ_R can affect the phase of the fundamental component, $B_1 \sin \omega_M t$, by only a change in sign; i.e., by ± 1 . The characteristic curve shape of the ranging phase detector (Figure 3.2.2-4) is not predicted in this model.

APPENDIX III.1

DELAY VARIATION CAUSED BY REFERENCE PHASE VARIATION IN THE DEMODULATION
OF A RANGING SIGNAL WHICH CONTAINS COMPLEX AMPLITUDE MODULATION

APPENDIX III.1

DELAY VARIATION CAUSED BY REFERENCE PHASE VARIATION IN THE DEMODULATION OF A RANGING SIGNAL WHICH CONTAINS COMPLEX AMPLITUDE MODULATION

A3.1. From Appendix II, let

$$e_o(\theta) = K \cos[\theta_R + f(\theta)] = \text{demodulated video waveform}$$

A3.2. Assume $K \neq$ constant

$$= 1 + A(\theta).$$

That is, assume the ranging signal envelope is amplitude modulated with an unwanted complex waveform having no symmetry conditions but with the same period as $f(\theta)$, the desired phase modulation waveform.

A3.3. Let $A(\theta)$ be represented by the Fourier series

$$A(\theta) = \frac{a_o}{2} + \sum_{m=1}^{\infty} (a_m \cos m\theta + b_m \sin m\theta)$$

$$A3.3.1 \quad e_o(\theta) = [1 + A(\theta)] \left\{ \cos[\theta_R + f(\theta)] \right\}$$

A3.4 Combining terms, using the Fourier series for $\cos[\theta_R + f(\theta)]$ obtained in Appendix II.

$$e_o(\theta) = \left[1 + \frac{a_o}{2} + \sum_{m=1}^{\infty} (a_m \cos m\theta + b_m \sin m\theta) \right] \left[\frac{A_o}{2} + \sum_{n=1}^{\infty} (A_n \cos n\theta + B_n \sin n\theta) \right]$$

$$\frac{B_3}{2}(b_2 \cos \theta + a_2 \sin \theta)$$

$$\frac{A_2}{2}(a_3 \cos \theta + b_3 \sin \theta)$$

$$\frac{A_4}{2}(a_3 \cos \theta - b_3 \sin \theta)$$

$$\frac{B_3}{2}(b_4 \cos \theta - a_4 \sin \theta)$$

$$\frac{B_5}{2}(b_4 \cos \theta + a_4 \sin \theta)$$

⋮

A3.7 The resultant phase angle is hence

$$\tan \Delta\theta_d = \frac{\frac{a_1}{2}(A_o + A_2) + \frac{b_2}{2}(B_1 + B_3) + \frac{a_3}{2}(A_2 + A_4) + \dots}{(1 + \frac{a_o}{2})(B_1) + \frac{b_1}{2}(A_o - A_2) - \frac{a_2}{2}(B_1 - B_3) + \frac{b_3}{2}(A_2 - A_4) + \dots}$$

A3.8 For $\phi \ll 1$ (modulation approaches square wave) and $a_o/2 \ll 1$, the expression simplifies to

$$\tan \Delta\theta_d \approx \frac{\frac{a_1 A_o}{2} + \frac{2b_2 B_1}{3}}{B_1 + \frac{b_1 A_o}{2} - \frac{a_2 B_1}{3}}$$

where

$$A_{\text{even}} \rightarrow 0$$

$$B_3 \rightarrow 1/3 B_1$$

$$B_5 \text{ etc} \rightarrow 0$$

$$e_o(\theta) = (1 + \frac{a_o}{2})(\frac{A_o}{2}) + (1 + \frac{a_o}{2}) \sum (A_n \cos n\theta + B_n \sin n\theta) \\ + (\frac{A_o}{2}) \sum (a_n \cos m\theta + b_n \sin m\theta) + \left[\sum (a_m \cos m\theta + b_m \sin m\theta) \right] \\ \left[\sum (A_m \cos m\theta + B_m \sin m\theta) \right]$$

A3.5 The last term then becomes

$$\sum_{n=1}^{\infty} \sum_{m=1}^{\infty} (a_m A_n \cos m\theta \sin n\theta + b_m B_n \sin m\theta \sin n\theta + a_m B_n \cos m\theta \sin n\theta + \\ b_n A_n \sin m\theta \cos n\theta) \\ \sum_{n=1}^{\infty} \sum_{m=1}^{\infty} \left[\frac{a_m A_n}{2} \left\{ \cos[(m+n)\theta] + \cos[(m-n)\theta] \right\} + \frac{b_m B_n}{2} \left\{ \cos[(m-n)\theta] - \cos[(m+n)\theta] \right\} + \right. \\ \left. \frac{a_m B_n}{2} \left\{ \sin[(m+n)\theta] - \sin[(m-n)\theta] \right\} + \frac{b_n A_n}{2} \left\{ \sin[(m-n)\theta] + \sin[(m+n)\theta] \right\} \right]$$

A3.6. Evaluating only for the fundamental term, and noting $A_{\text{odd}} = B_{\text{even}} = 0$ from Appendix II.

$$(e_o)_1 = (1 + \frac{a_o}{2})(B_1 \sin \theta) + (\frac{A_o}{2})(a_1 \cos \theta + b_1 \sin \theta) \\ + \frac{A_2}{2}(a_1 \cos \theta - b_1 \sin \theta) \\ + \frac{A_2}{2}(a_1 \cos \theta - b_1 \sin \theta) \\ + \frac{B_1}{2}(b_2 \cos \theta - a_2 \sin \theta)$$

APPENDIX III.2

DELAY VARIATION CAUSED BY REFERENCE PHASE VARIATION IN THE
DEMODULATION OF THE RANGING SIGNAL - AN IDEALIZED MODEL

APPENDIX III.2

DELAY VARIATION CAUSED BY REFERENCE PHASE VARIATION IN THE
DEMODULATION OF THE RANGING SIGNAL - AN IDEALIZED MODEL

A pictorial representation of ranging delay due to reference phase variation is illustrated in Figure A.3-3. Sketch A.3-3b shows the phase relationship between modulated and unmodulated carrier. At $t=t_0$, the phase deviation waveform (A.3-3a) advances the phase of the carrier $+180^\circ$. Again at $t=1/2 T_{498}$ the carrier phase is acted on and caused to shift -180° .

Of interest is the video output of this phase modulated waveform which is approximated by reference signal sampling of the ranging signal (A.3-3c). If the reference signal is exactly at -90° with respect to the unmodulated carrier, then it's output will be as shown in Sketch A.3-3d. However, if the reference signal is shifted, say $\pm 45^\circ$, the video output will undergo a delay variation as shown.

From Figure A.3-3

$$45^\circ \text{ at } 9.56 \text{ MHz} = \frac{45}{19.4} = 2.52^\circ \text{ at } 498 \text{ KHz.}$$

The following general relationship can be deduced:

$$\text{Phase Slope} = \frac{f_{498}}{f_{9.56}} = \frac{1}{19.4}$$

$$= 0.0515 \text{ degrees @ } 498 \text{ KHz per degree @ } 9.56 \text{ MHz.}$$

This simple illustration shows qualitatively the minimum delay in the demodulation process due to reference signal phase shifting.

A.3-5

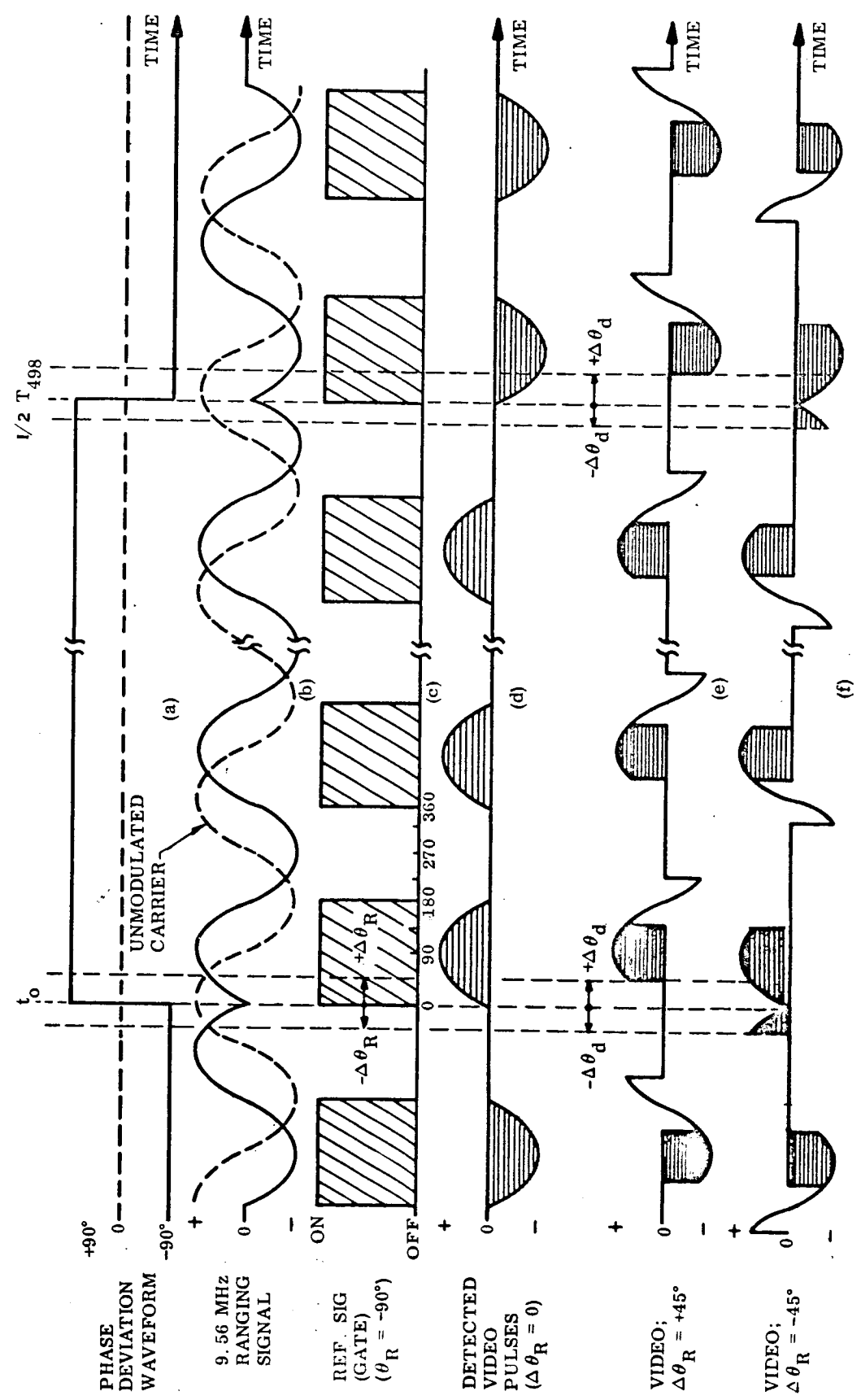
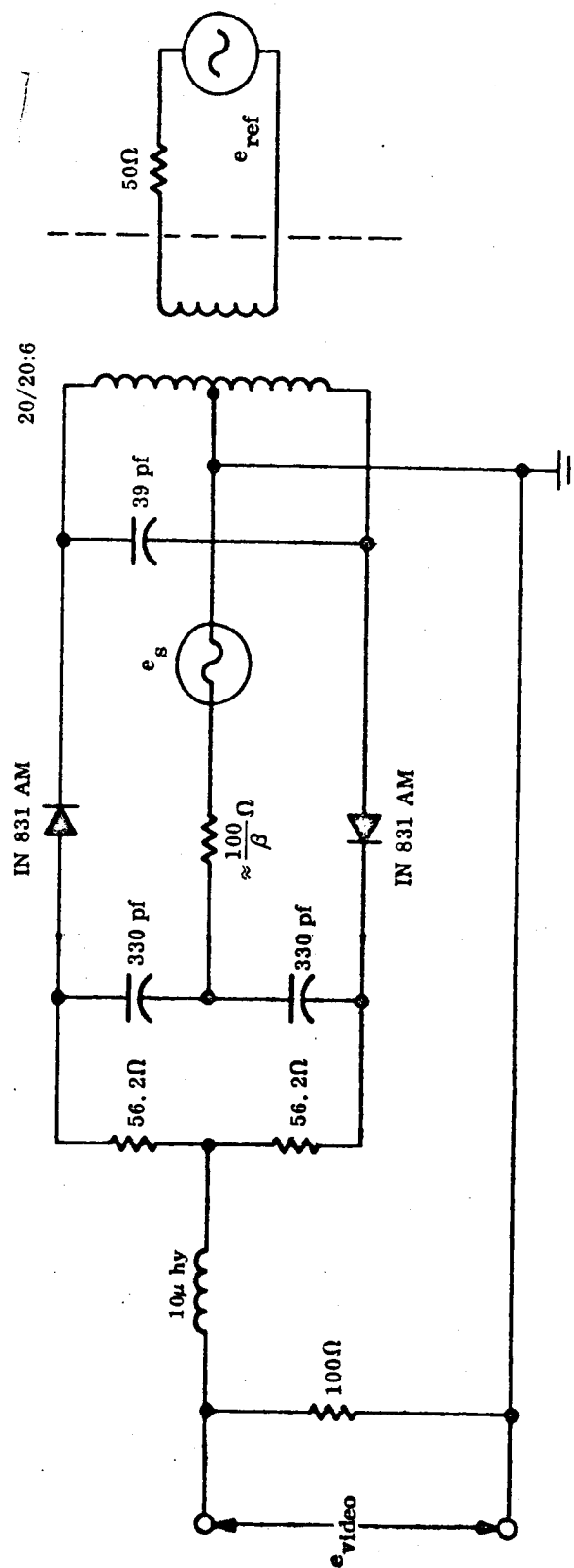


Figure A.3-3 Delay Produced in the Demodulation Process Due to Reference Phase Variation



A.3-7

Figure A.3-4 Ringing Phase Detector Reference Diagram

APPENDIX IV

TRAPEZOIDAL WAVEFORM PHASE MODULATION SPECTRUM ANALYSIS, USING
THE RESULTS OF THE DEMODULATION ANALYSIS

APPENDIX IV

TRAPEZOIDAL WAVEFORM PHASE MODULATION SPECTRUM ANALYSIS, USING
THE RESULTS OF THE DEMODULATION ANALYSIS

A.4.1. $e(t) = \cos[\omega_o t + f(\theta)]$

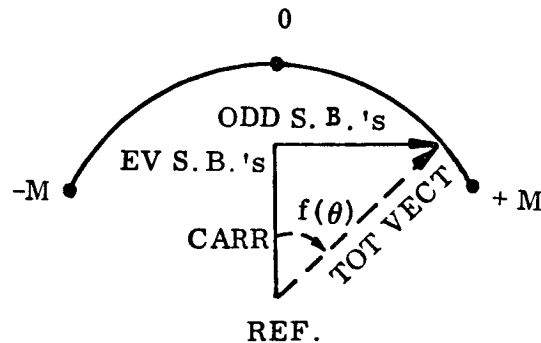
= instantaneous R.F. voltage

A.4.2. $f(\theta)$ and θ , θ_R , M , and ϕ as previously defined

A.4.3. carr + ev S.B.'s vect: $[\cos f(\theta)] \cos \omega_o t$

odd S.B.'s vect: $-\sin f(\theta) \sin \omega_o t$

A.4.4.



A.4.5. Evaluation of $\cos f(\theta)$ and $\sin f(\theta)$ from demodulation analysis (Appendix II)

$$\cos f(\theta) = \cos [\theta_R + f(\theta)] \quad \text{ev. @ } \theta_R = 0^\circ$$

$$\sin f(\theta) = \cos [\theta_R + f(\theta)] \quad \text{ev. @ } \theta_R = -90^\circ$$

A.4-1

$$\cos f(\theta) = \frac{A_0}{2} + \sum_{n=2,4,6,\dots} A_n \cos(n\omega_m t)$$

$$\sin f(\theta) = \sum_{n=1,3,5,\dots} B_n \sin(n\omega_m t)$$

where:

$$\frac{A_0}{2} \triangleq \frac{1}{\pi} \left[(\pi - 2\phi) \cos M + 2\phi \frac{\sin M}{M} \right]$$

$$A_n \triangleq \frac{2}{\pi} \left\{ \phi \left[\frac{\sin(M+n\phi)}{M+n\phi} + \frac{\sin(M-n\phi)}{M-n\phi} \right] - \frac{2}{n} \cos M \sin n\phi \right\}$$

$$n = 2, 4, 6, \dots$$

$$B_n \triangleq \frac{2}{\pi} \left\{ \frac{2}{n} \sin M \cos n\phi - \phi \left[\frac{\sin(M+n\phi)}{M+n\phi} - \frac{\sin(M-n\phi)}{M-n\phi} \right] \right\}$$

$$n = 1, 3, 5, \dots$$

$$A.4.6. \text{ Carrier} = \frac{A_0}{2} \cos \omega_0 t$$

$$A.4.7 \text{ ev sidebands: } (\sum A_n \cos n\omega_m t) \cos \omega_0 t$$

$$n = 2, 4, 6, \dots$$

$$= \sum \frac{A_n}{2} \cos(\omega_0 + n\omega_m)t$$

$$+ \sum \frac{A_n}{2} \cos(\omega_0 - n\omega_m)t$$

A.4-2

A.4.8. Odd sidbands: $-(\sum B_n \sin n\omega_M t) \sin \omega_o t$

$n = 1, 3, 5, \dots$

$$= \sum \frac{B_n}{2} \sin (\omega_o + n\omega_M)t$$

$$- \sum \frac{B_n}{2} \sin (\omega_o - n\omega_M)t$$

CALCULATED VALUES OF MODULATION SPECTRUM

CASE	ϕ	CARRIER	1	2	3	4	5	6	7	8	9	10
M=1.255	9.0°	9.0	4.4	27.1	14.1	27.3	19.0	27.8	22.6	28.3	25.7	29.1
M=0.4876	9.0°	1.0	10.5	42.3	20.4	42.6	25.4	43.0	29.2	43.6	32.6	44.4

NOTES: Spectrum is symmetric
All magnitudes in -db relative to the unmodulated carrier level
M is the peak phase deviation in radians

MEASURED VALUES OF MODULATION SPECTRUM

SIGNAL	ϕ	CARRIER	1	2	3	4	5	6	7	8	9	10
OUTPUT OF TEST SET		9.0	UPPER	5	21.5	17	26.5	23.5	31.5	27	34	42
			LOWER	3.5	19.5	15	22	20	25	24.5	28	31
OUTPUT OF TRANSP.		2.2	UPPER	7	19	21	23	28	35	38	*	*
			LOWER	7.5	19.5	18	23.5	28	33	37	44	45

NOTES: All magnitudes in -db relative to the unmodulated carrier level
* Not measured
Input signal level is -70 db
All values measured on HP 851B Spectrum Analyzer

Figure A4-1

APPENDIX V

TRANSPONDER PHASE ANALYSIS




APPENDIX V

TRANSPONDER PHASE ANALYSIS

A block diagram, Figure A.5-1, was developed to explain the transponder carrier phase measurements. Figure A.5.2 is a diagram of the transponder phase detection relationships.

Only elements known as significant contributors to phase shifts were noted. In addition, only transfer functions are shown. Driving point impedance interface effects were not taken into account although subsequent tests indicated interface problems do contribute to phase shift in some instances.

A.5.1 Explanation of Symbols for All Figures

-  = Summing Junction
 = Amplifier of Gain "N"
 = Composite representation of an amplifier which contributes a gain N and a phase shift, $\theta_{\text{amplifier}}$, where $\theta_{\text{amplifier}}$ is the sum of all phase shifts within the amplifier referenced to an equivalent output value.

A.5.2 Analysis of Transponder Carrier Phase Relationships

A.5.2.1 $G = \frac{1}{S} \left(\frac{1+\tau_2 S}{1+\tau_1 S} \right)$ and $K = K_D K_V$

A.5.2.2
$$\begin{aligned} \theta_{VCO} &= KG(\theta_{IV} - \theta_{III}) \\ &= KG \left\{ \left[\frac{1}{2} \theta_{VCO} + \theta_{\frac{1}{2}} \right] - [3\theta_{VCO} + \theta'_3 - (\theta_S)_{IN} + 108\theta_{VCO} + 36\theta'_3 \right. \right. \\ &\quad \left. \left. + \theta_{36} - \theta_{47.8} + \theta_{9.56} \right] \right\} \end{aligned}$$

A.5-1

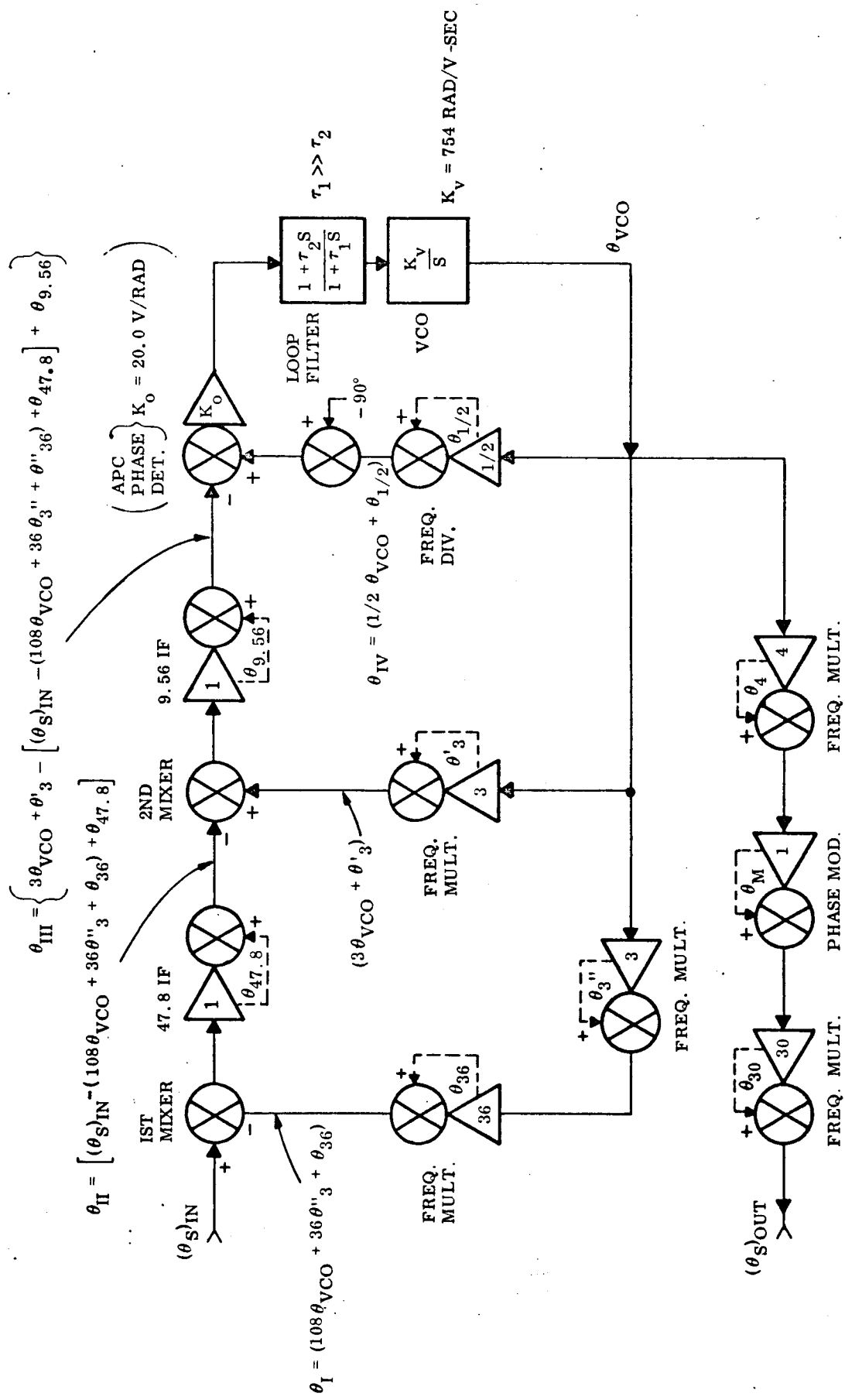


Figure A.5-1 Transponder Carrier Phase Block Diagram

194

TR-DA1522A

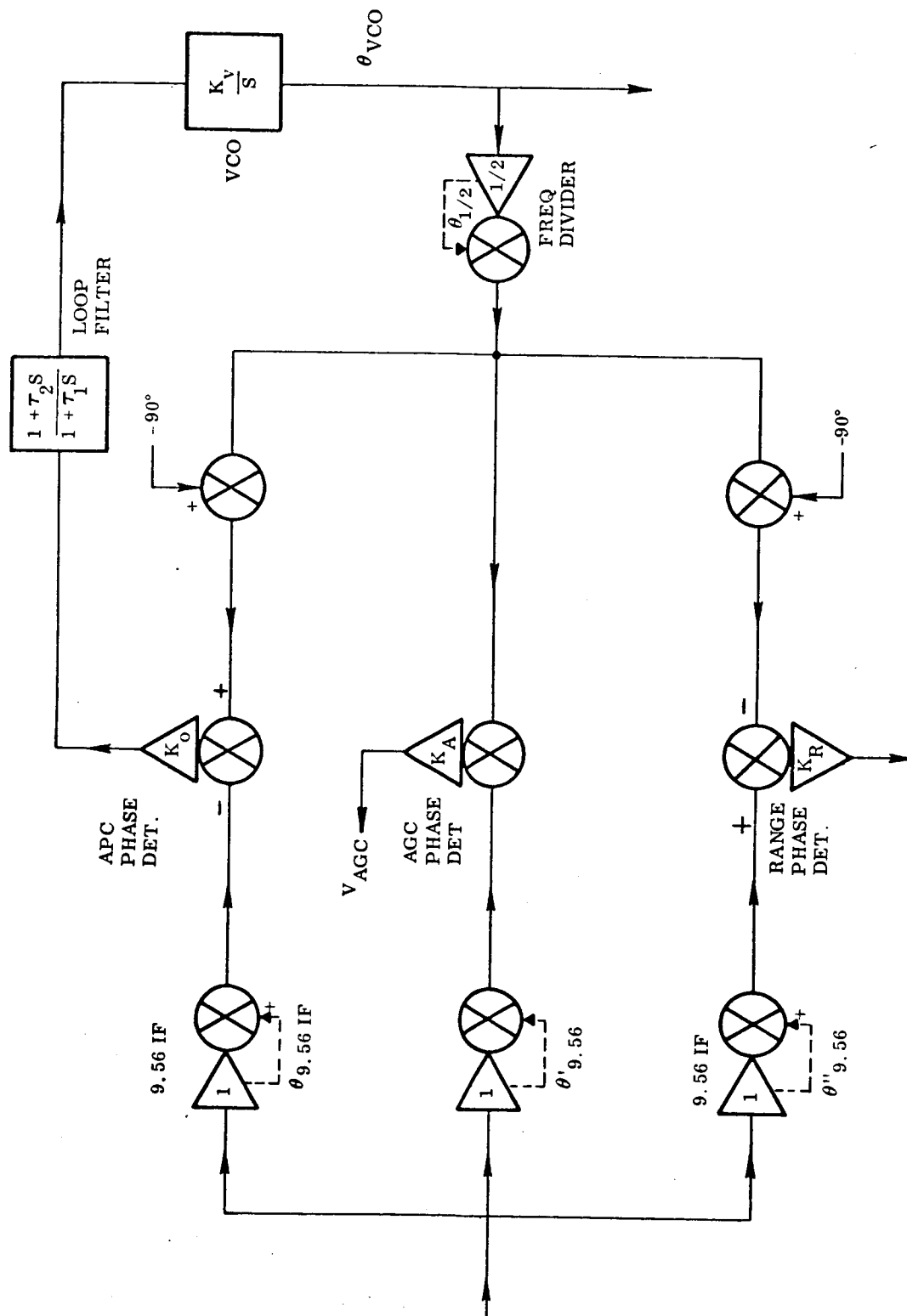


Figure A.5-2 Transponder Phase Detector Block Diagram

A.5-3

A.5.2.3. $\theta_{VCO} (1 + 110\frac{1}{2} KG) = KG(\theta_{\frac{1}{2}} - \theta_3' + (\theta_s)_{IV} - 36\theta_3'' - \theta_{36} + \theta_{47.8} - \theta_{9.56})$

A.5.2.4. $\phi = (\theta_s)_{IN} - \underbrace{(\theta_{36} - \theta_{47.8} + \theta_{9.56})}_{\text{Receiver, No.1 Six-Pack}} - \underbrace{(36\theta_3'' + \theta_3' - \theta_{\frac{1}{2}})}_{\text{Receiver, No.2 Six-Pack}}$

A5.2.5. $\theta_{VCO} = \frac{\phi KG}{110\frac{1}{2}KG+1}$

A.5.2.6. $\theta_{VCO} = \frac{\phi(s) \frac{\tau_2}{\tau_1} K_V K_D (s + 1/\tau_2)}{s^2 + \frac{110\frac{1}{2} K_V K_D \tau_2 + 1}{\tau_1} s + \frac{110\frac{1}{2} K_V K_D}{\tau_1}} = \frac{\phi(s) 4.098(s + 13.333)}{(s + 13.751)(s + 439.06)}$

A.5.2.7. $(\theta_s)_{OUT} = \underbrace{120 \theta_{VCO}}_{\text{Receiver No. 1 \& No. 2 six-packs}} + \underbrace{30(\theta_4 + \theta_M)}_{\text{Transmitter six-pack}} + \theta_{30}$

NOTE:

- $\phi = \phi(s) = \Sigma \theta(s)$ inputs, these inputs should be considered general functions having the angular amplitudes designated
- The APC loop is considered to be "inlock" for all time
- System constants are as follows:

$$\tau_1 = 276 \text{ sec}$$

$$\tau_2 = 75 \text{ Msec}$$

$$K_V = 754 \text{ radians/volt-sec}$$

$$K_D = 20 \text{ volts/radian}$$

- θ_3' and θ_3'' are in the VCO module.

A.5.2.3. $\theta_{VCO} (1 + 110\frac{1}{2} KG) = KG(\theta_{\frac{1}{2}} - \theta_3' + (\theta_s)_{IV} - 36\theta_3'' - \theta_{36} + \theta_{47.8} - \theta_{9.56})$

A.5.2.4. $\phi \triangleq (\theta_s)_{IN} - \underbrace{(\theta_{36} - \theta_{47.8} + \theta_{9.56})}_{\text{Receiver, No.1 Six-Pack}} - \underbrace{(36\theta_3'' + \theta_3' - \theta_{\frac{1}{2}})}_{\text{Receiver, No.2 Six-Pack}}$

A.5.2.5. $\theta_{VCO} = \frac{\phi KG}{110\frac{1}{2}KG+1}$

A.5.2.6. $\theta_{VCO} = \frac{\phi(s) \frac{\tau_2}{\tau_1} K_v K_D (s + 1/\tau_2)}{s^2 + \frac{110\frac{1}{2} K_v K_D \tau_2 + 1}{\tau_1} s + \frac{110\frac{1}{2} K_v K_D}{\tau_1}} = \frac{\phi(s) 4.098(s + 13.333)}{(s + 13.751)(s + 439.06)}$

A.5.2.7. $(\theta_s)_{OUT} = \underbrace{120 \theta_{VCO}}_{\text{Receiver No. 1 \& No. 2 six-packs}} + \underbrace{30(\theta_4 + \theta_M)}_{\text{Transmitter six-pack}} + \theta_{30}$

NOTE:

- $\phi = \phi(s) = \Sigma \theta(s)$ inputs, these inputs should be considered general functions having the angular amplitudes designated
- The APC loop is considered to be "inlock" for all time
- System constants are as follows:

$$\tau_1 = 276 \text{ sec}$$

$$\tau_2 = 75 \text{ Msec}$$

$$K_v = 754 \text{ radians/volt-sec}$$

$$K_D = 20 \text{ volts/radian}$$

- θ_3' and θ_3'' are in the VCO module.

A.5.3 An Analysis of the Effect of VCO Crystal Frequency Drifts Expressed as an Equivalent Input DC Voltage Change

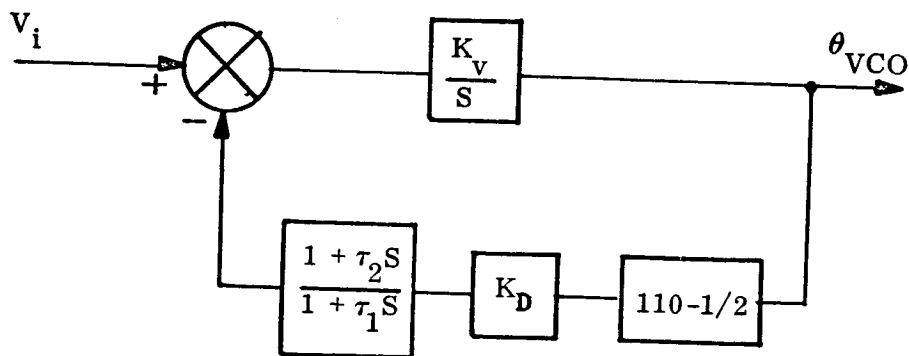


Figure A.5-3 VCO Loop Block Diagram

A.5.3.1

$$\frac{\theta_{VCO}(s)}{v_i(s)} = \frac{G(s)}{1+H(s)G(s)}$$

A.5.3.2

$$\theta_{VCO}(s) = \frac{v_i(s) \left(K_v (s + 1/\tau_1) \right)}{s^2 + \left(\frac{110^{1/2} K_v K_D \tau_2 + 1}{\tau_1} \right) s + \frac{110^{1/2} K_v K_D}{\tau_1}} = \frac{v_i(s) (754)(s + .0036232)}{(s + 13.751)(s + 439.06)}$$

NOTE: See Figure A.5-6 for typical graph of VCO equivalent D.C. bias change vs temperature

A.5-5

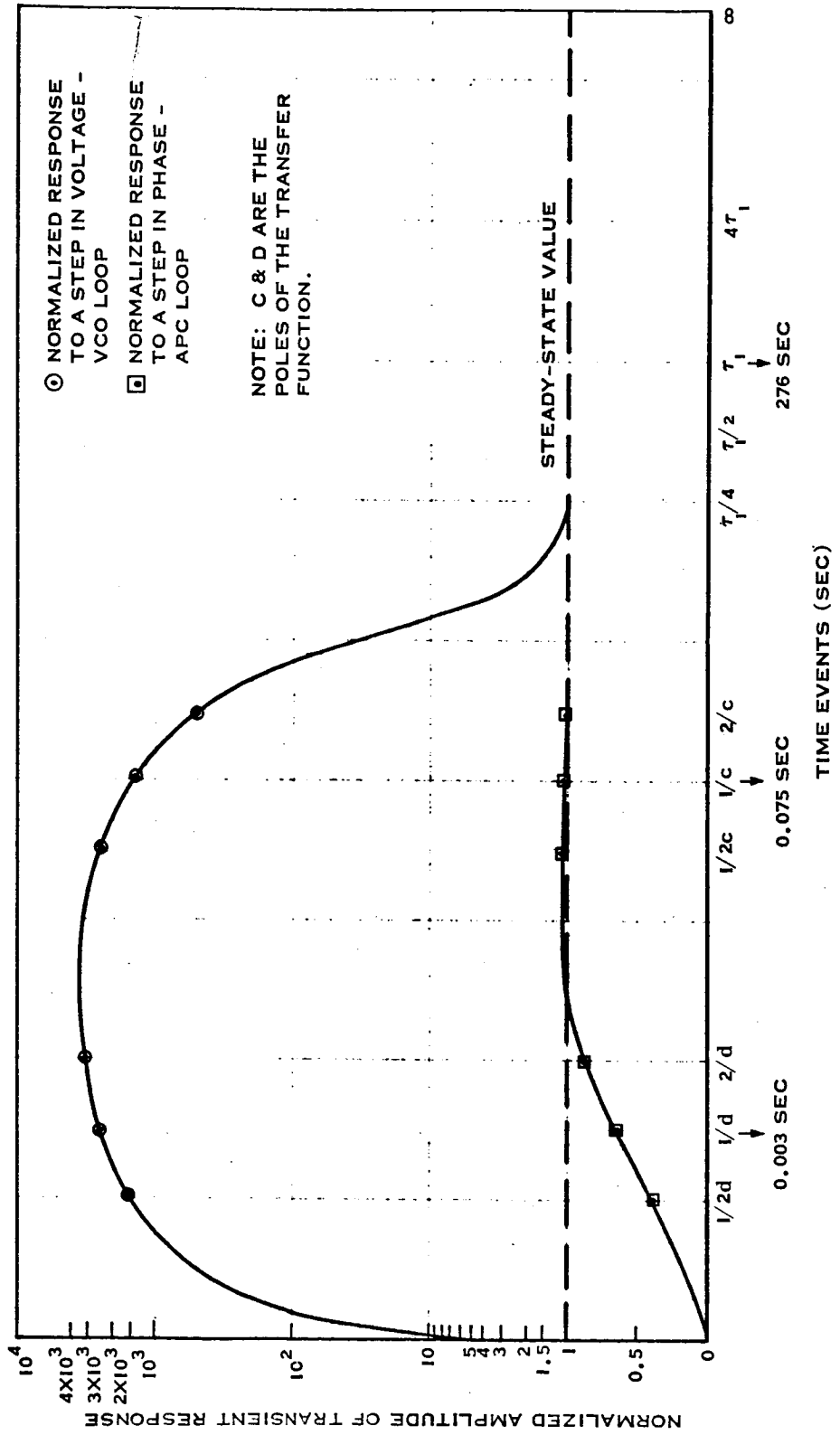


Figure A.5-4 Comparison of the APC and VCO Loops to Step Inputs.

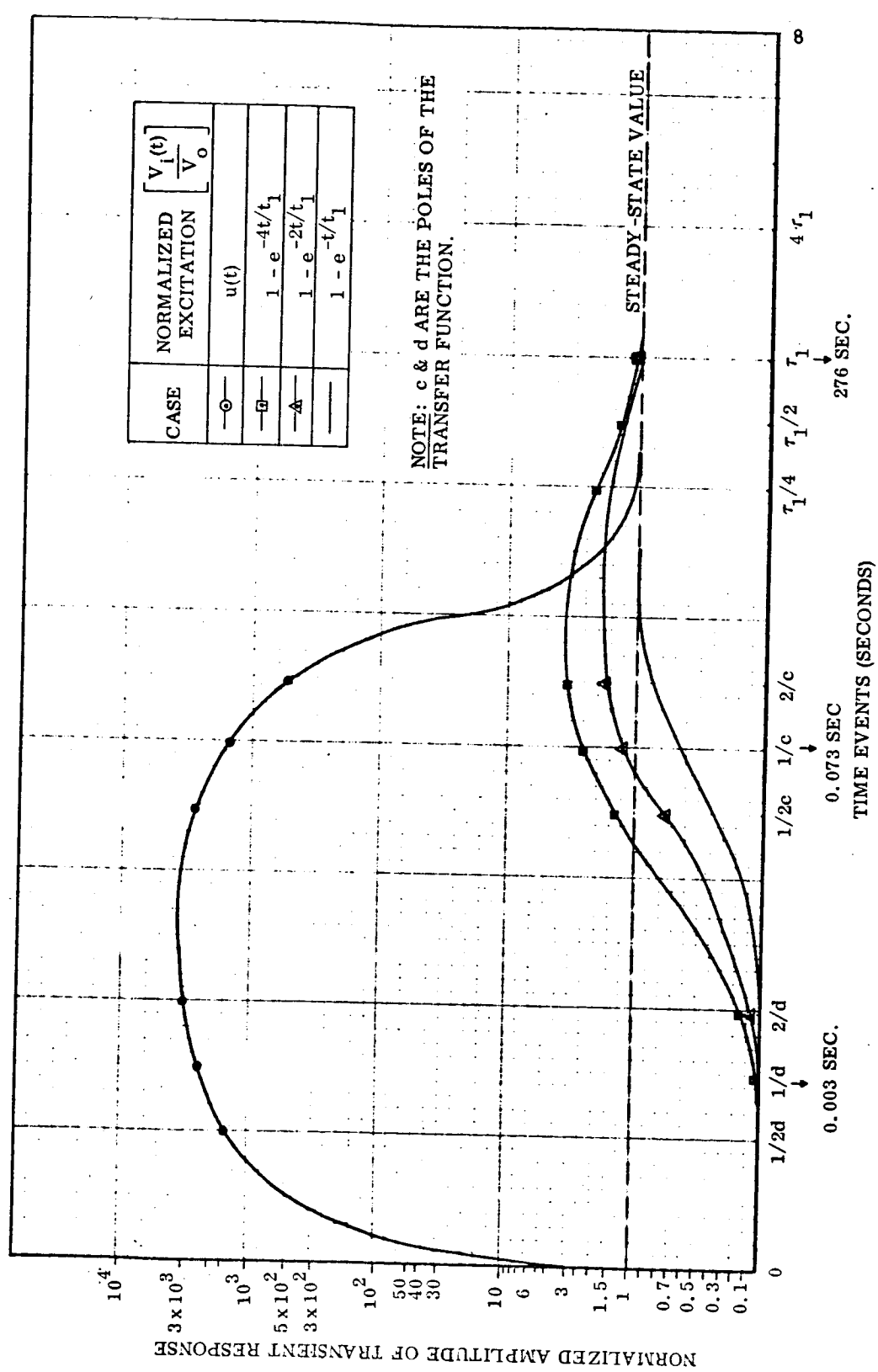
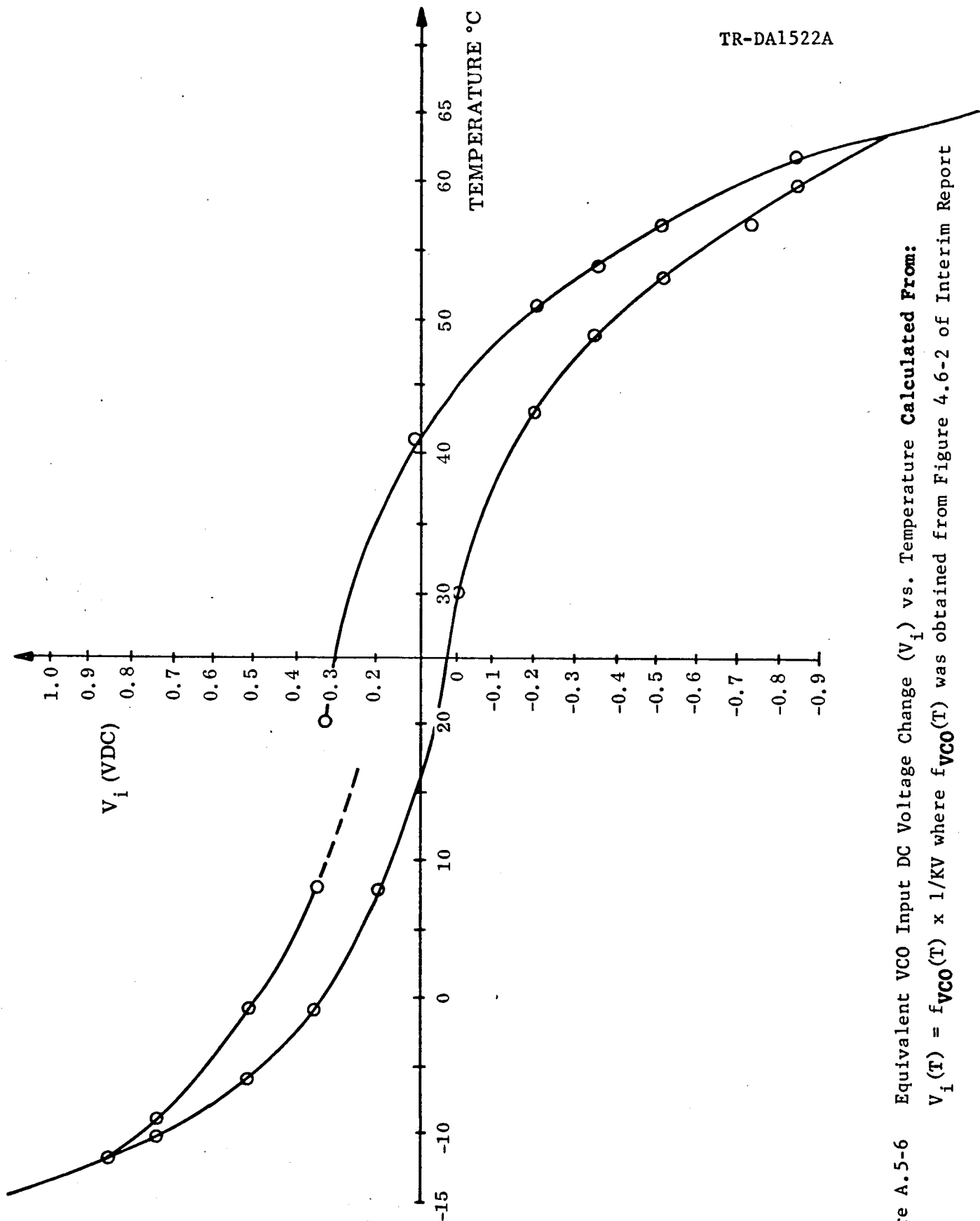


Figure A.5-5 VCO Loop Transient Response .

TR-DA1522A



A.5-8

Figure A.5-6 Equivalent VCO Input DC Voltage Change (V_i) vs. Temperature Calculated From:

$$V_i(T) = f_{VCO}(T) \times 1/\text{KV where } f_{VCO}(T) \text{ was obtained from Figure 4.6-2 of Interim Report}$$

APPENDIX VI

FREQUENCY RATIO STUDY; ANALYSIS OUTLINE

APPENDIX VI

FREQUENCY RATIO STUDY; ANALYSIS OUTLINE

TENTATIVE RESTRICTIONS

For purposes of analysis let

$k = 1, 2, 3 \dots$ (an arbitrary positive integer)

$$(R1)_6 \quad \left\{ \begin{array}{l} 1750 \text{ Mc} \leq f_u \leq 1850 \text{ Mc} \\ 2200 \text{ Mc} \leq f_d \leq 2300 \text{ Mc} \end{array} \right\}$$

$$\left\{ \begin{array}{l} 2300/1850 \leq f_d/f_u \leq 2200/1750 \\ 2300/1850 = 46/37 = 1.2432 \\ 2250/1800 = 5/4 = 1.2500 \\ 2200/1750 = 44/35 = 1.2571 \end{array} \right\} \quad \begin{array}{l} \text{For reference only} \\ \text{(not part of R1)} \end{array}$$

$$R2. \quad * \leq f_o \leq 50 \text{ Mc}$$

$$(R3)_4 \quad * \leq f_1 \leq 100 \text{ Mc}$$

$$(R4)_3 \quad 8 \text{ Mc} \leq f_2 \leq 12 \text{ Mc}$$

$$R5. \quad * < B_u < 2f_o$$

$$R6. \quad * < B_1 < 2f_o$$

$$R7. \quad * \leq B_2 \leq 4.7 \text{ Kc}$$

$$R8. \quad * < B_d < *$$

$$R9. \quad * < B_d < 2f_o$$

*Undermined limits.

$$(R10)_1 \quad f_u \neq kf_o$$

$$R11. \quad f_u \neq kf_2$$

$$R12. \quad f_u \neq kf_1$$

$$R13. \quad f_1 \neq kf_o$$

$$R14. \quad f_1 \neq kf_2$$

$$R15. \quad f_2 \neq kf_o$$

$$R16. \quad f_d = kf_o$$

$$(R17)_2 \quad f_u^{**} = f_d - (k \pm \frac{1}{2})f_o$$

$$(R18)_7 \quad a = \pi k, \quad 2 \leq k \leq 5$$

$$(19)_5 \quad b = k, \quad 2 \leq k \leq *$$

$$R20. \quad c = k_1/k_2, \quad k_2 > k_1$$

$$k_1 = 1, 2, 3, \dots$$

$$k_2 = 1, 2, 3, \dots$$

$$(R21)_8 \quad d = \pi k, \quad 2 \leq k \leq 5$$

NOTE: The brackets indicate only those restrictions actually used,
and the subscript indicates the order of usage.

** Locates f_u midway between harmonics of f_o .

* Undetermined limits.

A6.1 A Conditional Choice of "C"

Assumptions:

$$R10. \quad f_u \neq kf_o$$

$$R17. \quad f_u = f_d - (k \pm \frac{1}{2})f_o$$

Pertinent Formulas:

$$4.3.1.5. \quad f_d = df_o$$

$$4.3.2.1. \quad f_u/f_o = a \pm (b \pm c)$$

Results:

$$f_u/f_o = a \pm (b \pm c) \neq k$$

Since a, b, and k are integers, c is not an integer

$$f_u/f_o = a \pm (b \pm c) = d - (k \pm \frac{1}{2})$$

$$A.6.1.1 \quad c \equiv \frac{1}{2}$$

A.6.2 Bounds on f_o

Assumptions:

$$R4. \quad 8 \text{ Mc} \leq f_2 \leq 12 \text{ Mc}$$

$$A6.1.1. \quad c \equiv \frac{1}{2}$$

Pertinent Formulas:

$$4.3.1.4. \quad f_2 = cf_o$$

A.6-3

Results:

$$8 \text{ Mc} \leq 1/2 f_o \leq 12 \text{ Mc}$$

A6.2.1 $16 \text{ Mc} \leq f_o \leq 24 \text{ Mc}$

A6.3 Upper Bound on "b"

Assumptions:

R3. $* \leq f_1 \leq 100 \text{ Mc}$

R4. $8 \text{ Mc} \leq f_2 \leq 12 \text{ Mc}$

A6.1.1. $c \equiv \frac{1}{2}$

Pertinent Formulas:

A6.2.5. $f_1/f_2 = (b+c)/c$

Results

$$b_{\max} = c \left(\frac{f_{1 \max}}{f_{2 \min}} + 1 \right)$$

$$= 1/2 \left(\frac{100}{8} + 1 \right) = 6.75$$

A6.3.1 $b_{\max} = 6$

A.6.4 Lower Bound on f_1

Assumptions:

R4. $8 \text{ Mc} \leq f_2 \leq 12 \text{ Mc}$

R19. $b = k, 2 \leq k \leq *$

A6.1.1 $c \equiv \frac{1}{2}$

A.6-4

Pertinent Formulas:

$$A6.2.5. \quad f_1/f_2 = (b \pm c)/c$$

Results:

$$\begin{aligned} f_{1 \min} &= f_{2 \min} \left(\frac{b_{\min} - c}{c} \right) \\ &= (8 \text{ Mc}) \left(\frac{2 - \frac{1}{2}}{\frac{1}{2}} \right) \end{aligned}$$

$$A6.3.1 \quad \underline{f_{1 \min} = 24 \text{ Mc}}$$

A6.5 Bounds on "a" and "d"

Assumptions:

$$R1 \quad \left\{ \begin{array}{l} 1750 \text{ Mc} \leq f_u \leq 1850 \text{ Mc} \\ 2200 \text{ Mc} \leq f_d \leq 2300 \text{ Mc} \end{array} \right\}$$

$$R19 \quad b = k, \quad 2 \leq k \leq *$$

$$A6.1.1. \quad c \equiv 1/2$$

$$A6.2.1. \quad 16 \text{ Mc} \leq f_o \leq 24 \text{ Mc}$$

$$A6.3.1. \quad b_{\max} = 6$$

Pertinent Formulas:

$$4.3.2.1. \quad f_u/f_o = a \pm (b \pm c)$$

$$4.3.2.7. \quad f_d/f_o = d$$

Results:

$$\frac{f_{u \min}}{f_{o \max}} \leq a \pm (b \pm c) \leq \frac{f_{u \max}}{f_{o \min}}$$

$$\frac{f_{d \min}}{f_{o \max}} \leq d \leq \frac{f_{u \max}}{f_{o \min}}$$

$$[a \pm (b \pm c)]_{\min} = \frac{f_{u \min}}{f_{o \max}} = \frac{1750}{24} = 72\frac{1}{2}$$

$$[a \pm (b \pm c)]_{\max} = \frac{f_{u \max}}{f_{o \min}} = \frac{1850}{16} = 115\frac{5}{8}$$

$$d_{\min} = \frac{f_{d \min}}{f_{o \max}} = \frac{2200}{24} = 91\frac{2}{3}$$

$$d_{\max} = \frac{f_{d \max}}{f_{o \min}} = \frac{2300}{16} = 143\frac{3}{4}$$

A6.5.1 $72\frac{1}{2} \leq a \pm (b \pm c) \leq 115\frac{5}{8}$
 $91\frac{2}{3} \leq d \leq 143\frac{3}{4}$

Bounds on "d" using A6.5.1 and $C = \frac{1}{2}$

A.6.5.2 $92 \leq d \leq 143$

Minimum bounds on "a"

A6.5.3 $71 \leq a \leq 109$

A6.6 Prime Factors

Assumptions:

$$R19. \quad b = k, \quad 2 \leq k \leq *$$

$$A1.1. \quad c \equiv 1/2$$

$$A3.1. \quad b_{\max} = 6$$

$$A5.2. \quad 92 \leq d \leq 143$$

$$A5.3. \quad 71 \leq a \leq 109$$

Results:

No.	"a"	Prime No.'s	No.	"a"	Prime No.'s	No.	"a"	Prime No.'s
1	71	71	14	84	2,41	27	97	97
2	72	2,2,3,3	15	85	5,17	28	98	2,7,7
3	73	73	16	86	2,43	29	99	3,3,11
4	74	2,37	17	87	3,29	30	100	2,2,5,5
5	75	3,5,5	18	88	2,2,2,11	31	101	101
6	76	2,2,19	19	89	89	32	102	2,3,17
7	77	7,11	20	90	2,3,3,5	33	103	103
8	78	2,3,13	21	91	7,13	34	104	2,2,2,13
9	79	79	22	92	2,2,23	35	105	3,5,7
10	80	2,2,2,2,5	23	93	3,31	36	106	2,53
11	81	3,3,3,3	24	94	2,47	37	107	107
12	82	2,41	25	95	5,19	38	108	2,2,3,3,3
13	83	83	26	96	2,2,2,2,2,3	39	109	109

A.6-7

207

TR-DA1522A

<u>No.</u>	<u>"b"</u>	<u>Prime No.'s</u>	<u>No.</u>	<u>"b"</u>	<u>Prime No.'s</u>
1	2	2	4	5	5
2	3	3	5	6	2,3
3	4	2,2			

A.6-8

<u>No.</u>	<u>"d"</u>	<u>Prime No's.</u>	<u>No.</u>	<u>"d"</u>	<u>Prime No's.</u>
1	92	2,2,23	31	122	2,2,31
2	93	3,31	32	123	3,41
3	94	2,47	33	124	2,2,31
4	95	5,19	34	125	5,5,5
5	96	2,2,2,2,2,3	35	126	2,7,9
6	97	97	36	127	127
7	98	2,7,7	37	128	2,2,2,2,2,2,2
8	99	3,3,11	38	129	3,43
9	100	2,2,5,5	39	130	2,5,13
10	101	101	40	131	131
11	102	2,3,17	41	132	2,2,3,11
12	103	103	42	133	7,19
13	104	2,2,2,13	43	134	2,67
14	105	3,5,7	44	135	3,3,3,5
15	106	2,53	45	136	2,2,2,17
16	107	107	46	137	137
17	108	2,2,3,3,3	47	138	2,3,23
18	109	109	48	139	139
19	110	2,5,11	49	140	2,2,5,7
20	111	3,37	50	141	3,47
21	112	2,2,2,2,7	51	142	2,71
22	113	113	52	143	11,13
23	114	2,3,19			
24	115	5,23			
25	116	2,2,29			
26	117	3,3,13			
27	118	2,59			
28	119	7,17			
29	120	2,2,2,3,5			
30	121	11,11			

Summary of usable values:

Assumptions:

$$R18. \quad a = \pi k, \quad 2 \leq k \leq 5$$

$$R19. \quad b = k, \quad 2 \leq k \leq *$$

$$R21. \quad d = \pi k, \quad 2 \leq k \leq 5$$

$$A6.1. \quad c \equiv 1/2$$

$$A6.3. \quad b_{\max} = 6$$

$$A6.5.2. \quad 92 \leq d \leq 143$$

$$A6.5.3. \quad 71 \leq a \leq 109$$

No.	a	b	d
1	72(2,2,3,3)	2	96(2,2,2,2,2,3)
2	75(3,5,5)	3	100(2,2,5,5)
3	80(2,2,2,2,5)	4(2,2)	108(2,2,3,3,3)
4	81(3,3,3,3)	5	120(2,2,2,3,5)
5	90(2,3,3,5)	6(2,3)	125(5,5,5)
6	96(2,2,2,2,2,3)		128(2,2,2,2,2,2,2)
7	100(2,2,5,5)		135(3,3,3,5)
8	108(2,2,3,3,3)		

A6.7 Tentative Choice of $f_d/f_d = r$

Assumptions:

A6.1. $c \equiv 1/2$

A6.6. See table, summary of values on previous page

$$f_u > af_o$$

$$f_l < bf_o$$

Pertinent Formulas:

$$f_u/f_d = d/[a \pm (b \pm c)] \triangleq r$$

Results: (Using Mariner C sign choices)

$$r = d/[a + (b-c)]$$

A6.7.1 Table of $a+(b-c)$ for usable values of a, b , and c .

No.	<u>a</u>	<u>$a+2-\frac{1}{2}$</u>	<u>$a+3-\frac{1}{2}$</u>	<u>$a+4-\frac{1}{2}$</u>	<u>$a+5-\frac{1}{2}$</u>	<u>$a+b-\frac{1}{2}$</u>
1	72	73½	74½	75½	76½	77½
2	75	76½	77½	78½	79½	80½
3	80	81½	82½	83½	84½	85½
4	81	82½	83½	84½	85½	86½
5	90	91½	92½	93½	94½	95½
6	96	97½	98½	99½	100½	101½
7	100	101½	102½	103½	104½	105½
8	108	109½	110½	111½	112½	113½

A6.7.2 Prime Factors of $2[a+(b-c)]^*$

<u>No.</u>	<u>$a+(b-c)$</u>	<u>$2[a+(b-c)]$</u>	<u>Prime Factor</u>
1	$73\frac{1}{2}$	147	3,7,7
2	$74\frac{1}{2}$	149	
3	$75\frac{1}{2}$	151	
4	$76\frac{1}{2}$	153	3,3,17
5	$77\frac{1}{2}$	155	5,31
6	$78\frac{1}{2}$	157	
7	$79\frac{1}{2}$	159	3,53
8	$80\frac{1}{2}$	161	7,23
9	$81\frac{1}{2}$	163	
10	$82\frac{1}{2}$	165	3,5,11
11	$83\frac{1}{2}$	167	
12	$84\frac{1}{2}$	169	13,13
13	$85\frac{1}{2}$	171	3,3,19
14	$86\frac{1}{2}$	173	
	.		
15	$91\frac{1}{2}$	183	3,61
16	$92\frac{1}{2}$	185	5,37
17	$93\frac{1}{2}$	187	11,17
18	$94\frac{1}{2}$	189	3,3,3,7
19	$95\frac{1}{2}$	191	
	.		

* $[a + (b - c)]$ is multiplied by 2 in anticipation of a rational fraction
for $r = \frac{fd}{f_u}$.

A.6-12

<u>No.</u>	<u>a+(b-c)</u>	<u>2[a+(b-c)]</u>	<u>Prime Factor</u>
20	97½	195	3,5,13
21	98½	197	
22	99½	199	
23	100½	201	3,67
24	101½	203	7,29
25	102½	205	5,41
26	103½	207	3,3,23
27	104½	209	11,19
28	105½	211	
	.		
	.		
	.		
29	109½	219	3,73
30*	110½	221	13,17
31	111½	223	
32	112½	225	3,3,5,5
33	113½	227	

A6.7.3 Tentative Choices of a+(b-c)

<u>No.</u>	<u>a+(b-c)</u>	<u>a</u>	<u>b</u>	<u>c</u>
1	112½	108	5	1/2
2	94½	90	5	1/2
3	73½	72	2	1/2

* Present S-band value.

Prime Factors:

$$2(112\frac{1}{2}) = 225 = 3 \times 3 \times 5 \times 5$$

$$2(94\frac{1}{2}) = 189 = 3, 3, 3, 7$$

$$2(73\frac{1}{2}) = 147 = 3, 7, 7$$

$$a = 108 = 2 \times 2 \times 3 \times 3 \times 3$$

$$a = 90 = 2 \times 3 \times 3 \times 5$$

$$a = 72 = 2 \times 2 \times 3 \times 3$$

A6.7.4 Resultant $f_d/f_u = r$

<u>No.</u>	<u>a+b-c</u>	<u>d</u>	<u>r</u>
1	112½	135	1.2000
2	94½	120	1.2698
3	73½	96	1.3061

The best all-around choice is No. 2, and the final results are as follows:

$$r = \frac{f_d}{f_u} = \frac{d}{a+b-c} = \frac{120}{94\frac{1}{2}} = \frac{2 \times 2 \times 2 \times 3 \times 5}{(2 \times 3 \times 3 \times 5) + 5 - 1/2} = \frac{80}{63}$$

The final transponder configuration is shown in Figure 4.3-2.

A6.7.5 Loss In Tuning Range

$$r = \frac{5}{4} : \text{(This value provides optimum tuning range)}$$

$$f_{u \min} = \frac{4}{5} f_{d \min} = \frac{4}{5}(2200) = 1760 \text{ Mc}$$

$$f_{u \max} = \frac{4}{5} f_{d \max} = \frac{4}{5}(2300) = 1840 \text{ Mc}$$

$$r = 80/63:$$

$$f_{d \min} = \frac{80}{63} f_{u \min} = \frac{80}{63}(1750) = \frac{149000}{63} = 2,222\frac{2}{9}$$

$$f_{u \max} = \frac{63}{80} f_{d \max} = \frac{63}{80}(2300) = \frac{7,245}{4} = 1,811\frac{1}{4}$$

Result:

$\frac{r}{}$	$\frac{f_{u \min}}{}$	$\frac{f_{u \max}}{}$	$\frac{BW_u}{}$	$\frac{f_{d \min}}{}$	$\frac{f_{d \max}}{}$	$\frac{BW_d}{}$
5/4	1760	1840	80	2200	2300	100
80/63	1750	1811 $\frac{1}{4}$	61 $\frac{1}{4}$	2222 $\frac{2}{9}$	2300	77 $\frac{7}{9}$

$$\text{Loss of BW} = 80 - 61\frac{1}{4} = 18\frac{3}{4} \text{ Mc}$$

A6.7.6 Transponder Nominal Frequencies

$$\frac{f_{d \min}}{f_{u \min}} = \frac{f_{d \text{ mid}}}{f_{u \text{ mid}}} = \frac{f_{d \max}}{f_{u \max}} = r$$

$$\left(\frac{f_{d \text{ mid}}}{f_{u \text{ mid}}}\right)^2 = \left(\frac{f_{d \min}}{f_{u \min}}\right) \left(\frac{f_{d \max}}{f_{u \max}}\right)$$

$$\frac{f_{d \text{ mid}}}{f_{u \text{ mid}}} = \frac{\sqrt{f_{d \text{ min}} f_{d \text{ max}}}}{\sqrt{f_{u \text{ min}} f_{u \text{ max}}}}$$

$$f_{d \text{ mid}} = \sqrt{f_{d \text{ min}} f_{d \text{ max}}}$$

$$= \sqrt{\frac{140,000}{63} \cdot 2300} = \sqrt{5,111,111 \frac{1}{9}} = 2260.69$$

$$f_{d \text{ mid}} = 2260.79 \text{ Mc}$$

$$f_{u \text{ mid}} = \frac{2260.79}{1.2698} = 1780.43$$

$$f_{u \text{ mid}} = 1780.43 \text{ Mc}$$

$$f_o = \frac{f_d}{d} = \frac{2260.79}{120} = 18.840$$

$$f_o = 18.840 \text{ Mc}$$

$$f_2 = c f_o = \frac{1}{2}(18.840) = 9.420$$

$$f_2 = 9.420 \text{ Mc}$$

$$f_1 = \left(\frac{b-c}{c}\right) f_2 = \frac{5-\frac{1}{2}}{\frac{1}{2}}(9.420) = 84.780$$

$$f_1 = 84.780 \text{ Mc}$$

TR-DA1522A

REFERENCE
PRIME NUMBERS

1	113
2	127
3	131
5	137
7	139
11	149
13	151
17	157
19	163
23	167
29	173
31	179
37	181
41	191
43	193
47	197
53	199
59	211
61	223
67	227
71	229
73	233
79	239
83	241
89	251
97	257
101	263
103	269
107	271
109	277
	281

A.6-17

APPENDIX VII

TEST INFORMATION FOR S-BAND/"VCO"/RANGING PHASE SHIFT VS TEMPERATURE

APPENDIX VII

TEST INFORMATION FOR S-BAND/"VCO"/RANGING PHASE SHIFT VS TEMPERATURE

The test information that follows describes the application of the ranging equipment as utilized for the measurements made in this study. Information on theory and procedure of operation for the Motorola Mariner S-band transponder Test Set, can be found in Motorola documents 68-26429C and 68-26430C.

A.7.1 GENERAL POINTS OF INTEREST

1. The equipment was connected as shown in the test setup block diagram Figure 3.1-1.
2. The part of the transponder to be temperature tested was placed in the test environment. In order to insure that room temperature variations did not cause the rest of the test transponder to be the source of phase variations, the remaining portion of the test transponder was placed in a reference oven.
3. After connecting the module with the rest of the transponder, via appropriate interconnection cables, a preliminary check was made to see that everything was operating correctly (see preliminary transponder checks Section A.7.3)
4. The test set was left on continuously because, at the early part of the program, the daily log of ranging delay showed about a two day stabilization time after weekend shutdowns. The transponder was only shutdown during the time a different part of it was placed in the test oven.
5. The Rustrak recorder charts were adjusted at the beginning of each temperature test to correlate with the actual time of the day. Two other recorders, used to monitor room temperature and AC line voltage, were also adjusted to correlate with actual

A.7-1

time so that any variation observed on the S-band charts could be corrected for possible room temperature and line voltage effects. The recorder speed was one inch per hour which permitted convenient recording of the S-band phase changes.

6. Two transponders were used for the test. One was used only to supply coherent reference signals to the "VCO" and S-band phase detectors. To insure a phase stable reference, the temperature and power input of the reference transponder were maintained constant. A reference temperature of 45°C was used to eliminate a need for refrigeration to maintain constant temperature.
7. The DC supply power to the isolation amplifier of the reference transponder was disconnected to turn its ranging channel off. This made the S-band chart recordings trace smoother because of reduced phase noise in the reference signal. The ranging channel of the test transponder was left on continuously because the switching action caused cog jumps of the "VCO" phase. (See Section 4.2.1) The phase noise on the S-band recordings was only about a pen width in amplitude.

A.7.2 HIGHLIGHTS OF TEST METHOD

1. With the part of the test transponder to be tested placed in the test environment and properly connected to the rest of the test transponder in the reference oven, the test was begun by lowering the temperature to -10°C and allowing at least a two hour stabilization time. The chart recorders were not started at this time.
2. After stabilization, ranging phase was measured at three power levels, -70 DBM, -90 DBM, and -110 DBM. This measurement was done by first making a doppler phase reading with the transponder connected to the test set. Then, the frequency converter was

A.7-2

connected to the test set, and, by means of the test receiver input attenuator and the ranging modulation level control, the test receiver AGC and the ranging correlation voltage, respectively, were made to match those recorded while the transponder was being measured. The doppler phase reading of the frequency converter was subtracted from the transponder reading to give the transponder delay. Since the delay through the frequency converter wasn't actually zero, the absolute delay of the transponder is in slight error. However, since the frequency converter reading was taken at each power level at all temperature being tested, the relative ranging delay change with temperature is accurate.

3. The S-band phase voltages were read on a digital voltmeter as a function of input power to the test transponder. "VCO" phase shift was also recorded at the same levels which was from -70 DBM to -140 DBM in 10 DB steps. At the same time all the data asked for on the data sheet (Figure A.7.1) was recorded.
4. The input power was then returned to -70 DBM and the S-band chart recorders were fixed to record. The temperature at this time was changed to the next higher value. If the S-band phase changed considerably with temperature, 5°C temperature steps were made to keep the recordings legible. If little S-band phase change was noticed with temperature, the complete temperature change was made in one step. When whole six packs were being temperature tested, an hour was allowed for stabilization, while only 45 minutes was used in module tests.
5. At the end of the stabilization time, the S-band recorders were set to stop recording, but allowed to keep running to keep the chart correlated with the actual time of the day. The ranging S-band and "VCO" phase measurement were made at this time and upon setting the charts to record, the procedure repeated until 75°C was reached.

A.7.3 PRELIMINARY TRANSPONDER CHECKS

1. All connectors tight (especially microdot)
2. X30 output spectrum
3. (a) Receiver in, and out, of lock
(b) Ranging on, and off
3. No signal receiver SPE $< \pm 100$ mv.
4. Receiver phase noise maximum peak $< 9^\circ$, measured at transponder receiver SPE test jack; Pin = -70 dbm
5. Transmitter phase noise maximum peak $> 6^\circ$, measured at test set receiver SPE test jack
6. Receiver AGC curve (approx. values)

Pin	VAGC
(dbm)	(vdc)
-70	-7.0
-90	-6.5
-110	-5.8
-152	-2.0 (threshold)
$-\infty$	+1.8 (no signal)

7. False lock is indicated if VAGC is some negative value
8. Check X36 spectrum (2.0655Gc) at transponder input
9. Check TLM modulation sensitivity
10. Check frequency for "0" volts SPE
 - a. "receiver phase error"
 - b. "transmitter phase error"

A.7.4 Stability of the Test Set Frequency

The manner in which the stability of the test set VCO was determined was by the observation of the transponder SPE. During the testing of the transponder when the VCO module was in the test oven, the SPE was noticed to change only .02 volts throughout an entire temperature test. The manual setting of the test set VCO frequency was not changed during any particular temperature test. Since the temperature of the transponder VCO was kept constant in a reference oven, any SPE change will be due to test set frequency changes. The VCO frequency sensitivity is 120 Hertz per volt. This means, for a .02 volt change, there is only a 2.4 Hertz drift in the transponder VCO frequency due to the change in test set VCO frequency change with varying room temperature.

TABLE A.7-1

JPL MARINER S-BAND TRANSPONDER TEST SET SERIAL NO. 12

1. 1362 Dynamics Microvoltmeter	J2-13423
2. Type M TEK Plug In (Scope)	J2-19778
3. 45A TEK (Scope)	J2-22612
4. RAN. RCVR	J1-862
5. 802 B HARR (Pwr. Sup)	J2-19541
6. TP-12 Pwr. Sup. (CCC)	J2-12003
7. TP-12 Pwr. Sup. (CCC)	J2-11994
8. BL-10 Card Files	J2-11981
9. B6-10 Card Files	J2-11985
10. 122AR Scope	J2-13422
11. Test Xmit	J1-863
12. Test Revr.	J1-839
13. Conv. RF	J1-29461
14. R-100B Philbk. Pwr. Sup.	J2-33325
15. 480M Lambda Pwr. Sup.	J2-33324
16. QR. 10-10 NJE-Pwr. Sup.	J2-33326
17. 802B Harrison Pwr. Sup.	J2-33327

TEMP °C

POWER
SUPPLIES

S-BAND
(Cycles)

SPE

RCVR -15
+15

EXCITER 15
-25

POWER LEVEL	S-BAND 0°	S-BAND 90°		CONV θ	XPNDR θ	θ _d	AGC	TEST SET I.F. ATTN	CORR. VOLTS
	Volts		Degrees				No. MOD.		
-70DBM									
-80									
-90									
-100									
-110									
-120									
-140									

NOTES:

1. S-band cycles are measure from the preceeding temperature
2. (+) above at S-band cycles means advancing ∅

Figure A.7-1 JPL Transponder Temperature Test
(Sample Data Sheet)